



**MINERALOGICAL & PETROPHYSICAL CHARACTERISATION OF GAS
SHALES: COLORADO GROUP, WESTERN CANADA SEDIMENTARY BASIN**

A thesis submitted to the Newcastle University in partial fulfillment of the requirements for
the degree of Doctor of Philosophy in the Faculty of Science, Agriculture and Engineering

by

Mohammed Bello Adamu

School of Civil Engineering and Geosciences
Newcastle University,
Newcastle upon Tyne united kingdom

March, 2012

DECLARATION

I hereby certify that this work is my own, except where otherwise acknowledged, and that it has not been submitted previously for a degree at this or any other university.

Mohammed Bello Adamu

ACKNOWLEDGEMENT

I would like to express my profound and sincere thanks to my supervisor Professor Andrew Aplin for his supervision, advice and patience. I'll forever appreciate the guardianship you provided me throughout my entire stay in the UK.

My thanks also go to Dr Martin Jones for help and advice in the lab. I am particularly grateful to Philip Green for his tireless assistance in running sedigraph and porosimetry analyses. Mr. Bernie Bowler has been a wonderful host at CEG, the constant smile on your face has made even the most glooming times bright. Special thanks to Kuncho Kurtev and Eliza Mathia for their assistance and discussions.

I must specially thank Nykky Allen for his friendship, encouragements and being there at my most trying times, thank you for taking me in and out of the ward. I am also grateful to my friends at Newcastle: Sani Yahaya, Kasim Muhammad, Aminu Bayawa, Mu'allim Bello, Sani Makarfi, Idris Musa and Habib Abdulkarim. I really appreciate your company and moral supports; you have been my family far away from home.

My colleagues, Sulaiman Dodo and Aliyu Maikobi were very supportive and kind looking after my interests in Nigeria.

ATBU and Petroleum Technology Development Fund (PTDF) are acknowledged for providing the sponsorship to carry out this programme.

Lastly but most importantly, my deepest gratitude goes to my family for their sacrifice, support and encouragement. The supports of my mother; Mallama Sa'adatu Usman, and father; Mallam Adamu Mohammed have been invaluable throughout, and I am eternally grateful. May Allah shower you with His mercies the way you raised me since kindergarten. I also appreciate the patience of my wife; Fatima and my daughter; Aisha! Sorry I couldn't be there all the times, but you were always very close to my heart.

ABSTRACT

The Colorado Group mudstones within the Western Canada Sedimentary Basin (WCSB), have been characterised for their shale gas potential using a range of mineralogical, geochemical (LECO and Rock-Eval), and petrophysical (lithology, porosity, pore size distributions and microfabric) techniques in order to gain an understanding of the shales' characteristics as suitable source rocks and reservoirs for shale gas.

Semi-quantitative mineralogy of the shales was computed using a chemometric technique developed in this study, combining Attenuated Total Reflection Fourier Transform Infra-red Spectroscopy (ATR-FTIR) and multivariate Partial Least Squares (PLS) analysis. The technique estimates quartz, total clay (illite-smectite, kaolinite, chlorite) and total carbonate (calcite, dolomite) to within 5% absolute of true value and demonstrates potential application for high sample throughput and thus high density sampling strategies for ultra-high resolution or multi-well studies.

The mineralogy of the Colorado Group shales shows that clay minerals dominate the composition of each Formation, followed by quartz. Minor amounts of calcite, dolomite and feldspars are also present. Grain size data indicate that the Colorado Group lithology consists of substantial amount of clay-grade plus fine silt materials dominated by grains <10µm deposited as floccules. Pore size distributions are predominantly unimodal with an average mean pore radius (r_{mean}) value of 50nm, although some samples exhibit bimodal pore size distributions reflecting mixture of mudstones and silt size materials.

The pore size distributions of the Colorado Group Formations are generally influenced by the relative percentages of clay and silt, as well as by the level of compaction. Clay-rich sediments tend to be unimodal with tight pore size distributions while sediments with both clay-sized and silt materials tend to have broader and occasionally bimodal pore size distributions. The unimodal porosity nature of the Colorado Group formations, and the dominance of clay-sized and silt sediments may promotes the adhesion of gas molecules, which makes these sediments optimal for gas adsorption.

Integration of the various data revealed that the Colorado Group depositional system is complex with widely changing seaway conditions showing no simple correlations between mineralogy, grain size and organic facies, or their spatial variation from palaeosource. The presence of sands and reworked shell fragments indicate a dominantly advective transport of sediments within the Colorado Group. Mud and clay cements are observed throughout the Upper Colorado Group, whereas calcareous cements are present only within the Second White Specks Formation, Medicine Hat Member and First White Specks Member. Laminations of calcareous coccoliths within the Second White Specks Formation typically display calcite overgrowths. Calcite overgrowths are also observed within mudstones in the basal part of the Medicine Hat Member. Such differences in appearance show the occurrence of temporal and lateral facies changes; the presence of facies changes is an important factor that can affect shale gas production patterns within a single, seemingly laterally-continuous lithological unit.

High TOC (>2wt. %) and Type II kerogen appear to indicate that biogenic gas may be a dominant component of the total gas-in-place in the Colorado Group. The Middle Carlile member is likely the best shale gas target within the Upper Colorado Group. The Carlile

Formation and Verger Member also appear to have the highest sorption capacity, based on a dominant clay sized fractions. However, mudstones within all formations and members display moderate to high clay minerals (fluid sensitivity), have poor fraccability and contain clay and mud cements. The presence of muddy siltstone within Middle Carlile member and its high potential for gas adsorption is likely to make the unit a viable target for possible horizontal drilling for gas shale.

Table of Contents

ABSTRACT	iv
1 CHAPTER ONE: INTRODUCTION	1
1.1 Introduction	1
1.2 Depositional and Geologic Controls on Shale Gas Potential	3
1.3 Western Canada Sedimentary Basin (WCSB)	7
1.4 Geologic History	9
1.5 Thesis objectives	14
1.6 Thesis structure	15
2 CHAPTER TWO: METHODOLOGY	16
2.1 Analytical Techniques.....	16
2.1.1 Fourier Transform Infrared (FTIR) Spectroscopy	16
2.1.2 Quantitative X-Ray diffraction (QXRD)	17
2.1.3 Mercury Injection Capillary Pressure (MICP).....	17
2.1.4 Grain Size Distribution (GSD).....	20
2.1.5 Thin section & Scanning Electron Microscopy (SEM) analysis.....	22
2.1.6 Total Carbon and Sulphur Analysis & Organic Carbon	22
2.1.7 Rock-Eval Analysis	23
3 CHAPTER THREE: QUANTITATIVE MINERALOGY OF SHALE ROCKS USING FOURIER TRANSFORM INFRARED SPECTROSCOPY	24
3.1 Introduction	24
3.2 Fourier Transform Infrared Spectroscopy	25
3.2.1 Background	25
3.3 Methodology	30
3.3.1 Samples and sample preparations	30
3.3.2 Pure Mineral Mixtures	30
3.3.3 Shale Samples	30
3.3.4 Nile Delta shales	30
3.3.5 Western Canada Shales	32
3.3.6 Sample preparations	32
3.3.7 Sample Preparation for Transmission Spectra	34
3.3.8 Sample preparations for DRIFT Spectra	35
3.4 Mineral Standard Spectra	35

3.5	Spectra Repeatability	43
3.6	Spectra Pre-processing	45
3.7	Calibrations	46
3.8	Results and discussions of the ATR-PLS-MM model	49
3.8.1	Application of ATR-PLS-MM model to independent shale rock samples	52
3.8.2	ATR-PLS-SR model of shale rocks	58
3.8.3	Application of the (ATR-PLS-SR) model of shale rocks to Independent shale samples.....	64
3.8.4	ATR-PLS model of semi-artificial shale rocks (ATR-PLS-SMM)	71
3.8.5	Application of ATR-PLS-SMM to independent shale samples	74
3.9	Application of the FTIR Mineralogy to create a Mineralogy Log	80
3.10	Summary of FT-ATR spectroscopy quantitative mineralogy calibration models	82
4	CHAPTER FOUR: MINERALOGY, GRAIN SIZE AND PORE SIZE DISTRIBUTIONS FOR THE COLORADO GROUP.....	85
4.1	Introduction	85
4.2	Bulk mineralogical results of the lower Colorado Group	88
4.3	Mineral Distributions by Formation.....	89
4.3.1	Viking Formation.....	89
4.3.2	Westgate Formation.....	89
4.3.3	Fish Scales Formation.....	91
4.3.4	Belle Fourche Formation	91
4.3.5	Second White Specks Formation	93
4.4	Grain Size Distribution of the Colorado Group	96
4.4.1	Kranck model fitting	96
4.5	Pore Size Distribution of the Colorado Group	113
4.6	Summary	126
5	CHAPTER FIVE: SPATIAL AND STRATIGRAPHIC VARIATIONS OF THE COLORADO GROUP.....	128
5.1	Introduction	128
5.2	Spatial trends in Mineralogy, Grain Size and Palynofacies	133
5.2.1	Westgate Formation.....	133
5.2.2	Fish Scales Formation.....	138
5.2.3	Belle Fourche Formation	141
5.2.4	Second White Specks Formation	144

5.3	Stratigraphic Variations	150
5.3.1	Controls on Colorado Group Sediment Deposition	157
5.3.2	Summary	160
6	CHAPTER SIX: SHALE GAS POTENTIAL OF THE UPPER COLORADO GROUP, SOUTHWESTERN SASKATCHEWAN (12-19-013-28W3 WELL)	162
6.1	Introduction	162
6.2	Background to the Upper Colorado Group	162
6.3	Bulk mineralogical results of 12-19-013-28W3 well	167
6.4	Grain size distributions and thin sections of 12-19-013-28W3 well	171
6.4.1	Carlile Formation	171
6.4.2	Niobrara Formation	178
6.5	PSD, porosity and permeability of 12-19-013-28W3	186
6.6	Total Organic Carbon (TOC) distribution within the 12-19-013-28W3	192
6.7	Rock-Eval Analyses of 12-19-013-28W3	194
6.8	Shale gas reservoir properties of the Upper Colorado Group	198
6.9	Summary	203
7	CHAPTER SEVEN: CONCLUSIONS & FUTURE WORK	205
7.1	GENERAL CONCLUSIONS	205
7.2	FUTURE WORK	208
7.3	REFERENCES	209
7.4	APPENDICES	219

1 CHAPTER ONE: INTRODUCTION

1.1 Introduction

Until recently (approximately two decades ago) shale was regarded only as a potential source rock and/or seal/cap rock for conventional hydrocarbon reservoirs, although, gas has been produced in low quantities since the early 1820s from the Devonian Shale in the United States (Ross and Bustin, 2008). The depletion in conventional petroleum sources, and the exploitation of gas shales in the United States (e.g. Barnett, Caney, Woodford, Fayetteville, Antrim, Ohio, New Albany and Lewis shales) have led to the realisation that shale or indeed, fine grained rocks can also act as potential unconventional reservoirs for hydrocarbons (e.g. Jarvie et al. 2007; Montgomery et al. 2005; Curtis, 2002; Martini et al. 1996).

Successful shale gas production in each of the known U.S. shales indicates that natural gas is stored in a wide spectrum of mud, siliceous or carbonate lithologies and textures ranging from mudstone to siltstone and fine-grained sandstones. Therefore, a shale gas reservoir is not comprised of a single lithology but a collection of any fine-grained rocks capable of storing significant amounts of gas. Several authors (Bustin et al. 2008; Ross and Bustin, 2008; Ross and Bustin, 2007; Montgomery et al. 2005; Faraj et al. 2004) describe shale gas as unconventional, continuous-type (pervasive over large area), self-sourced resources contained in fine grained, organic-rich, low permeability reservoirs in which thermogenic or biogenic methane is stored as free gas in the matrix or fracture porosity, or as adsorbed/dissolved gas on the organics and/or clays.

Thermogenic gas is associated with mature organic matter (1.0-1.1%Ro) that has been subjected to relatively high temperature and pressure or generated from the secondary cracking of oil (Martini et al. 1998). The decomposition of organic material in an oxygen-poor environment, with the aid of anaerobic bacteria, results in the formation of methane. Biogenic gas is also generated at low temperatures (<70°C) by microbes including bacteria in areas of fresh water recharge (Schoell, 1983; Rice and Claypool, 1981). Therefore, biogenic methane production is influenced by low temperature, anoxic and sulfate deficient environments as well as sufficient organic matter and storage sites.

A firm knowledge of the reservoir characteristics i.e TOC, thermal maturity, lithology, mineralogy, depth, fracturing, production technique and infrastructure of the shale gas systems in the U.S contributed to improved exploration results (Ross and Bustin, 2008). In the western Canada sedimentary basin, finding organic rich, gas-prone shale is generally not difficult but, rather, finding the permeable or the most brittle layers is the main issue (Faraj et al. 2004). Gas shales have characteristically low permeabilities (in the milli-nano Darcy range) and the gas can be stored in more than one way. In fact, there are varying opinions on the forms of gas storage in the rock: one being in the open spaces between the rock, as free gas in the matrix or fracture porosity, therefore, quantifying total porosity is important (Ross and Bustin, 2008). The second mode is adsorbed/dissolved gas on the organic matter (kerogen) and mineral surfaces (Ross and Bustin, 2008). In all cases, economic shale reservoirs require natural or induced fractures which must be maintained open to accumulate and produce hydrocarbons. Brittle behaviour is necessary for fracture maintenance and this in turn requires a rock of suitable mechanical properties; mineralogy, to a large extent, can determine whether or not shale can maintain the fracture system (Bloch, 1995).

The generation of optimal hydraulically-induced fractures is a key factor in the stimulation of shale gas production (Ross and Bustin, 2007; Montgomery et al. 2005; Pollastro, 2003). Silica-rich shales have previously been targeted in the Barnett Shale, Fort Worth Basin, Texas, as the mechanical properties are conducive to hydraulic fracturing (Matthews et al. 2007). The presence of swelling clays (i. e., smectite) can lead to formation damage during drilling operations, completion, stimulation, and workover (Zhou and Law, 1998). Such problems arise when incompatible drilling fluids (i.e. water) are used during completion, which can enter the reservoir from the borehole and cause clays within the reservoir to swell, reducing both porosity and permeability. The use of compatible drilling fluids is crucial in clay-rich shale gas reservoirs, as an abundance of clay minerals is typically associated with poor reservoir quality due to swelling and formation damage (Zhou and Law, 1998). Therefore, quantifying the mineralogical abundances is critical and must be placed at the heart of shale gas prospecting.

Much of the current knowledge on shale gas is based on experience with analogues for many other systems (Montgomery et al. 2005). For example, previous work on gas shales has only considered the characteristics of producing shales within the United States (Jarvie et al. 2007; Curtis, 2002; Martini et al. 1996). However, there is the need for the individual assessment of each play in order to evaluate its shale gas potential due to differences in geological controls between basins and heterogeneity of shales and mudrocks which exists at nanometer scale (Passey et al. 2010; Ross and Bustin, 2008).

1.2 Depositional and Geologic Controls on Shale Gas Potential

Shales are generally described as variable mixtures of clay minerals (illite, mixed layer illite-smectite, kaolinite, and chlorite), quartz, feldspars, carbonates (calcite, dolomite, and siderite), sulfides (mainly pyrite), amorphous material and organic matter (Aplin and Macquaker, 2012). Most mudstone successions exhibit enormous variability in mineralogies, grain size, textures, fossil contents, and organic geochemical compositions (Passey et al. 2010) due to varying detrital inputs to the basin, primary production within the basin, and chemical conditions at the sediment water interface as well as in the bottom water layers (Passey et al. 2010).

The accumulation of organic matter in a depositional environment is critical for a rock to function as an effective hydrocarbon source or a shale-gas reservoir. Organic rich rocks have been described to be a function of non-linear interactions of the rates of organic matter production, destruction and dilution (Bohacs et al. 2005). Primary producers photosynthesise using solar energy, nutrients and water to generate the amount of particulate and dissolved organic matter in the sedimentary system (Bohacs et al. 2005), while secondary consumers such as radiolarian provide brittle materials such as silica (Passey et al. 2010). Optimum organic accumulation is shown to occur at intermediate rates of primary production as very high rates lead to significant dilution by non-hydrogen rich biogenic material, while during very low rates organic matter is destroyed by consumer organisms (Bohacs et al. 2005).

The destruction of organic matter occurs through ingestion by metazoans, microbial respiration, and inorganic oxidation. Further degradation of organic matter occurs by microbial activities which include methanogens (Claypool and Kaplan, 1974). Dilution of organic matter by material that is not hydrogen rich (either clastic or biogenic or both) is the predominant control on significant accumulations of organic matter because it has the widest range of mass accumulation rates and grain size variations (Bohacs et al. 2005). Dilution rates are also used to infer the environment and conditions of sediment deposition, and therefore the location of 'sweet spots'. For example, low dilution rate are commonly associated with distal, relatively low energy settings prone to accumulation of fine grained rocks rich in clay sediments and organic matter (Tyson, 1995). Similarly, proximal, high energy environments are associated with coarse clastic materials and thus high dilution rates. Although, dilution can also be affected by high biogenic material which can produce relatively organic lean rocks in distal (from sediment source), quiet energy environments (Bohacs et al. 2005).

The presence of multiple fine-grained rock types in organic-rich shale means that the shale properties vary in space and time, and on scales ranging over many orders of magnitude, from millimeters to several meters. For example, the Upper Jurassic, Kimmeridge Clay Formation, Dorset, England comprises stacked mudstone successions of bed-sets that are compositionally different from each other. This compositional variability causes them to be variably resistant to weathering (Aplin and Macquaker, 2012).

Mineralogy and grain size exert a primary control on the nature of pore systems and on other physical properties including geomechanical properties (Mondol et al. 2007; Aplin et al. 2006). The mineralogy of fine-grained sedimentary rocks is controlled by the initial supply of sedimentary materials (which include diverse and unstable assemblages of soil-derived minerals and amorphous matter, biogenic opal and carbonate minerals, and organic matter) and the subsequent diagenetic changes that convert mud into a mudstone.

Mechanical and chemical compactions are the primary processes affecting muds, reducing absolute permeability and porosity. Mechanical compaction is driven by grain rearrangement and deformation of brittle materials, while chemical compaction is caused by pressure solution (mineral dissolution). Mechanical processes dominate low temperature diagenesis in siliciclastic systems while chemical processes play a much greater role in biogenic muds.

The rate of compaction (compressibility) is in turn strongly influenced by grain size and mineralogy (Mondol et al., 2007; Aplin et al., 2006); finer-grained muds have higher depositional porosities but are more compressible. However, finer-grained smectite have been shown to be substantially less compressible than kaolinite. For example, Mondol et al. (2007) showed that at 50MPa effective stress, the porosity of experimentally compacted pure kaolinite was 10%, while that of pure smectite was 35%.

Within the first few meters of burial, diagenesis is dominated by redox processes in which organic matter is oxidized primarily by microbes which use oxygen, nitrates, Mn, iron oxides and sulfate as terminal electron acceptors (Canfield et al. 1993). Carbonate, sulfide and reduced iron are generated as key by-products of these reactions and form early diagenetic minerals such as calcite, siderite and pyrite (Canfield and Raiswell, 1991a). The form of these minerals ranges from micrometer-size crystals that largely infill primary porosity, in which case the diagenetic minerals form up to 90% of the bulk sediment to patchy distribution constituting <50% of the rock volume (Aplin and Macquaker, 2012).

The physical change in mudstones at temperatures above ~ 70°C is dominantly controlled by clay mineralogy. Potassium, derived from the breakdown of potassium feldspar between ~ 70 and 100°C, leads to illitisation whereby smectite, or mixed layer illitesmectite (I-S), converts to illite or more illitic I-S ($\text{Smectite} + \text{K Feldspar} = \text{Illite} + \text{Quartz} + \text{Chlorite} + \text{Water}$) (Hower et al. 1976).

Illitisation has important implications for the elastic and mechanical properties of shales generating excess silica believed to be retained within the mudstone, and precipitates as microcrystalline quartz within the clay matrix (Peltonen et al. 2009). At approximately 6 km burial and 200°C, porosity is shown to reduce to less than 5% and the mineral assemblage is dominated by quartz, illite and chlorite (Mondol et al. 2007).

Biogenic silica converts from opal-A to opal-CT and then to quartz during burial diagenesis through dissolution – dehydration – reprecipitation reactions leading to rapid loss of permeability and porosity due to the formation of cements. Cementation is caused when silica is precipitated as overgrowths or layers on quartz grains (Rushing and Blasingame, 2008).

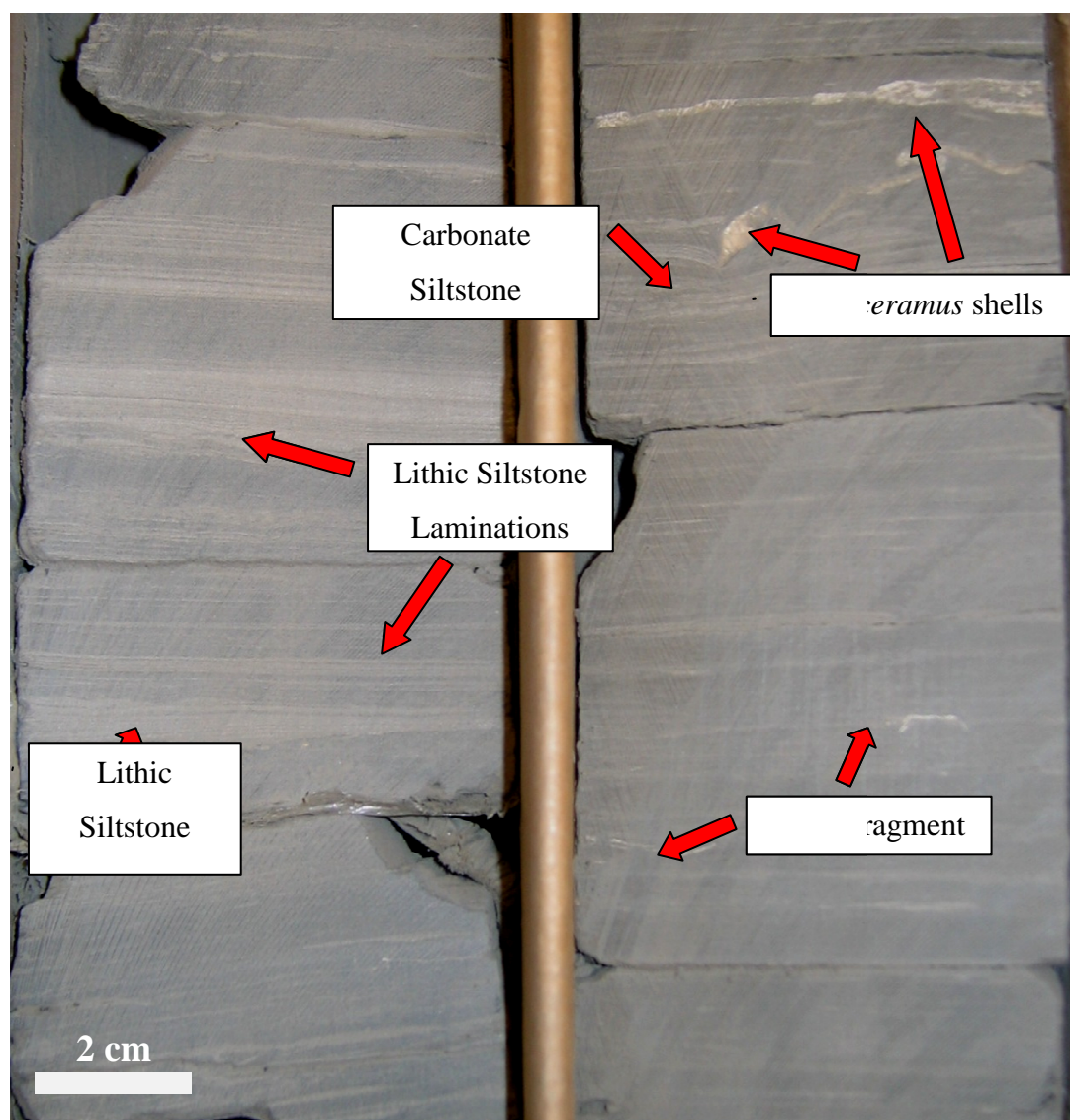


Figure 1.1: Core photo from the First White Specks Member, within the Upper Colorado illustrating the occurrence of cm-scale variability. This figure also shows ripples and *Inoceramus* shell fragments –the carbonate siltstone laminations on the right.

Similarly, carbonate cements are precipitated soon after deposition filling pore spaces between framework grains. However, recrystallization of both biogenic silica and carbonate can embrittle shales, with important consequences for induced hydraulic stimulation (Pollastro, 2003). Porosity and permeability values display wide variation in shale gas reservoirs, having values of a typical conventional reservoir only on occasion. It is mentioned by Shurr and Ridgley, (2002) that values of high porosity and permeability within a shale gas

reservoir may “represent only localized areas within otherwise tight, continuous-type reservoirs”, or “sweet spots”.

Millimeter scale variability (e.g. Figure 1.1), common in mudstones, means that high resolution studies are required to adequately characterise them. Although most techniques used to characterise a conventional source/reservoir rock (e.g. TOC, XRD, core description, thin sections e.t.c) are applicable to unconventional shale gas, most cannot be utilised for high resolution purposes. For example, it is not practical to analyse the mineralogy of hundreds of samples using XRD as it is both expensive and time consuming. Therefore, it becomes important to develop pragmatic techniques for the characterisation of gas shales.

1.3 Western Canada Sedimentary Basin (WCSB)

The Western Canada Sedimentary Basin (WCSB) has a large inventory of laterally extensive shale and silt-dominated Cretaceous formations and existing biogenic gas production (Shurr and Ridgley 2002); therefore, it represents a suitable setting for potential shale gas system. Conventional sandstone reservoirs in the Cretaceous Colorado Group and equivalent formations are well studied (Buckley, 2004; Bloch et al. 1999; McNeil and Gilboy, 1999; White et al. 1999; Schröder-Adams et al. 1996; Leckie et al. 1994). However, much less is known about the shale, and very little is known concerning the reservoir characteristics of the Colorado Group shale (Bloch, 1995).

Since previous shale gas studies within the WCSB focused on selected shale units (Ross and Bustin, 2008; Walsh et al. 2006; Faraj *et al.* 2004; Shurr and Ridgley, 2002) further work is now needed in order to characterise the shales across the vast basin. Porosity and permeability values of Cretaceous reservoir rock in the northern Great Plains were reported by Shurr and Ridgley (2002). The study showed that although there are fairly large ranges in permeability and porosity, higher porosities and permeabilities are only found within localized areas, otherwise known as ‘sweet spots’. These areas are separated by tight, laterally extensive beds of the same stratigraphic unit that have considerably lower porosity and permeability. However, biogenic shale gas production from the Colorado Group has a long history dating back to 1904 with around $140,000 \times 10^6 \text{ m}^3$ (880 Bcf) produced from the

south-eastern Alberta and south-western Saskatchewan within the Belle Fourche Formation, Second White Specks Formation, and the Medicine Hat Member of the Niobrara Formation (Leckie et al. 2008).

Faraj et al. (2004) conducted a preliminary study evaluating the geochemical, geological and structural characteristics of the shale packages within western Alberta and eastern British Columbia. A study by the British Columbia Ministry of Energy, Mines and Petroleum Resources focused on Devonian shale gas potential (EMPR, CBM Solutions, 2005). The study centred on the Exshaw, Besa River, Fort Simpson and Muskwa formations and estimated gas-in-place capacity of more than 500 trillion billion cubic feet (Tcf) in northeast BC. The study of Walsh et al. (2006) evaluated the regional shale gas potential of the Triassic Doig and Montney Formations of northeast British Columbia.

The study quantified the potential original gas-in-place via spatial analysis. Walsh et al. (2006) provided original gas-in-place estimates of 30 to 200 Tcf for the Upper Montney, 50 to 500 Tcf for the Lower Montney, 40 to 200 Tcf for the Doig Formation and approximately 70 Tcf for the organic rich Doig Phosphate unit. The study noted that original gas-in place estimates must be taken in context and cannot be compared directly with estimates for conventional plays as critical reservoir characteristics remain poorly understood. Ross and Bustin (2008) conducted a multidisciplinary evaluation of the Devonian-Mississippian strata in the northwestern region, investigating the shale gas potential of the thermally mature strata of the Base River, Horn River, Muskwa and Fort Simpson formations. They estimated total organic content of up to 5.7wt% with total gas capacities between 60 and 600bcf/section.

1.4 Geologic History

The Western Canada Sedimentary Basin (WCSB) has been described as a clastic foreland petroleum province (Bloch, 1995). The basin is well documented, with a well understood tectonic and depositional history (Leckie et al. 2008). Deposition within the Western Interior Seaway was controlled by changes in eustatic sea level, sediment flux (Bhattacharya and Walker, 1991; Caldwell, 1984) and tectonic influences (Varban and Plint, 2008). The Colorado Group shales were deposited during a global sea level rise over an approximately 25 to 30 million year period during the Cretaceous (Leckie et al. 1994; Bloch et al. 1993). It incorporates the provinces of British Columbia, Alberta, Saskatchewan, Manitoba and Northwest Territories (Figure 1.1), and measures $1.9 \times 10^6 \text{ km}^2$ (Leckie et al. 2008). The biostratigraphy of both the western and eastern margins of the basin has been studied in great detail (Bloch et al. 1999; McNeil and Caldwell, 1981).

Initial sedimentation within the North American Foreland Basin coincides with downflexing of the continent's western interior during the early to middle Jurassic (Leckie et al. 2008; Leckie et al. 1994). This foreland basin encompassed eastern Alberta, Saskatchewan and western Manitoba. Oceanic transgression of the foreland basin led to basin flooding and the birth of the Western Interior Seaway (WIS), marked by deposition of the thick marine shales of the lower Colorado Group. Bloch et al. (1993) reports that the Lower Colorado Group (Albian-Turonian) was deposited during the major pulse of eustatic level rise and revised the nomenclature into four main formations throughout much of the basin. They are the Westgate, Fish Scales, Belle Fourche and Second Whites Specks in ascending order (Figure 1.2).

Sedimentation continued throughout the remainder of the Albian age in shoreface, deltaic, estuarine and shallow marine settings. Overall, this time was characterised by general transgression in the basin, but the seaway frequently experienced sudden, regressive lowstands (Leckie et al. 1994). The Fish Scales Zone denotes a major basin-wide transgression (Leckie et al. 2008), at which time the Arctic Ocean and Gulf of Mexico were connected, leading to speculation that the Fish Scales Zone may represent the combining of the two oceans within the seaway (Leckie et al. 2008).

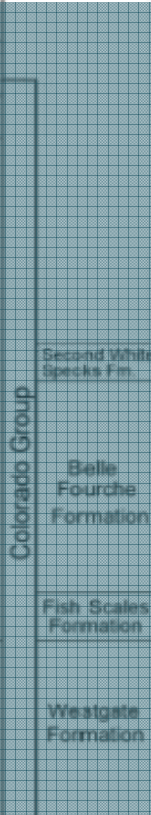
PERIOD	EPOCH	STAGE	Southern Foothills	Central Foothills	Northwest Plains	Central Plains	Southern Plains	Bloch et al. 1999
CRETACEOUS	LATE	Campanian	Belly River Fm.	Brazeau Formation	Puskwakua Fm.	Belly River Fm.	Belly River Fm.	
		84	First White	Speckled Shale		Lea Park Fm.	Milk River Fm.	
		Santonian	Wapiabi Formation	Wapiabi Formation	Badheart Fm.	Medicine Hat Sandstone	Medicine Hat Sandstone	
		87			Muskiki Fm.			
		Coniacian	Cardium Formation	Cardium Formation	Cardium Formation	Cardium Formation		
		89						
		Turonian	Opabin Member				Jumping Pound Mbr.	
		93	Haven Member					
			Vimy Member					
	EARLY	Cenomanian	Sunkay Member	Dunvegan Formation	Dunvegan Formation		Philips SS	
		97-99		Cruiser Formation			Barons Sand	
				Goodrich Formation	Shaftsbury Formation			
		Albian		Hassler Formation				
				Boulder Creek Fm.		Viking Fm.	Bow Is. Fm.	
				Hillcross Formation	Peace River Fm.	Joli Fou Fm.	Joli Fou Fm.	
						Basal Colorado Sand	Basal Colorado Sand	
						Mannville Group	Mannville Group	

Figure 1.2: Stratigraphy of the Cretaceous Colorado Group (after (Bloch et al. 1999). Highlighted column indicates stratigraphy used in this study

LATE CRETACEOUS				McNeil and Caldwell (1981)		Wall and Rosene(1977)		Donaldson, 1998		Stott (1963)		Bloch et al. (1993) Nielsen et al., (2003)													
PERIOD				STAGE		AGE (Ma)		SEDIMENTARY CYCLES		ALBERTA SOUTHERN FOOTHILLS		WEST-CENTRAL FOOTHILLS AND PLAINS ALBERTA		ALBERTA CENTRAL PLAINS		ALBERTA SOUTHERN PLAINS & SOUTH-WESTERN SASK.									
LATE CRETACEOUS				CAMPANIAN		84		NIOBRARA MARINE CYCLE REGRESSION		BELLY RIVER FORMATION		NOT STUDIED		BELLY RIVER FORMATION		NOT STUDIED									
				CONIACIAN		87		TRANSREGRESSION		WAPIABI FM.				LEA PARK FORMATION		MILK RIVER FORMATION									
				TURONIAN		89		TRANSREGRESSION		ALBERTA GROUP		CHUNGO		PUSKWASKAU FM.		FIRST WHITE SPECKLED SHALE		NIOBRARA FM.		FIRST WHITE SPECKS MBR.					
												HANSON								BAD HEART FM.		UNNAMED COLORADO SHALE		VERGER MEMBER	
												THISTLE													
								TRANSREGRESSION		ALBERTA GROUP		DOWLING		MUSKIKI FORMATION		CARDIUM FORMATION		CARLILE FORMATION		BENTONITE MARKER					
												MARSHYBANK													
												MUSKIKI													
												OPABIN													
								TRANSREGRESSION		ALBERTA GROUP		BLACKSTONE FM.		NOT STUDIED		SECOND WHITE SPECKLED SHALE				SECOND WHITE SPECKS FORMATION					
HAVEN																									
VIMY																									

Figure 1.3: A lithostratigraphic chart of the Upper Colorado Group, for southern Alberta and southwestern Saskatchewan. The highlighted column indicates the stratigraphy used in this work, (after Nielsen et al. 2003).

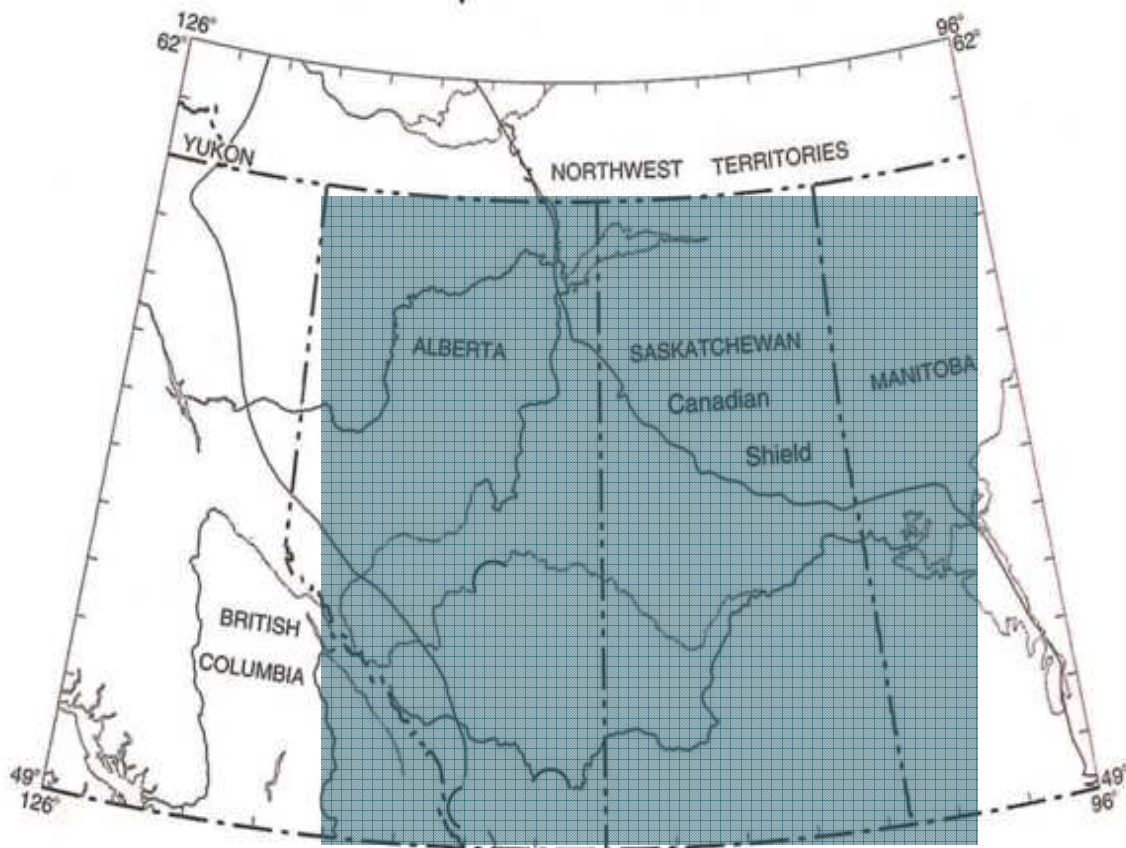


Figure 1.4: Provincial map of the Western Canada showing the study areas (modified After Leckie et al. 2008).

Eustatic sea level rise during the Cenomanian (98-93 Ma), accompanied by increased sediment flux, deposited stacked depositional cycles, shoreface and deltaic deposits along the western coast of the seaway (Bhattacharya and Walker, 1991). In addition to changes in eustatic sea level, periodic tectonic influences also affected sediment deposition. Active sedimentation to the foreland basin occurred due to mechanical loading from compressional and dextral faulting to the west, followed by subsequent erosion of the uplifting Rocky Mountain fold-thrust belt. This likely happened in concurrence with eustatic sea level increase in the Cenomanian (Leckie et al. 1994).

Maximum global transgression occurred during Late Cenomanian to Early Turonian, correlative to the basin-wide deposition of the Second White Specks (Leckie et al. 2008). A major regression occurred within the seaway during the Turonian (93-88 Ma), which is responsible for the deposition of Cardium Formation sands. During to this lowstand, narrowing of the Western Interior Seaway generated numerous partial and basin-wide unconformities. It is during this time that depositional patterns within the seaway become quite complex. Changing depositional patterns are likely due to a combination of frequent sea level fluctuations and pulses in sedimentation. Rapidly changing depositional conditions continued until the end of the Santonian age (83 Ma), at which time another transgression initiated the highstand deposition of the First White Specks Member. The end of the Santonian demarcates a return to fully marine conditions within the Western Interior Seaway. Deposition of the Milk River Formation commenced at approximately 84.5-83.5 Ma (Leckie et al. 2008), recording both the initial deposition of the Montana Group and the return to a deltaic and fluvially-influenced regime until the end of the Cretaceous.

Due to fluctuating eustatic sea level and periodic sedimentation, downflexing of the interior North American continent, and deposition of bentonite clays from related volcanic activity, the Upper Colorado Group formations are largely composed of fine-grained sediments (mud, silt, clay) with a varying degree of Tethyan influence (Nielsen et al. 2003). Sediment input, sourced from erosion of the uplifting Rocky Mountain fold-thrust belt, enters the Western Interior Seaway through river systems along the western margin of the Foreland Basin. Input from these rivers promoted the mixing of terrigenous waters and ocean waters along the western margin while the eastern side of the basin experienced marine-dominated conditions (Nielsen et al. 2003). Sedimentation of the entire Upper Colorado Group mainly took place in a distal but shallow marine environment when maximum water depth in the foreland basin was between 150-300 metres during the Late Cretaceous (Leckie et al. 2008). Current estimations of water depth are significantly shallower at 40-100 metres (Varban and Plint, 2008).

The compositional variability of the Colorado Group and changing conditions of the Western Interior Seaway and foreland basin may represent significant implications with regards to shale gas prospectivity. Therefore characterising the shales may aid the understanding of the shale gas system deposition and formation interaction on a regional, basin-wide scale. Such characterisation of the shales requires detailed knowledge of their properties and the integration of sedimentology, lithology, geochemistry, mineralogy, porosity and permeability.

1.5 Thesis objectives

This thesis investigates the spatial and temporal variations in mineralogy, grain size and pore properties of the Colorado Group shales in order to understand the shale gas potential on a basin-wide scale. This required the analysis of a lot of samples; therefore, the primary aims of this study include:

- 1) To test the feasibility of using Attenuated Total Reflectance Fourier Transform Infrared Spectroscopy to develop a rapid semi-quantitative mineralogical tool.
- 2) To evaluate the spatial and temporal variations in shale characteristics using mineralogy, grain size, porosity and permeability combined with existing geochemical and palynology data (Buckley, 2004) and examine the implications for gas shale prospectivity.
- 3) Evaluate target zones for shale gas production from a single core within south-western Saskatchewan (Fig. 1.3).

1.6 Thesis structure

This thesis is structured as follows: Chapter two gives a brief description and background to the analytical techniques utilised. Chapter three gives a detailed description of the chemometric technique developed in this study for the semi-quantitative determination of shale mineralogy using various calibration models. Chapter three is structured as a standalone chapter; with its introduction, methodology, results and discussions.

Chapter four describes the bulk mineralogy data and petrophysical (grain size distributions, thin sections & SEM and pore size as well as porosity and permeability calculations) data of the Colorado Group samples. In addition to this, grain size data is fitted with the Kranck et al. model (1996a) with the purpose of identifying sediment deposition and transport patterns and hydrodynamic conditions of the sea water. Chapter five builds on chapter four, integrating the mineralogy, grain size, pore size data and organic facies to discuss (a) main controls on organic richness, (b) influence of grain size and porosity on the pore size distributions and (c) spatial and temporal variations in mineralogy, grain size and TOC and their implications to shale gas prospects.

Chapter six describes an integrated study of a single well to characterise the shale gas potential of the Upper Colorado Group. The study integrates mineralogy, petrophysics (grain size & pore size distributions, porosity and permeability calculations) and geochemical (TOC and Rock-Eval) data with the purpose of identifying organic rich intervals and establishing organic matter type within the formations, the gas capacity and producibility of the shales. Chapter six is also presented as a standalone piece with its discussions and conclusions.

Chapter seven provides general conclusions of each of the chapters and their findings and recommendation is proffered for areas of future work and improvements.

2 CHAPTER TWO: METHODOLOGY

2.1 Analytical Techniques

2.1.1 Fourier Transform Infrared (FTIR) Spectroscopy

Fourier transform infra-red (FTIR) spectroscopy was used to compute semi-quantitative mineralogy for the shale samples. Spectroscopy is “the study of light as a function of wavelength that has been emitted, reflected or scattered from a solid, liquid, or gas” (Clark, 1999). The capability of photons to be absorbed in minerals depending on their wavelength therefore enables us to derive information about the chemistry of minerals from its reflected or emitted light. The ability to combine spectra together with multivariate statistical analysis (Breen et al. 2008; Breen et al. 2007; Karakassides et al. 1997; Crowley and Vergo, 1988; Hunt and Hall, 1981) to quantify an analyte in a mixture has made FTIR a useful quantitative analytical tool.

Transmission and diffuse reflectance (DRIFTS) are the most widely used FTIR techniques. In transmission, IR beam (I_o) incident on a sample is partly absorbed and partly transmitted (I). Quantification is possible because the absorbance is directly proportional to the concentration (c) of the absorbing material according to Beer-Lambert’s equation:

$$I = I_o e^{-kx} = \epsilon lc \text{ ----- Equation 2:1}$$

Where, k is an absorption coefficient

x is the distance travelled through the medium

ϵ (proportionality constant) is the absorptivity.

Chapter three describes in full a methodology developed in this study for the semi-quantitative determination of shale mineralogy using various calibration models. The models were developed by combining various IR spectra with multivariate partial least squares (PLS) fitting using Pirouette software. The spectra were recorded using a Thermo Nicolet Nexus 870 FTIR spectrometer and data were acquired using OMINC 6.1a software.

2.1.2 Quantitative X-Ray diffraction (QXRD)

Selected shale samples from the Colorado Group and Nile delta were analysed for quantitative X-ray mineralogy for the IR calibrations according to Hillier (2003) at the Macaulay Institute, Aberdeen. The bulk samples were dried at 105°C, wet ground in a McCrone mill and spray dried to produce random powders. X-ray powder diffraction (XRPD) patterns were recorded from 2-75°2 θ using Cobalt K α radiation. Quantitative analysis was done by a normalised full pattern reference intensity ratio (RIR) method. Expanded uncertainty using a coverage factor of 2, i.e. 95% confidence, is given by $\pm X0.35$, where X = concentration in wt. %, e.g. 30 wt. % ± 3.3 . For phases present at the trace level (<1%) there may also be uncertainty as to whether or not the phase is truly present in the sample. This is both phase and sample dependent. It arises because at trace concentrations identification is often based on the presence of a single peak and the judgement of the analyst in assigning that peak to a likely mineral.

Additional XRD data for shale rock samples supplied by Conoco Philips were also utilised in the IR calibrations. The sample sets were independently quantified by Conoco Philips and Core Laboratory (Core Labs). The two datasets are generally similar but some variations exist in some samples. These discrepancies are assumed to results from possible differences in standard used by each company as well as differences in sample preparations. In either case, both data were used to compare the IR mineralogy.

2.1.3 Mercury Injection Capillary Pressure (MICP)

Mercury porosimetry has been used extensively to characterise porous materials (Cranganu et al. 2009; Giesche, 2006; Yang and Aplin, 1998) between 500 μ m and 3.5nm. It provides information about pore throat size and pore size distributions, total porosity, as well as bulk density. It also provides data for the determination of permeability, capillary entry pressure and other petrophysical properties.

The technique involves injecting mercury at pressures up to 60,000psi, increasing the pressure in a stepwise manner inside a porosimeter. Samples are first oven dried and stored in a desiccator prior to analysis. During the mercury intrusion technique, a completely dry,

weighed sample is placed inside a penetrometer and the penetrometer is loaded into a low pressure system of the porosimeter. A range of low pressure is then applied to the mercury according to a programmed step-wise manner after which the penetrometer containing the sample and the intruded mercury is removed and weighed. The penetrometer is then loaded into a high pressure system, where a series of high pressures are applied to inject the mercury into the sample. The volume of the sample is then derived according to equation 2:2.

$$V = V_p - \frac{m_{p+s+Hg} - m_{p+s}}{G_{hg}} \text{-----Equation 2:2}$$

Where V is the volume of the sample (L³),

V_p is the volume of the penetrometer (L³),

m_{p+s+Hg} is the mass of penetrometer loaded with sample and filled with mercury (M),

m_{p+s} is the mass of penetrometer plus sample (M), and

G_{hg} is the density of mercury (M/L³).

Total porosity is derived from the bulk and grain density of the sample, calculated according to Borst (1982) represented in equation 2:3:

$$\emptyset = 1 - \frac{\rho_d}{G_s} \text{-----Equation 2:3}$$

Where, \emptyset is the total porosity

ρ_d is the bulk density defined as the ratio of the total mass to the total volume determined from the volume of a known mass of the sample (equation 2:4).

$$\rho = \frac{M}{V} \text{-----Equation 2:4}$$

Where, ρ is the bulk density, (g/cm³)

M is the total mass, (g)

V is the total volume, (cm³)

G_s is the grain density determined from the volume of the dry mass of the sample calculated from the mass of water displaced by the sample in a pyknometer; a

grain density of 2.66g/cm^3 is normally assumed for mudstones (Aplin, pers. comm.).

The incremental pressure is plotted against mercury saturation and the intrusion pressure values are converted into the corresponding pore size using the (Washburn, 1921) equation, thus:

$$r = \frac{-2\gamma\cos\theta}{P} \text{ --- Equation 2:5}$$

Where:

r = pore size (nm)

γ = interfacial tension between air-mercury-solid contact angle (0.485N/m)

θ = contact angle (140°)

P = pressure (psi)

The applied pressures force mercury through pore throats which act to control access to the pores (Purcell, 1949). In effect, the pores acts as bottlenecks in the system and may results in potential overestimation of pores with small radii (Hildenbrand and Urai, 2003). Also, high pressures may result in the destruction of natural pores or creation of artificial pores, representing a potentially significant issue for accurate petrophysical measurements. Another important limitation of the technique is that it measures the largest entrance towards a pore instead of the actual inner size of the pore and does not see closed pores (Giesche, 2006). Furthermore, oven drying of samples may lead to shrinkage of clay minerals.

In order to minimise errors, samples were dried by first freeze drying at -40°C before oven drying at 105°C and then stored in a desiccator prior to analysis. To ensure that only the applied pressure acts on the mercury, and that no back pressure due to entrapped air is present, the low pressure system was evacuated to less than $30\mu\text{m Hg}$ before introducing mercury into the penetrometer during the analysis of the shale samples in this study.

2.1.4 Grain Size Distribution (GSD)

Grain size data is important in constraining the fluid flow properties of mudstones (Yang and Aplin, 1998) and in correlating deposits to sedimentary processes (Kranck and Milligan, 1991a). Published permeability data for fine grained clastic sediments has been shown to vary over a range of six orders of magnitude, with a three order of magnitude range at a single porosity that can be attributed to differences in grain size (Dewhurst et al. 1998; Yang and Aplin, 1998a). For example, Yang and Aplin (1998) presented pore throat size data for three samples with different lithologies but the same levels of burial depth. Their MICP and GSD data show that the siltier samples contained higher porosities and a mean pore radius which is almost two orders of magnitude greater than that of the finer, clay-rich samples. Therefore, it has been established that the pore size distributions and hence permeability of mudstones are fundamentally controlled by the extent of compaction (porosity) and grain size distribution (Dewhurst et al., 1998). As one of the objectives of this study is to investigate the influence of grain size on the pore size distributions of the mudstones, samples were selected for grain size analysis.

Grain size distribution can be defined as the relative distribution of grain size expressed as weight percentage. This study utilised the freeze-thaw disaggregation technique and ultrasonic treatment of Yang and Aplin (1997) for sample preparation. During sample preparation, a sample is initially disaggregated and made into a suspension in distilled water and a deflocculating agent. The particle sizes are then determined using either a pipette or X-Ray sedimentation method in a Sedigraph Particle Size Analyser. The time, t , for particles of certain size to settle at a specified depth in the suspension is determined from Stoke's equation:

$$D = 0.005531 \left\{ \frac{\zeta H}{(G_s - G_f)t} \right\}^{0.5} \text{ --- Equation 2:6}$$

Where D is the equivalent particle diameter (mm),

ζ is the dynamic viscosity of water at the test temperature (mPa.s),

H is the sampling depth (mm),

G_s is the grain density of the particles (g/cm^3),

G_f is the density of the water with dispersant containing the sample suspension (g/cm^3)

t is sampling time (min)

The X-Ray sedimentation technique was used in this study. It uses the transmission of X-rays to detect concentration changes caused by sedimentation. As the concentration of suspended particles decreases with time, the signals of the X-ray reaching the detector are recorded continuously. The recorded strength with time is a reflection of particle size distribution.

The freeze-thaw technique of Yang and Aplin (1997) was used to prepare the samples for the analysis briefly described below:

1. About 1g of approximately 1cm³ rock size were sieved and spread in drying tins for the analysis
2. The samples were then subjected to a series of freeze-thaw cycles which gently disaggregate them in distilled water
3. The disaggregated samples were then introduced into a ~100ml solution of 5ml of dispersant (33g/L sodium hexametaphosphate and 7g/L sodium carbonate)
4. Further disaggregation of the samples was done by subjecting the solution to ultrasonic treatment for about 1 hour
5. A further 5ml of dispersant was added to the solution and agitated for 30 minutes using a magnetic stirrer to ensure no flocculation occur
6. The solution was then placed into the Sedigraph's settling cell and the sub-63µm grain size distribution determined using a Sedigraph 5000ET following the technique of Coakley and Syvitski (1991)
7. The remaining solution was then sieved at 63µm to remove any sand fraction which was then dried , weighed and recorded
8. The grain size cumulative curves were corrected for the >63µm component according to Yang and Aplin, (1997) :

$$X_{\text{corr}} = X_{\text{sedi}} (1 - X_{63}) \text{-----Equation 2.7}$$

$$X_{\text{pip}} = 5.64 + 0.41386X_{\text{corr}} + 0.004518X_{\text{corr}}^2 \text{-----Equation 2.8}$$

Where

X_{sedi} =

values recorded directly from the cumulative curve generated from the Sedigraph

X_{63} = weight % of the material removed from sieving at 63 μ m

X_{corr} = values corrected for the *> 63 μ m material*

X_{sedi} = values calibrated to the pipette method

2.1.5 Thin section & Scanning Electron Microscopy (SEM) analysis

Thin sections and SEM analysis were used to analyse small grains, mineralogy, rock pore as well fossils content and diagenetic features. Thin sections were prepared by Wagner Petrographic, Lindon, Utah, USA. SEM analysis was conducted at Durham University using a Hitachi SU-70 High Resolution Analytical Scanning Electron Microscope, equipped with an Oxford Instrument Energy Dispersive X-ray microanalysis system (INCA Energy 700). The rocks were coated with a conductive material (carbon) prior to scanning.

2.1.6 Total Carbon and Sulphur Analysis & Organic Carbon

Total Carbon and sulphur were determined using a LECO CS-244 carbon and sulphur analyser. Approximately 100mg of the sample was weighed into a crucible and ignited at high temperature combustion in a stream of oxygen. Tungsten accelerator and iron chips were added to facilitate combustion. During combustion, carbon and sulphur are oxidised to carbon dioxide and sulphur respectively which are then quantified by infrared detection. LECO carbon (%C = 0.834 \pm 0.005) and sulphur steel (%S = 0.0044 \pm 0.0003) were analysed between samples as reference materials to determine accuracy and precision.

Organic carbon was determined in the same manner but the samples were treated with 4M hydrochloric acid in a porous crucible to remove inorganic carbonates. Once the acid has drained, distilled water was used to wash the acids several times and then dried overnight at 65°C

2.1.7 Rock-Eval Analysis

Rock-Eval pyrolysis is used to identify the type and maturity of organic matter and assess its petroleum potential. The Rock-Eval pyrolysis was carried out according to the methods of Peters (1986) using an Oil Show Analyser. Briefly, about 100 mg of the sample was weighed into a crucible and pyrolysed in a stream of helium gas. The heating programme involved three phases. Phase one involves holding the sample at 100°C for 1 minute, in order to remove volatile (gaseous) hydrocarbons from the sample. Volatile hydrocarbons are quantified by flame ionisation detector (FID), and they are defined as peak 1 or S₀ (mg/g sediment). In the second phase, temperature was increased at 25°C/minute to 300°C and held for 2 minutes. The volatile hydrocarbons produced are defined as peak 2 or S₁ (mg/g sediment). The final phase involved increasing the temperature to 550°C, at 25°C/minute, and held for 1.5 minutes. The third phase produced hydrocarbon pyrolysate from the nonvolatile organic matter, which is quantified and, recorded as peak 3 (S₂ mg/g sediment).

The temperature at the peak of S₂ generation is also recorded as T_{max}. The production index (PI) and Hydrogen Index, were computed according to (Peters, 1986; Espitalie et al. 1985) from the S₁ and S₂ peak areas using equation:

$$HI = \frac{S_2}{TOC} \times 100 \quad \text{--- Equation 2:9}$$

$$PI = \frac{S_1}{S_1 + S_2} \quad \text{--- Equation 2:10}$$

Only samples from the Bigstick Field from the Upper Colorado were analysed for total carbon, organic carbon and Rock-Eval in this study, while data from Buckley (2004) were used for the lower Colorado Group samples.

3 CHAPTER THREE: QUANTITATIVE MINERALOGY OF SHALE ROCKS USING FOURIER TRANSFORM INFRARED SPECTROSCOPY

3.1 Introduction

Mineralogical composition is a key variable to determine shale gas potential. Successful exploitation of shale gas resources has been shown to require knowledge of the shale sequences because of high variability (heterogeneity) at various scales (Passey et al. 2010) and therefore, the need to obtain high resolution data. For example, grain composition governs the type and severity of diagenesis, some minerals (i.e. the clays) are more reactive to natural fluids within the pores and may be altered by adverse chemical reactions. Similarly, clays can vary widely in their structure or morphology and generally reduce both permeability and primary porosity (Rushing and Blasingame, 2008). Smectite, illite and chlorite have been identified to significantly affect rock permeability and quality of reservoir (Zhou and Law, 1998). On the other hand, the sorption capacity of shale depends on the amount and types of clays and organic matter present (Javadpour et al. 2007). This is because the adsorption or the adhesion of gas molecules on the surfaces of sediment grains, and/or organic matter is highest in sediments with a large surface area (i.e. significant microporosity). Carbonates and biogenic silica are more brittle than the clays and therefore more susceptible to compaction and failure during induced fracturing. One of the key aspects of the Barnett's prospectivity is its anomalously strong nature due to silica cementation (Jarvie et al. 2007) with important implications for the reservoir's geomechanical behavior. Therefore, when characterising shale gas, it is imperative to know the mineral contents of the samples.

While X-ray Diffraction is the best technique for mineralogical analysis, it is used mainly as a method to identify and quantify crystallised minerals. Shale gas has a large amount of non-diffracting matter due to the presence of kerogen, which is amorphous. Furthermore, XRD requires 1g or more amounts of sample for analysis plus the procedure is time consuming and expensive makes it a less desirable technique for high resolution data studies. Infrared spectroscopy has been suggested previously (McKelvy et al. 1996) as a cheaper and faster way of evaluating mineral contents in rocks. IR has the advantage of rapidly acquiring potentially quantitative results of both shale organic and mineral matter in a non-destructive manner (Snyder et al. 1983).

3.2 Fourier Transform Infrared Spectroscopy

3.2.1 Background

Infrared (IR) is part of the electromagnetic radiation between the high frequency end of the visible region and the low frequency end of the microwave region. Essentially, it covers the electromagnetic spectrum with wavelength between $13,000 - 10 \text{ cm}^{-1}$ ($0.78 - 1000 \mu\text{m}$). The IR region is further divided into near IR (NIR) covering $13000 - 4000 \text{ cm}^{-1}$ ($0.78 - 2.5 \mu\text{m}$); mid IR (MIR) covering $4000 - 400 \text{ cm}^{-1}$ ($2.5 - 25 \mu\text{m}$); and far IR (FIR) covering $400 - 10 \text{ cm}^{-1}$ ($25 - 1000 \mu\text{m}$). All these regions have applications in chemical sciences, but, MIR was specifically used in this study because minerals exhibit most of their fundamental molecular vibration modes in the MIR (Matteson and Herron, 1993; Painter et al. 1981).

An FTIR spectrum of a compound represents the molecular absorption (emissions) of electromagnetic radiations, creating a molecular finger print with peaks which correspond to the frequencies of vibrations between the bonds of the atoms making up the compound. The size and position of the peaks in the spectrum is a direct indication of the amount of the material present since different bonds have different vibration frequencies (because of differences in bond strength and masses of the atoms) and can provide both qualitative and quantitative information.

IR and, in particular, the more versatile Fourier Transform IR spectroscopy have been used extensively to identify and characterise clays and other minerals in rocks and soils (McKelvy et al. 1996). These studies cover applications ranging from qualitative interrogation of structural features to quantitative estimation of bulk components. Several studies (Karakassides et al. 1997; Crowley and Vergo, 1988; Griffiths, 1983; Hunt and Hall, 1981; Ishii et al. 1967; Farmer and Russell, 1964) highlight the success of applying different infrared spectroscopy techniques for the characterisation of clay minerals. These techniques include: transmission (absorption KBr) technique, reflectance techniques, including diffuse and specular, and Attenuated Total Reflectance (ATR). Each technique is best suited for different state of the material being analysed. The theory and instrumentation for Fourier transform infrared spectrometry are discussed in Griffiths (1983).

Painter et al. (1981) applied a least square curve-fitting program in conjunction with a spectral subtraction method to Fourier transform spectra for the quantitative determination of mineral matter in coal. The spectral fitting was able to identify the right components and quantitative measures of the clays present that are in good agreement with weighed quantities of artificial mixtures. Furthermore, the fitting was able to distinguish between two different kaolinite standards.

Cronauer (1982) performed a similar spectra subtraction technique for the characterisation of oil shale by FTIR. The study quantified the shale minerals from a library of FTIR standard minerals spectra by subtracting the spectrum of the mineral standard from that of the shale. The subtraction parameter results in the complete elimination of the bands of the particular mineral being subtracted which then provides a measure of the weight fraction of that mineral in the shale.

Crowley and Vergo (1988) conducted a quantitative study of kaolin mixtures using near-infrared (NIR) reflectance spectra for mixtures of ordered kaolinite and ordered dickite. They simulated the spectral response of disordered kaolinite to discern structural disorder problems and also demonstrated how NIR spectra of laboratory mixtures of ordered kaolinite and halloysite could be used to roughly estimate their proportions in unknown natural samples.

A methodology for obtaining quantitative mineral concentrations from transmission FTIR spectroscopy was presented by Matteson and Herron (1993). Their method used absorbance spectra that were reproducible to within $\pm 5\%$ relative standard deviation to perform whole-spectrum least-squares spectral processing. The technique produced an average absolute difference between known and derived mineral concentrations of $\pm 2.6\text{wt } \%$. The error reduced to $\pm 1.2\text{wt } \%$ when they applied non-negative spectrum least-squares spectral processing.

Janik and Skjemstad (1995) applied partial least squares (PLS) analysis to Diffuse Reflectance Infrared Fourier-transform (DRIFT) spectra of whole soils to identify and quantify a number of minerals (smectite, kaolinite and gibbsite clay minerals) and also organic (alkyl, carboxylic and amide species) components.

In a subsequent study, Janik et al. (1995) demonstrated how experimentally derived soil mineralogical and organic components may be correlated with the infrared spectra based on the theory that mid-infrared diffuse reflectance Fourier transform (DRIFT) spectra of powdered soils present the major components, relative to their concentrations. They used PLS to model the properties of some 298 eastern and southern Australian soils and their spectra and then used the model to classify the soil spectra and their associated major oxides including SiO_2 , Al_2O_3 , Fe_2O_3 , TiO_2 , MgO and CaO . The PLS predicted values for SiO_2 , Al_2O_3 and Fe_2O_3 versus XRF resulted with linear regression R^2 values of 0.97 - 0.92. Regressions for the other oxides, e.g. TiO_2 , MgO and CaO , were generally underestimated at high concentrations.

Quantitative analysis using high quality Fourier transforms infrared (FTIR) spectra of cements obtained by diffuse reflectance mid-infrared Fourier transform spectroscopy (DRIFTS) method was carried out by Hughes et al. (1995). They used the FTIR spectra of 156 cements of varied origin and known elemental composition to construct multivariate calibration models in order to estimate nine mineral components and five minor oxides. The model allowed the composition of unknown cements to be determined rapidly from the FTIR spectrum alone with sufficient accuracy.

Marko et al. (2000) developed a method based on diffuse reflectance infrared Fourier transform spectroscopy (DRIFTS) together with partial least squares (PLS) modeling to rapidly determine the hydroxyl group content in calcined silica. They used samples that were not used in the construction of the models to validate the calibration model and to predict the hydroxyl content in unknown samples previously analysed by Thermogravimetry (TG). The model was able, with sufficient accuracy, to predict the hydroxyl content of several calcined silica samples with different physical properties.

Most of the quantitative estimation of minerals in shales and other rock types have been conducted using transmission and DRIFT spectroscopy while ATR spectroscopy has been mostly applied for structural investigations. The study of Holman et al. (1994) highlights the fact that ATR-FTIR spectroscopy can provide accurate quantitative results when applied to analyse complex mixtures. They performed multicomponent analyses on the ATR spectra to

determine Sulfur-Oxygen anion concentrations in aqueous solution and were able to quantify the concentrations of seven components with a root-mean square error of 0.0002M.

Despite the obvious potential and advantages of the Transmission and DRIFT methods, there are still major problems. In both techniques, sample preparation is required in order to record a good quality spectrum. In transmission, samples have to be diluted in a KBr matrix and pressed into a pellet disc due to the high absorptivities associated with clay minerals (Karakassides et al. 1997). The pressing of KBr pellet with clay is often associated with alteration in spectra through absorption or exchange of the K into the clay structure (Ray and Ursula, 1998). KBr is hygroscopic and it is difficult to prepare a pellet completely free of contaminating moisture; it cannot therefore eliminate interference of water bands in the clay mineral spectra. The DRIFTS method is applicable to powder samples, however, the samples still need to be mixed with KBr matrix to minimise interference effect created by particle size and the incident IR wavelengths (towards the low frequency region, normally below 1000 cm^{-1}) known as the Reststrahlen effects (Ray and Ursula, 1998).

This work employed FT-ATR analysis together with a multivariate statistical analysis to estimate the major mineral components in shale rock. The ATR technique involves the collection of radiation reflected from the interface between the sample and a crystal (ZnSe), in which an evanescent wave penetrates from the crystal into the powder samples. This evanescent ray permits sampling in the close vicinity of the interface because reflected beam will be attenuated by absorption in this limited thickness of the less-dense medium (sample). The attenuated total reflection (ATR) spectrum produces the features of an absorption spectrum in a semi-quantitative manner. It is hoped that the ATR technique combats the most challenging aspects of Transmission and DRIFT analyses such as sample preparation and concentration since analyses is conducted on whole rock powders without the need to dilute in a KBr matrix.

Fourier Transform Infra-Red (FTIR) spectroscopy has been applied in the studies of organic and reservoir geochemistry (Hakuli et al. 1995; Landais, 1995; Tanaka et al. 2001; Lis et al., 2005; Bhargava et al. 2005; Permanyer et al. 2007; Leach et al. 2008). However, it is not the intent of this work to estimate the organic phase of the shale gas using IR technique.

This section of the work is generally aimed at investigating the feasibility of applying multivariate statistical models based on Partial Least Squares (PLS) to mid-infrared spectra obtained via Attenuated Total Reflectance Fourier Transform Spectroscopy in order to estimate bulk mineralogy of shale rocks. Objectives of the study are:

- a) To compare the ATR spectra of the various shale minerals with FTIR transmission spectra using KBr pellets and with DRIFT spectra to elucidate the strengths and weaknesses of the method.
- b) To provide a semi quantitative mineralogy of the major minerals in shale using the ATR technique. This would be achieved by:
 - i. Developing a PLS multivariate calibration model using spectra of artificial mixtures of standard pure minerals.
 - ii. Comparing predicted values with known XRD values for validations.
 - iii. Predicting the relative concentrations of the modelled minerals in natural shale rock samples using the calibrated spectra model.

3.3 Methodology

3.3.1 Samples and sample preparations

3.3.2 Pure Mineral Mixtures

A suite of clastic and carbonate mineral mixtures were prepared from five mineral standards based on mineral combinations commonly found in shale reservoir rocks. The five minerals chosen to make up the mineral mixtures are: quartz, illite-smectite (70:30), kaolinite, calcite and dolomite and were obtained from the Clay Minerals Society repository with all standards having a percentage purity of 99.7%. All the minerals were used as received, without further treatment. Standard mixture sets were created by mixing known concentrations (wt. %) of each pure mineral to make up 100mg. Each mineral in the mixture sets was distributed within concentration ranges typical of sedimentary rock (Table 3.3). Independent shale rock samples rich in clastic and carbonates minerals were selected and quantified independently using the XRD technique (Hillier, 2003) for comparison.

3.3.3 Shale Samples

Two sets of shale samples with pre-existing XRD data were used in optimising the IR calibrations. These include samples from the Nile Delta and Western Canada.

3.3.4 Nile Delta shales

A total of 26 Nile Delta shales (Table..) previously characterised for quantitative bulk mineralogy by the Macaulay Institute, Aberdeen were utilised. These samples were generally used to (a) validate mineral mixture calibration, (b) construct and validate a calibration of natural shale. The rationale for choosing these samples is because they have XRD data that can be used to check the accuracy of the IR calibration and also provided more accurate estimates of the mineral assemblage compared to the weights of the mixtures used for the mineral mixtures calibrations.

Table 3.1: XRD data for Shale samples used in optimising IR calibrations (A) Nile Delta shales, (B) Bigstick shales and (C) Wildmere shales – within the Bigstick Field. All the XRD data in this table were generated by the Macaulay institute, Aberdeen.

A												
XRD												
Labcodes	Pattern Name	Quartz	Plagioclase	K-feldspar	Calcite	Dolomite	Siderite	Pyrite	Anatase	Kaolinite	Chlorite	Illite+ Illite-Smectite
937969	Raven-4-4339-25-B	15	4.7	1.3	1.9	0	5.2	0.7	0.9	24.5	8.8	36.9
937970	Raven-4-4346-23-B	13.6	4.4	1.2	0.3	0	2.2	1.7	1	26.5	6.1	43
937971	Raven-4-4354-38-B	12.7	4.8	1.3	0.2	0	5.8	3.8	1	24.8	5.7	40
937972	Raven-4-4364-41-B	15.9	6.8	1.4	0.4	0	8.6	1.1	0.9	21.1	8.9	35.1
937973	Raven-4-4367-35-B	12.9	6.4	1.1	0.3	0	6	1.3	1	22.5	6.2	42.2
937974	Raven-4-4370-47-B	9.2	4.2	1.3	2.3	0	2.1	2.4	0.7	27.2	5.5	45.3
937975	Raven-4-4377-47-B	14.4	4.9	1.1	0.1	0	0.3	0.9	1.1	25.8	6.2	45.2
937976	Raven-4-4382-30-B	13.6	4.5	1	0.1	0	2	0.9	1.1	27	6.9	42.8
937977	Raven-4-4393-30-B	12.6	4.1	0.8	0.1	0	13.4	1	0.7	22.6	6.7	37.9
937978	Raven-4-4401-50-B	14.9	5	1.2	0	0	1.4	0.5	1.3	29.6	7	39.2
937979	Raven-4-4409-42-B	13.7	4.3	1	0	0	0.8	1.2	1.1	29.5	6	42.6
937980	Raven-4-4415-36-B	12.7	4	0.8	0	0	2.6	0.4	1	29.4	6.7	42.6
937981	Raven-4-4421-50-B	9.1	2.6	0.6	0	0	26.3	0.8	0.6	18	8.7	33.3
937982	Raven-4-4427-48-B	12.1	3.9	0.9	0.1	0	3.7	0.6	1.2	30.2	6.3	41
937983	Raven-4-4432-54-B	12.5	4.2	1	0.1	0	5.7	0.4	1.2	28.5	5.9	40.6
937984	Raven-4-4440-40-B	14.1	5.2	0.8	0.3	0	5.8	0.6	1	24.8	7.6	39.8
937985	Raven-4-4447-53-B	15.5	5.8	1.2	0.6	0	10.5	0.7	1.1	22.3	9	33.3
937986	Raven-4-4459-52-B	20.9	6.7	2	0.5	0	4.3	0.7	1.3	19.5	7.7	36.5
937987	Raven-4-4468-56-B	9.9	4	1.5	0.8	0	7	0.7	1.3	25.4	5.9	43.6
937988	Raven-4-4474-45-B	21.5	4.4	1.3	1.3	0	4.8	0.5	1.1	16.4	6.4	42.3
937989	Raven-4-4480-50-B	24.4	5.2	1.6	2	0	4	0.6	1.2	13.9	7.7	39.6
937990	Raven-4-4486-60-B	11.5	4.1	1	1.1	0	8.6	0.6	1	22.7	5.2	44.4
937991	Raven-4-4496-40-B	15.8	4.2	1.3	17.6	0.3	2.9	2.5	0.6	17.2	6.1	31.6
937992	Raven-4-4520-55-B	16.9	6	0.6	3.3	0	6.9	0.5	0.7	24.6	7.5	32.9
937993	Raven-4-4524-60-B	14.8	5.8	1.4	0.2	0	2.5	1.7	1	22.9	4.1	45.8
937994	Raven-4-4537-58-B	11.5	5.6	0.9	0.2	0	7.4	0.4	0.9	25.7	2.9	44.6
937995	Raven-4-4630-52-B	85.6	8.6	0	0.2	0	1.3	0	0.4	0	3.9	0
937996	Raven-4-4632-62-B	23	9.3	2.2	0.1	0	10.4	0.9	1	13.6	4	35.6
937997	Raven-4-4634-15-B	14.5	7.1	1.7	0.1	0	6.2	0.9	1.3	22.3	2.1	43.9

B												
Labcode	Sample	Quartz	Plagioclase	K-feldspar	Calcite	Dolomite	Siderite	Pyrite	Anatase	Gypsum	Basanite	Halite
1023267	MT3 1575.4m	58.1	3.7	2.7	0.2	0.2	1.2	3.0	0.2	0.0	0.0	6.1
1023268	CR43 156.4m	0.5	0.0	0.0	87.7	0.0	0.0	0.0	0.0	2.6	0.0	9.2
1023269	AER20 1340"	17.2	1.4	1.8	47.7	2.5	0.3	3.0	0.0	1.6	0.0	2.3
1023270	Sample 2 682.92m	36.1	2.0	2.4	0.3	0.0	0.3	0.5	0.3	0.0	0.0	3.9
1023271	Sample 13 668.85m	27.5	2.8	3.5	0.0	0.0	0.0	1.6	0.5	0.0	0.0	2.4
1023272	Sample 27 650.91m	26.9	1.3	0.9	17.9	0.8	0.0	6.8	0.0	0.0	1.4	0.0
1023273	Sample 31 646.25m	3.9	0.1	0.7	88.8	2.3	0.4	2.9	0.0	0.0	0.0	0.4
1023274	Sample 36 640.52m	16.6	1.1	1.5	60.5	1.7	0.3	2.2	0.0	0.0	0.8	0.9
1023275	Sample 42 629.91m	19.4	1.1	1.6	42.4	0.9	0.6	4.1	0.1	0.2	0.5	0.0
1023276	Sample 49 621.05m	41.0	1.4	1.9	1.2	0.2	0.2	1.9	0.5	0.0	0.2	0.0
1023277	Sample 74 589.3m	6.4	0.0	0.5	88.4	0.0	0.0	1.7	0.0	0.0	0.0	3.0
1023278	Sample 79 585.6m	29.8	2.0	1.7	0.7	0.1	0.2	23.1	0.3	0.5	0.4	0.0
1023279	Sample 86 573.6m	11.2	1.2	0.4	0.6	0.0	0.0	3.9	0.4	0.0	0.0	0.3
1023280	Sample 93 563.8m	32.1	1.3	1.5	8.9	0.5	0.3	7.1	0.4	0.0	1.8	0.0
1023281	Sample 96 558.8m	17.2	0.9	2.2	19.3	27.7	0.2	3.8	0.1	0.6	0.1	0.0
1023282	Sample 99 558.8m	36.1	1.7	1.6	7.8	0.4	0.0	3.0	0.5	0.0	0.0	7.1
1023283	Sample 107 549.6m	38.3	1.9	1.8	4.6	0.7	0.0	3.1	0.0	0.0	0.0	7.8
1023284	Sample 119 539.35m	43.9	2.6	2.5	0.4	0.2	0.0	2.1	0.0	0.0	0.0	5.2
1023285	Sample 144 501.4m	42.2	2.2	1.9	1.4	1.8	0.0	3.7	0.0	0.0	0.0	6.5
1023286	Sample 150 492.9m	44.1	2.7	3.1	5.0	4.5	0.0	3.8	0.0	0.0	0.0	7.9
1023287	Sample 156 485.9m	36.3	2.5	3.3	9.8	9.3	0.0	3.4	0.0	0.8	0.0	6.2
1023288	Sample 163 477.3m	28.8	1.7	1.9	15.5	2.4	0.0	4.5	0.0	1.3	0.0	6.6
1023289	Sample 167 474.2m	25.4	1.9	2.0	20.6	20.0	0.0	3.2	0.0	1.8	0.0	6.3
1023290	Sample 175 463.2m	28.0	1.7	2.4	24.2	4.5	0.0	3.8	0.0	0.0	0.0	6.4

C												
Labcode	Sample	Quartz	Plagioclase	K-feldspar	Calcite	Dolomite	Siderite	Pyrite	Anatase	Gypsum	Basanite	Halite
1023291	PRG 6208 T597	25.5	2.3	2.8	16.9	0.4	0.0	5.0	0.0	4.1	0.0	0.1
1023292	PRG 6239 T682	41.9	2.1	3.2	0.4	0.2	0.0	1.2	0.0	0.0	0.0	0.4
1023293	PRG 6262 T742	17.6	0.9	1.4	57.5	2.1	0.0	1.7	0.0	0.0	0.0	2.8
1023294	PRG 6294 T946	29.8	3.5	3.4	0.3	0.1	0.0	2.6	0.0	0.0	0.0	0.1

3.3.5 Western Canada Shales

A range of Western Canada shales were also utilised for the calibrations. Twelve samples were supplied by Conoco Phillips characterised by two independent XRD companies; Conoco Phillips and Core Laboratories (Table 3.2). Additional 9 Canadian samples obtained from the Bigstick Field (Fig. 6.1) comprising 5 samples from Bigstick core and 4 samples from Wildmere core. These samples were also characterised by the Macaulay Institute for bulk XRD mineralogy (Table 3.1). These samples provided a broader range of mineralogical compositions and were utilised to (a) validate calibrations constructed from the Nile Delta shales (b) validate calibrations constructed with a composite of natural shale and altered shales whose natural compositions have been altered by mixing with pure minerals.

3.3.6 Sample preparations

The pure standard minerals and the shale samples were pulverised to less than 10 μm using a micronising mill for 10 minutes. 100mg of each pure mineral mixture were prepared by weighing the individual mineral material to within ± 0.1 mg of the pre-assigned amounts. The mixture was then mixed with a pestle and mortar for another 10 minutes to a consistent homogeneity of less than 2 μm . The powdered mixtures were then stored in a dessicator for the FTIR analysis.

About 2mg of the samples were scanned over a wavelength of 400-4000 cm^{-1} collecting 32 scans at a resolution of 8 cm^{-1} using a Fourier Transform AVATAR 360 FTIR ESP spectrometer with OMNIC software fitted with an ATR Performer accessory and equipped with a DTGS detector. A background scan was performed for every sample and the sample chamber was purged with purified compressed air to remove water vapour and CO_2 prior to scanning the samples. ATR spectra were also recorded on the whole rock samples.

Table 3.2: XRD data for Shale samples supplied by Conoco Phillips used in optimising IR calibrations. XRD data was generated by (a) Conoco Phillips –designated as ‘base’ and (b) Core Laboratory- designated as ‘terra’

Title	illit	kao	mont	chl	qtz	ortho	plagio	Cal	dol	sid	pyt	apat	kero	total
base--Indian Castle--calc silic shale	6	1	0	0	38	0	13	29	9	0	4	0	0	100
terra--Indian Castle--calc silic shale	23	0	0	0	24	0	17	30	4	0	2	0	0	100
base--Nordegg--xtline limestone	0	0	0	0	0	0	4	93	2	0	0	1	0	100
terra--Nordegg--xtline limestone	0	0	0	0	2	0	0	98	0	0	0	0	0	100
base--Ferne--shale	29	9	24	3	24	0	0	0	7	0	4	0	0	100
terra--Ferne--shale	45	13	0	0	26	0	0	0	11	0	5	0	0	100
base--Nordegg--black chert	0	0	0	0	92	1	1	3	0	0	1	2	0	100
terra--Nordegg--black chert	0	0	0	0	94	0	0	0	0	0	2	4	0	100
base--Nordegg--calc sand	0	0	0	0	66	0	7	17	1	0	0	9	0	100
terra--Nordegg--calc sand	0	0	0	0	53	0	5	31	0	0	0	11	0	100
base--Montney--argil silt	17	0	0	0	40	8	13	6	8	0	3	0	5	100
terra--Montney--argil silt	25	0	0	0	36	10	14	7	7	0	1	0	0	100
base--Montney--dolom silt	4	0	0	0	16	3	5	21	46	0	1	0	4	100
terra--Montney--dolom silt	12	0	0	0	20	4	7	21	35	0	1	0	0	100
base--Montney--plag silt	11	0	0	0	42	8	13	5	9	0	3	0	9	100
terra--Montney--plag silt	20	0	0	0	38	10	15	7	8	0	2	0	0	100
base--Montney--calc silt	11	0	0	0	29	5	10	19	7	0	5	0	14	100
terra--Montney--calc silt	22	0	0	0	29	7	13	19	8	0	2	0	0	100
base--Montney--calc silt	6	0	0	0	27	5	10	33	11	0	2	0	6	100
terra--Montney--calc silt	18	0	0	0	24	6	9	31	10	0	2	0	0	100
base--Duvernay--calc shale	10	0	0	0	20	7	0	61	0	0	2	0	0	100
terra--Duvernay--calc shale	11	0	0	0	32	14	0	40	0	1	2	0	0	100
base--Duvernay--silic shale	22	0	0	0	51	13	0	7	0	7	0	0	0	100
terra--Duvernay--silic shale	27	0	0	0	45	15	0	11	0	1	1	0	0	100
base--Duvernay--calc shale	11	0	0	0	34	6	0	47	0	0	2	0	0	100
terra--Duvernay--calc shale	16	0	0	0	20	4	0	59	0	0	1	0	0	100
base--Duvernay--calc shale	6	0	0	0	24	3	0	63	0	0	4	0	0	100
terra--Duvernay--calc shale	7	0	0	0	8	2	0	81	0	1	1	0	0	100
base--Duvernay--pyrite nodule	35	0	0	0	28	8	0	0	0	0	29	0	0	100
terra--Duvernay--pyrite nodule	19	0	0	0	44	18	0	6	0	3	10	0	0	100

Illit- % illite, kao- % kaolinite, mont- % montmorillonite, chl- %chlorite, qtz-%quartz, orth-% orthoclase, plagio- % plagioclase, cal-%calcite, dol-% dolomite, sid- % siderite, pyt- % pyrite, apat- % apatite, ker-% kerogen,

The success of obtaining accurate mineralogy from FTIR spectroscopy depends on several factors (Matteson and Herron, 1993):

- a) That the FTIR spectra of the different mineral standards are distinguishable from one another.
- b) That the analytical procedures minimises variance between spectra of the same sample.
- c) That the appropriate spectral processing programs are implemented.

The analytical procedures followed in this study ensured that absorbance bands are in the linear region of Beer's law (equation 2.1). The spectrum of each of the five pure minerals chosen were recorded and compared to identify the diagnostic bands in each. Appropriate spectral processing were applied (discussed in section 3.6) to account for spectral variability that may occur due to unavoidable sample variability. However, meticulous sample preparation was ensured; all samples were pulverized and ground in a consistent manner. Furthermore, the mineral spectra for the five standards were recorded using the KBr Transmission and DRIFT techniques to allow for comparison with the ATR spectra.

3.3.7 Sample Preparation for Transmission Spectra

- 1) 0.0015g of sample was then mixed with 0.2985g of Potassium bromide (KBr) and ground again to a homogeneous blend for another 10 minutes.
- 2) The mixture was then compressed under 10×10^3 Kg pressure for ten minutes into a small transparent disc 13mm in diameter using a 15 ton-press.
- 3) Samples were stored in an oven to prevent water contamination and then transferred into a desiccator to cool down for at least 24 hours before recording the spectrum.
- 4) This disc was then placed in the infrared spectrometer and the spectrum is collected
- 5) Transmitted spectra were converted to absorbance spectra at each frequency and absorbance is plotted against frequency to make the spectrum of the samples.

3.3.8 Sample preparations for DRIFT Spectra

All samples were ground for 10 minutes in an agate and mortar and dispersed at 5wt% in a FTIR grade KBr. Each sample was then packed into the sample cup gently tamped at the base and smoothed at the surface using a micro spatula. Homogeneous samples and sample packing are critical to obtaining reproducible spectra which in turn determine the success of the quantification (Osborne and Fearn, 1986). Therefore, all samples were milled to at least <10 microns and an updrift accessory designed to minimise scatter was used in recording the spectra. All samples were scanned over the MIR region ($400\text{--}4000\text{cm}^{-1}$) at 8cm^{-1} resolution and 32 scans using a FTIR (Thermo Nicolet AVATAR 360 FTIR) using a Collector DRIFTS accessory.

3.4 Mineral Standard Spectra

The absorbance FT-ATR spectra of the mineral standards are shown in Fig. 3.1. Generally, the mineral standards in this set of mixtures fall into three major groups: the tectosilicates (framework silicates, e.g., quartz), phyllosilicates (layer silicates, e.g., clays), and the carbonates. The mineral groups have FTIR absorbance band features that make them clearly different from one another (Figs. 3.2 & 3.3 and Table 3.3). However, within each group the spectra have similar bands at certain frequencies. For example, both the calcite and dolomite are characterised by strong absorption bands due to asymmetric stretching vibrations of the CO_3^{2-} which occur between 1540 and 1400 cm^{-1} (Clark, 1999; Matteson and Herron, 1993).

The diagnostic bands for calcite on a transmission spectrum occur at 1428 , 878 and 714 cm^{-1} while the spectrum of dolomite shows similar bands shift to higher frequency (Clark, 1999; Wilson, 1996; Vagenas et al., 2003). The spectra of the ATR show similar pattern with calcite having diagnostic bands at 1413 , 873 & 711cm^{-1} while dolomite shows bands at slightly higher frequencies of 1438 , 881 & 729 cm^{-1} (Fig. 3.2b).

The silicates are characterised by Si-O stretching and bending vibrations between 1200 and 400 cm^{-1} (Wilson, 1996). However, the phyllosilicates can be separated from the tectosilicates based on the occurrence of the O-H stretch vibrations at 3750 to 3400 cm^{-1} and O-H deformation band at 916 cm^{-1} characteristic of the clays (Peussa et al. 2000). The 796 & 778 cm^{-1} doublet characteristics of quartz spectrum are clearly absent in the clays enabling quartz

and kaolinite to be distinguished (Fig. 3.2a). The quartz doublet occur at 800 & 781 cm^{-1} on a transmission spectrum and together are regarded as the most diagnostic bands for the quartz (Clark, 1999; Matteson and Herron, 1993).

The O-H stretching doublet 3700 & 3620 cm^{-1} bands and the OH deformation band at 916 cm^{-1} have been identified as characteristic of kaolinite, distinguishing it from other clay minerals (Clark, 1999; Matteson and Herron, 1993). This is evident in the ATR spectrum at 3695, 3620 cm^{-1} (Fig. 3.3a) despite the strong similarity between the kaolinite and illite-smectite spectra.

The illite-smectite shows a single and broader OH band at 3643 cm^{-1} close to that of the inner OH groups in kaolinite and shows more resolved OH deformation bands at 999 cm^{-1} and 929 cm^{-1} than the kaolinite (Figs. 3.3a+b). These bands occur at lower frequency for individual illite and smectite; in transmission, smectite shows the broader OH band at 3622 cm^{-1} and the resolved OH deformation bands at 1029, 915 and 840 cm^{-1} (Clark, 1999; Matteson and Herron, 1993).

Table 3.3 : FT-ATR spectra of the five standard minerals and their diagnostic bands

Pure Mineral	Absorption Diagnostic bands (cm^{-1})
Quartz	1058, 796, 778, & 615
Calcite	1413 , 873 & 711
Dolomite	1438 , 881 & 729
Kaolinite	3695, 3620, 1002 & 912
Illite-smectite	3643, 999 & 929

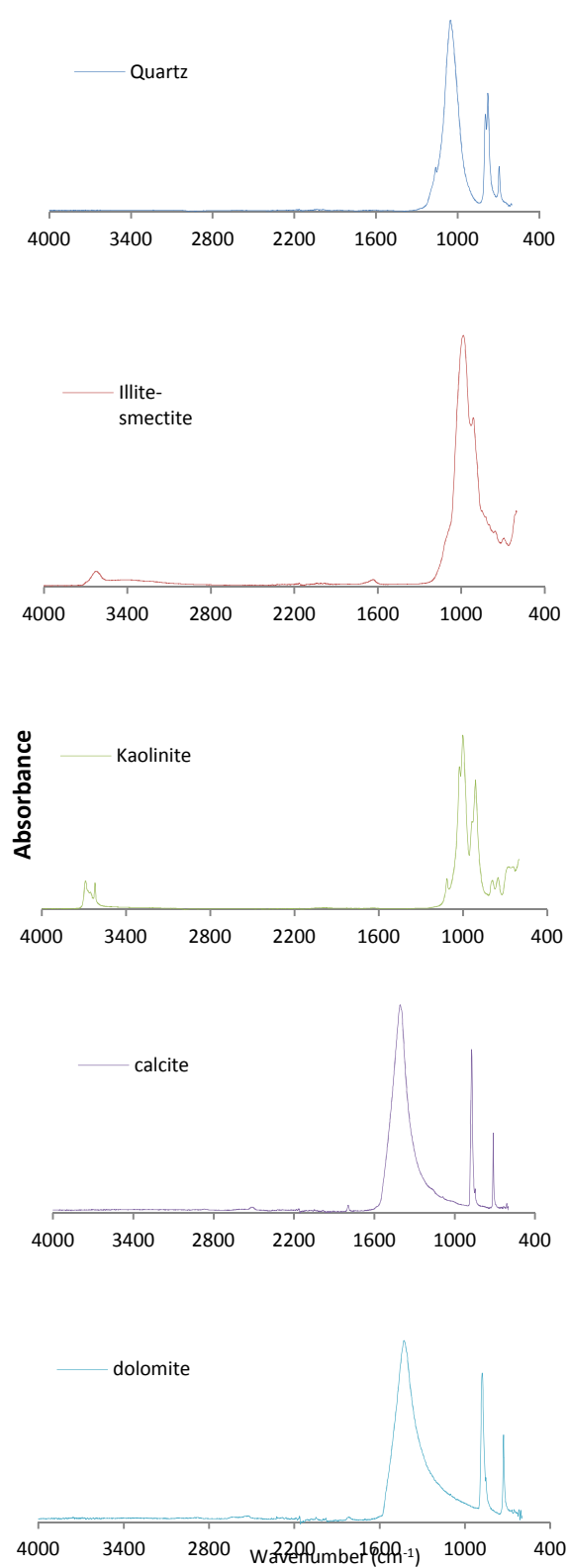
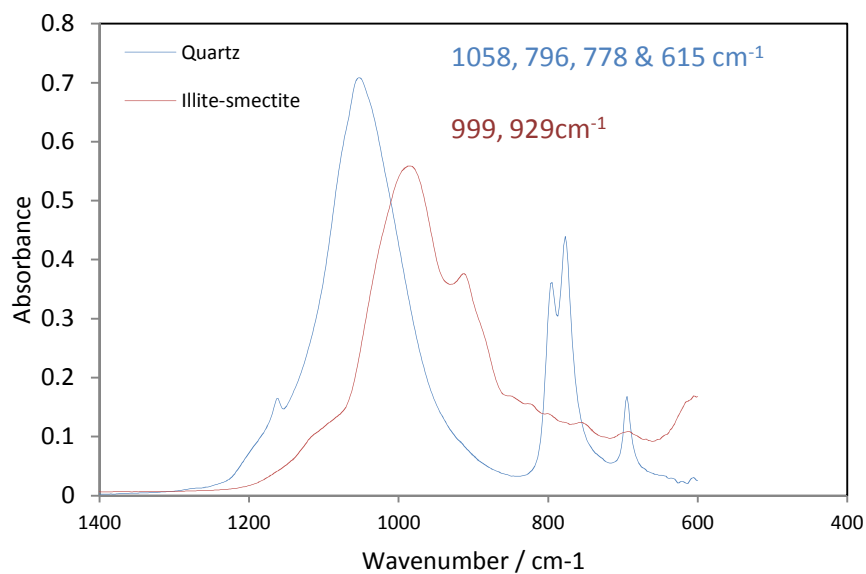


Figure 3.1: The FT-ATR spectra of the five standard minerals used to develop the calibration, showing their characteristic diagnostic bands

a)



b)

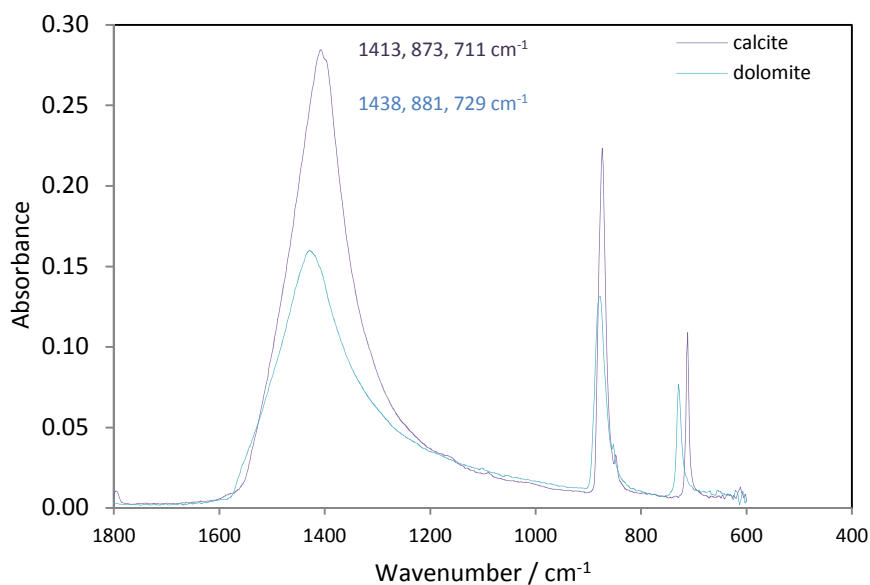
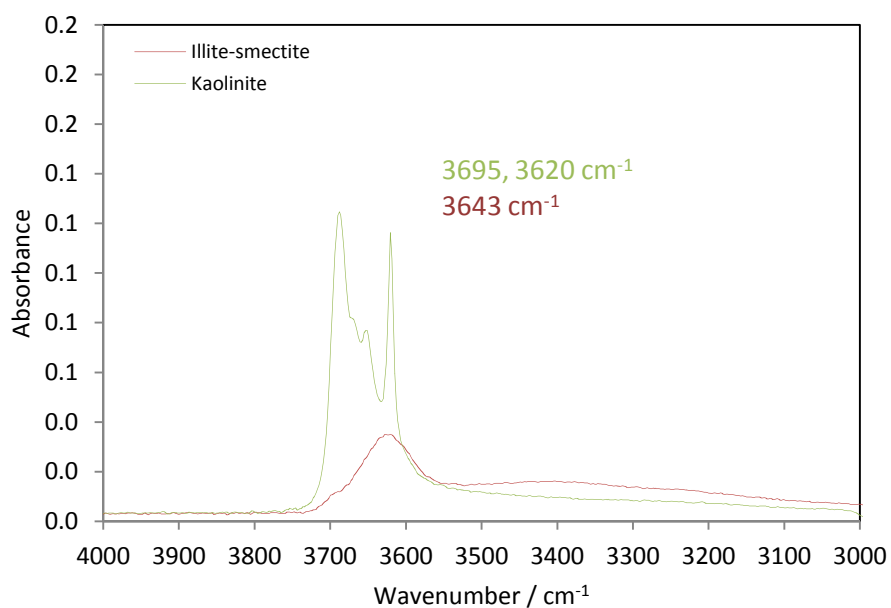


Figure 3.2: The FT-ATR spectra of: (a) silicates showing comparison between quartz and illite-smectite; (b) the carbonate showing comparison between calcite and dolomite. The spectra have been offset to (1800 to 400 cm^{-1}) for visual enhancement. Quartz can be separated from the illite-smectite based on the occurrence of the 796 & 778 cm^{-1} doublet which are clearly absent in the illite-smectite. The only difference between the carbonate is that dolomite diagnostic bands occur at slightly higher frequencies than the calcite.

a)



b)

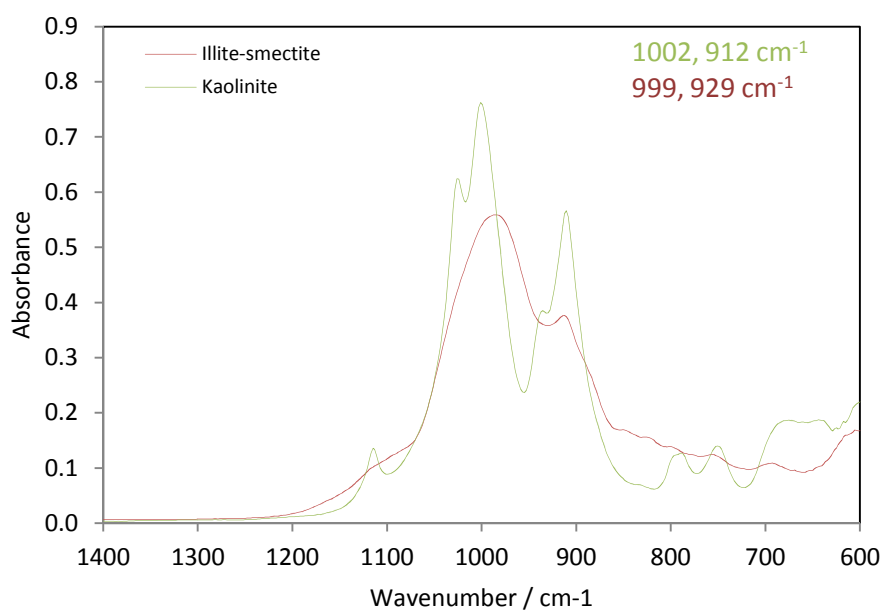


Figure 3.3: The FT-ATR spectra of the clays: (a) OH stretching bands for kaolinite and illite smectite (b) Si-O stretching and OH deformation bands for kaolinite and illite smectite. The spectra have been offset for visual enhancement. Kaolinite can be distinguished from illite-smectite by the well-resolved 3695, 3620 cm^{-1} doublet and the Si-O band at a higher frequency of 1002. Illite-smectite can be distinguished by a more resolved OH deformation band at 929 cm^{-1}

Figures 3.4-3.5 show comparisons of ATR spectra with transmission and DRIFT spectra for the five pure minerals showing similarities and differences between the techniques. There is a general agreement between the spectra for all the minerals with respect to the major characteristic bands in the stretching and deformation areas. However, there are many differences with respect to the position of the bands and quality of the spectra. Below is a summary of the major differences between the techniques:

1. The ATR spectrum has a better linear baseline than either the transmission or DRIFT. A linear baseline ensures a uniform base: peak ratio which in turn results in a more accurate quantitative analysis.
2. The CO₂/moisture bands are clearly visible in the transmission spectrum between the regions of 2402 – 2348cm⁻¹ but are generally absent in the ATR spectrum (Fig. 3.4). The presence of the moisture bands affects both the relative positions of the fundamental bands as well as the overall quality of the spectrum.
3. Fundamental bands present between the 600-400cm⁻¹ in the transmission spectrum are absent in the ATR and the DRIFT spectra. This is a major limitation of the ATR technique.
4. Although spectra of the clays show some family resemblance between 600 – 400cm⁻¹, there are slight differences in positions of the bands that distinguish them from quartz and from one another. For example, the Si-O bending bands at 528, 468cm⁻¹ in illite-smectite occur at 539, 470cm⁻¹ in kaolinite and at 512, 460cm⁻¹ in quartz (Figs 5a-c).
5. The carbonates did not show any bands beyond the 600cm⁻¹ region for both the ATR and transmission spectrum. Wilson (1996) show a transmission spectrum for calcite and dolomite with well resolved bands at 322, 228cm⁻¹ for calcite and 369, 262cm⁻¹; these are outside the mid-infrared region.
6. The DRIFT spectra exhibit more spectral features than both the ATR and Transmission. However, the DRIFT spectra are significantly affected by the Reststrahlen effects which appear as spikes below the 1000 cm⁻¹ region.

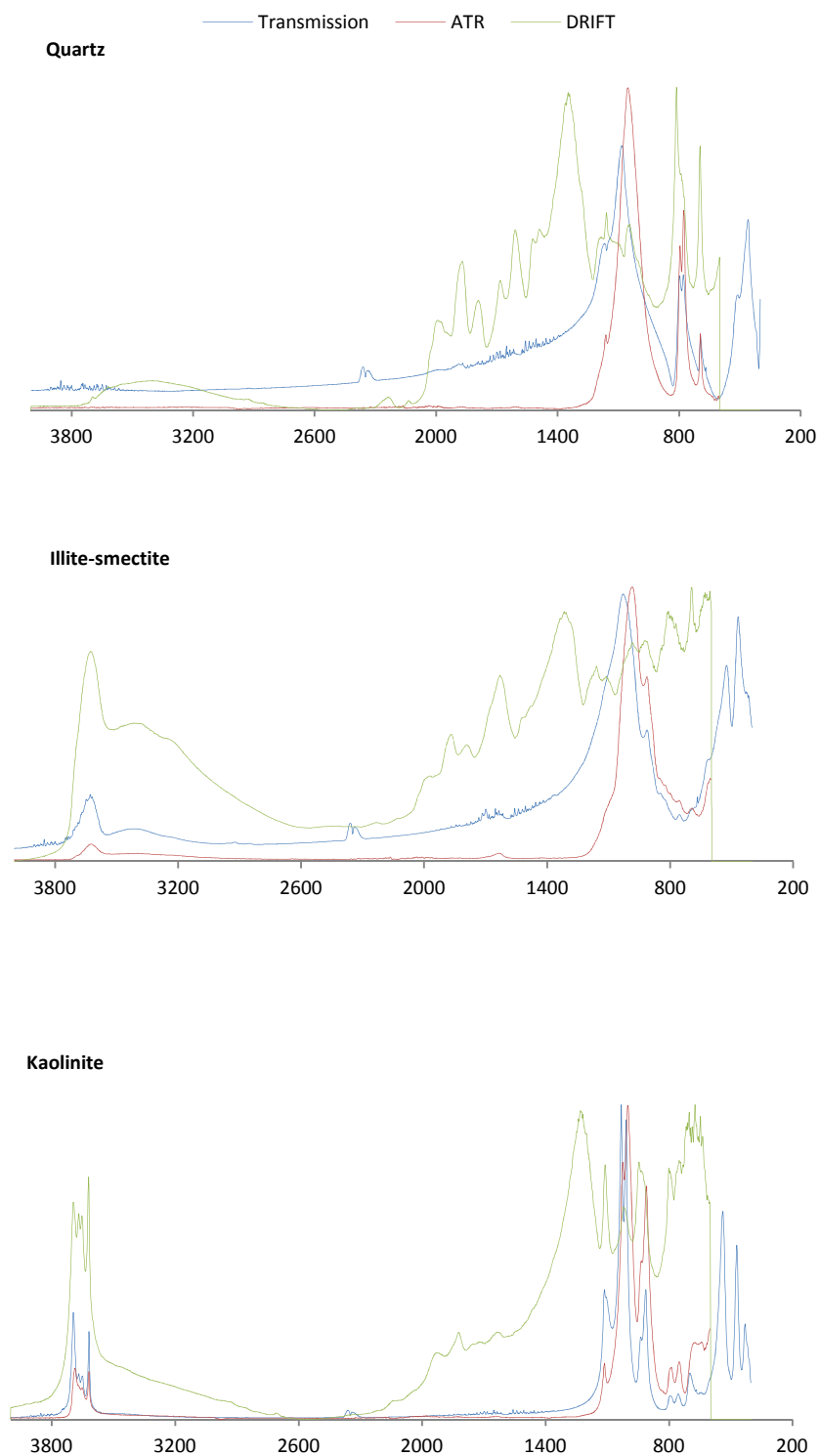


Figure 3.4: Comparison between ATR , Transmission and DRIFT spectra for (a) quartz, (b) Illite-smectite, (c) kaolinite

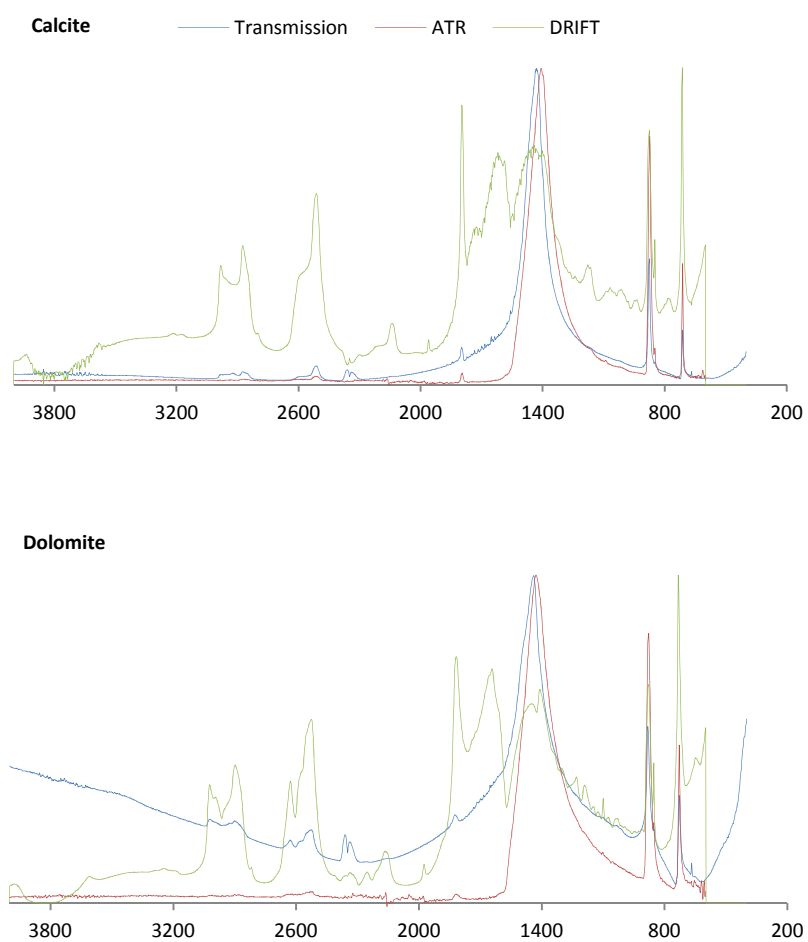


Figure 3.5: Comparison between ATR , Transmission and DRIFT spectra for (d) calcite and (e) dolomite

3.5 Spectra Repeatability

The analytical procedures followed in this study ensured that absorbance bands are in the linear region of Beer's law (equation 2.1). Analytical errors were calculated by measuring the standard deviation of the maximum absorbance peak (three spectra per sample) for each standard (Table 3.4; Fig. 3.6). Figure 3.7 shows the overlay plots of the pure minerals spectra (three spectra) for each mineral. Spectra differ by absorbance values of 0.02 for quartz; 0.05 for illite-smectite; 0.01 for kaolinite; 0.03 for calcite and dolomite. This shows that the ATR produce highly reproducible spectra and therefore it is feasible to perform quantitative analysis.

Table 3.4: Errors in spectral repeatability

Minerals	Illite-Smectite	Kaolinite	Quartz	Calcite	Dolomite
Peak height1	0.3065	0.7898	0.4603	0.2963	0.2617
Peak height2	0.3306	0.7876	0.4654	0.3082	0.2530
Peak height3	0.2823	0.7846	0.4448	0.2828	0.2336
average	0.3064	0.7873	0.4568	0.2958	0.2494
std dev	0.0241	0.0026	0.0107	0.0127	0.0144
std err	0.0139	0.0015	0.0062	0.0073	0.0083

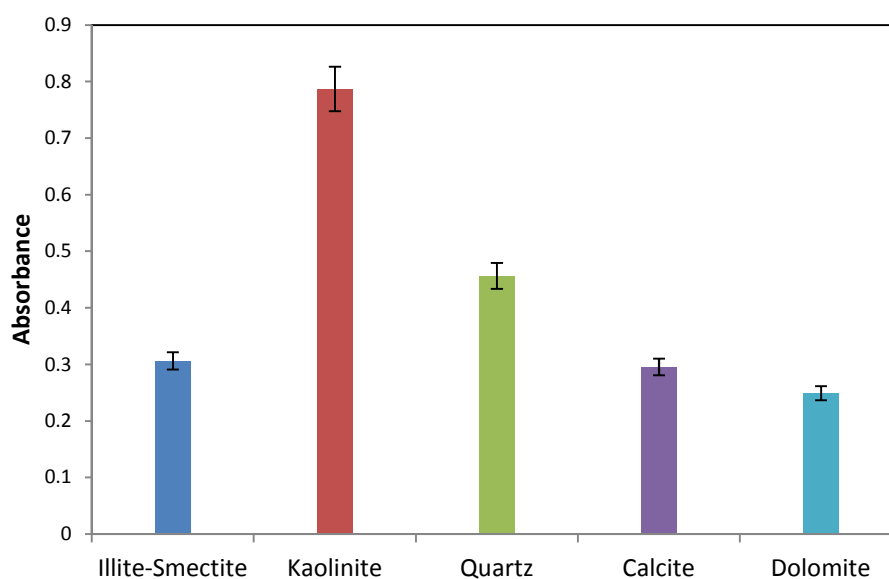


Figure 3.6: Bar charts showing error bars for repeated spectra of pure minerals

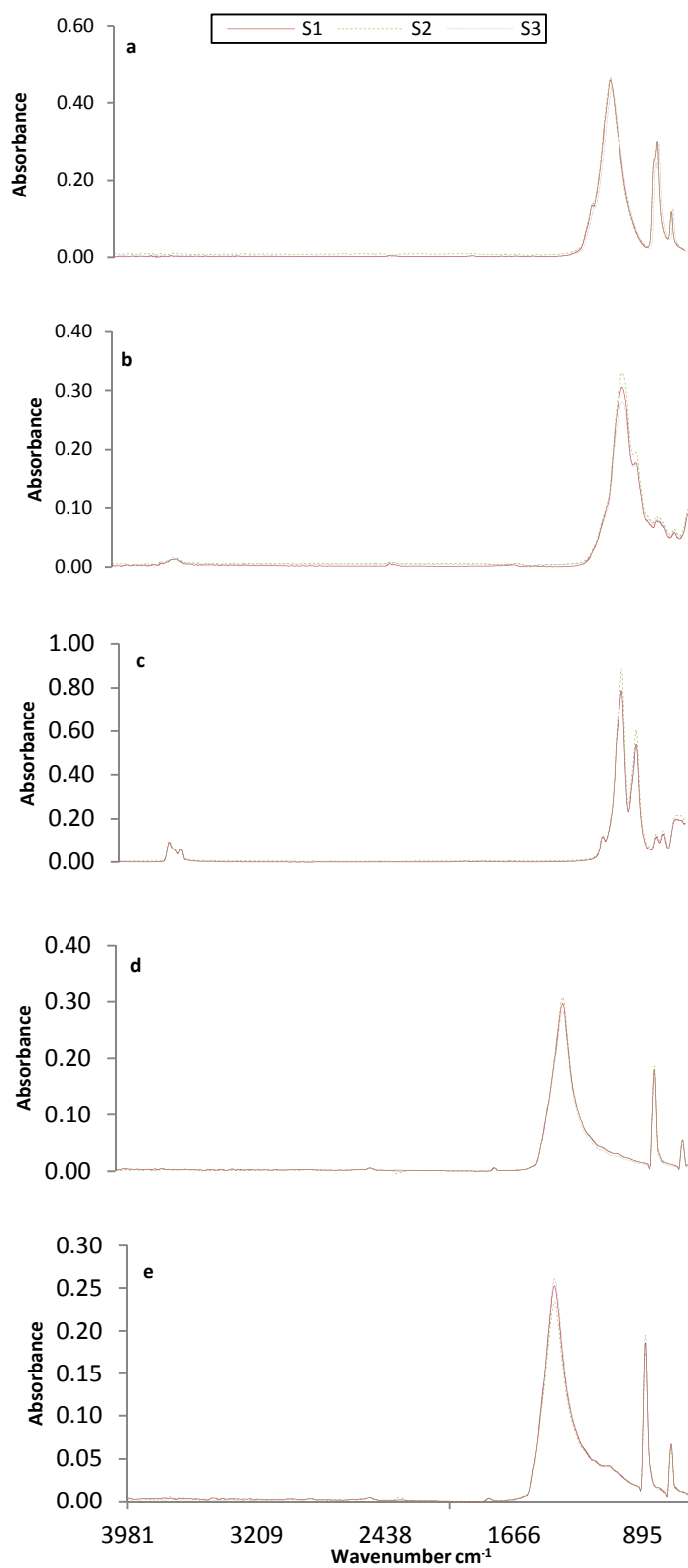
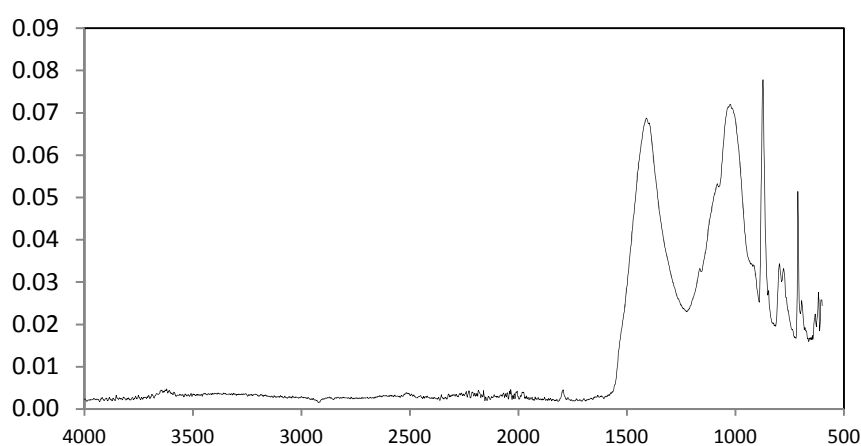


Figure 3.7: Overlay plots for three repeated spectra for each (a) quartz, (b) Illite-smectite, (c) Kaolinite, (d) Calcite, (e) Dolomite

3.6 Spectra Pre-processing

The spectra were baseline linearised using multipoint options and adjusted to zero absorbance. Smoothing to reduce noise in the data was done using Savitzky-Golay algorithm (Savitzky and Golay, 1964) with second degree polynomial convolution function at 15 points to ensure the structural feature of the spectra were not altered. Figure 3.8 shows a typical spectrum before and after pre-processing. Prior to calibration, each spectrum was normalised by dividing the entire spectrum by the highest peak intensity in the spectrum such that the optimum absorption is between 0 and 1 using the Thermo Nicolet Grams AI software.

a



b

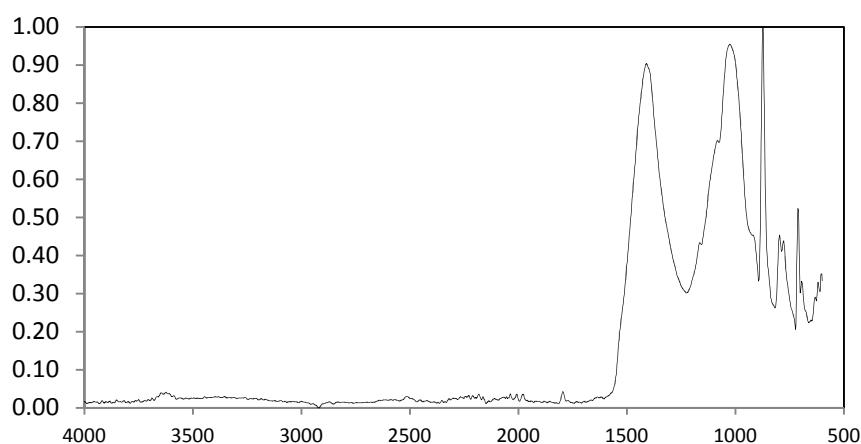


Figure 3.8: Illite-smectite, quartz, calcite mixtures before (a) and after (b) the applications of baseline, smoothing and normalisation

3.7 Calibrations

A total of 26 pure mineral mixtures were used to develop and validate the model called-ATR-PLS-MM model. Seventeen of the twenty-six mixtures were used to develop the model, and the remaining nine were used in the validation process (Appendix I). The weight percent ranges (concentrations) of the pure mineral components used in developing the model are given in Table 3.5. Furthermore, the mineral content of twelve reservoir shale core samples from the Nile Delta and the Western Canada Sedimentary Basin were analysed using quantitative XRD and the ATR-PLS model. This was done in order to assess the prediction capability of the model.

Table 3.5: The relative compositions of mineral standards used to develop the calibration model

Mineral	Typical structural formula	Weight % ranges
Illite/ Smectite	$(K,H_3O)(Al,Mg,Fe)_2(Si,Al)_4O_{10}[(OH)_2,(H_2O)]/$ $(Na,Ca)_{0.33}(Al,Mg)_2(Si_4O_{10})(OH)_2 \cdot nH_2O$	0-80
Kaolinite	$Al_4Si_4O_{10}(OH)_8$	0-30
Quartz	SiO_2	0-80
Calcite	$CaCO_3$	0-60
Dolomite	$CaMg(CO_3)_2$	0-30

The PLS model was developed on the Pirouette software platform (<http://www.infometrix.com>). The optimum number for factors used in the model development was determined from the predicted error sum of squares (PRESS). PLS is a multivariate statistical technique (Geladi and Kowalski, 1986; Beebe and Kowalski, 1987) that can be used to quantify analyte in infrared spectra that are expressed using the Beer-Lambert law for absorbance or the Kubelka Munk equivalent for spectra obtained using DRIFTS. This technique is particularly appropriate when analysing complex multiple spectra, which contain broad and overlapping bands. In essence the PLS algorithm examines regions of the spectra to determine which areas vary as a function of component concentration (Beebe and Kowalski, 1987).

In PLS computation, the complex relationship between a very large number of \mathbf{X} independent variables and dependent \mathbf{Y} variables is compressed into small number of linear combinations of the original \mathbf{X} variables, and only those components are used in the calibration (Beebe and Kowalski, 1987). In addition, the dependent \mathbf{Y} variables are used explicitly in how each factor (component) is computed from spectra (Bjorsvik and Martens, 2000). The most important advantage of PLS regression in comparison to more simple regression methods is that many co-linear, independent \mathbf{X} variables can be handled, which is essential in FTIR analysis because of the large number of spectral data points which correlate with each other (Martens and Naes, 1989).

A PLS regression model is established between a matrix \mathbf{X} , containing absorbance at m wave-numbers for n samples; a \mathbf{Y} matrix containing the concentration-path length product of p components in the n samples and a \mathbf{K} which is a p by m matrix. Each row of \mathbf{K} corresponds to the spectrum of one of the p analytes at unit concentration and unit path length. Each row of \mathbf{X} is the spectrum of one of the n samples, containing the absorbance values at different wave numbers. The matrix formulation of Beer's Law is:

$$\mathbf{X} = \mathbf{YK} \text{ --- Equation 3.1}$$

Where:

\mathbf{X} is the n by m matrix of absorbance of the samples

\mathbf{Y} is the n by p matrix containing the concentration-pathlength product of the p components in the n samples

\mathbf{K} is a p by m matrix.

Any sample's spectrum is assumed to be the sum of the spectra of p components in the sample. Prior to modelling, the mixtures are divided into calibration and validation sets. The composition of new samples (*i.e.*, unknowns) can be determined immediately from their spectra and \mathbf{K} . Designating the spectrum of a single new sample as \mathbf{X}_{new} , equation (1) can be rearranged to give a vector of estimated concentrations for this sample:

$$Y_{\text{new}} = X_{\text{new}} \beta = X_{\text{new}} K^T (K K^T)^{-1} \text{-----Equation 3.2}$$

Where β is a **matrix** containing p column vectors, one for each component.

The individual regression vectors are thus the columns of the pseudo-inverse of \mathbf{K} , symbolized by \mathbf{K}^\dagger :

$$\beta = K^T (K K^T)^{-1} \text{-----Equation 3.3}$$

3.8 Results and discussions of the ATR-PLS-MM model

The calibration model was validated by first comparing predicted results to the actual concentrations of the individual minerals, for subsets of mixtures not included in the calibration, as well as for independent shale samples. Because the weight percent of the mixtures in the validation set and the XRD data for the shale samples known, the calibration model could be tested for accuracy by statistically comparing the ATR-PLS predicted values for the known mixtures and the shale samples against their known values. This provides an indication of the likely performance of the calibration model in predicting the mineral composition of unknown samples in the future.

The composition of samples (mixtures) predicted using the calibration model, occasionally gave negative mineral predictions when the concentrations are low. This is a problem encountered in all multivariate models, and can either be ignored or assigned as containing none of the specified components (Beebe and Kowalski, 1987). All negative values were reported as computed by the model in this study in order to gain full insight of any variability.

The ability of the pure mineral mixture model to successfully predict the concentration of each mineral standard in the validation mixture set is represented in Fig. 3.9. The figure shows the cross plots of predicted concentration against measured concentration as well as correlation coefficients. A one to one solid line is drawn through the origin to represent predicted concentrations equal to actual concentrations to demonstrate the accuracy of the model. Similarly, dashed lines were drawn above and below the actual values to represent the $\pm 10\%$ lines.

The correlation show there is a good agreement between the IR-derived and the known (measured wt %) concentrations with correlation coefficients of 0.96, 0.94, and 0.90 for quartz, kaolinite and calcite respectively. Illite-smectite and dolomite exhibit lower correlation coefficients of 0.88 and 0.78 respectively.

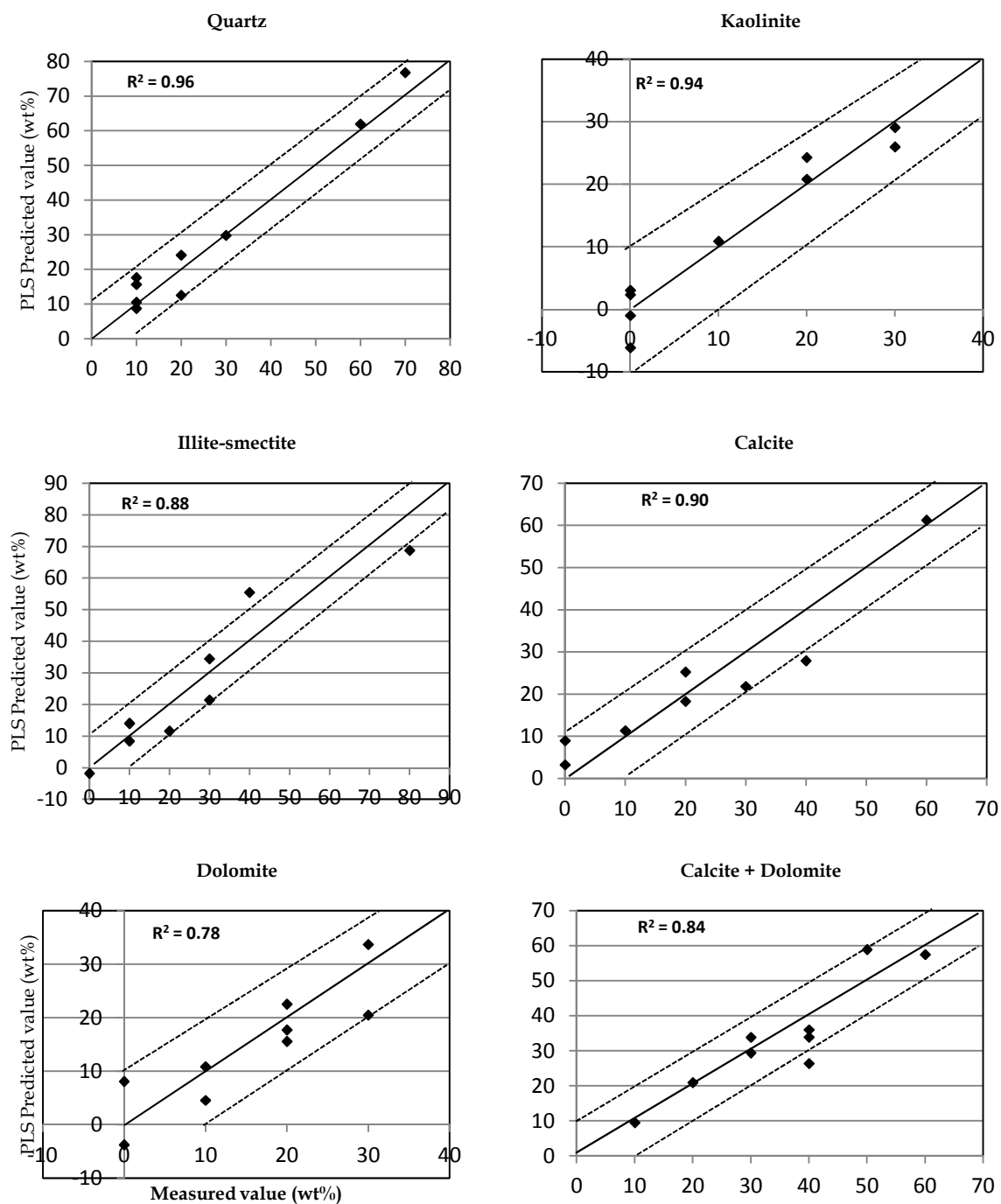


Figure 3.9: Calibration model on pure mineral mixtures. Plots of measured mineral concentrations against the PLS-predicted concentration for the validation sets showing correlation coefficients

The average absolute difference between measured and predicted concentrations is calculated for each mineral and presented in Table 3.4. The absolute average error between actual and predicted values were <5wt % for all the minerals except illite-smectite which have 6.6wt %. The absolute weight difference between measured and predicted values for more than 80% of all the mixtures is < 10 wt % for all the minerals (Fig. 3.9).

The low correlation coefficients for illite-smectite and dolomite are an indication that the model is likely to work better in predicting quartz, calcite and kaolinite compared to illite-smectite and dolomite.

Table 3.6: Errors for the pure mineral mixtures model on validation mineral mixtures

	Quartz	Calcite	Dolomite	Kaolinite	Illite-smectite
Average error (wt %)	4.0	4.8	4.5	2.6	6.6
STD	3.0	6.5	5.4	3.4	8.4
std error	1.0	2.2	1.8	1.1	2.8

Table 3.7: Errors associated with minerals for the pure mineral mixtures model on independent shale samples

	Quartz	Calcite	Dolomite	Kaolinite	Illite-smectite	Clays	Carbonates
Average error (wt %)	8.1	10.6	7.2	10.2	8.2	10.4	14.7
STD	9.6	11.5	8.6	11.7	8.2	13.4	11.8
std error	2.8	3.3	2.5	3.4	2.4	3.9	3.4

3.8.1 Application of ATR-PLS-MM model to independent shale rock samples

The model was also validated using independent shale samples that were different from the calibration samples. Figure 3.10 shows plots of mineral concentrations measured by XRD versus ATR-PLS-MM predicted concentrations for shale samples. The shales were drawn from two different settings to account for natural variability in concentrations and crystallinity. A total of 12 samples were used; nine samples were selected from two fields in the Western Canada Sedimentary Basin and three samples from the Nile Delta.

The average absolute differences between measured (XRD) and IR predicted (ATR-PLS-MM) concentrations for each mineral are shown in Table 3.5. The concentrations of the clays predicted by the ATR-PLS-MM model were generally lower for kaolinite compared to those obtained by the XRD in the Nile Delta samples but predicted higher in the Canadian samples with an average error up to 10wt % and a p – value of 0.53 (Fig. 3.10). Generally, the Nile Delta shale contains high concentrations of kaolinite but the high discrepancies may also be because the shale rocks contain small amounts of other clays (chlorite). These clay minerals exhibit infrared bands in similar spectral regions to those of the mixed layer in the OH stretching region as well as the Si-O bands thus making the distinction between the clays difficult. The model however, predicted values for the illite-smectite which compared well with the XRD values despite the low correlation coefficients (0.88) observed in the mineral mixture validations. Average error for the illite-smectite is 8.2 wt % and a t-test indicated a p value of 0.15 (Table 3.5) revealing that the two measurements do not differ statistically.

The correlation between the two measurements for calcite was good ($R^2 = 0.90$) but have an average error of 11.5wt %, although a p – value of 0.58 suggests that the measurement do not differ significantly over the range of samples analysed. Like the kaolinite, most of the errors come from the Nile Delta shales. The large variation between the IR and XRD calcite values can be attributed to the presence of other carbonates (siderite) present in these shales but uncounted for in the calibration. Siderite and magnesite have been reported to exhibit infrared bands in similar spectral regions to those of dolomite (Breen et al., 2008), and even though they were not included in the model, they might have contributed to the results, thus making the prediction for the carbonates less accurate.

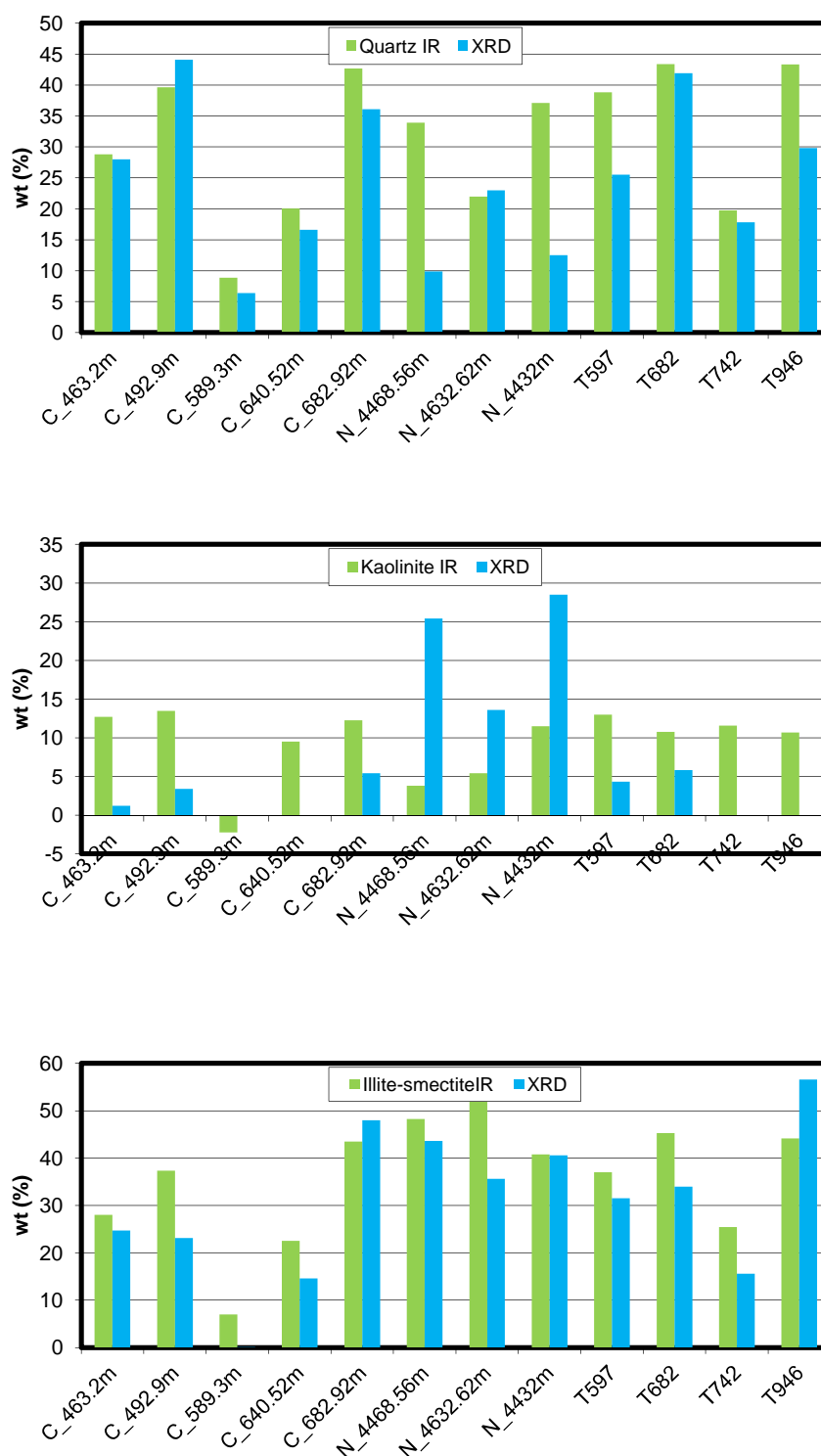


Figure 3.10: Bar charts showing comparison of known concentrations of mineral (quartz, kaolinite and illite-smectite) (XRD) and ATR-PLS model predicted mineral concentrations in independent shale

C – samples from Western Canada Bigstick core; N- samples from the Nile Delta; T - samples from Western Canada Wildmere core (from Table 3.1)

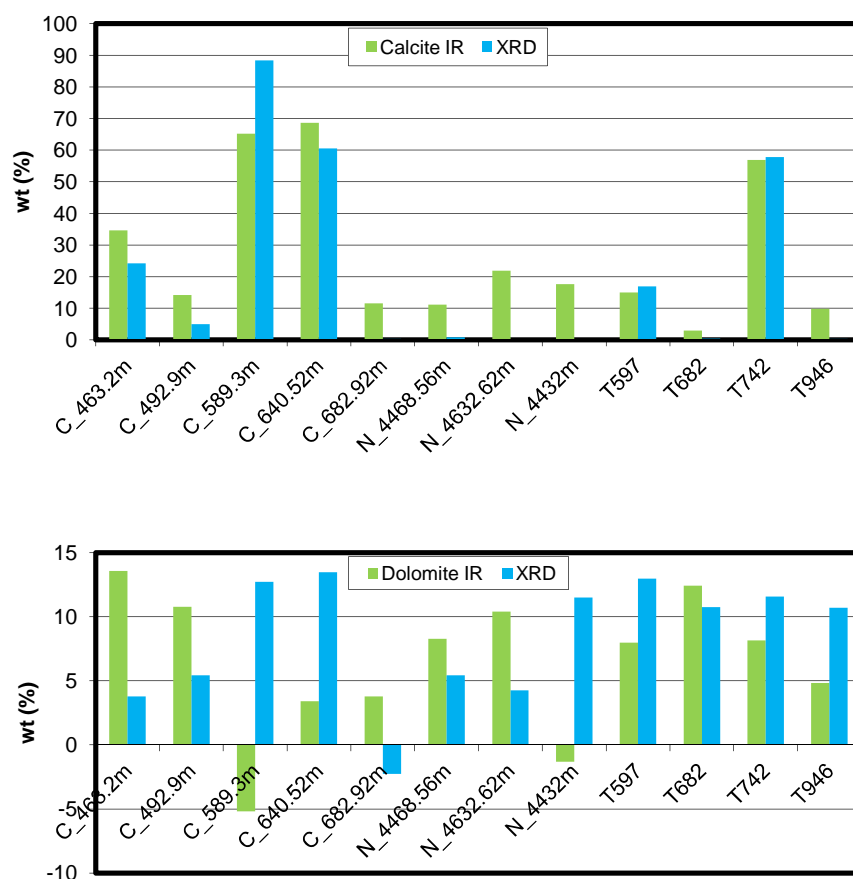


Figure 3.11: Bar charts showing comparison of known concentrations of mineral (calcite and dolomite) XRD and ATR-PLS model predicted mineral concentrations in independent shale

C – samples from Western Canada Bigstick core; N- samples from the Nile Delta; T - samples from Western Canada Wildmere core (from Table 3.1)

The XRD values for dolomite compared against the IR values for these shales are actual combination of the (dolomite and siderite) because siderite was not included in the calibration. The average error between IR and XRD dolomite values is 7.2 wt% and t-test show that the values are significantly comparable with a p-value of 0.38 despite a very low correlation coefficient of 0.1.

Previous IR quantitative mineralogy using transmission and DRIFT analysis (Matteson and Herron, 1993) suggests that prediction accuracy is increased if class of minerals are compared rather than individually. Ideally, the spectral information in each mineral spectrum should be unique. Consequently, if the spectra of two or more components are similar then correlations

between spectra and concentration information will be difficult to distinguish and quantitative results will be inaccurate.

In their study, Matterson & Herron (1993) show correlation coefficients for the transmission FTIR spectra of illite, smectite, kaolinite, chlorite, biotite and muscovite and suggest that it might be difficult to differentiate these minerals from one another but demonstrates that the four clay types can be quantified on average. Similarly, Breen et al. (2008)) developed a PLS model from the DRIFTS spectra of mixtures of seven mineral standards encountered in sandstone-type rocks; quartz, dolomite, montmorillonite, illite, kaolinite, chlorite and albite. The results of the PLS–DRIFTS model show that the sum of the individual clay concentrations compares better with XRD concentrations than the individual clay minerals.

A plot of (a) the combined carbonate (calcite and dolomite) and (b) clays (kaolinite and illite-smectite) concentrations are presented (Fig. 3.12) because the model produced relatively poor predictions for the kaolinite and the dolomite. This was anticipated for the carbonates as the attenuated spectra of calcite and dolomite are very similar which might be because of their similar intra-atomic bonds in the carbonate radicals (CO_3)²⁻, structure and properties (Harris et al., 1995). However, the combined predicted concentrations of the minerals were better than the individual mineral. The correlation coefficient between the IR carbonates and the XRD carbonate value ($R^2 = 0.89$) is slightly less than that of calcite alone but significantly more than dolomite alone. The average error for the total carbonates increased to 14.7wt%; although more than half the samples have absolute errors <10wt%, *p* –value of 0.30 shows the two measurements are still statistically comparable. The same trend is observed for the clays (kaolinite + illite-smectite) where the correlation for individual illite-smectite is better than when combined with kaolinite. The combined clays returned average error of 10wt% between the IR predicted and XRD measured concentrations and a *p* – value of 0.38 over the range of samples considered.

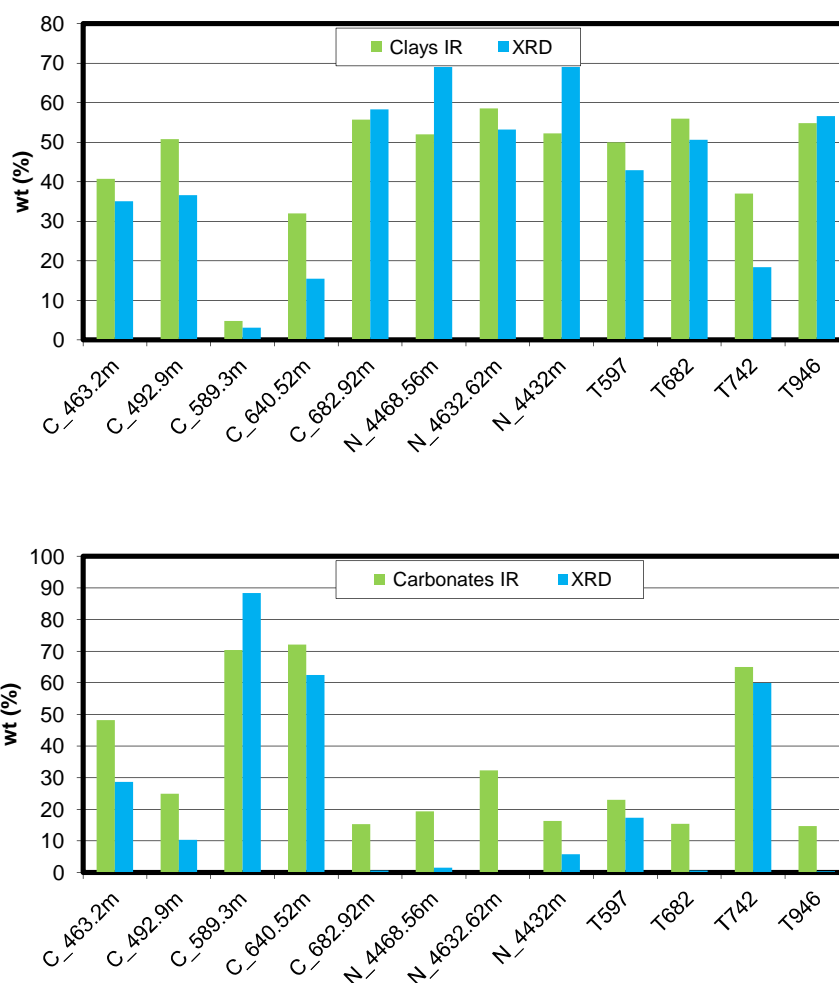


Figure 3.12: Bar charts showing comparison of known concentrations of mineral mixtures (combined clays and carbonates) XRD and ATR-PLS model predicted mineral concentrations in independent shale

C – samples from Western Canada Bigstick core; N- samples from the Nile Delta; T - samples from Western Canada Wildmere core (from Table 3.1)

Despite these limitations for the dolomite and kaolinite minerals, the ATR-PLS model produced good predictions for all the minerals included in the mixtures calibration with average errors of no more than 10 wt %. Previous studies indicate that minerals can be estimated using the IR technique to within 5wt %. For example the DRIFT study of Breen et al. (2008), whose calibration was not able to differentiate between montmorillonite and illite, due to the similarity of the DRIFT spectra of these minerals, but was able to quantify the combined (montmorillonite + illite) concentrations to within 1 wt. %.

Similarly, the results obtained when they applied the PLS–DRIFTS model to several sandstone-type quarry rocks and a suite of oilfield reservoir rocks did not describe all the mineral components present in the samples as is the case with the ATR pure mixtures calibration in this study. They report over-prediction of the concentration of albite in the quarry rocks due to the presence of K-feldspar, which has a similar DRIFTS spectrum and was not included in their model. However, the model predicted the total (albite and K-feldspar) concentration to within 4 wt. %. When they applied a separate PLS–DRIFTS model constructed using the DRIFTS spectra of the oilfield reservoir rocks for the prediction, the carbonate components, calcite and dolomite could be differentiated and quantified to within 5.0 and 3.6 wt. %, respectively.

This shows that more sophisticated models, which incorporate and describe a higher percentage of the variance in unknowns, might further improve the predictions. Such a model could be constructed from data set of cored shales.

3.8.2 ATR-PLS-SR model of shale rocks

As a result of the constraints encountered with the mineral mixture model, a second PLS model was constructed from the ATR spectra recorded from core shale rocks called ATR-PLS-SR in order to determine whether a data set containing natural variability in mineral concentration and crystallinity would affect its ability to predict the concentration of samples of a similar nature. Forty-seven shale samples were selected from the western Canada sedimentary basin and the Nile delta to account for variability from different settings. All the Nile Delta samples (23) come from the same area (Raven Field) whereas 20 samples come from the Bigstick area and four (4) samples from the Wildmere area of the Canada basin. All the shales have been independently analysed for quantitative mineralogy using XRD by the Macaulay Institute, Aberdeen.

ATR spectra of thirty four of the shale samples were used to create the ATR-PLS shale rocks calibration model, while the remaining thirteen were used to validate the model (Appendix I). The model was extended to include two more minerals which are common to these shales and which were not included in the pure mineral mixture model. These are chlorite and feldspars, the feldspar concentrations used in the calibration are a combination of plagioclase and K-feldspars. These were added because their spectra are similar, i.e. do not have unique diagnostic bands distinguishing them, and also because they occur in small concentrations in these shales. Similarly, the dolomite and siderite concentrations were summed together and considered as 'dolomite' prior to the calibration. The shales contain some other minerals such as pyrite and anatase that occur in minor concentrations but which were not included in the calibration. Because it is essential that the total mineral concentrations add up to 100 for the calibration to be accurate, all the minerals were normalised to account for the minor minerals not included in the calibration.

The ability of the ATR-shale model to predict mineral concentrations in independent samples is shown in Figures 3.13 to 3.16. Figure 3.13 show cross plots of the model predicted values against their known XRD values for all the minerals together with their respective correlation coefficients. The solid line passing through the origin represents a one-to-one comparison of the two methods with dotted lines above and below indicating prediction within ± 5 wt. %.

The model predictions for quartz and calcite were very good with correlation coefficients > 0.9 and absolute errors within $\pm 5\text{wt } \%$ for 90% and more than 50% of the samples for the quartz and calcite respectively. The correlation coefficients for the kaolinite and illite-smectite are 0.89 and 0.80 with about 85% of the data falling within $\pm 5\text{wt } \%$ absolute error for the kaolinite concentrations. There is more scatter for the illite-smectite prediction where more than 50% of the samples fell outside the $\pm 5\text{wt } \%$ absolute error margin. The feldspars and chlorite were predicted within absolute errors of $\pm 2\text{wt } \%$ and $\pm 4\text{wt } \%$ despite having low correlation coefficients of 0.77 and 0.53 respectively.

Generally, all the mineral concentrations were estimated with an average error of $< 5\text{wt } \%$ (Table 3.6; quartz, 3.1; feldspars, 0.6, kaolinite, 3.1; chlorite, 1.5) except, for illite-smectite with 5.8wt% and calcite and dolomite with 9.6wt % and 5.9wt % respectively. This highlights the problem of distinguishing between the clays and carbonates minerals using the multivariate analysis mostly due to spectral similarities that arises due to similarities in chemical compositions of minerals in the same group.

The results show that the ability of the model to predict the mineral concentrations was reasonable despite the low correlation coefficients, although, the relative error at low concentrations is high. This model was able to predict the minerals separately with improved accuracy compared to the pure mineral mixture model.

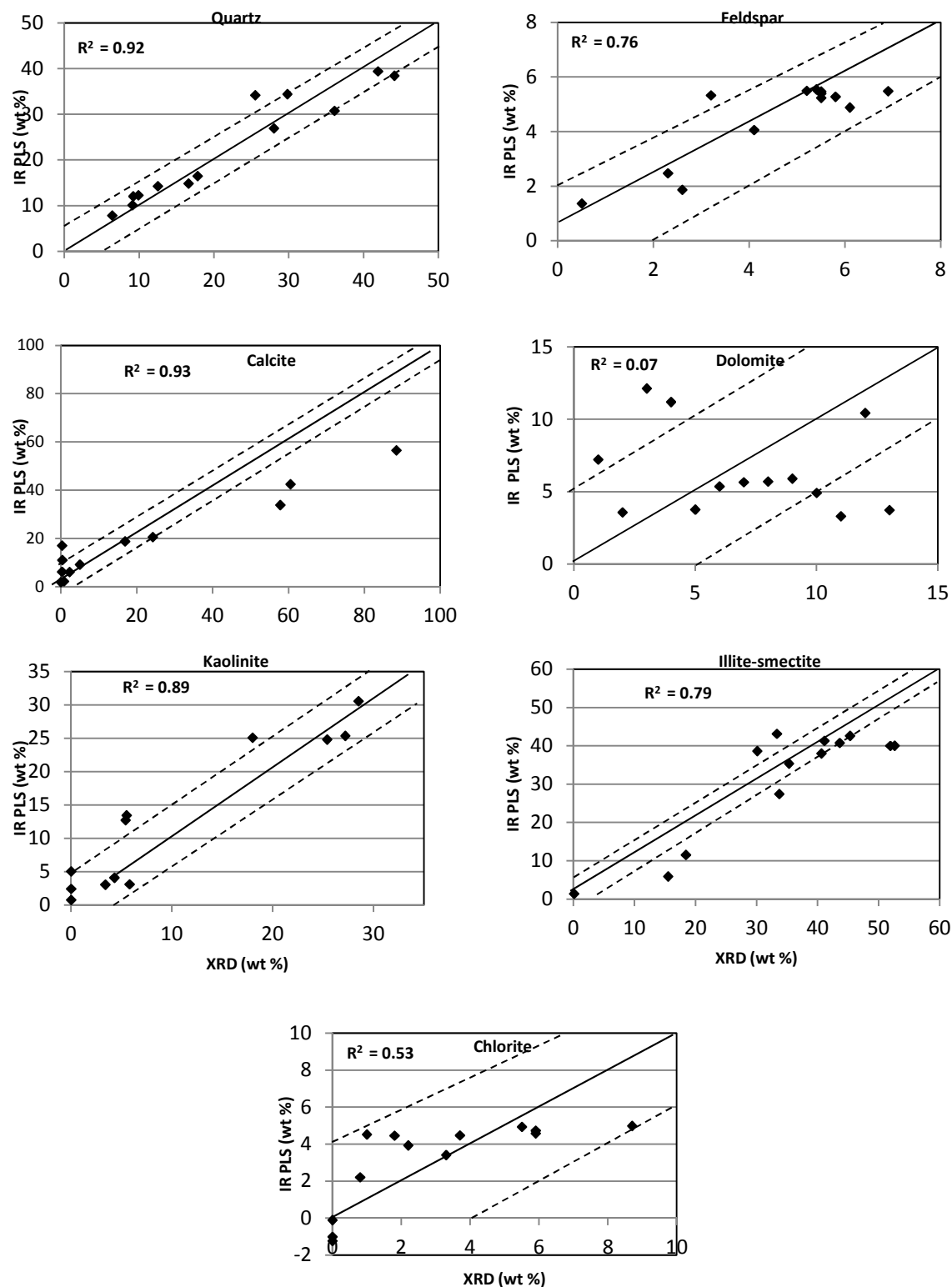


Figure 3.13: Plots of measured minerals concentration against the PLS-predicted concentration for the validation sets showing correlation coefficients for the ATR-PLS-Shale Model



Figure 3.14: Bar charts showing comparison of known concentrations of mineral mixtures (XRD) and ATR-PLS model predicted mineral concentrations for validation set shales

C – samples from Western Canada Bigstick core; N- samples from the Nile Delta; T - samples from Western Canada Wildmere core (from Table 3.1)

The combined plots of the total clays and carbonates are given in Figures 3.15 and 3.16. The scatter plots show that overall, the estimation for the total clays which was obtained by adding by the predictions of chlorite, kaolinite and illite-smectite, significantly improved with a correlation coefficient of 0.95 and more than 80% of the samples estimated were within $\pm 5\text{wt } \%$ error and average error of $4.4\text{wt } \%$. In contrast, the combined plot show that the ability of the ATR-PLS model to predict carbonates (calcite + dolomite) concentration is less accurate with a correlation coefficient of 0.86 and values generally having absolute errors up to $10\text{wt } \%$ and average error of $10.5\text{wt } \%$.

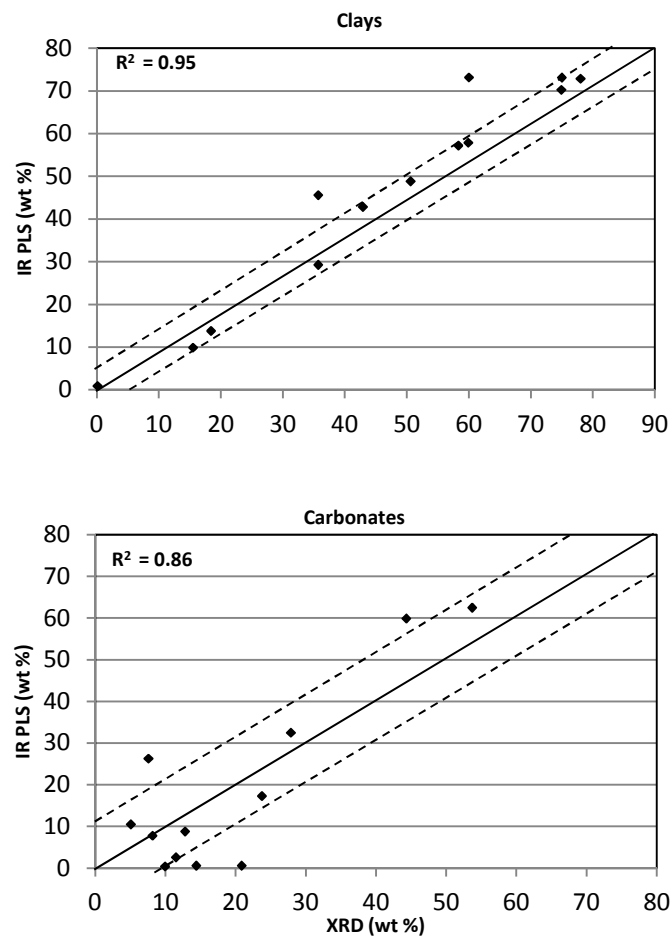


Figure 3.15: Plots of measured minerals concentration for the combined clays and carbonates against the PLS-predicted concentration for the validation sets showing correlation coefficients for the ATR-PLS-Shale Model. Carbonate shows a better correlation overall, because calcite $R^2 = 0.93$ and Dolomite $R^2 = 0.07$

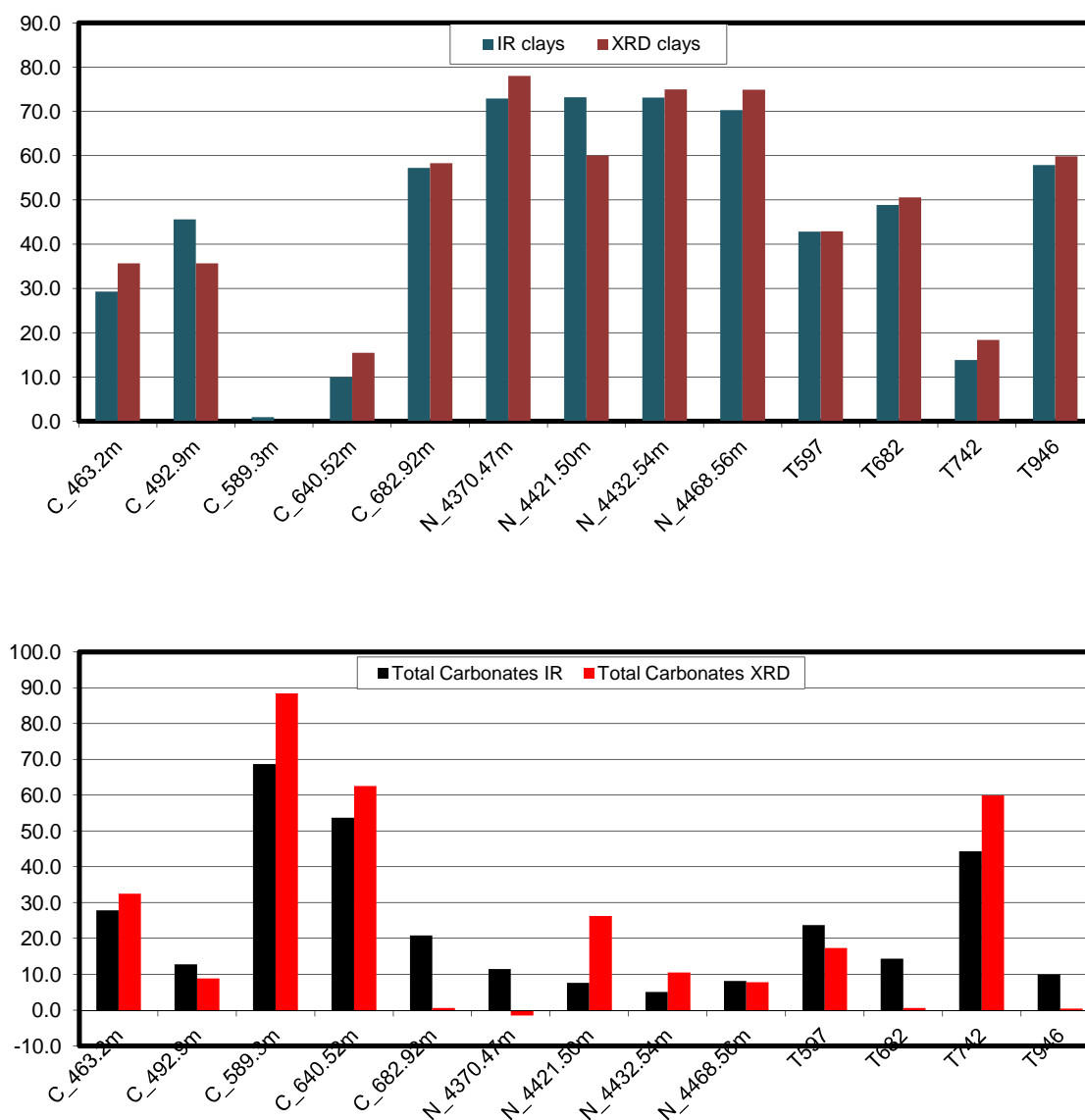


Figure 3.16: Bar charts showing comparison of known mineral concentrations (XRD) and ATR-PLS-Shale model predicted mineral concentrations for validation set (samples from Western Canada and Nile Delta) on combined clays and carbonates

C – samples from Western Canada Bigstick core; N- samples from the Nile Delta; T - samples from Western Canada Wildmere core (from Table 3.1)

The bar charts demonstrate that although the model occasionally under or over predicts the mineral concentration the patterns are similar to those predicted by XRD and most importantly within $\pm 5\text{wt}\%$ of the true XRD values.

3.8.3 Application of the (ATR-PLS-SR) model of shale rocks to Independent shale samples

The ATR-PLS model of shale rocks was applied to predict the mineral concentration in entirely new shale samples different from the ones used in the calibration set. Twelve shale samples of varying mineral composition supplied by Conoco Phillips with two independent XRD measurements conducted by Conoco Phillips referred to as base XRD in this report and XRD measurements conducted by Core Laboratories referred to as terra in this study (Appendix I) were compared against the IR predicted concentrations using the shale rock model. The shales were derived from five different formations including: Indian Castle, Nordegg, Fernie, Montney and Duvernay and captures a wide range of shale compositions from siliclastic-shale to calcareous shale and limestone.

The predictions for quartz compare reasonably well with the two XRD measurements in all the samples with an absolute error <5wt % (Fig 3.17). The only exceptions are the Nordegg-black chert sample where the IR underpredicted by 10wt% and the Nordegg-calcareous sand where there is significant underestimation compared to both XRD values. While this is a major concern, it is thought that small scale heterogeneity may have caused the wide error since analyses were not run on the same sample aliquots.

The results indicate that the ability of the ATR-PLS-SR model to predict kaolinite and the feldspars in independent sample set was poorer than the validation sub-sample sets of similar shales have suggested (Fig. 3.18). Chlorite and kaolinite are always identified by IR but not generally picked up the XRD. This was possibly due to artefacts errors associated with the software as the range of these two minerals is within the error margin of around 5wt%, and also possibly due to the fact that the spread of kaolinite and feldspars concentration of the shale samples used in the calibration did not cover the optimum ranges. The maximum concentration of feldspars in the calibration set is <10wt% whereas the range in some of these shales (i.e. Montney shales) measured by XRD is over 20wt%. Apart from the Indian Castle shale and the Fernie Shale, kaolinite has not been detected by the two XRD measurements for all the samples as against the IR prediction which predicts kaolinite concentrations of < 9% in all the samples (Fig 3.18). However, all the kaolinite IR predicted concentrations are within 8wt %, with a mean value of 6.8, sufficient to say that the average errors are still within

10wt %. This implies that model predictions for mineral concentrations below 10% is less accurate compared to minerals that occur in higher concentrations (>10%).

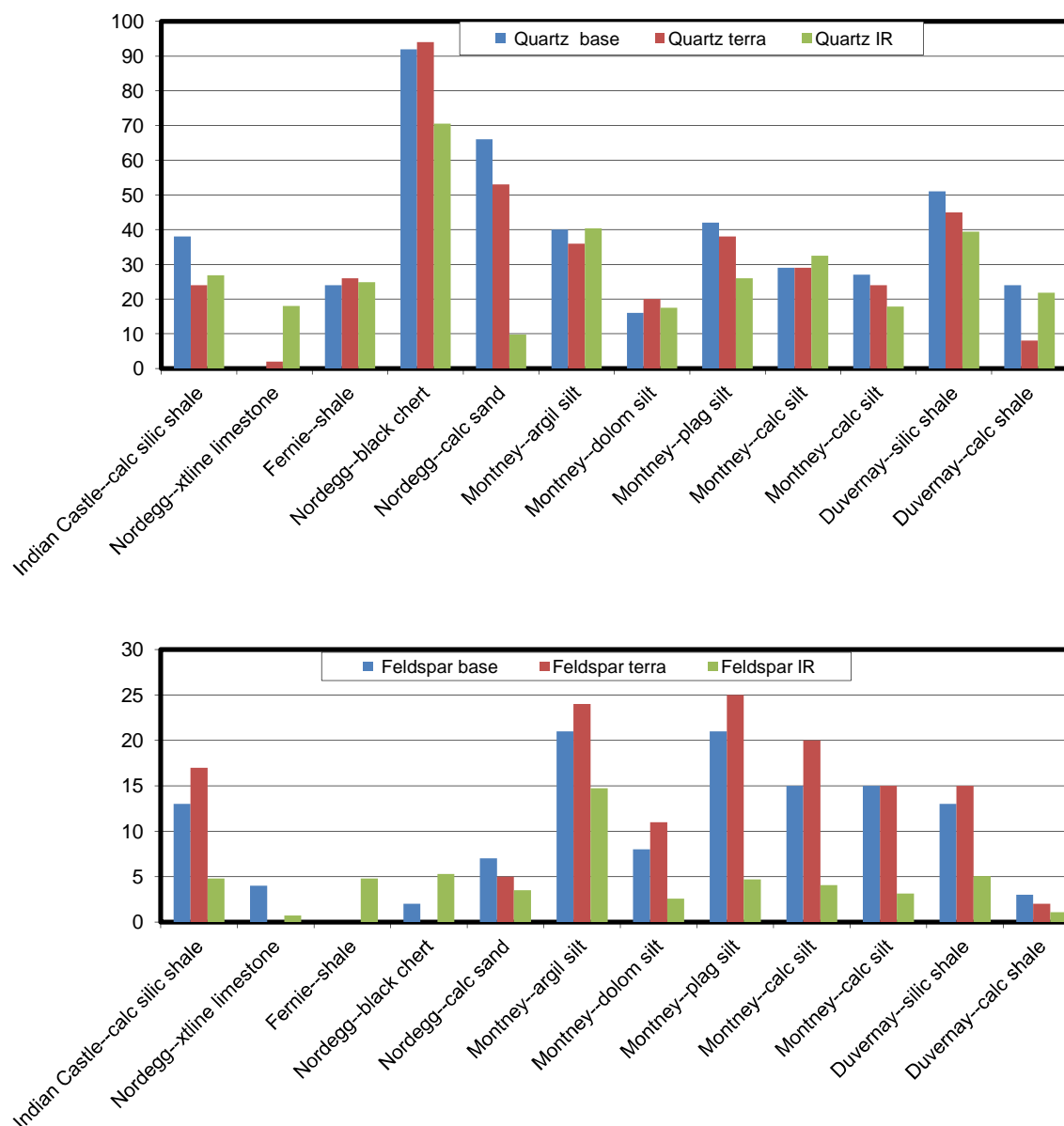


Figure 3.17: Bar charts showing comparison of known concentrations of quartz and feldspars(XRD) and ATR-PLS-Shale model predicted mineral concentrations for independent shales. Base-Conoco Phillips XRD measurements, Terra- Core Labs XRD measurements.

The IR predicted concentrations for the mixed layer I-S compared better with the Core Labs terra XRD values than with Conoco Phillips base XRD values. The Nordegg-calcareous sand and Montney-plagioclase shales show the highest deviations (~20 wt %).

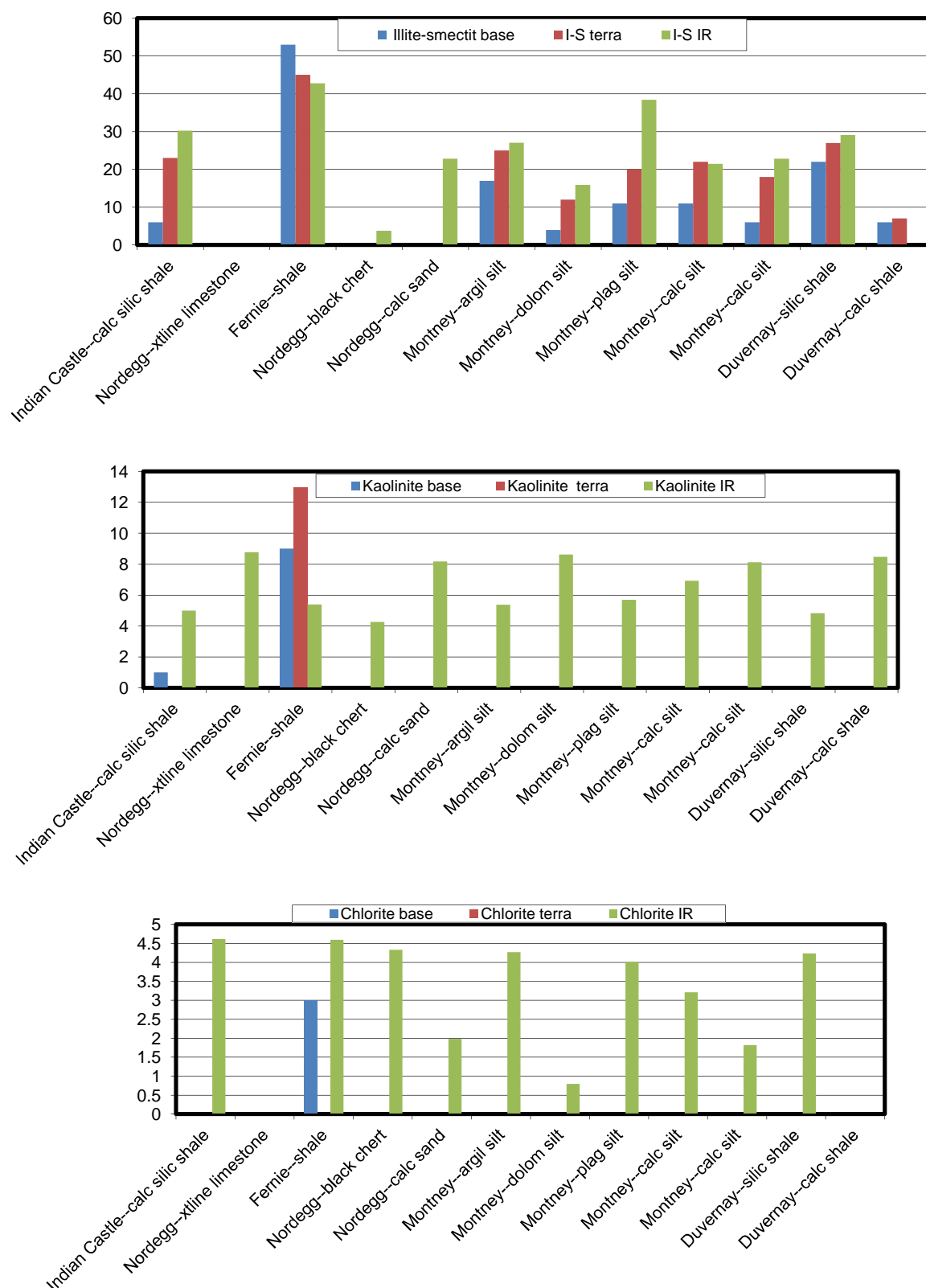


Figure 3.18: Bar charts showing comparison of known concentrations for the clays (XRD) and ATR-PLS-Shale model predicted mineral concentrations for independent shales. Base-Conoco Phillips XRD measurements, Terra- Core Labs XRD measurements.

The difference between the two XRD measurements in the Indian Castle shale for the illite-smectite is ~17wt% and this shows that significant difference can occur even within different XRD measurements of the same sample. This may be due to differences in sample preparations or simply because of subtle differences in mineralogy due to sample heterogeneity. Furthermore, differences in XRD standards may potentially results in different quantification of the same mineral. The illite-smectite predictions in all the other samples compares well between both XRD measurements with absolute error of <2wt%. The fact that neither the IR nor the two XRD analysis detected illite-smectite in the Nordegg limestone demonstrates the strength of the IR technique in estimating the mineral concentrations.

The prediction for the calcite and dolomite show significant improvement compared with the mineral mixture model prediction on blind shale samples. The IR values agree with the two XRD values, however, the predictions in the Indian Castle and Montney samples indicate that the distinction between the carbonates remain a problem. The IR did not detect any calcite in the Indian Castle shale while the XRD values both show calcite concentration of 23wt % and in turn the IR estimated 37% dolomite while the XRD analyses all measure just <10% in the same sample (Fig. 3.19). Similarly, in the Montney dolomite shale, the IR predicted the dolomite as calcite, estimating 43% calcite and 0% dolomite where as the XRD measures 20% calcite and 35% dolomite (Fig. 3.19). Although the model was not able to distinguish between calcite and dolomite with sufficient accuracy, the calcite predictions compare well with measured values with absolute error within 10wt % for 70% of the samples with an average error of 12.3%.

Figure 3.20 shows plots for the combined clays and carbonates indicating that the prediction ability of the shale model is significantly improved in estimating combined species than in predicting individual mineral within a group.

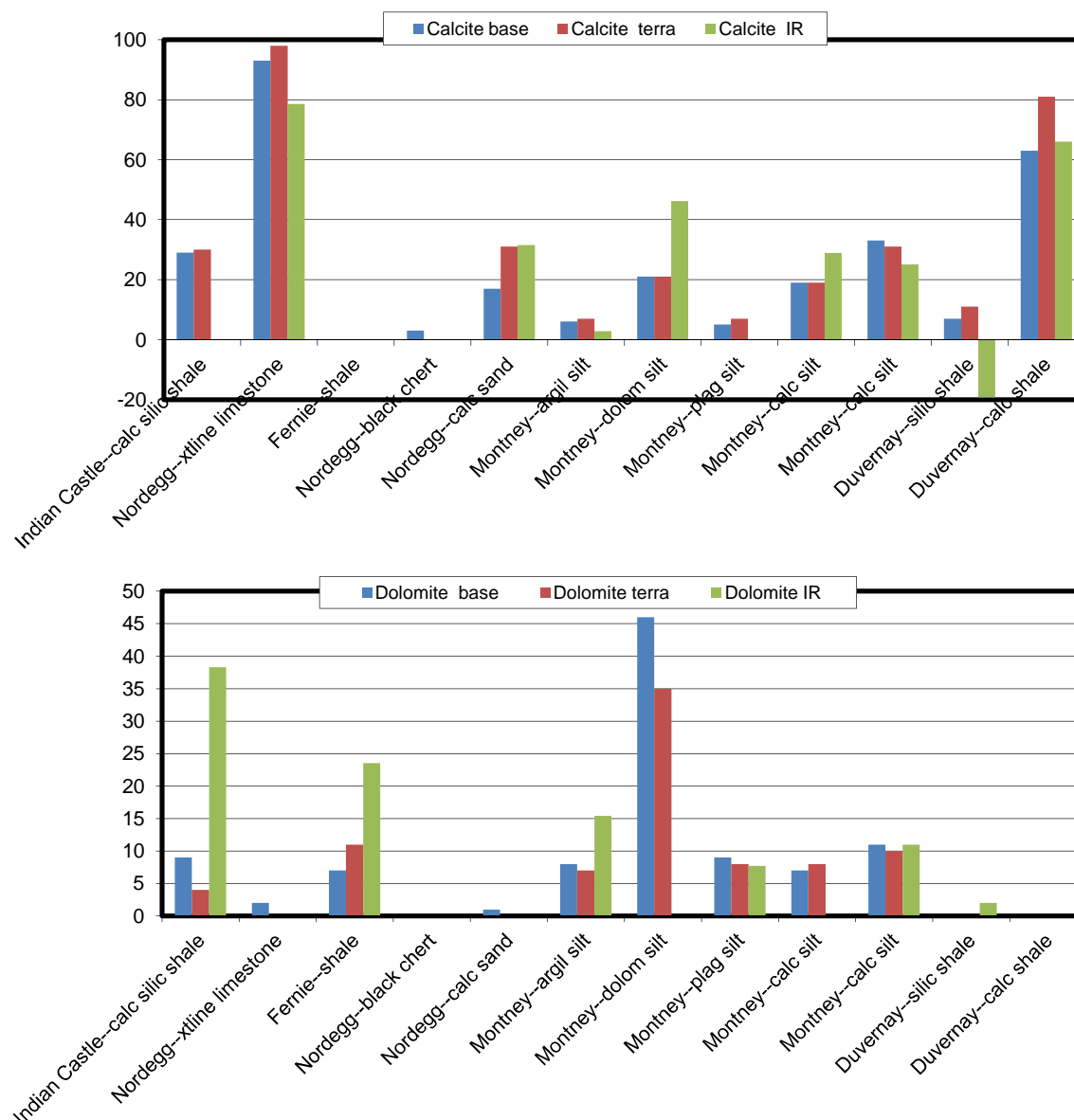


Figure 3.19: Bar charts showing comparison of known concentrations for the carbonates (XRD) and ATR-PLS-Shale model predicted mineral concentrations for independent shales. Base-Conoco Phillips XRD measurements, Terra- Core Labs XRD measurements.

The IR combined clays compares better with the Conoco-Phillips base XRD measurements than with the Core labs terra measurements, unlike the I-S which compares better with the Core labs terra measurements than with the Conoco-Phillips base. The absolute errors for the clays and carbonates are within 10wt% with an absolute average error of 6.4 and 9.0 for the clays and carbonates respectively. A statistical summary for the IR measurements against the XRD measurements is presented in Tables 3.6 & 3.7.

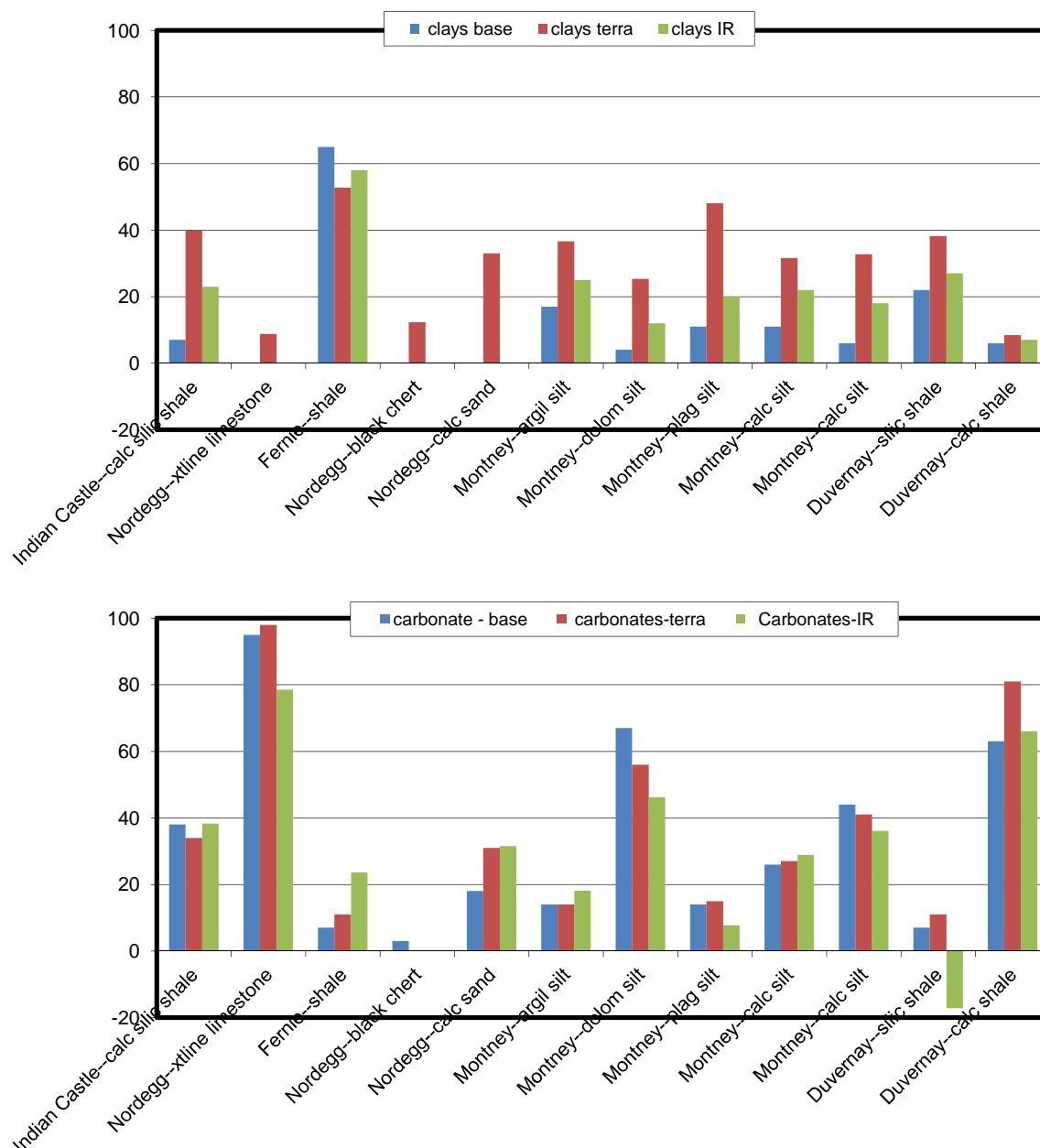


Figure 3.20: Bar charts showing comparison of known concentrations for total clays and total carbonates (XRD) and ATR-PLS-Shale model predicted mineral concentrations for independent shales. Base-Conoco Phillips XRD measurements, Terra- Core Labs XRD measurements.

In summary, the ATR-PLS-SR model has shown that prediction on a sub set samples of the same origin as the calibration set is accurate to within 5wt % for all the minerals except for the carbonates. The prediction for the total clays and carbonates has shown that the clays can be estimated within 5wt% but up to 10wt% for the carbonates.

Table 3.8: Errors for the ATR-PLS-SR model on validation set shales

	Quartz	Feldspars	Calcite	Dolomite	Kaolinite	chlorite	Illite-smectite	Clays	Carbonates
Average error (wt %)	3.1	0.6	9.6	5.9	3.1	1.5	5.8	4.4	10.5
STD	3.9	0.9	13.9	8.1	3.7	1.9	6.9	5.9	12.7
std error	1.1	0.3	3.9	2.3	1.0	0.5	1.9	1.6	3.5

Table 3.9: Errors for the ATR-PLS –SR model on independent (blind) shales

	Quartz	Feldspars	Calcite	Dolomite	Kaolinite	chlorite	Illite-smectite	Clays	Carbonates
Average error (wt %)	11.2	8.4	12.3	8.5	6.8	2.8	6.2	6.4	9.0
STD	16.2	8.2	15.9	15.6	4.5	1.8	8.4	6.6	11.5
std error	4.7	2.4	4.6	4.5	1.3	0.5	2.4	1.9	3.3

Application of the ATR-PLS-SR model to independent shales from different formations resulted in greater errors but predictions are still within 5-10wt% for all the minerals. These errors can be attributed to the fact that the spread of mineral concentrations did not cover the optimum ranges. The range of kaolinites in the calibration samples is concentrated between 0-10% and 20-30%, samples with concentrations in the range of 10-20wt% were generally absent. The range of quartz at high concentrations (60wt% and over) were not well spread. Therefore, further development on the calibration is necessary to include a larger number of real samples and pure minerals with concentrations that covers all the expected variability.

3.8.4 ATR-PLS model of semi-artificial shale rocks (ATR-PLS-SMM)

Since the samples used as a calibration set in the ATR-PLS-SR did not cover the optimum ranges for all the minerals, the calibration dataset was extended to include broader range of shales concentrations amended by adding known weights of pure minerals. In essence, the shale mineralogy was altered by mixing with pure minerals thereby creating semi-artificial mixtures containing new concentrations of the minerals. The pure standard minerals were added in known amounts as (wt %) to selected rocks from the Western Canada Sedimentary Basin and from the Nile Delta (Appendix I) thus increasing the concentration of the added mineral and reducing the concentrations of the remaining minerals which were then normalised to give the relative concentrations of all the minerals in each sample.

Sixty-three natural shale samples and mixtures of shale plus pure minerals were used in creating the third model (ATR-PLS-SMM) from spectra of shales plus mineral mixtures in order to obtain a calibration that captures a wide range of mineralogies. This was important because the calibration will be able to account for variabilities that may arise between the same mineral deposited or formed in different environmental settings. Differences in crystallinity between the shales and the pure minerals may mean the model predictions are less reliable. Forty-five of the mixtures were included in the calibration while the remaining 18 were used in the model validation.

Figure 20 shows the modelled results comparing the PLS predicted values against the known weight values for the minerals. The correlations coefficient shown on the graph is for the validation samples. Generally, strong correlations were obtained for all the minerals between the model predicted values and the known values. The figure also shows the range of values used for each mineral and their distributions. In all the minerals have $R^2 > 0.8$, except for the chlorite.

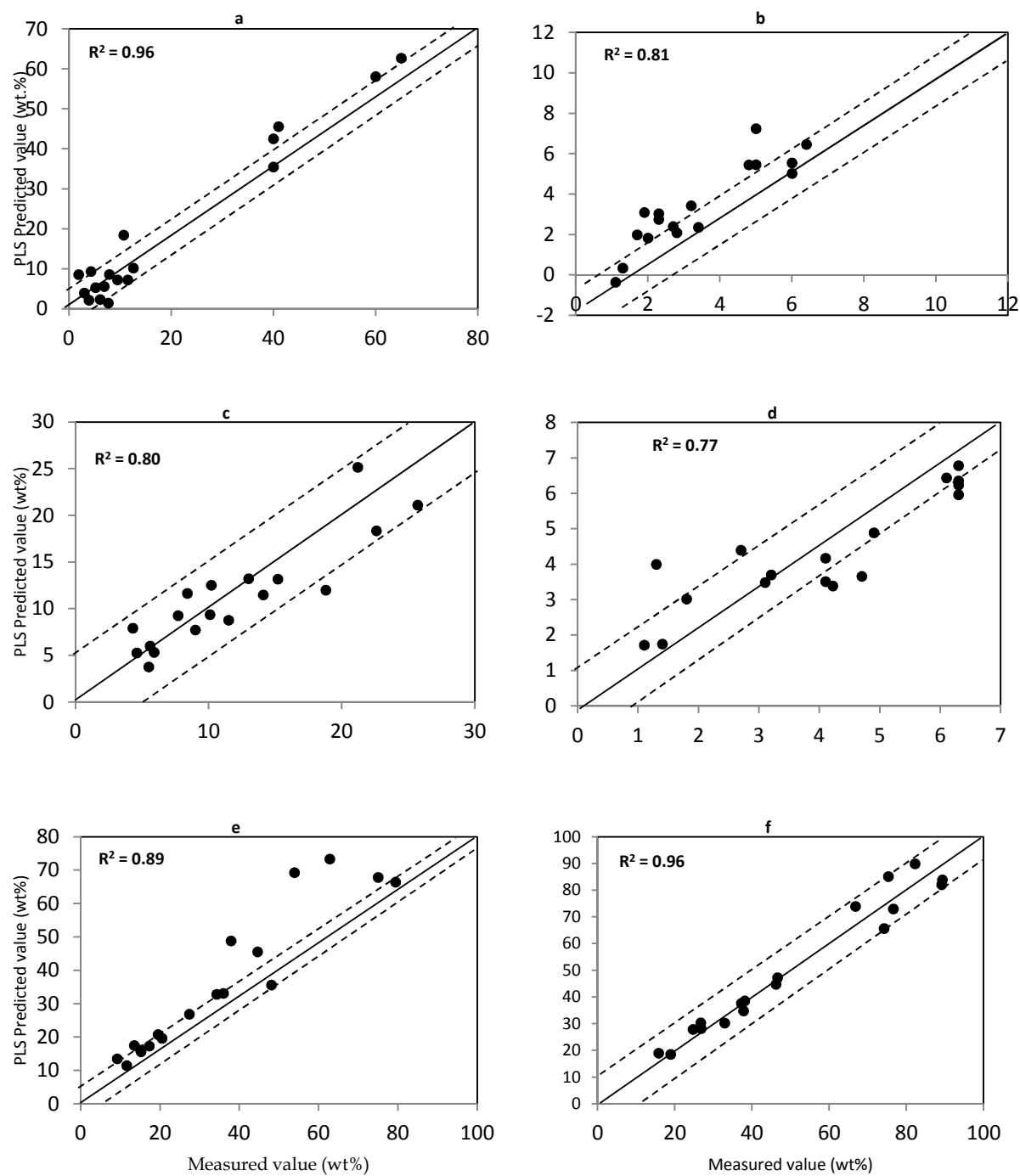


Figure 3.21: Plots of measured minerals concentration for (a) quartz, (b) feldspar, (c) kaolinite, (d) chlorite, (e) illite-smectite and (f) combined clays against the PLS-predicted concentration for the validation sets showing correlation coefficients for the ATR-PLS-SMM Model

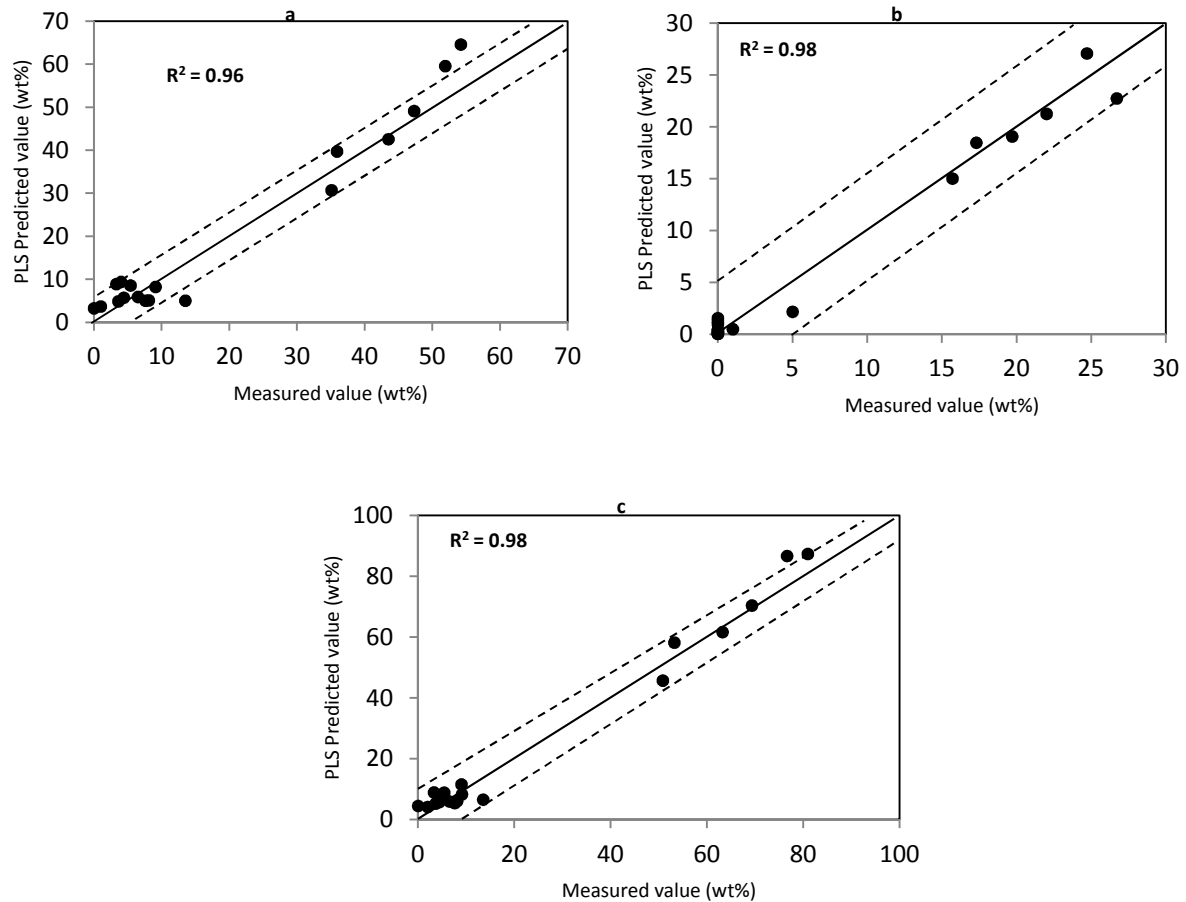


Figure 3.22: Plots of measured minerals concentration for (a) calcite, (b) dolomite, (c) combined carbonates against the PLS-predicted concentration for the validation sets showing correlation coefficients for the ATR-PLS-SMM Model

The correlation coefficient of the predicted vs. measured quartz wt% is > 0.96 and using the ATR-PLS-SMM Model improved the combined clays and carbonates to more than 0.9 indicating that that prediction is more accurate for the combined groups than individual clay or carbonate minerals. The plots show that the model is able to distinguish between the clays and carbonates although the prediction accuracy is greater when each group is combined. All the minerals were estimated with an average error within 5wt% (Table 3.8). The average errors of 3.3wt & 3.7wt% were calculated for quartz and calcite respectively. The feldspars, dolomite and chlorite were estimated with an average errors of $< 1\text{wt}\%$; 0.7 for feldspar and chlorite and 1wt % for dolomite. The highest errors were calculated for the illite-smectite with average value of 4.9wt% but kaolinite has an average error of only 2.4wt%. Combined clays and carbonates were predicted with average errors of 3.9 and 3.5wt% respectively. This

shows that a robust calibration is capable of estimating mineral concentrations of similar samples with accuracies between 0 - 5 wt percent for all minerals.

Table 3.10: Errors for the ATR-PLS-SMM model on validation set shales

	Quartz	Feldspars	Calcite	Dolomite	Kaolinite	chlorite	Illite-smectite	Clays	Carbonates
Average error (wt %)	3.3	0.7	3.7	1.0	2.4	0.7	4.9	3.9	3.5
STD	4.0	0.9	4.5	1.5	3.0	0.9	7.2	5.0	4.2
std error	0.9	0.2	1.1	0.4	0.7	0.2	1.7	1.2	1.0

3.8.5 Application of ATR-PLS-SMM to independent shale samples

The ATR-PLS-SMM model was used to predict the mineral concentrations in 9 shale samples supplied by Conoco Phillips; results are presented in Figures 3.23 to 3.25.

Figure 3.23 shows the comparisons between three types of Duvemay shales; a siliceous shale, calcareous shale and pyrite-rich shale. IR predicted values compared very well for the siliceous and calcareous shales (error within 5wt% for most minerals, but up to 10wt% in some) but did poorly in the pyrite nodule.

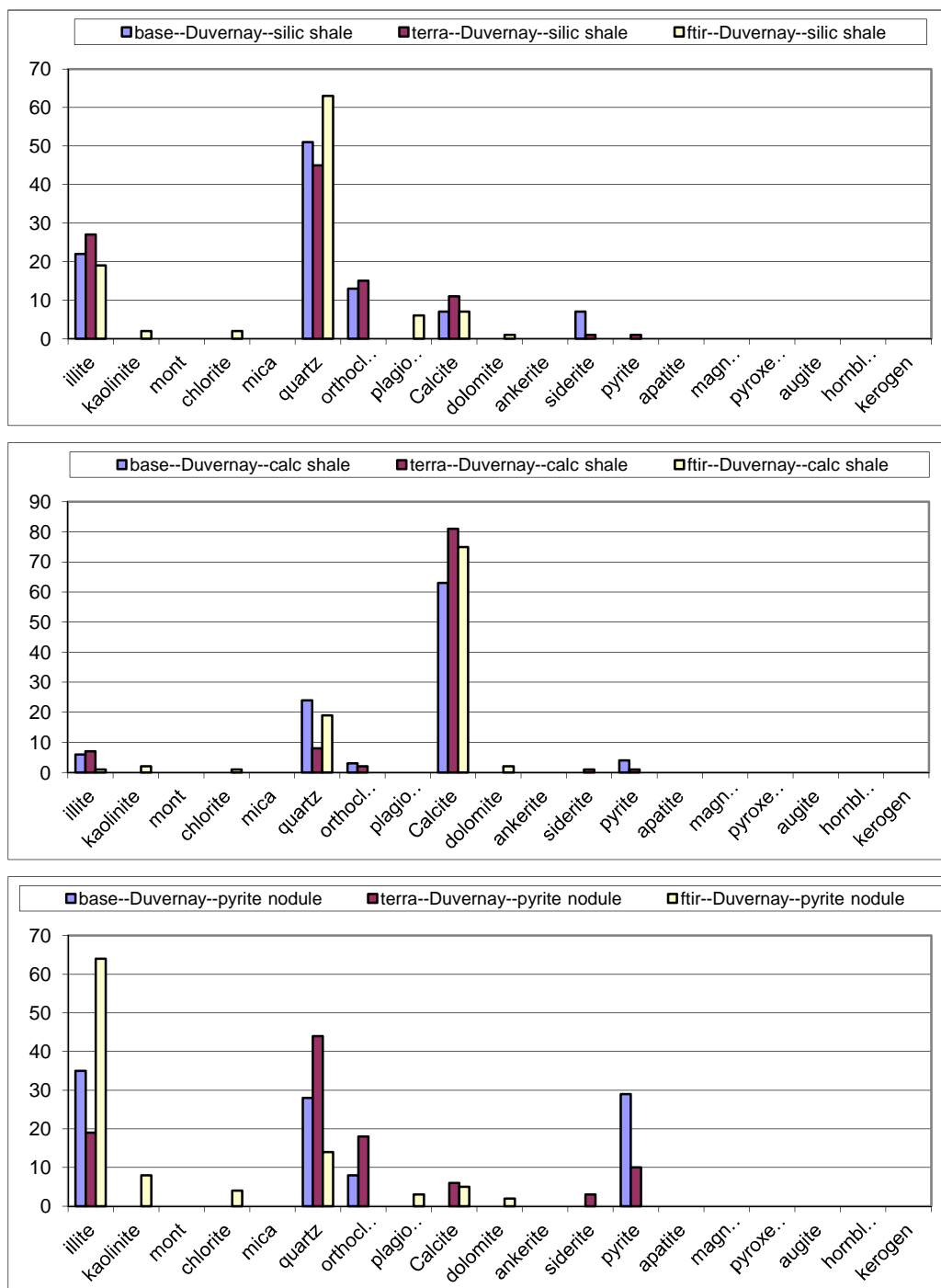


Figure 3.23: Bar charts comparing two XRD mineral concentration for Duvernay siliceous, calcareous and a pyrite type shales against the IR-predicted concentration for the ATR-PLS-SMM Model

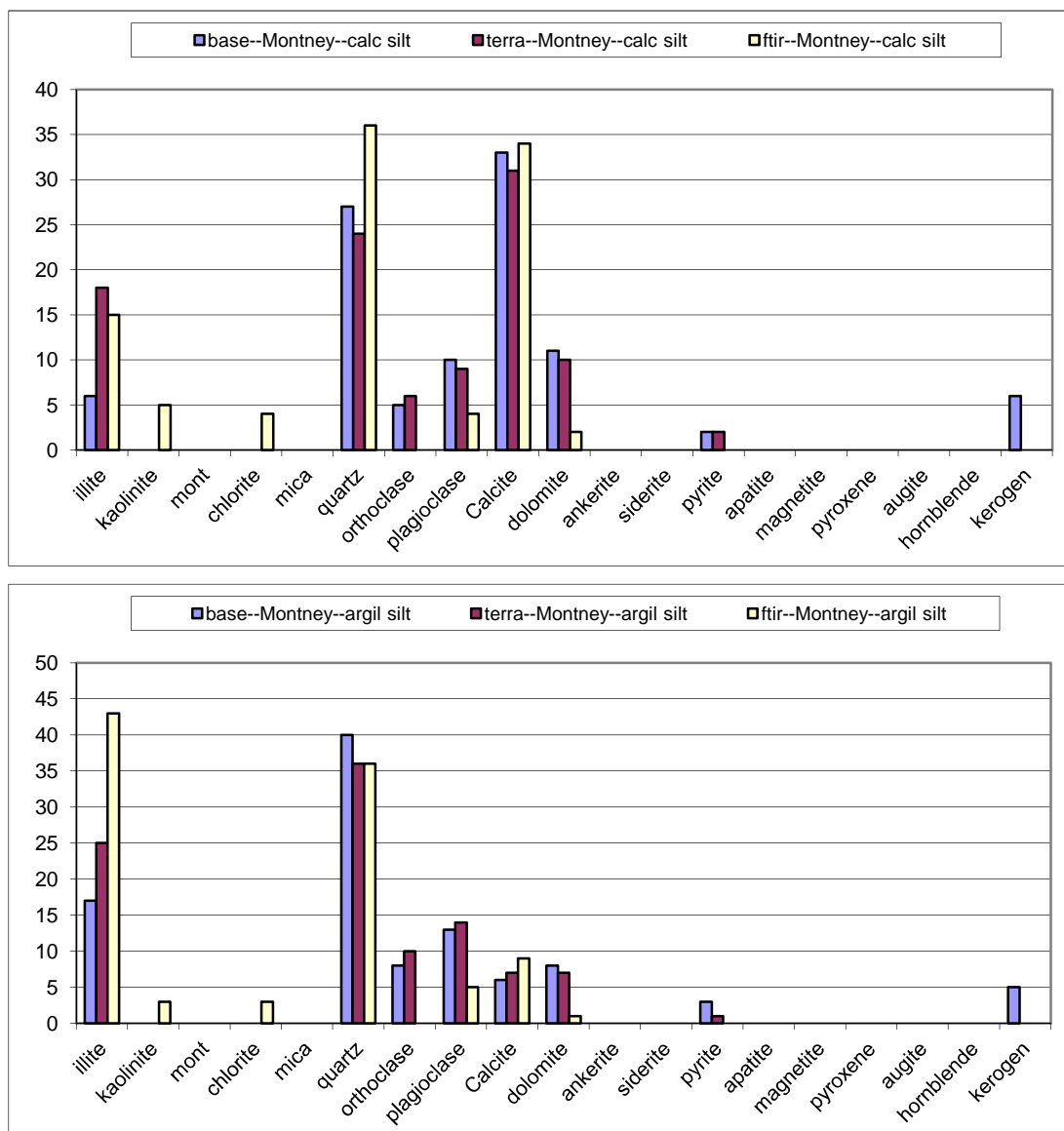


Figure 3.24: Bar charts comparing two XRD minerals concentration for Montney calcareous and an argillaceous type shales against the IR -predicted concentration for the ATR-PLS-SMM Model

This is not unexpected because pyrite (FeS_2) which occurs in concentrations up to ~30%, as measured by the base XRD, and has not been included in the calibration. The pyrite is interpreted to result in the overestimation of the mixed-layer clays since both contain Fe^{+2} .

The mineralogy of two types of Montney shales; calcareous siltstones and argillaceous siltstones are presented in figure 3.24 showing the comparison of IR predicted concentrations against XRD measurements. Both shales contain about 2% pyrite and 5% kerogen which were not accounted for in the ATR-PLS-SMM model calibrations. Despite this, the model predicted well for all the minerals in both shales with errors <10wt%.

In Figure 3.25 the ability of the IR to estimate the concentration of a single dominant mineralogy is demonstrated. Two Nordegg shales consisting of a dominantly crystalline limestone and calcareous sandstone show the IR predicted values compares with the XRD measurements to within 5-10wt % error margin. The XRD techniques measured 10% apatite in the calcareous sandstone and none of the clays, whereas the IR predicted ~10% mixed layer clays in the Nordegg calcareous shale. Because apatite ($\text{Ca}_{10}(\text{PO}_4)_6(\text{OH}, \text{F}, \text{Cl}, \text{Br})_2$) was not part of the calibration, it is assumed that the model assigned the apatite concentration to the clays because both contain high concentration of hydroxyl groups and thus both minerals may contain similar absorption bands in the OH stretching and bending regions of the spectrum, although this needs to be investigated.

The mineralogy of two additional shales; the Indian Castle shale and the Fernie shale are presented in figure 3.26. The plots show the limitation of the model in distinguishing between minerals of the same group when the model is applied to estimate mineralogy in independent (blind) samples. In the Fernie shale, IR predicted 8% calcite 0% dolomite; whereas, the XRD measurements calculated 0% calcite and 8-12% of the dolomite. The IR estimation for the mixed layer (illite-53%) is closer to the terra XRD (illite-46%) values than with the base (illite-29%). However, the base XRD calculated 23% of montmorillonite which when combined with the illite gives a total of 52%.

The mineral concentrations for the two XRD and IR measurements in the Indian Castle shale highlights that some of the differences could be due to sample variability and differences in sample preparation. For example, the terra XRD and IR estimated equal concentrations for the illite (21% each), but the base XRD measured only 6% illite. In contrast, the base XRD and IR compares better in the estimation of quartz with 38% and 48% respectively, while the terra XRD measured only 22%. The XRD measurements compared better for the plagioclase and the carbonates than either with the IR values.

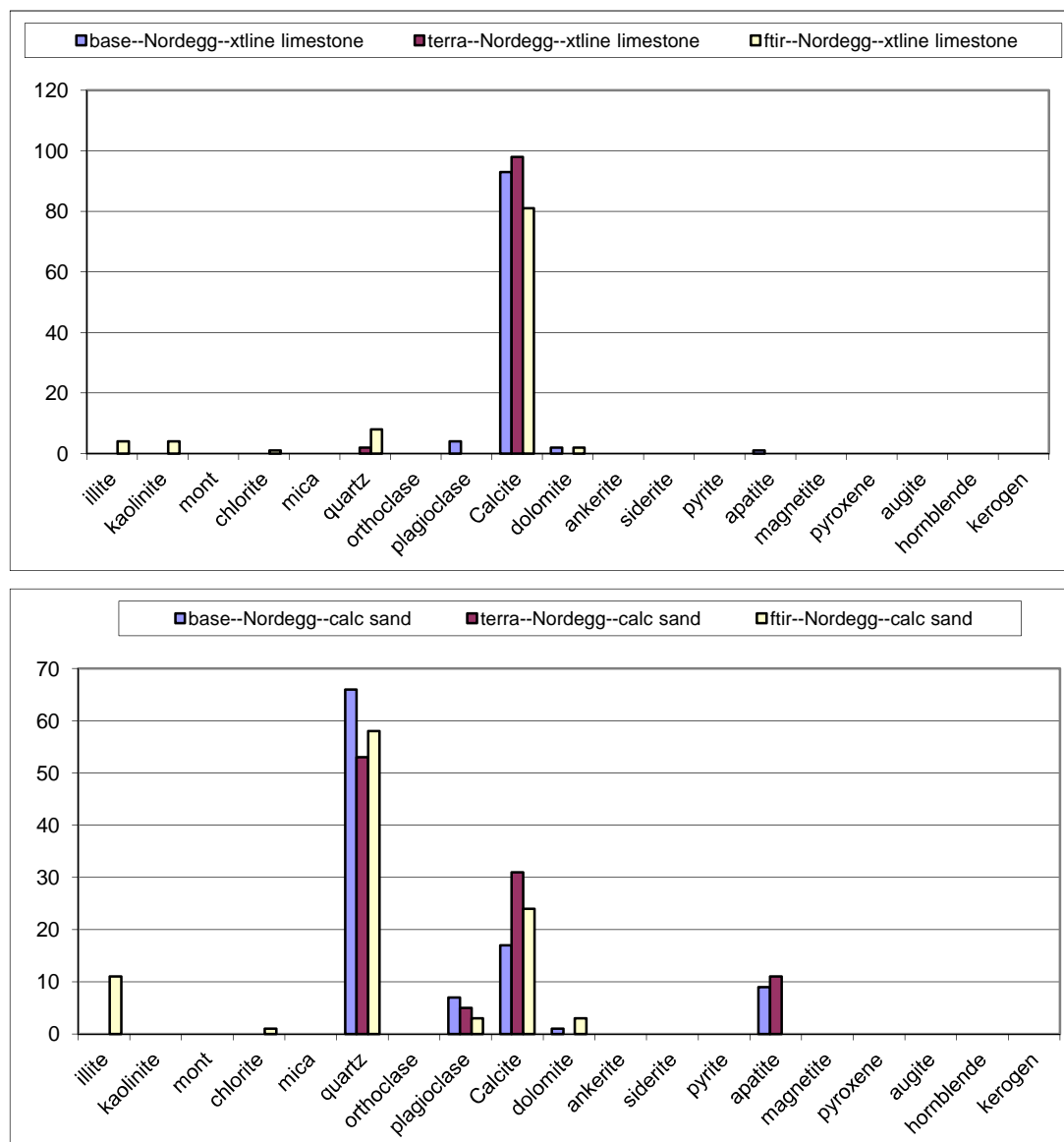


Figure 3.25: Bar charts comparing two XRD minerals concentration for Nordegg crystalline and a calcareous type shales against the IR -predicted concentration for the ATR-PLS-SMM Model

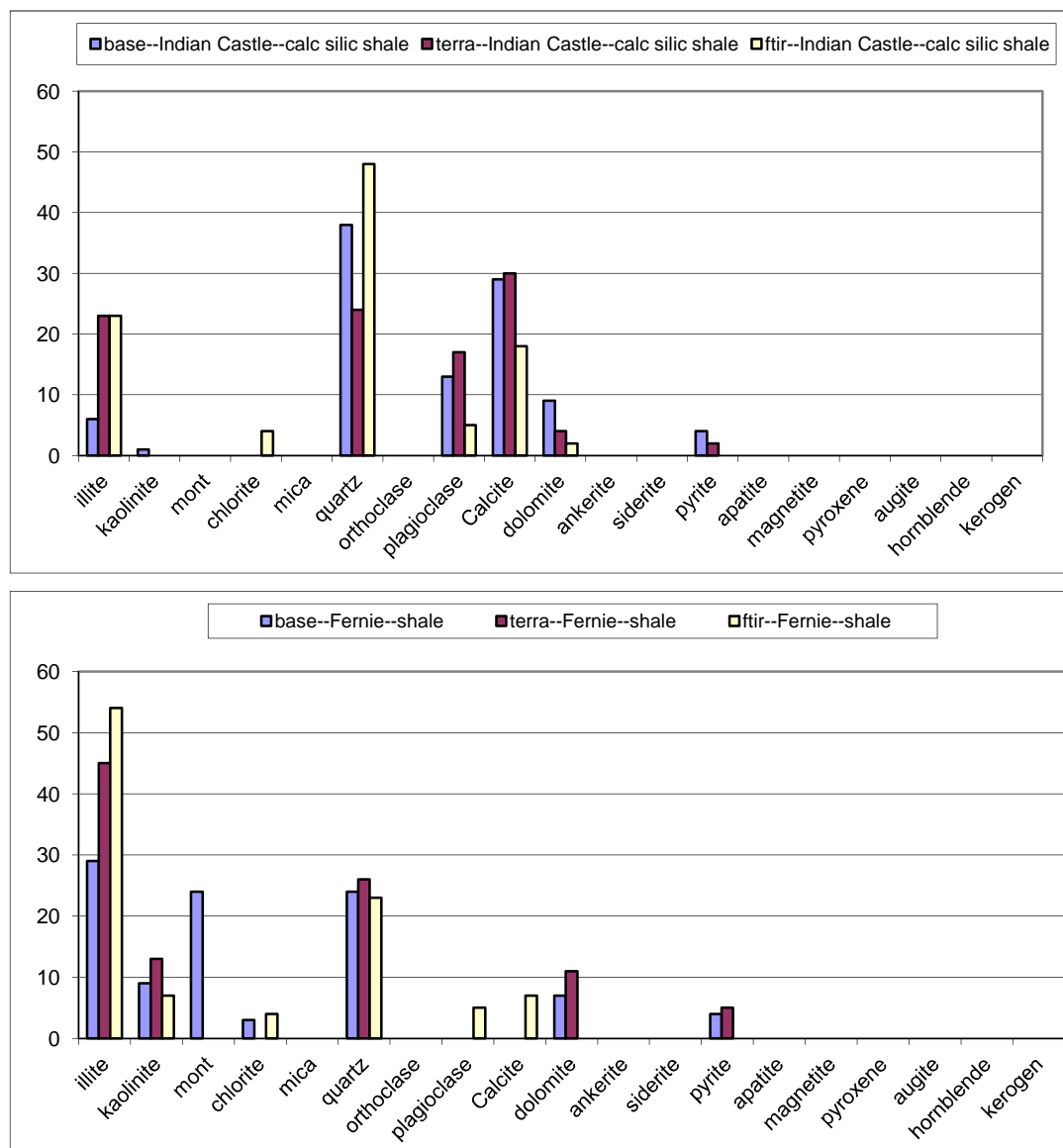


Figure 3.26: Bar charts comparing two XRD minerals concentration for Nordegg crystalline and a calcareous type shales against the IR -predicted concentration for the ATR-PLS-SMM Model

3.9 Application of the FTIR Mineralogy to create a Mineralogy Log

The ATR-PLS-SMM calibration was run on a 22m thick shale gas formation, and a mineralogy concentration log created (Fig. 3.27). The data represent 209 core samples from a single wellbore taken at 1cm intervals. The interval between 506-507m was not sampled. The log shows that the most abundant mineral found is the illite-smectite with an average concentration of 59.7%. The average value for quartz is 14.4%, kaolinite with 9.6%, feldspars 3.2% and chlorite 2.6%. The average concentration of 6.5% and 1.6% values were measured for calcite and dolomite but calcite is present in concentration between 5 and 22%. Three distribution patterns can be gleaned from the data. The interval between 498.0 – 504.7m contain variable amount of quartz and illite-smectite. This is followed again by an interval of variable amount of quartz and illite-smectite between 513.3-519.2m and an interval of carbonate streak at 519.3-520m.

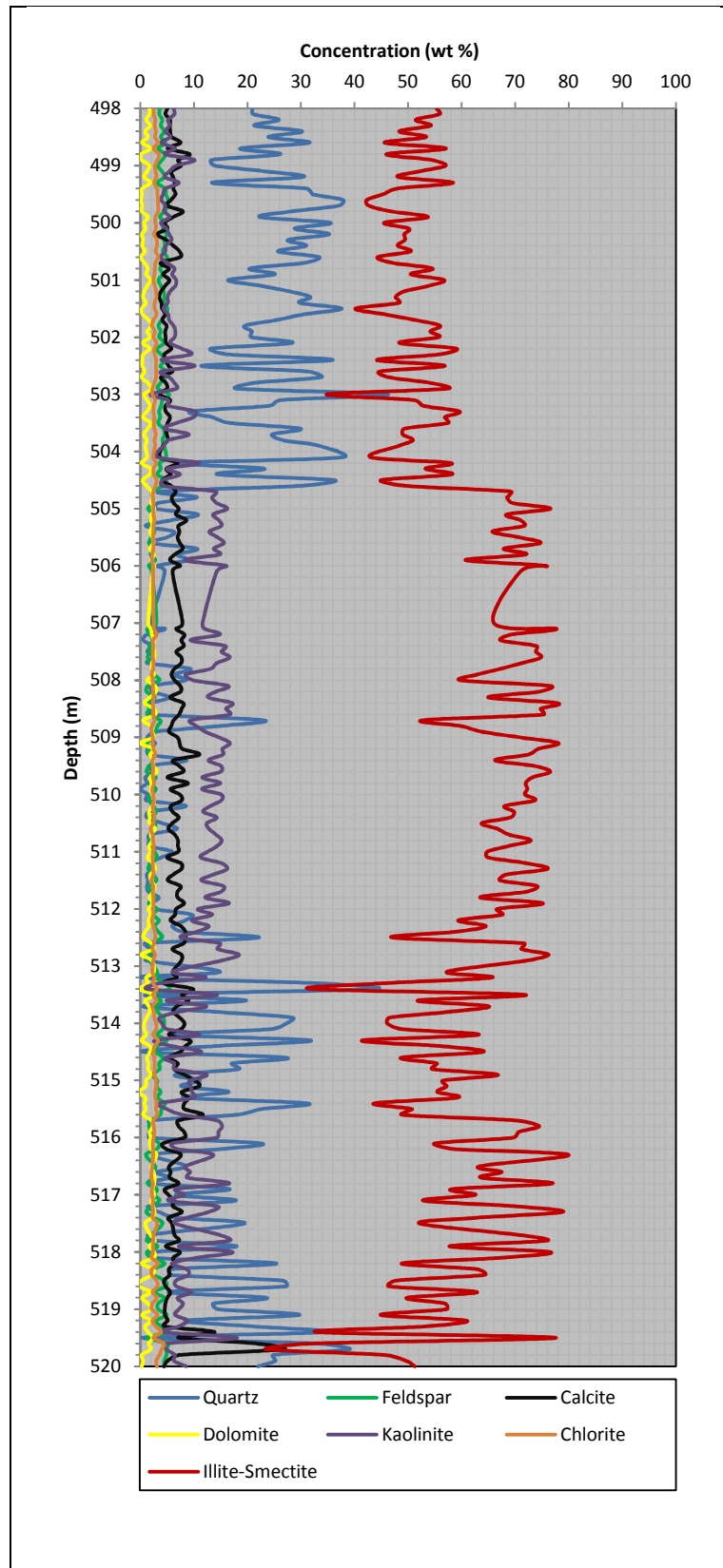


Figure 3.27: Mineralogy Log for a Shale Gas Well

3.10 Summary of FT-ATR spectroscopy quantitative mineralogy calibration models

1. A feasibility study was conducted in order to investigate the potential of combining ATR spectroscopy with PLS multivariate statistical technique for quantitative mineralogical analyses of shales.
2. The ATR technique produced spectra that are reproducible to within 0.05 absorbance value.
3. Comparison of the ATR spectra with DRIFT and Transmission indicate that important diagnostic band below the 650 wave number were absent (these include bands at 522, 464 cm^{-1} for quartz; 530, 472 cm^{-1} for illite-smectite; 543, 472, 462 cm^{-1} for kaolinite)
4. Three different calibration models were developed from ATR recorded spectra and tested with independent shale rocks of varying mineralogical content determined using quantitative XRD analyses.
5. The first model, ATR-PLS-MM, was constructed from a set of pure mineral mixtures. The mineral mixtures were designed to reflect five major mineral components found in clastic and carbonates formations, namely: illite-smectite, kaolinite, quartz, calcite and dolomite.
6. Application of the ATR-PLS-MM model on a subset of mixtures prepared from the same pure minerals gave predictions with average absolute errors of 6.6wt% for illite/smectite, 2.6wt% for kaolinite, 4.0wt% for quartz, 4.8wt% for calcite and 4.5wt% for the dolomites.
7. Application of the ATR-PLS-MM model on 12 independent shales from Western Canada basin and the Nile Delta gave predictions with average absolute errors up to 10wt% for calcite and kaolinite. The average errors for quartz, dolomite and illite/smectite were 8.1wt%, 7.2wt% and 8.2wt% respectively.
8. The sum of the clays and carbonates did not significantly improve the results. The average error for the clays is 10.4wt% and 14.7wt% for the carbonates.
9. The large errors were attributed to unavoidable differences in crystalline structures between the pure minerals and the shale, although all samples were ground in the same manner. Also, the shales contain other minerals in small quantities that were unaccounted for in the calibration model.

10. The second model (ATR-PLS-shale) which incorporates and describes a higher percentage of the variance in unknowns, was constructed from a data set containing naturally varying minerals.
11. The model accounted for two additional minerals including feldspars and chlorite. The model predicted the concentrations of seven minerals for a sub-set of the shales with an average error of < 5wt% for quartz, feldspars, kaolinite and chlorite. The calcite, dolomite and illite-smectite gave average errors of 9.69wt%, 5.9wt% 5.8wt% respectively.
12. The degrees of similarity between the clays and carbonates spectra indicate that it is difficult to determine individual minerals, thus resulting in the large errors.
13. The agreement between the IR derived and XRD mineralogy is better when the sum of the clays are compared, with a combined average error of 4.4wt%.
14. The agreement between IR derived and known carbonates is poor, with a combined average error up to 10wt % and leads to the conclusion that it is difficult to quantify the carbonates with sufficient accuracy using ATR spectroscopy.
15. Application of the ATR-PLS-Shale model on 13 independent shale samples gave estimations with errors between 5-10wt%. The prediction for the combined clays and carbonates compared better with the measured XRD values than the individual minerals.
16. The major constraint of the second model in predicting the mineral concentrations in independent (blind) samples is that it did not cover the optimum spread of mineral concentrations. The model was therefore, extended to include concentration ranges of the shale plus added known weights of pure minerals to construct the third model (ATR-PLS-SMM).
17. The third model was able to quantify the minerals in independent natural shale rocks to within 5wt% but occasionally with error up to 10wt%, especially when the unknown shale contain other minor minerals not included as part of shale rock calibration occurring in large quantities.
18. Generally, in all the models, prediction is more accurate when applied on samples similar in nature and concentration ranges than on an entirely different set of samples.

19. The major limitation of the ATR technique is its inability to scan beyond the 650 wave number where Transmission spectra revealed there are important diagnostic bands for the silicates.
20. The feasibility study demonstrates that applying multivariate non-linear regression analysis on attenuated spectra of shale rocks has high potential for quantitative mineralogy.
21. The study also shows that quantitative mineralogy using the FT-ATR technique is not as accurate as other IR techniques such as Transmission and DRIFT in which quantification is achieved with errors within 1-5wt% (e.g Breen et al. 2008 & Hughes et al. 1995). However, the speed of spectral acquisition and data processing together with small sample size requirement makes the ATR technique more desirable than the other techniques. The ATR can be used as a semi-quantitative technique for acquiring and building high resolution data quickly and cheaply.

4 CHAPTER FOUR: MINERALOGY, GRAIN SIZE AND PORE SIZE DISTRIBUTIONS FOR THE COLORADO GROUP

4.1 Introduction

The Cretaceous Colorado Group (Albian to Santonian) comprises of predominantly marine shales that extends more than 1300km from the Rocky Mountains to the Manitoba Escarpment (Bloch et al. 1993). The Colorado Group mudstones have been studied extensively (Buckley, 2004; Bloch et al. 1999 & 1995; McNeil and Gilboy, 1999; White et al. 1999; Schröder-Adams et al. 1996; Leckie et al. 1994) in terms of their sedimentology, micropalaeontology, organic facies, geochemistry and source rock potential. The mineralogy and petrophysics of the shales must however also be understood in order to evaluate their potential as gas shales.

This chapter presents the results of mineralogical and petrophysical analyses conducted on a suite of 409 Cretaceous samples from 40 wells and comprising five stratigraphic formations from the lower Colorado Group (Fig. 4.1, Table 4.1 & Appendix II). These samples have been previously characterised for palynofacies and geochemistry (Buckley, 2004) to study a west-east transect in organic facies. All the samples were analysed for quantitative mineralogy using Fourier Transform Infra-Red (FTIR) spectroscopy. A total of 79 samples were selected and examined petrophysically, by MICP to determine pore size distributions, and were disaggregated to determine grain size distribution. The samples selected for grain size and MICP were drawn from five formations including: the Viking Group, Westgate, Fish Scales, Belle Fourche, and Second White Specks Formations, therefore the sampling strategy covers all the stratigraphic units. The general stratigraphy of the lower Colorado Group is reviewed by Bloch et al. (1993 & 1999) and is shown in Figure 1.2.

The main aim of this chapter is to describe the bulk mineralogy and grain size distributions of the Colorado Group mudstone samples. In addition to this, grain size data is fitted with the Kranck et al. (1996b) model and then used to determine sediment depositional processes and hydrodynamic conditions. Data from MICP is also used to determine pore size distributions as well as total porosity and permeability. The results are described formation by formation while drawing general trends within and between the formations.



Figure 4.1: Map of the Western Canada Sedimentary Basin with location of studied cores (adopted from Buckley and Tyson, 2003)

Table 4.1: Locations of wells within the WCSB map

Sample	Location	Latitude	Longitude	Well Name	Location on map
CSO	06-07-12-28W4	49° 58' 46.75" N	113° 48' 58.77" W	Canadian Superior Oxley	1
SCD	03-07-13-27W4	50° 03' 52.80" N	113° 40' 35.81" W	Sinclair C & E Dahl 2A	2
IW	05-09-72-08W6	55° 13' 10.83" N	119° 10' 29.51" W	Imperial Wembley	3
MB	11-21-12-23W4	50° 00' 48.72" N	113° 05' 21.82" W	Melaar Barons	4
EFR	06-10-39-09W5	52° 20' 18.41" N	115° 13' 02.50" W	Esso Ferrier	5
BSR	16-10-12-23W4	49° 59' 15.51" N	113° 03' 17.94" W	Barons Superior No 1	6
SAF	14-22-39-08W5	52° 22' 31.83" N	115° 04' 15.95" W	Pembina Unit 1 Ferrier	7
BEI0	07-09-12-21W4	49° 58' 55.10" N	112° 48' 37.02" W	Banner et al Ironsp	8
TBR	12-35-45-13W5	52° 55' 32.67" N	115° 47' 03.28" W	Trilogy et al Brazr	9
GBR	16-30-45-12W5	52° 54' 47.01" N	115° 43' 19.98" W	Gulf et al Brazr	10
REW	16-18-39-05W5	52° 21' 38.15" N	114° 41' 53.82" W	Resman et al Willgr	11
MSL	16-28-37-05W5	52° 12' 50.23" N	114° 38' 54.53" W	Murphy et al Sylvan Lake 16-28-37-05	12
BVW	04-27-39-06W5	52° 22' 48.84" N	114° 47' 16.17" W	BVI Willgr 10-27-39-06	13
CLF	16-15-39-05W5	52° 21' 41.59" N	114° 37' 40.01" W	CPOG Leaf	14
AC	11-12-06-16W4	49° 27' 37.37" N	112° 02' 14.72" W	Amoco Conrad	15
PH	10-09-28-21W4	51° 22' 54.70" N	112° 53' 49.06" W	PCP et al Hussar 10-09-28-21	16
MT	14-18-36-25W4	52° 05' 44.97" N	113° 34' 02.01" W	Marathon Threehick 14-18-36-25	17
PS	07-14-01-05W4	49° 01' 58.28" N	110° 34' 07.59" W	Pacific Amoco Sapphire	18
HLC	08-06-40-25W4	52° 24' 31.94" N	113° 34' 45.90" W	Husky et al Lacombe	19
CRB	06-23-14-10W4	50° 11' 04.34" N	111° 16' 08.39" W	CPOG Rainbow	20
IK	05-01-77-20W5	55° 38' 29.04" N	116° 58' 17.27" W	Imperial Kathleen	21
CB	10-34-42-22W4	52° 38' 05.08" N	112° 57' 33.93" W	CNRL et al Bashaw	22
PFV	09-03-36-19W4	52° 03' 47.13" N	112° 37' 39.75" W	Paz Fennbv	23
DR	08-33-30-12W4	51° 36' 34.57" N	111° 37' 36.74" W	Dome Richdale 08-33-30-12	24
MDA	11-30-41-18W4	52° 33' 29.72" N	112° 35' 01.56" W	Merland Donalda	25
MPD	11-15-41-18W4	52° 31' 51.08" N	112° 30' 52.84" W	Mobil Penzl 1B Donalda	26
AY	06-34-30-08W4	51° 36' 35.15" N	111° 03' 05.93" W	Amoco B1 Youngstown	27
HP	15-07-32-25W3	51° 44' 08.39" N	109° 31' 59.94" W	Hardy Prairiedale	28
AER	06-18-45-01W4	52° 52' 39.01" N	110° 08' 27.63" W	Anderson et al Ribstone	29
AHR	10-35-45-02W4	52° 55' 32.39" N	110° 10' 47.64" W	Anderson Husky Roros 10-35-45-02	30
NH	07-28-29-20W3	51° 30' 42.96" N	108° 45' 25.19" W	Netherhill No 1 Strat Test	31
CV	11-16-35-8W3	52° 00' 33.98" N	107° 05' 25.43" W	C M & S Vanscoy 11-16-35-8	32
IF	16-04-21-25W2	50° 45' 44.19" N	105° 24' 10.01" W	Imperial Findlater	33
GS	16-10-44-27W2	52° 47' 05.42" N	105° 49' 46.64" W	Grey Owl Syndicate	34
DT	11-36-10-13W2	49° 52' 06.65" N	103° 38' 48.32" W	Dome Talmage	35
LR1	04-23-46-16W2			Kennecott Leather River I-09-01	36
MG	08-11-33-09W2	51° 48' 58.05" N	103° 10' 03.63" W	Margo 8 11	37
IY	01-24-20-33W1	50° 43' 48.00" N	101° 55' 55.92" W	International Yarbo NO 17S	38
SWB	11-36-22-1W2	50° 56' 30.49" N	102° 01' 15.77" W	SWP Bredenbury*	39
CR	01-04-45-10W2			Kennecott Crooked River SK-16B-93-1	40

4.2 Bulk mineralogical results of the lower Colorado Group

Fourier Transform Infrared Spectroscopy was used to compute semi-quantitative bulk mineralogy on 409 Colorado Group samples by applying the model constructed from ATR-PLS-SMM derived spectra to predict quartz, feldspars, calcite, dolomite, kaolinite, chlorite and illite-smectite. All the samples were treated in the same manner as the samples in the calibration. Spectra of the rocks were obtained using a Fourier Transform AVATAR 360 FTIR ESP spectrometer with OMNIC software fitted with an ATR Performer accessory and equipped with a DTGS detector recording 32 scans at a resolution of 8cm^{-1} .

Figure 4.2a shows a plot of IR determined carbonates (calcite + dolomite) vs LECO determined calcium carbonate computed as the [total inorganic content * 8] as a general check on the accuracy of results predicted by the model. The strong correlation coefficient ($r^2 = 0.87$) show that the FTIR mineralogical calibration used produced predictions with a reasonable degree of accuracy with about 80% of the sample set within $\pm 5\text{wt}\%$ of the LECO values. Figure 4.2b is a scatter plot of clays vs quartz for the lower Colorado Group samples with $<20\%$ carbonates content showing a strong negative correlation ($r^2 = 0.83$). This relationship indicates that the clays and quartz constitute the dominant mineralogy distributions for the lower Colorado Group.

The bulk mineralogy of the five major minerals for the lower Colorado Group is shown in Table 4.2. Ternary plots exhibiting the bulk mineralogy of the major species (quartz, clays and carbonates) for the Colorado Group are shown in Figure 4.3. The percentage of quartz for the whole dataset ranges from 0.4 – 61.3% (mean 28.8%) with over 80% of samples containing between 20-60%. Illite-smectite content varies from 1.4 – 78.6%, with a mean of 38.5%. Kaolinite ranges from 0 – 24.8% with a mean of 8.79%. The concentration of calcite ranges from 2.6 – 73.7% (mean 11.7%); over 70% of samples contain less than 10% calcite. Low dolomite concentration was measured with values ranging from 0-26.9% (mean 2.4%); with about 80% of the samples containing between 1-2%.

The mineralogical analysis for the entire dataset suggests that the lower Colorado Group formations are dominated by the clays and quartz; however, each formation is different with different mineralogical compositions, hence they were described separately. Table 4.2 provides a summary of the bulk mineralogy analysed for each formation, displaying the variability in all the minerals throughout the section.

4.3 Mineral Distributions by Formation

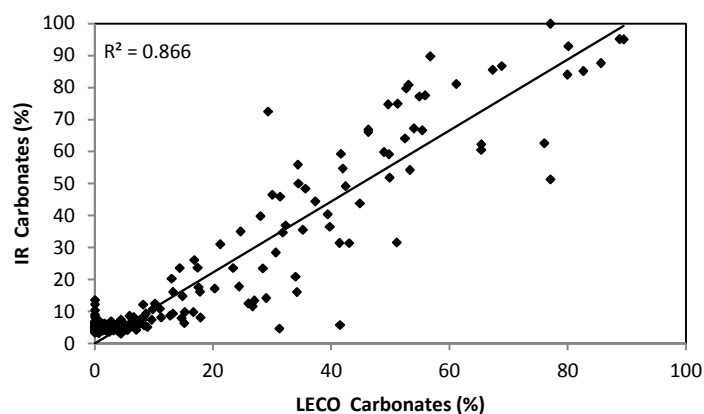
4.3.1 Viking Formation

FTIR mineralogical analyses have been conducted on 19 Viking Formation samples. Figure 4.3 is a ternary plot showing the range of mineralogy data obtained for total clays, quartz and combined carbonates. A restricted mineralogical distribution is observed dominated by quartz and clays which comprise a significant proportion of the total mineralogy, indicative of significant continental input. Quartz ranges from 19.2 to 46.8% and a mean of 34.2%. The Illite-smectite contents of the Viking Formation ranges from 25.9-56.8% (mean value of 39.8), while the samples contain between 2-14% (mean 9.9%) values for kaolinite. Both calcite and dolomite account for only up to 10% of the bulk mineralogy of samples analysed, with mean values of 4.9 and 0.4% respectively.

4.3.2 Westgate Formation

FTIR mineralogical analyses have been conducted on 133 Westgate Formation samples. Generally the Westgate Formation exhibits a similar but a much broader range of mineralogical distributions than the Viking Formation. Quartz and clays are the dominant mineralogy with very low carbonate contents. Quartz ranges from less than 5% to 50% with more than 75% of the samples analysed containing between 20 – 50%. The illite-smectite contents of the Westgate Formation ranges from ~25-70% with majority of the samples (57%) containing between 30-45%. Almost all the Westgate samples contain between 0-15% kaolinite with the exception of a few which contain up to 25%. Both calcite and dolomite account for only 5% in over 70% of samples analysed, although calcite values of up to 25% were measured in a very few samples.

a



b

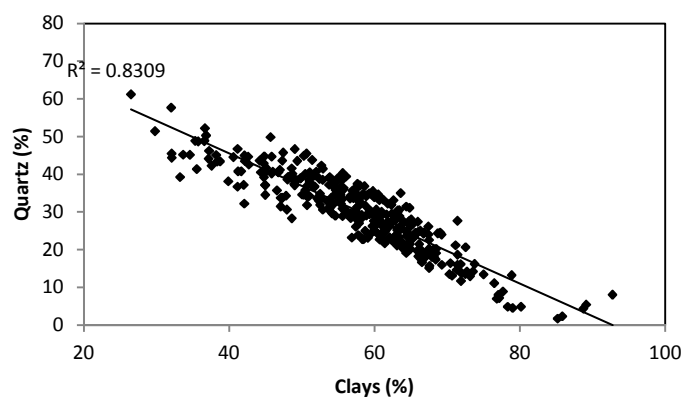


Figure 4.2: Cross plots of (a) LECO determined carbonates versus IR determined carbonates, (b) Clays vs quartz for samples with <20% carbonates for the lower Colorado Group data set

The range of mineralogy measured indicates that the Westgate Formation is consistent with heterogeneous mixture of mudstones and silty shales suggested by (Bloch et al., 1999), and indicative of transition in space between shelf to basin (Tyson, 1995).

4.3.3 Fish Scales Formation

Mineralogical data have been obtained for 44 Fish Scales Formation samples from 14 cores. Quartz percentage ranges between 4.6-61.3% (mean 35.5%). Illite-smectite concentration varies between 11.1- 66.8% (mean 38%). Kaolinite values range from 0-16.6% (mean 8.4%). Like the Westgate Formation, the Fish Scales Formation exhibit very low abundance of carbonates; calcite (3.1 – 30.6) with a mean of 5.4%, and dolomite concentration between 0-13.3% (mean 0.78%). However, an increase in calcite concentration is observed in some samples reaching up to 30% in the lower section of the formation.

4.3.4 Belle Fourche Formation

Ninety nine Belle Fourche Formation samples from 17 cores were subjected to the FTIR mineralogical analyses. The Belle Fourche Formation exhibits a broader range of mineralogy than the underlying Fish Scales Formation, with a relative increase in the proportion of carbonates. Quartz concentrations vary between 6.6-48.8% (mean 25.0%). Illite-smectite values vary from 8.7-64.1% (mean 44.4%) significantly higher than quartz. The range of kaolinite values measured in the Belle Fourche Formation (0.9- 19.8%; mean 10.6%) is similar to the concentrations determined in the underlying Fish Scales Formation. Calcite values ranges from 2.9-52.5% (mean 6.7%), and dolomite concentration vary from 0-22.2% (mean 1.44%). The broad range of carbonate concentrations and its positive covariance with clay is interpreted to represent transition in space from proximal-shelf to distal basin (Tyson, 1995).

Table 4.2: Mineralogical Composition of the lower Colorado Group Shales

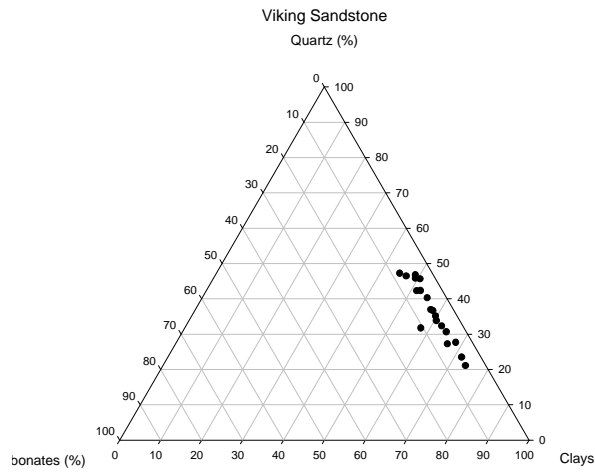
FORMATION	N	Minimum	Maximum	Mean	Std. Deviation
VIKING					
% Quartz	19	19.20	46.80	34.19	8.22
% Calcite	19	3.40	9.90	4.88	1.58
% Dolomite	19	0.00	1.40	0.35	0.42
% Kaolinite	19	2.60	13.70	9.90	3.14
% Illite-Smectite	19	25.9	56.80	39.38	7.91
WESTGATE					
% Quartz	133	2.40	49.90	31.43	9.25
% Calcite	133	2.60	24.30	4.65	2.02
% Dolomite	133	0.00	4.80	0.39	0.70
% Kaolinite	133	1.30	24.80	10.30	3.80
% Illite-Smectite	133	26.20	66.20	43.23	9.82
BELLE FOURCHE					
% Quartz	99	6.60	48.80	24.96	8.16
% Calcite	99	2.90	52.50	6.72	8.25
% Dolomite	99	0.00	22.20	1.44	3.68
% Kaolinite	99	0.90	19.80	10.56	4.47
% Illite-Smectite	99	8.70	64.10	44.44	10.48
FISH SCALES					
% Quartz	44	4.6	61.3	35.53	12.95
% Calcite	44	3.1	30.6	5.41	4.07
% Dolomite	44	0.0	13.3	0.78	2.17
% Kaolinite	44	0.0	16.6	8.41	4.09
% Illite-Smectite	44	11.1	66.8	37.96	12.86
SECOND WHITE SPECKS					
% Quartz	93	0.40	56.10	25.15	14.35
% Calcite	93	3.10	73.70	29.38	21.81
% Dolomite	93	0.00	26.90	7.45	8.75
% Kaolinite	93	0.00	22.00	4.65	4.60
% Illite-Smectite	93	1.40	78.60	25.31	17.45
UPPER COLORADO					
% Quartz	21	0.80	45.30	26.40	11.88
% Calcite	21	4.00	67.10	10.47	15.14
% Dolomite	21	0.00	20.60	2.74	5.69
% Kaolinite	21	0.00	20.90	8.90	5.17
% Illite-Smectite	21	12.20	58.60	39.61	11.13

4.3.5 Second White Specks Formation

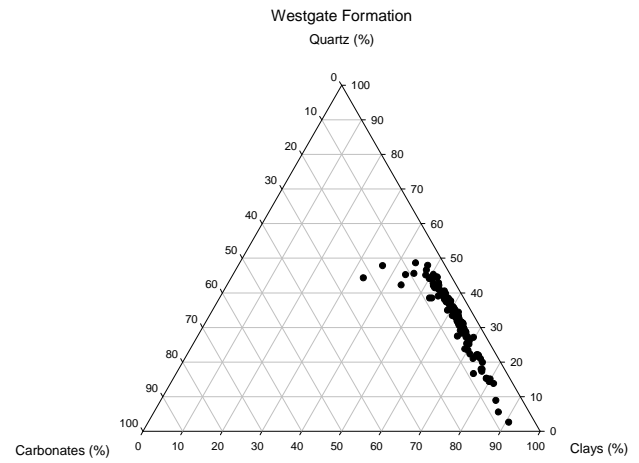
Mineralogical analysis was conducted on 93 Second White Specks samples from 17 cores (Fig. 4.3e). The mineralogy differs significantly from the other Colorado Group shales, exhibiting the greatest variation of all the formations as well as the greatest carbonate contents of all the samples analysed. Abundant carbonates of up to 93% have been measured. Calcite values range from 3.1-73.7% (mean 29.3%). Dolomite values of between 0- 26% (7.5%) were measured and are supported by SEM images analysis (to be discussed further later); although about 66% of the samples have dolomite concentrations of less than 1%. High quartz concentrations up to 56.1% (mean 25.2%) have been measured in some samples, indicative of continental contribution. The clays are dominated by the mixed layer illite-smectites (1.4- 78.6%; mean 25.3%), but only few samples (~6%) have Illite-smectite values up to 50% and above. Kaolinite varies from 0-22% (mean 4.7%).

Thin section and SEM examination of the Colorado Group show that pyrite is abundant within all the formations, although it was not determined in the IR mineralogy. Pyrite is present in framboids and small cubes within intergranular pore spaces, and within foraminifera. This pyrite was most likely formed during the early stages of burial as organic matter was oxidized during microbially mediated sulfate reduction; this is a common process within most present-day shallow shelf environments (Bloch et al., 1999), (Fig. 4.4).

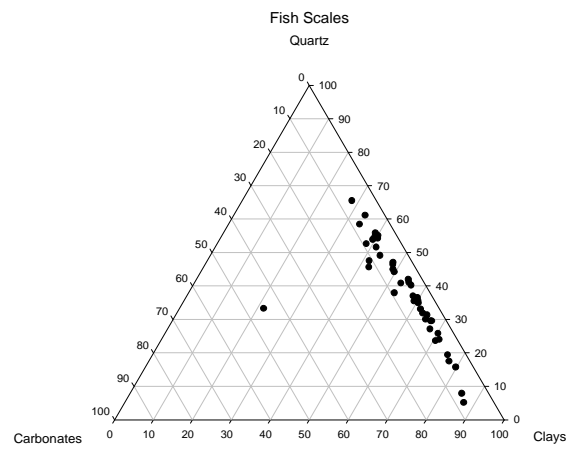
a



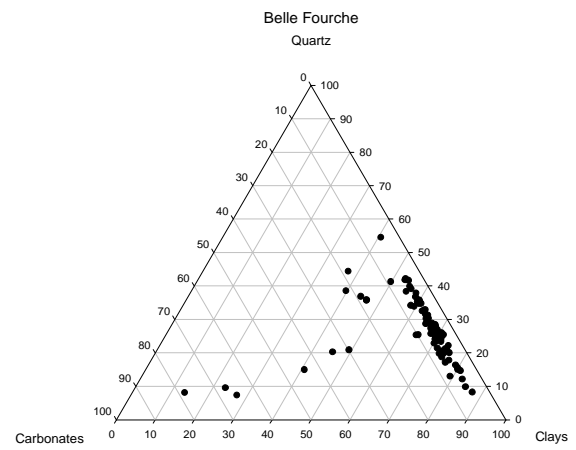
b



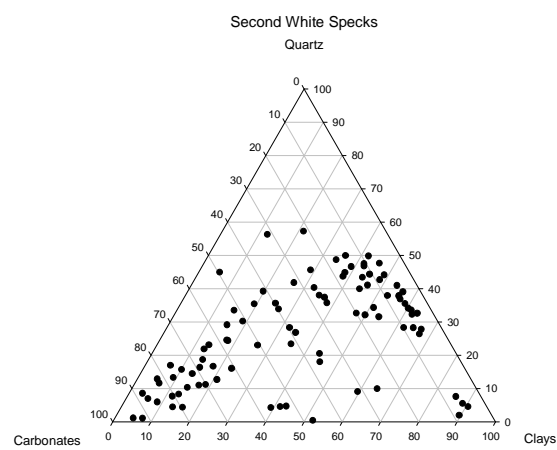
c



d



e



f

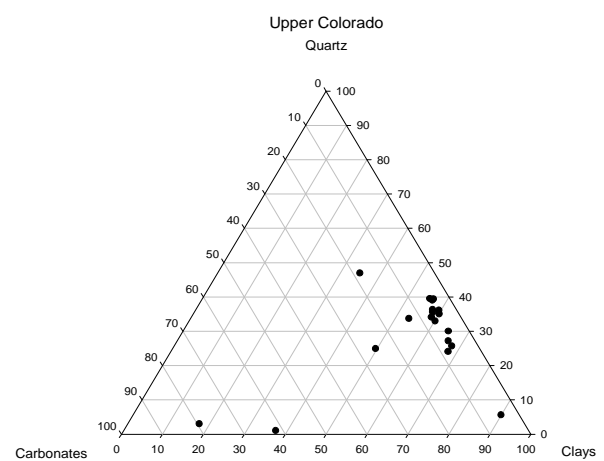


Figure 4.3: Ternary plots of Quartz-Clay-Carbonate for the Colorado Group formations

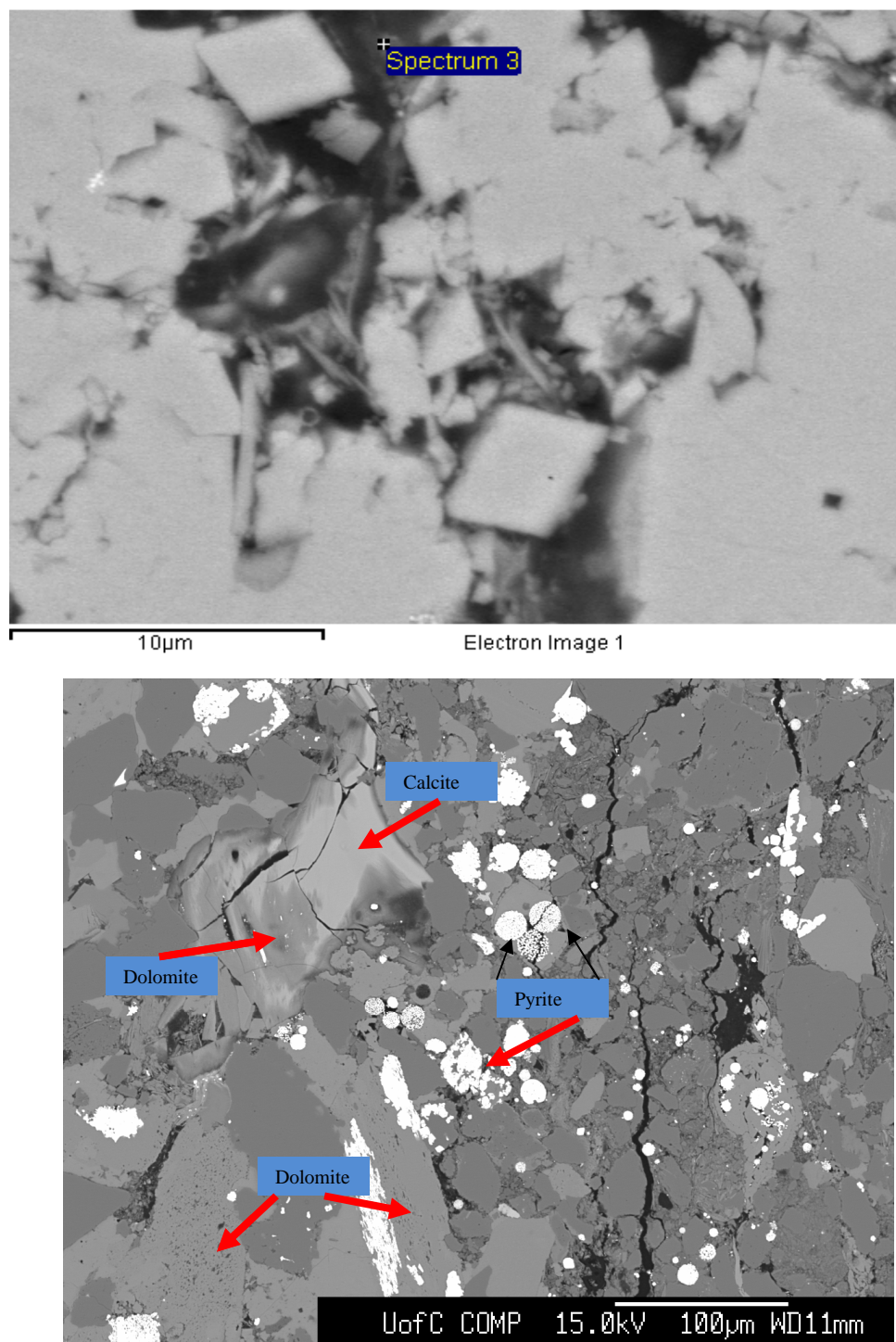


Figure 4.4 (A) SEM of a carbonate rich sample within the Second White Specks Formation, at a depth of 275.6 m in the SWB core showing the presence of calcites **(B)** SEM image within the Second White Specks Formation showing the presence of both calcite and dolomite. Pyrite is also present as framboids and cubes

4.4 Grain Size Distribution of the Colorado Group

A total of 79 core samples were selected for the GSD and MICP analyses incorporating the Viking Formation, through to the Second White Specks. Samples for GSD were drawn from Alberta to Saskatchewan (Fig. 4.1) wells and represent the upper, middle and lower sections of each of the formations in order to observe temporal trends and to account for any variability. Tables 4.4 and 4.5 show that the individual unit formation show subtle variation in the grain size distributions. Some of the samples could not be disaggregated either because they have been deeply buried and were therefore too consolidated, as in the case of the Viking Formation or have been cemented by carbonate minerals; this is more pronounced in the Second White Specks Formation due to their calcareous nature.

Grain size distributions for 45 samples taken from the lower Colorado Group show that all samples comprise between 50-80% combined clay and fine silt (Tables 4.4 & 4.5) that can be incorporated into flocs, and are considered to be either shale or clayshale. All the formations have ~ 20-40% sortable silt (10-62.5 μ m). The Second White Specks Formation has relatively higher combined silt and sand content than the other formations. Highest clay content values were found within the Westgate Formation and Belle Fourche Formation, where up to 80% of the samples comprised 50% and over of clay-sized materials.

4.4.1 Kranck model fitting

The grain size distribution of muds in seawater environments has been used to infer their modes of transportation, deposition as well as the energy of the environment (Kranck et al. 1996b). These in turn have significant implications in understanding sedimentary features and in correlating stratigraphic units. The grain size models classify particle size distributions of weathered rock in the water column as a mixture of single grains and flocs, and each is defined by a set of hydrodynamic properties. Particles smaller than ~ 10 μ m act in a cohesive manner and are deposited as unsorted flocs, whereas larger particles, sometimes referred to as ‘sortable silt’ mainly settle as single grains in responses to hydrodynamic processes and its properties may be used in some way to infer palaeocurrent (Kranck et al. 1996b; Kranck et al. 1996a; Kranck and Milligan, 1991b). The deposition of flocs to the sediment surface, compared to single grains, is related to the energy and sediment concentration of the water column such that the rates of floc formation exceeds floc destruction in lower energy

environments and where suspended sediment concentrations are high (Curran et al. 2004; Hill et al. 2001). Therefore, the grain size distribution of muds is considered as a representation of “the respective fluxes of flocs and single grains to the sediment-water interface, which in turn depends on the concentration of each component and the energy of the environment” (Aplin and Macquaker, 2012).

In terms of sediment transport, muddy sediments are therefore largely regarded to be composed of two components: the first one is an unsorted component which mainly comprises phyllosilicate grains less than $\sim 10 \mu\text{m}$ incapable of basin-scale ripple migration, and a second component which is coarser and mainly comprises tectosilicates; quartz, mica and feldspars i.e. “sortable silt”; (McCave and Syvitski, 1995) and which may be organised into ripples. However, recent studies (Schieber et al. 2010; Schieber and Southard, 2009; Schieber et al. 2007) have demonstrated that both flocs and sortable silt can be transported as bedload post deposition. These studies demonstrate that since clay-sized and silt-sized sediments are able to flocculate and form a single ‘floc’ that is held together by weak Van der Waals forces, it is therefore, capable of being transported in ripple form in a similar fashion to sand-sized particles (Schieber and Southard, 2009). This analysis also indicates that although clay-sized particles are largely deposited as flocs, their occurrence in the geological record cannot be restricted to low energy depositional environments (Macquaker et al. 2007).

The grain size cumulative curves were digitised, generating grain size frequency distributions and fitted with Kranck et al.’s. (1996) model. Grain size frequency distributions were then plotted as log-log spectra of grain size (μm) versus weight %. The model assumes that deposition of fine particles occurs at rates proportional to the exponential of their settling rate from an unsorted turbulent source suspension (Kranck and Milligan, 1991b), simply represented by:

$$C = \Delta Q w^{(m+n)} e^{-Kw} \text{ — — — — — Equation 4.1}$$

Where:

C = concentration in a size class

ΔQ = concentration at a reference settling velocity

m =

slope of the source suspension with a value between 1 and -1 (Kranck et al., 1996)

exponent n = controls the nature of the GSD model fit either flocculated or single grain

K = defines the extent to which the coarser grains have settled ($s\text{ cm}^{-1}$)

Putting equation 4.3 into linear form by taking the log of both sides gives:

$$\ln C = \ln \Delta Q + (m + n) \ln w - Kw - - - - - \text{after Kranck et al., (1996a), Equation 4.2}$$

The parameters ($\ln \Delta Q$, $(m + n)$ and K) were estimated using least square regression according to equation 4.2. Another parameter (D_f) defined as the floc-silt intersection (Curran et al., 2004) was calculated where appropriate. The floc-silt intersection estimates the maximum particle size that will be incorporated into flocs which was used to classify the grain size distributions. Moore (2005) proposed six mudstone grain size distribution types reflecting largely the relative contributions of a flocculated, clay rich component and unflocculated silt/sand –rich grain size components. The study integrates grain size data and petrographic observations to discriminate between floc dominated, floc silt mixtures and silt dominated grain size distributions (Table 4.2 & Fig. 4.3).

The frequency distributions generated from digitizing the grain size curve is believed to have generated artefacts and therefore fitting the data with the Kranck's model was very difficult for many of the samples. Kranck's model is generally more accurate for clastic fine grained sediments; since the Colorado Group samples contain fine grained carbonates the accuracy of the sorting (fitting) is quite poor. This likely affected the datasets in this study; however, there is still use for the current data in samples that consists of a dominant clastic lithology.

The grain size distributions and type of grain size spectra for the lower Colorado samples are given in Tables 4.4 & 4.5. The type of grain size distributions were characterised according to Moore's (2005) classification after fitting with Kranck's model. The data show variable grain size distributions representing the different types of mudstone in all the formations.

Table 4.3: Grain Size distribution and types and their depositional environments attributes and properties according to (Moore, 2005)

Type	Nature of spectra	Characteristic of grain size distribution
Type 1	Floc -dominated	Grain size distribution is characterised by a low flocculated concentrations of particles in suspension and has high K values (average 239.5) and results from slow deposition at the distal end of the sediment transport path
Type 2	High concentration Floc	The grain size distribution is similar to Type 1 but with low K- values (average 27) parameter. It is characterised by a significant silt component in the floc deposited material and assumed to be deposited from a flow or water column with a high suspended sediment concentration
Type 3	Dominant floc-settled component and a minor Silt component	Grain size distribution composed of a component deposited as single grains either from a static water column or from a dilute flow (Moore, 2005). Grain size distribution spectra are characterised by a floc-non-cohesive silt intersection (D_f) value ranging from 9-18 μ m; average of 10 μ m.
Type 4	Approximately equal proportions of Flocs settled and Stokes settled silt material	Flocs and silt deposited simultaneously and do not form discrete layers. They exhibit D_f values ranging between 3-19 μ m (average 9.6 μ m)
Type 5	Coarse, silt-rich component and a minor Floc component	Characterised by an average floc-non-cohesive silt intersection value D_f of 7.9 μ m, ranging between 2-13 μ m
Type 6	Sand-rich mudstones and siltstones.	Mudstones with a sand content greater than 10% further sub-divided into floc dominated sandy mudstones; floc-silt-sand mixtures; and clay-silt-sand mixture

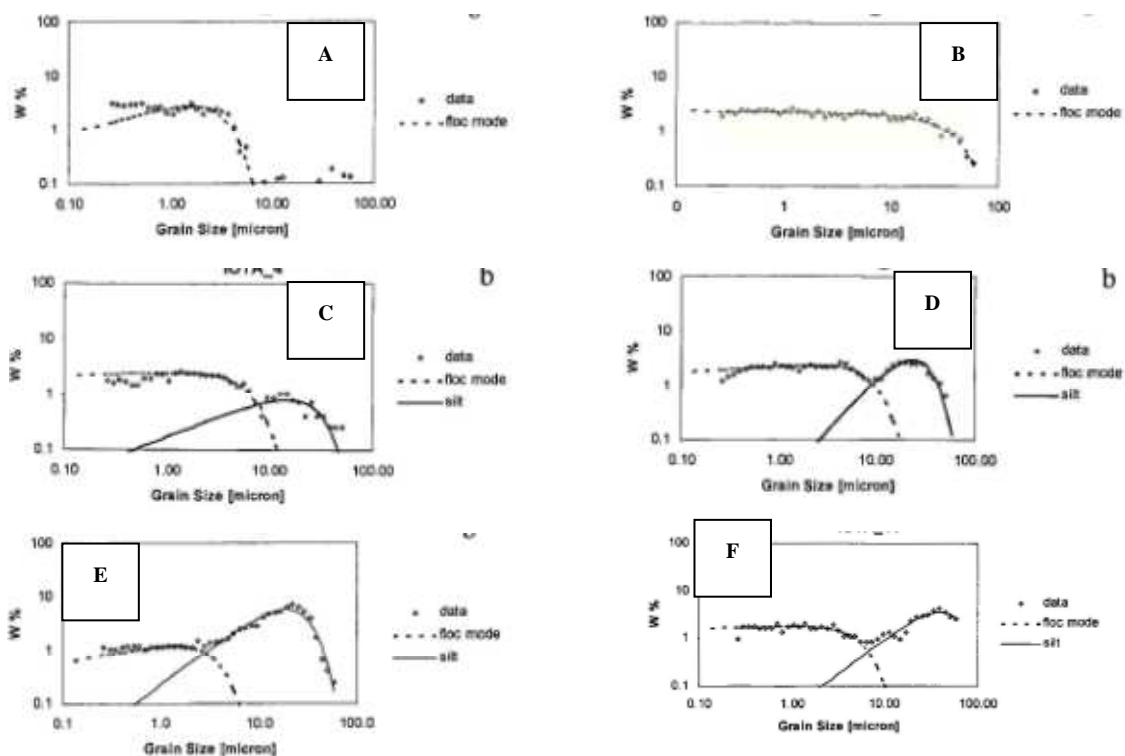
**Figure 4.5: Moore's (2005) mudstone classification (A) Type 1 - Floc –dominated, (B) Type 2 – High concentration Floc, (C) Type 3 - Dominant floc-settled component and a minor Silt component, (D) Type 4 - Approximately equal proportions of Flocs settled and Stokes settled silt material, (E) Type 5 - Coarse, silt-rich component and a minor Floc component and (F) Type 6 – Sand-rich mudstones and siltstones (Moore, 2005).**

Table 4.4: Grain Size Distribution from disaggregation and sedigraph for the Upper Colorado, SWS and Fish Scales Formations

Formation	Sample	% clay (<2um)	% Fine silt (2 – 10um)	% Coarse silt (10 – 62.5um)	% Sand (>63um)	Total Silt (2 – 63um)
Upper Colorado	AHR65	52.7	26.2	20.9	0.2	47.1
Upper Colorado	HP5	48.1	24.4	25.7	1.8	50.2
Upper Colorado	IF9	46.0	18.1	22.8	13.1	40.9
SWS	AC14	ND	ND	ND	ND	ND
SWS	AC17	46.9	23.1	29.8	0.2	52.9
SWS	AER21	47.2	31.9	20.3	0.6	52.3
SWS	AHR53	45.1	33.1	21.5	0.3	54.6
SWS	AY11	ND	ND	ND	ND	ND
SWS	CB1	31.0	22.4	45.5	1.1	67.9
SWS	CB8	ND	ND	ND	ND	ND
SWS	CR44	ND	ND	ND	ND	ND
SWS	CSO15	ND	ND	ND	ND	ND
SWS	CV17	53.1	14.9	31.7	0.4	46.6
SWS	DT2	56.2	4.9	38.5	0.4	43.4
SWS	DT6	ND	ND	ND	ND	ND
SWS	GS6	ND	ND	ND	ND	ND
SWS	HP1	49.2	29.8	20.8	0.3	50.5
SWS	IF6	ND	ND	ND		
SWS	IY15	ND	ND	ND	ND	ND
SWS	LR24	58.3	24.1	16.9	0.6	41.1
SWS	MB10	ND	ND	ND	ND	ND
SWS	MB14	33.1	41.3	25.1	0.5	66.4
SWS	PS6	ND	ND	ND	ND	ND
SWS	SWB25	41.2	26.5	30.3	1.9	56.9
Fish Scale	AER9	24.7	36.9	37.8	0.6	74.7
Fish Scale	AHR26	ND	ND	ND	ND	ND
Fish Scale	BVW7	ND	ND	ND	ND	ND
Fish Scale	CR30	62.2	18.3	19.1	0.4	37.4
Fish Scale	IK12	39.0	35.6	24.3	1.1	59.9
Fish Scale	IY9	ND	ND	ND	ND	ND
Fish Scale	MB3	ND	ND	ND	ND	ND
Fish Scale	MG5	44.0	26.5	28.9	0.6	55.4
Fish Scale	MSL 11	38.1	22.9	27.8	11.2	50.7
Fish Scale	MSL13	ND	ND	ND	ND	ND
Fish Scale	NH4	55.1	23.6	21.1	0.2	44.7

ND* = Not Disaggregated

Table 4.5: Grain Size Distribution from disaggregation and sedigraph for Belle Fourche, Westgate and Viking Formations

Formation	Sample	% clay (<2um)	% Fine silt (2 – 10um)	% Coarse silt (10 – 62.5um)	% Sand (>63um)	Total Silt (2 – 63um)
Belle Fourche	AC10	41.3	17.0	41.4	0.3	58.4
Belle Fourche	AC7	43.7	14.1	41.6	0.6	55.7
Belle Fourche	AER17	58.2	23.3	18.2	0.3	41.5
Belle Fourche	AHR30	ND	ND	ND	ND	ND
Belle Fourche	AY6	ND	ND	ND	ND	ND
Belle Fourche	CR35	60.3	22.8	16.3	0.6	39.1
Belle Fourche	CSO30	ND	ND	ND	ND	ND
Belle Fourche	CV12	59.9	15.8	24.2	0.1	40.0
Belle Fourche	IF1	57.7	22.4	19.5	0.4	41.9
Belle Fourche	IK16	63.8	19.6	16.4	0.2	36.0
Belle Fourche	IW18	33.4	26.9	39.1	0.7	66.0
Belle Fourche	IW22	33.2	32.5	33.5	0.8	66.0
Belle Fourche	LR21	50.9	28.6	19.1	1.4	47.7
Belle Fourche	MB6	43.0	21.0	35.5	0.5	56.6
Belle Fourche	MSL16	39.8	38.7	21.2	0.3	59.9
Belle Fourche	NH6	ND	ND	ND	ND	ND
Belle Fourche	PS2	ND	ND	ND	ND	ND
Belle Fourche	SWB14	73.3	13.9	12.7	0.0	26.7
Westgate	AER3	53.0	7.9	26.6	12.5	34.5
Westgate	AHR8	67.4	23.0	9.7	0.0	32.7
Westgate	AY5	ND	ND	ND	ND	ND
Westgate	BVW1	ND	ND	ND	ND	ND
Westgate	CR19	56.1	25.1	18.7	0.2	43.7
Westgate	CV1	ND	ND	ND	ND	ND
Westgate	CV8	59.8	18.1	21.9	0.1	40.0
Westgate	DR1	54.6	23.1	21.1	1.2	44.2
Westgate	DR7	ND	ND	ND	ND	ND
Westgate	IK1	57.8	16.4	24.9	0.9	41.4
Westgate	IK9	65.1	18.8	16.0	0.1	34.8
Westgate	IW4	34.0	13.6	51.3	1.1	65.0
Westgate	IW9	33.4	16.2	49.3	1.1	65.5
Westgate	LR11	ND	ND	ND	ND	ND
Westgate	LR9	56.9	21.4	21.5	0.1	42.9
Westgate	MG1	ND	ND	ND	ND	ND
Westgate	MSL5	ND	ND	ND	ND	ND
Westgate	MT5	45.3	29.1	25.0	0.6	54.1
Westgate	PH7	ND	ND	ND	ND	ND
Westgate	SWB9	55.6	29.8	14.5	0.1	44.3
Viking	CR3	54.5	14.4	19.6	11.6	34.0
Viking	IY2	ND	ND	ND	ND	ND
Viking	MT2	ND	ND	ND	ND	ND

The majority of samples analysed in all the formations show a flocculated grain size distribution characteristic of Type 1 and 2 mudstones using Moore's (2005) classification, suggesting that the sediments were mainly deposited at the distal ends of the sediment transport paths or in a low energy environment. The grain size spectra for Type 2 are dominated by a floc settled component but also incorporate a significant silt component within the floc deposited material. However, this is interpreted as indicating that the flocs incorporate material $>10\mu\text{m}$ and the sediment were deposited from a flow or water with high suspended sediment concentrations (Moore, 2005), contradicting low energy deposition.

Moore (2005) observed that the Type 2 mudstone has characteristic mudstone clasts in the photographic image and argued that the presence of clay clasts in the matrix suggests re-suspension from primary deposition and for the clast to be transported and re-deposited; it requires flow of high concentrations and as concentration of the sediments increases, the grain size incorporated into the floc components also increases. Clay clasts are a common feature seen in the thin sections of the samples analysed in this study (to be discussed later).

Fig 4.6 shows the grain size distribution spectra for the Westgate Formation samples. The majority of the samples exhibit a flocculated grain size distribution with high concentration flocculated components composed of more than 60% cohesive components. For example, sample IK9 has 65% clay, 19% cohesive silt, and only 16% sortable silt component. The Formation is also characterised by floc-silt mixtures, for example, sample CV8 from the Conrad Vanscoy core and IW9 from the Imperial Wembley core exhibit grain size distributions spectra characteristic of floc-dominated and silt-dominated - floc silt mixtures respectively. They are composed of a dominant floc-settled component and a minor silt component and a floc-non-cohesive silt intersection (D_f) value of $6.3\mu\text{m}$ deposited as single grains which suggests deposition from a static water column or from a dilute flow (Moore, 2005). Thin section analysis show that the Westgate Formation generally comprises homogeneous mudstones with irregular discrete organic matter particles and with occasional carbonate rich layers alternating with the fine particles (Figs. 4.7).

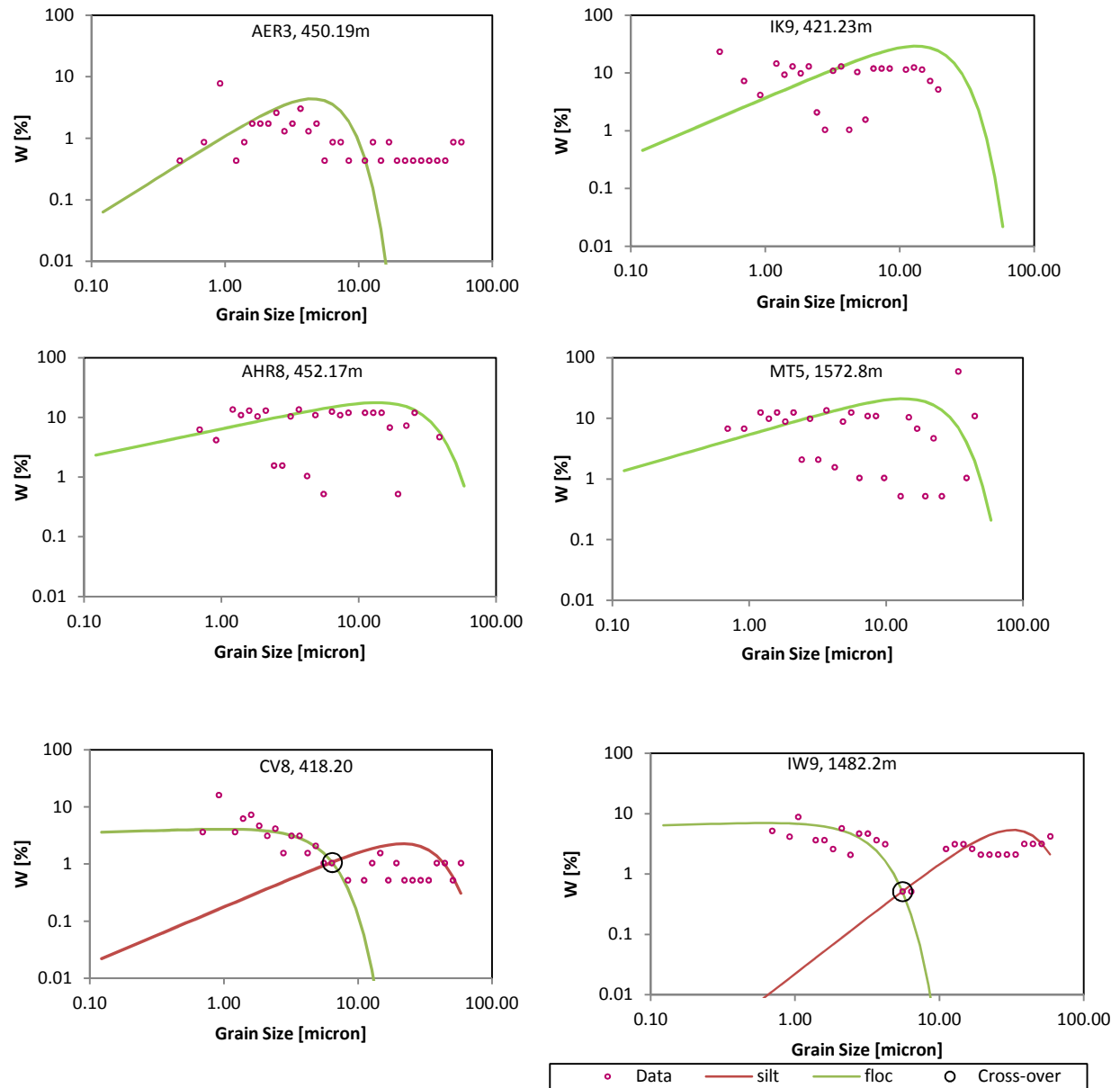


Figure 4.6: Grain size spectra for the Westgate Formation dominated by highly concentrated flocculated sediments that represents deposition from flow or water column with high suspended concentration (Moore, 2005). Samples from Conrad Vascoy (CV8) and Imperial Wembley (IW9) show floc- silt mixtures distribution representing deposition in a static water column or from a dilute flow (Moore, 2005).

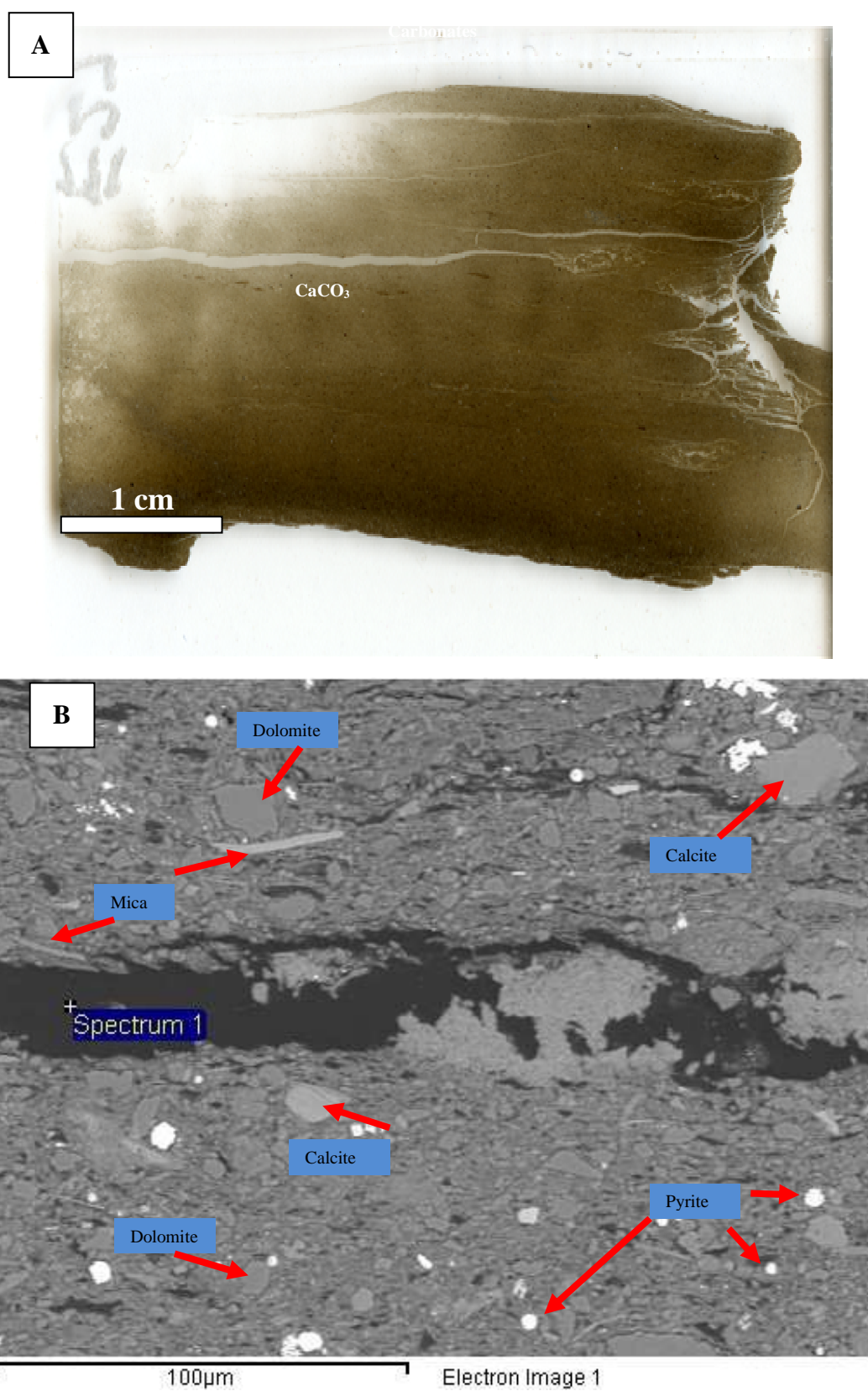


Figure 4.7: (A) Thin section of the sample within the Westgate Formation, at a depth of 418.2m m in the CV core showing fine-grained mudstone. (B) SEM shows regions rich in calcite, dolomite and pyrite.

The Fish Scale Formation exhibits more variable grain spectra incorporating more samples with both Floc-silt mixtures and flocculated Type mudstones, suggesting greater fluctuations in sea conditions. Sample MSL11 from the Marathon Threehick core contains a sand component of 11% (Fig. 4.8) and can be categorised as Type 6 (sand rich mudstones) according to the Moore (2005) classification, indicating a simultaneous floc-silt components deposition which do not form discrete layers deposited as single grains either from a static water column or dilute flow. The high proportion of sortable silt materials suggests deposition in high energy proximal environments causing the hydrodynamic condition that make the sediments to act as single grains and non cohesively (Moore, 2005).

Thin section of a sample from the Fish Scales Formation show that it is comprised of calcareous, clay to silty mudstone which show gradual grading with coarse grains at the base (Fig. 4.9). It shows that the formation is mud and clay-dominated, and contains siliciclastic siltstone and/or sandstone laminae. The mudstones contain abundant clay clasts, lenses of organic matter and floating quartz grains. Variations occur on a millimetre scale changing from bright grey to grey and dark layers of organic matter patches. Abundant pyrite was observed during the SEM analysis. The SEM images also show the presence of feldspars, dolomite and calcite.

The grain size spectra of the Belle Fourche Formation are similar to the underlying Fish Scales Formation but the majority of the samples exhibit grain size distribution spectra of flocculated components (Type 1 mudstone; Fig. 4.11). Samples from the C M & S Vanscoy core (CV12) show a floc dominated floc-silt mixture (Type 3 mudstone) whereas samples from the Amoco Conrad well (AC7 & AC10) show a Silt dominated floc-silt mixture Type 4 after (Moore, 2005) with a higher non-cohesive coarse silt component (41%, Fig. 4.12).

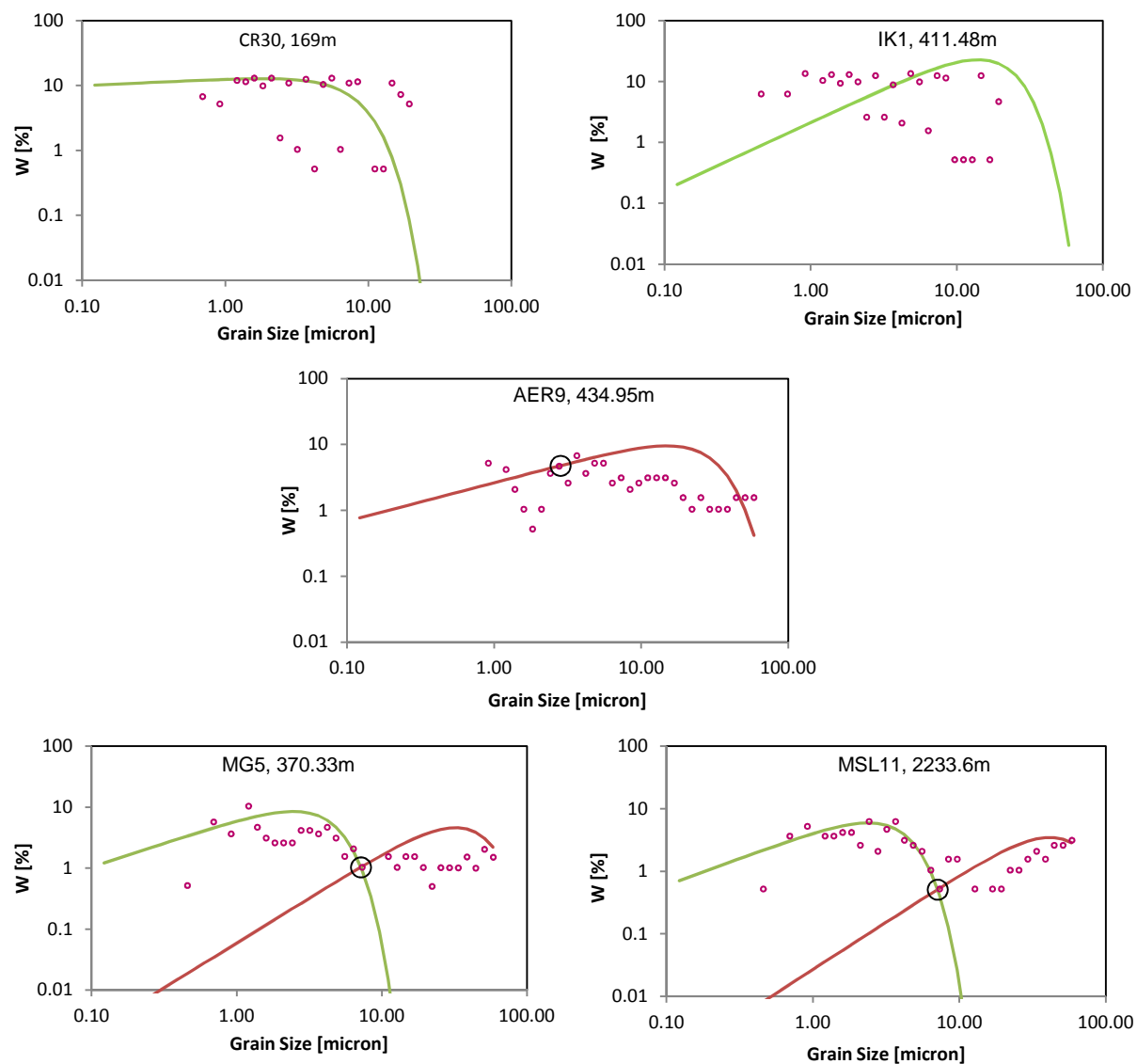


Figure 4.6: Grain size spectra of the Fish Scales Formation. Spectra are composed of floc-Silt settled components deposited as single grains from a static water column or from a dilute flow (Moore, 2005) representing proximal high energy setting. MSL 11 show a grain size spectrum consisting Floc-settled component and minor silt components deposited from a static water flow and simultaneously deposited with sand particles >10% classified as sand rich mudstones and siltstones (Moore, 2005)

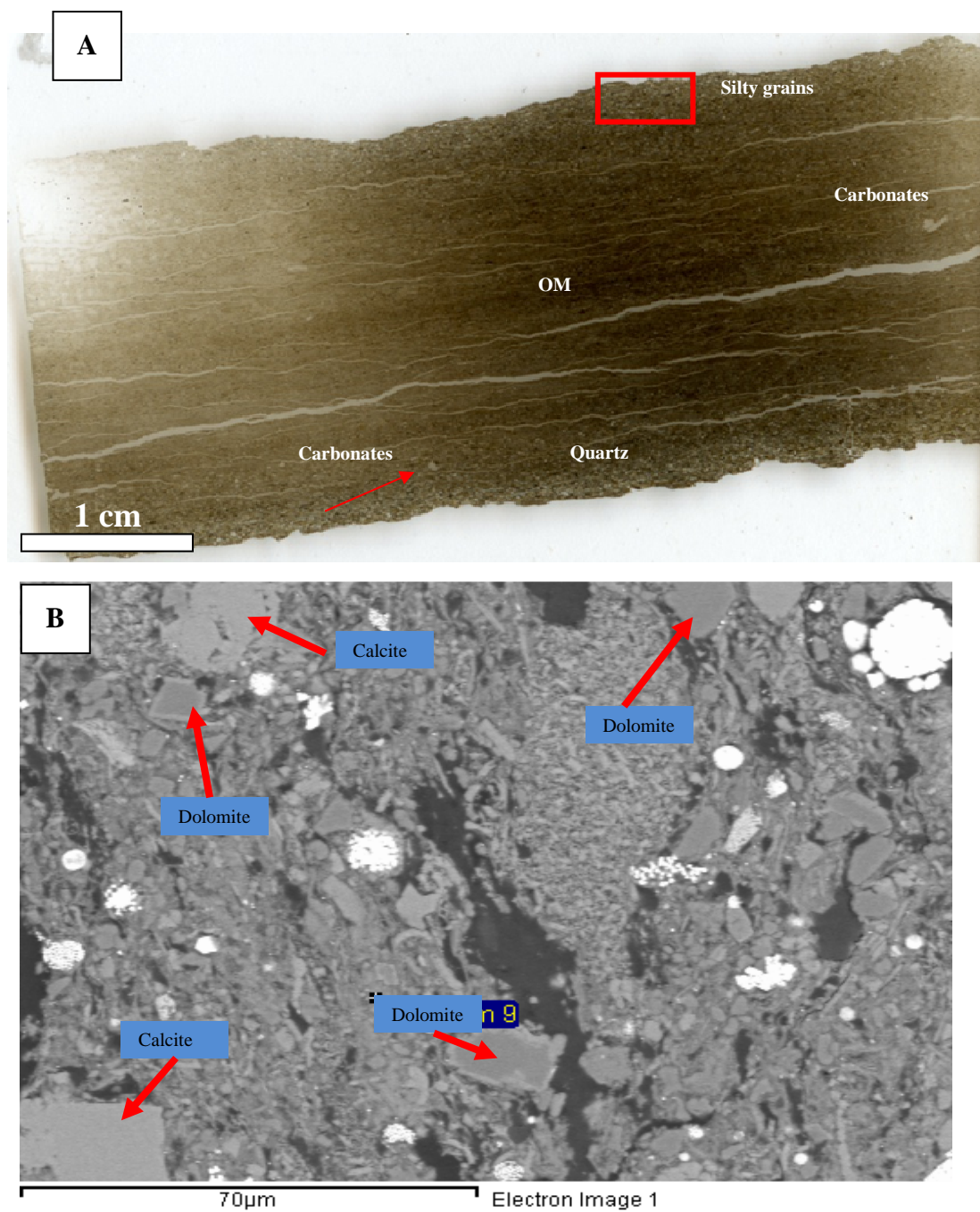


Figure 4.7: (A) Thin section of the sample within the Fish Scales Formation, within the AER core at a depth of 410m. The sample is rich in quartz, and silt-size grains carbonate patches. The red rectangle denotes the area within which view of the SEM image is taken. (B) SEM shows the presence of calcites, dolomite and pyrite.

The grain size spectra of the Second White Specks Formation show an increased contribution of unflocculated silt grains with about 80% of the samples composed of floc-silt mixtures. Five samples from different cores all exhibit grain size distribution characteristic of Floc-dominated and/or silt-dominated floc-silt mixtures deposited as single grains from a static water column or from a dilute flow. The grain size spectra of the SWS Formation suggests that it is the siltiest of the lower Colorado Formation, but it is worth noting that it is the most calcareous formation and half of the samples could not be disaggregated due to the high carbonate content nature of the formation. Thin section and SEM images show that the formation is mostly comprised of, organic-rich sediments, clayey mudstone or clay and mud-rich siltstone laminae/beds with occasional clay-sized or silt-sized quartz grains and sand-sized carbonate laminae (Fig. 4.10). The silty mudstone contains abundant stringers of organic matter and occasional floating quartz grains (Fig. 4.10).

The calcareous laminations within the Second White Specks Formation comprise coccoliths, (Fig. 4.15). Internal pore space within the coccoliths are recrystallised and filled with calcite, forming overgrowths (Fig. 4.15B). Other areas between the coccoliths are filled with mudstone (Fig. 4.15B).

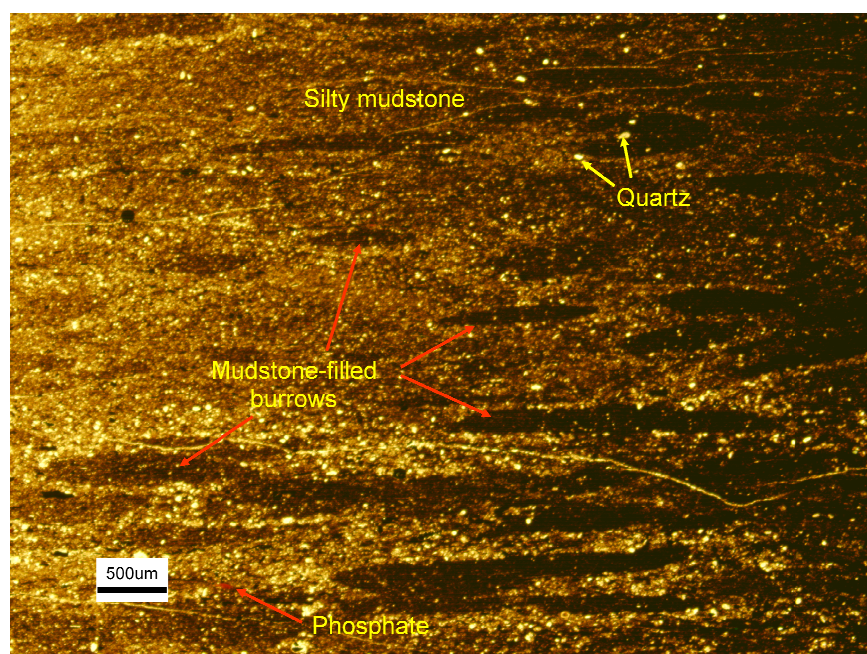


Figure 4.8: Petrographic image of a sample within the Second White Specks Formation, at a depth of 628.4 m filled burrows within a silty mudstone bed. The elongated shape of the burrows indicates that the sediments have been compacted during burial.

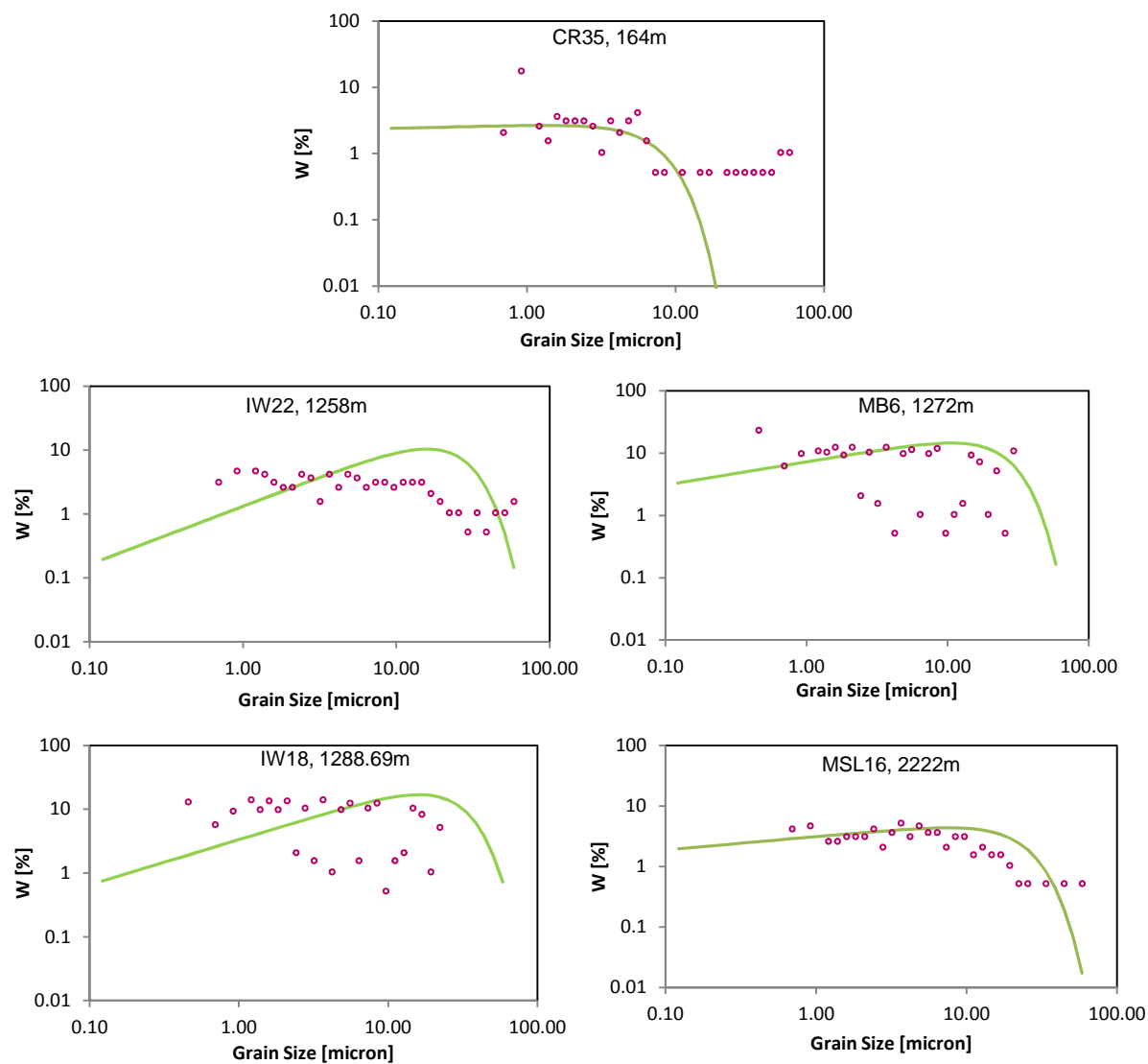


Figure 4.9: Grain size spectra of the Belle Fourche Formation. Grain size spectra of samples from the Belle Fourche Formation with flocculated components (Type 2 mudstone) grain size spectra

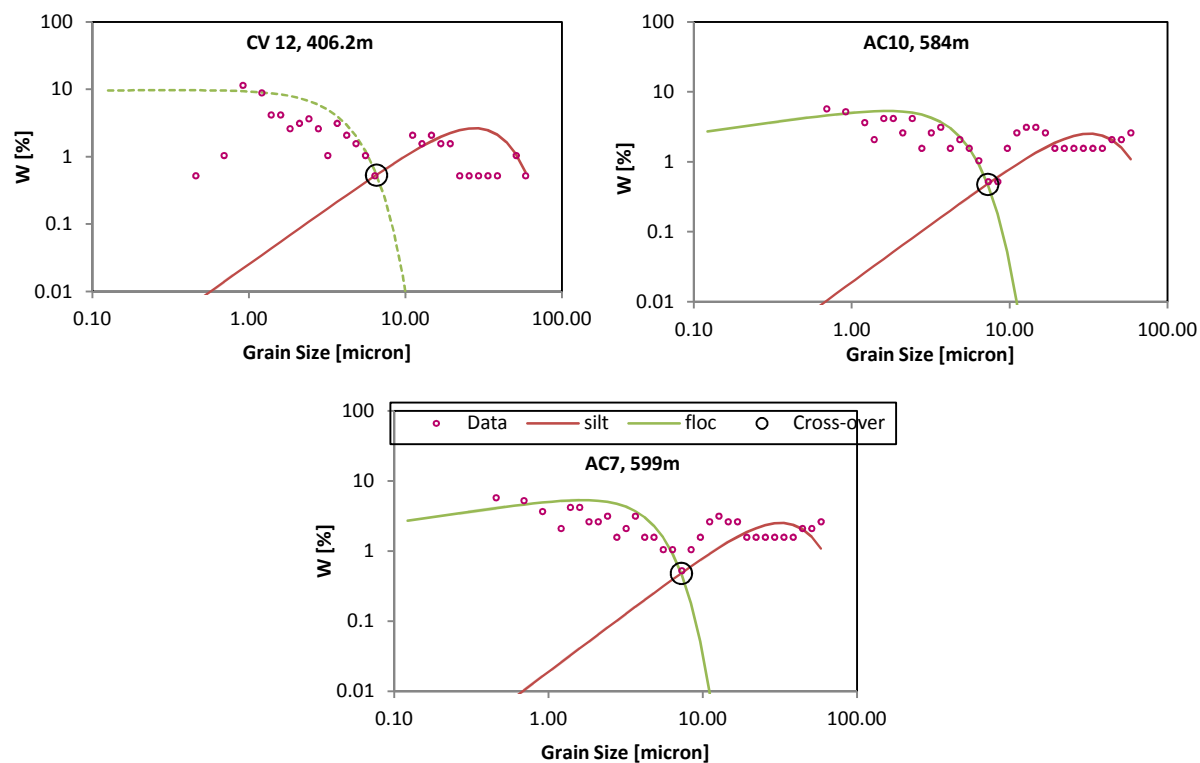


Figure 4.10: Grain size spectra of the Belle Fourche Formation showing samples with Silt dominated floc-silt mixture after (Moore, 2005) with a higher non-cohesive coarse silt component (41%, Table 4.3).

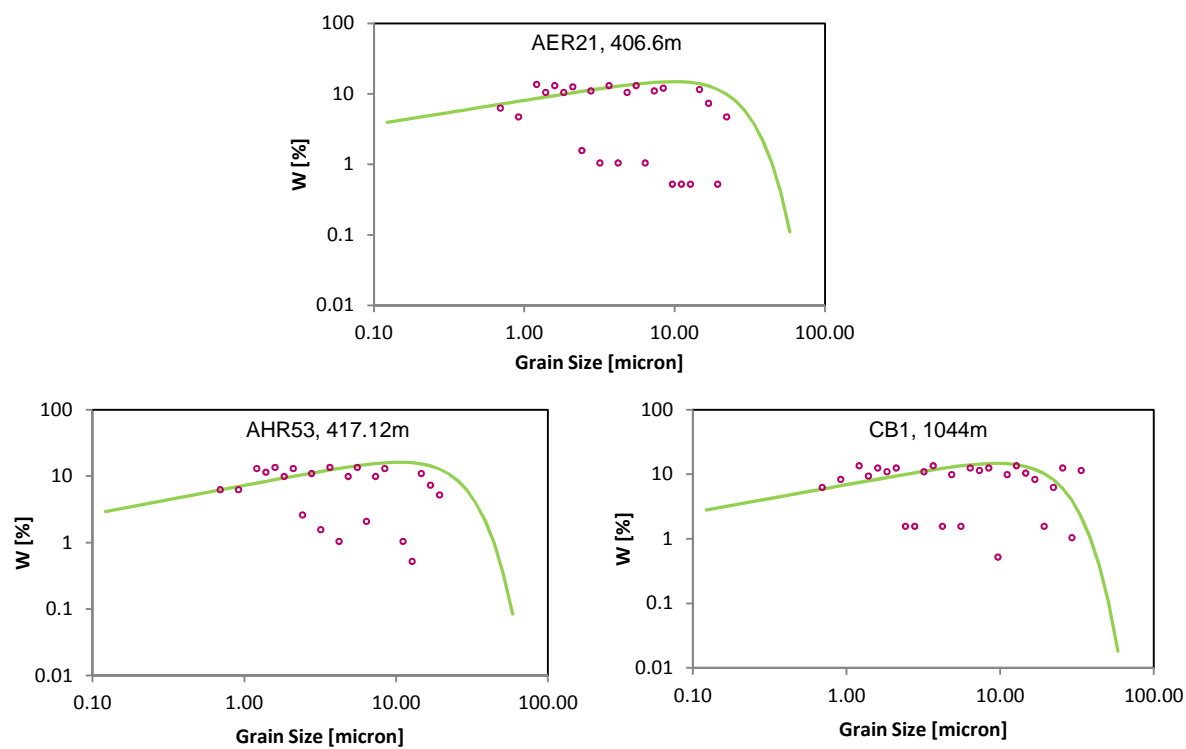


Figure 4.11: Grain size spectra of samples from the SWS Formation with flocculated grain size spectra

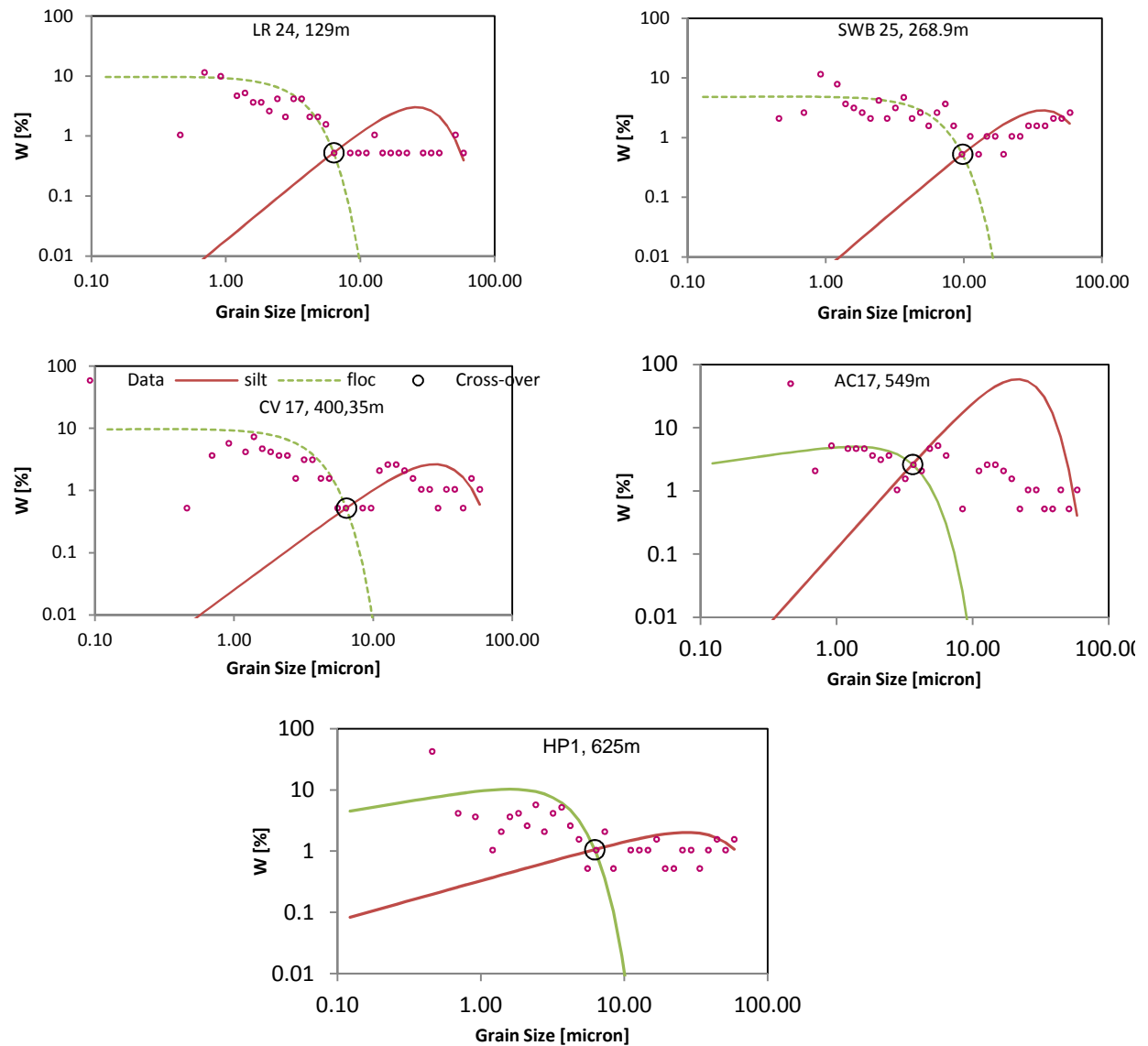


Figure 4.12: Grain size spectra of the Second White Specks Formation with a silt dominated floc-silt mixture after (Moore, 2005) with a higher non-cohesive coarse silt component.

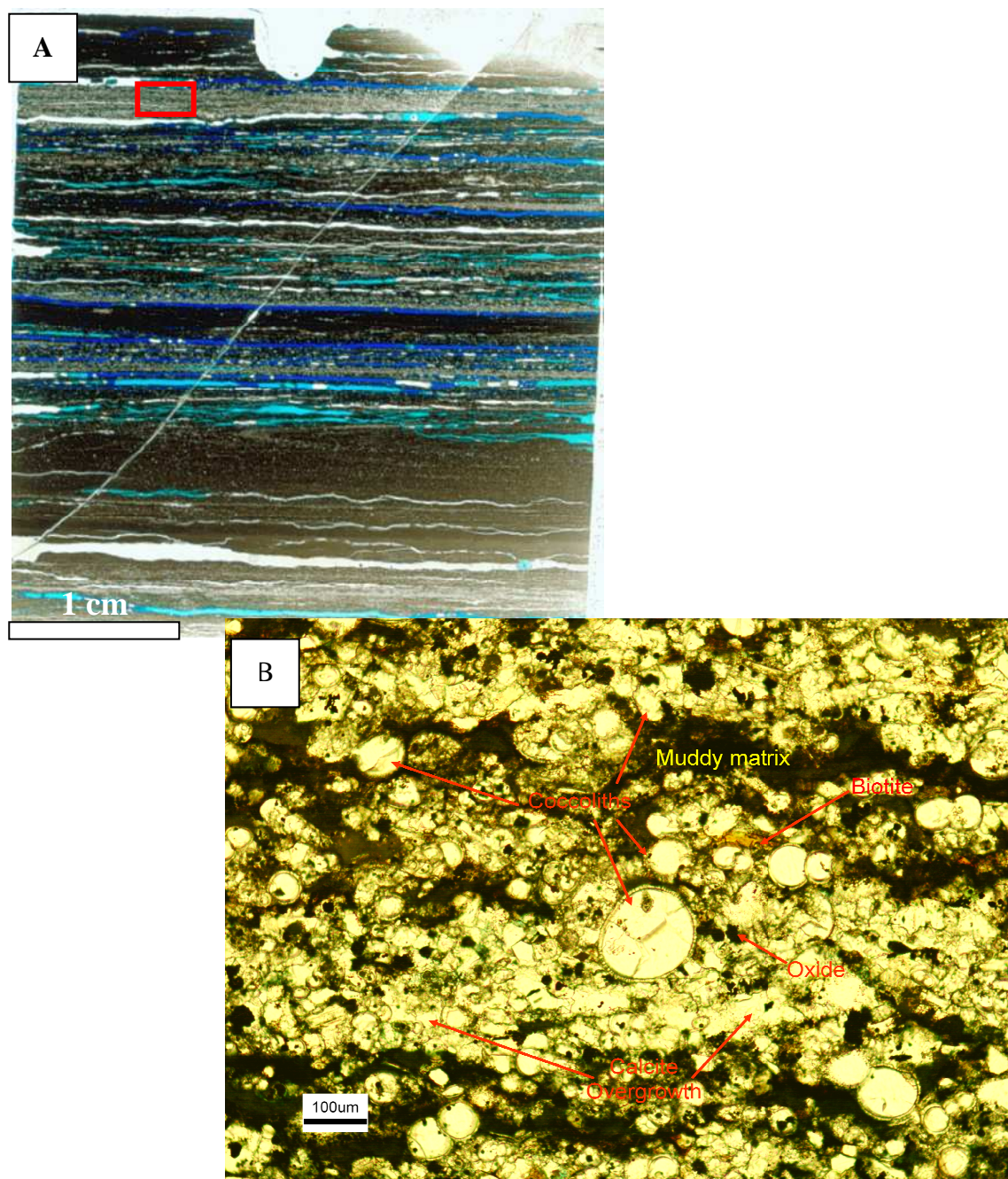


Figure 4.13: (A) Thin section of a sample within the Second White Specks Formation comprised of calcareous laminations, coccoliths, at a depth of 647.6 m. The red rectangle denotes the area within which the light microscopy image is taken. (B) Show coccoliths in the lamination are recrystallized and cemented by calcite overgrowths.

4.5 Pore Size Distribution of the Colorado Group

Porosity and permeability values for the lower Colorado Group were determined using mercury injection techniques. The background and description of the MICP technique is given in chapter two. Small pieces of core of $\sim 1 \text{ cm}^3$ were prepared for the determination of porosity and the pore throat radius distribution using a Micromeritics® Autopore II 9220 Series mercury porosimeter. The rock samples were freeze dried for 24hr at 40°C to remove any free water present in the pore, and therefore minimising the clay shrinkage effects associated with oven drying. The pore throat size distributions were measured assuming the surface tension of mercury to be 0.48 N/m and the contact angle between mercury and the particle surface to be 141° (Yang and Aplin, 1998; Purcell, 1949):

$$r = \frac{746,000}{p} \text{ --- Equation 4.3}$$

Where r is the pore throat radius (nm) and p is the pressure in kPa.

The distributions were corrected for artefacts which may arise during sample preparation, the creation of large cracks (Yang and Aplin, 1998) represented as a small second peak at large pore radii on the pore size frequency distributions. The second mode was rejected and the true distribution assumed to end at the turning point between the two peaks (Fig. 4.16). All calculations were performed using the pore-throat size distribution defined by genuine pore-throats as a function of cumulative porosity.

Permeability was calculated from pore size distributions following the Yang and Aplin (1998) model. The model estimates permeability in terms of porosity, the average alignment of pores, the pore shape and the pore throat size:

$$K_x = \frac{9 \cdot 10^{-18} \phi (\cos(\alpha))^2}{16} \frac{J1^3}{J2 (1+J1+J1^2)^2} \text{ --- Equation 4.4}$$

$$K_y = \frac{9 \cdot 10^{-18} \phi (\sin(\alpha))^2}{16} \frac{J1^3}{J2 (1+J1+J1^2)^2} \text{ --- Equation 4.5}$$

Where K_x = *absolute permeability of the sediment along the bedding direction*

K_y

= *absolute permeability of the sediment along the direction perpendicular to the bedding plane*

α = *pore alignment*

$J1$ & $J2$ = *pore shape of the sediment at half length and pore throat respectively*

The sediment pore shape is a function of lithology and compaction; $J1$ decreases with increasing compaction and loss of porosity, while $J2$ will increase (Yang and Aplin, 1998) (refer to reference for more explanation). Permeabilities were calculated using the clay content determined from the grain size analysis; permeability was computed assuming clay contents of 40% for samples that could not be disaggregated during grain size analysis.

The MICP porosities and permeabilities for selected samples of the Colorado Group formations are shown in Tables 4.6 & 4.7. Samples for the MICP analysis were selected from different wells and incorporating the top, middle and lower sections of each formation with more samples towards lithological boundaries, where samples are available. The rationale for this is to capture any variability in compaction due to burial depth and hence the porosity throughout the formations.

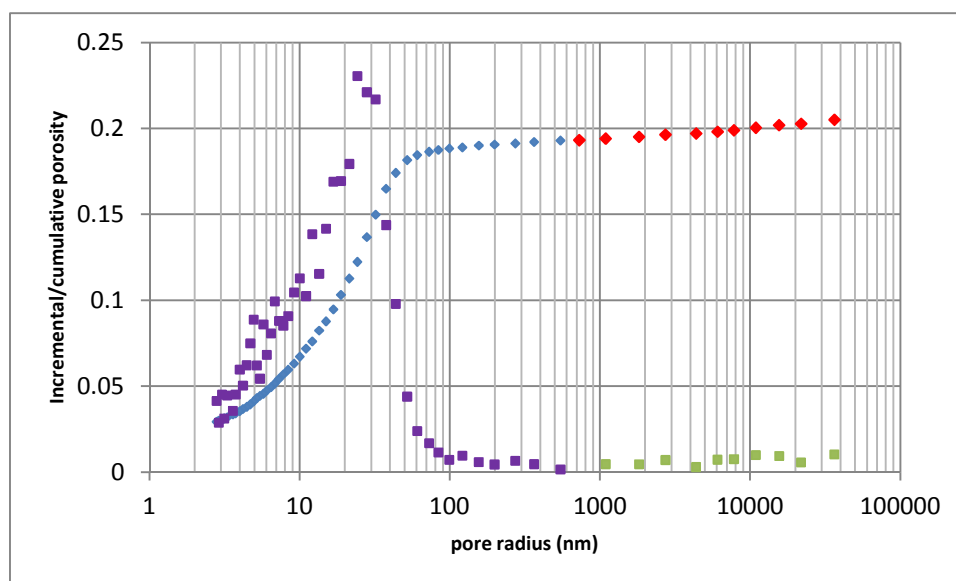


Figure 4.14: MICP Pore-throat size distribution. The distribution in blue show genuine pore-throats while pore throats distribution believed to be generated during sampling process are shown in red and green. This corresponds to the point where the Density distribution meets the baseline; all pores larger than this (i.e, the green density distribution) are assumed to be due to sample damage

The lowermost Viking Formation samples have porosities between 7 – 23% (average 14%), and mean pore radius between 15.9 – 81.0nm (average 38.5nm). The porosities for the Westgate Formation are shown in Figure 4.16- 4.17. Porosities range between 5.1 – 29.1% with an average of 16.0%. It appears that the PSD are influenced more by the level of compaction (porosity) rather than the grain size distributions. For example the pore size distributions for the Westgate Formation exhibit two trends: samples with porosity between 0 – 15% have tight pore size distribution of generally <10nm (Fig. 4.17) while samples with porosities > 15% have broader pore size distributions >10nm (Fig. 4.18). The clay fractions for both samples with tight and broad PSDs are relatively similar, ranging between 45- 60%. However, samples AER3 (Fig. 4.18) shows the broadest PSD and is characterised by bimodal pore size distributions, suggesting a contribution of silt size materials in the mudstones (e.g Dewhurst et al. 1998; Yang and Aplin, 1998). Grain size data (Table 4.4) show that sample AER3 is a sandy mudstone with sand (fractions >62.5µm) content greater than 10%, which is reflected as a second peak in the pore size distributions.

Table 4.6: MICP data for the Colorado Group (Viking, Westgate and Fish Scales)

Formation	Sample Well	Depth (m)	Total Porosity	Corrected Porosity	rmean (nm)	Modelled Kx (m ²)	Modelled Kz (m ²)
Viking	CR3	196.7	0.25	0.23	35.1	6.0E-20	1.7E-20
Viking	IY2	351.13	0.21	0.19	81.0	1.1E-19	4.6E-20
Viking	PH1	1254.6	0.15	0.15	16.0	1.4E-20	5.7E-21
Viking	MT2	1577.1	0.08	0.08	29.6	1.4E-20	5.0E-21
Viking	REW02	2202.9	0.08	0.07	30.9	1.3E-20	4.8E-21
Westgate	LR9	150	0.25	0.24	17.6	3.1E-20	8.3E-21
Westgate	CR19	180	0.29	0.29	23.3	4.1E-20	2.0E-20
Westgate	SW9	314.07	0.22	0.22	30.0	4.8E-20	1.3E-20
Westgate	MG1	385.88	0.26	0.25	25.3	4.1E-20	1.9E-20
Westgate	CV8	418.2	0.23	0.22	15.3	2.5E-20	5.8E-21
Westgate	AER3	450.19	0.22	0.21	35.6	5.4E-20	1.6E-20
Westgate	AHR8	452.17	0.24	0.20	15.2	2.3E-20	3.6E-21
Westgate	CV1	484.8	0.17	0.17	13.3	1.3E-20	5.5E-21
Westgate	MDA01	907.77	0.12	0.11	5.2	3.2E-21	1.2E-21
Westgate	MDA02	910.84	0.16	0.15	8.1	6.9E-21	2.8E-21
Westgate	DR1	930.3	0.17	0.16	23.4	2.7E-20	7.0E-21
Westgate	MPD01	1000.42	0.11	0.10	6.8	3.8E-21	1.5E-21
Westgate	PH7	1236	0.11	0.10	9.0	5.1E-21	1.9E-21
Westgate	BSR12	1260	0.09	0.08	59.1	3.2E-20	1.2E-20
Westgate	MT5	1572.8	0.08	0.08	25.2	1.2E-20	3.9E-21
Westgate	MSL5	2247.5	0.06	0.05	6.3	1.7E-21	6.3E-22
Fish Scales	CR30	169	0.20	0.18	12.8	1.7E-20	3.3E-21
Fish Scales	IY9	299.47	0.22	0.22	9.8	1.3E-20	5.6E-21
Fish Scales	MG5	370.33	0.15	0.15	30.4	3.0E-20	1.1E-20
Fish Scales	AER9	434.95	0.22	0.21	20.8	2.4E-20	1.5E-20
Fish Scales	AHR26	442.87	0.25	0.23	10.6	1.4E-20	6.3E-21
Fish Scales	NH4	618.1	0.21	0.20	13.3	1.8E-20	4.8E-21
Fish Scales	BVW7	2129.9	0.03	0.03	65.4	1.1E-20	3.8E-21
Fish Scales	MSL11	2233.6	0.07	0.07	72.0	3.0E-20	1.1E-20

Table 4.7: MICP data for the Colorado Group (Belle Fourche, SWS and Upper Colorado)

Formation		Sample Well	Depth (m)	Total Porosity	Corrected Porosity	rmean (nm)	Modelled K _x (m ²)	Modelled K _z (m ²)
Belle Fourche		LR21	132	0.31	0.31	138.5	2.8E-19	1.4E-19
Belle Fourche		CR35	164	0.24	0.22	12.9	2.1E-20	4.7E-21
Belle Fourche		SWB14	291.7	0.23	0.22	12.4	2.1E-20	2.6E-21
Belle Fourche		CV12	406.2	0.20	0.19	20.2	2.8E-20	6.1E-21
Belle Fourche		AER17	446.84	0.22	0.20	953.1	1.8E-18	4.3E-19
Belle Fourche		IF1	505.36	0.19	0.18	14.8	1.9E-20	4.4E-21
Belle Fourche		IY11	508	0.31	0.31	7.6	1.2E-20	6.3E-21
Belle Fourche		NH6	692.2	0.21	0.20	24.7	3.1E-20	1.3E-20
Belle Fourche		AHR30	1448.5	0.24	0.23	16.0	2.2E-20	9.9E-21
Belle Fourche		SCD02	2055.1	0.04	0.04	79.0	1.8E-20	6.2E-21
Second Specks		White LR24	129	0.36	0.35	35.2	8.1E-20	2.5E-20
Second Specks		White IY15	261.52	0.20	0.19	89.5	1.2E-19	5.0E-20
Second Specks		White SWB25	268.9	0.35	0.32	25.1	4.6E-20	2.3E-20
Second Specks		White SWB23	340.5	0.35	0.35	88.6	1.8E-19	9.6E-20
Second Specks		White GS6	359.36	0.34	0.33	17.9	3.2E-20	1.7E-20
Second Specks		White CV17	400.35	0.25	0.24	142.2	2.9E-19	8.7E-20
Second Specks		White AHR53	413.12	0.41	0.29	36.8	7.0E-20	3.0E-20
Second Specks		White IF6	489.81	0.27	0.26	19.5	3.2E-20	1.5E-20
Second Specks		White AC14	564	0.07	0.06	316.0	1.4E-19	5.2E-20
Second Specks		White CRB02	574.4	0.15	0.15	9.7	8.5E-21	3.4E-21
Second Specks		White HP1	625.1	0.30	0.26	38.7	7.1E-20	2.5E-20
Second Specks		White DT6	692.2	0.25	0.24	21.5	3.3E-20	1.5E-20
Second Specks		White CB8	1028.2	0.11	0.11	92.0	6.8E-20	2.6E-20
Second Specks		White CB1	1044	0.12	0.11	21.5	1.3E-20	6.2E-21
Second Specks		White HLC01	1446.52	0.07	0.07	2.7	8.9E-22	3.2E-22
Second Specks		White DT2	2294.5	0.24	0.22	21.2	3.5E-20	9.2E-21
Upper Colorado		IF9	480.67	0.25	0.24	19.0	3.0E-20	1.2E-20
Upper Colorado		BEI 01	582.2	0.07	0.06	3.9	1.0E-21	3.8E-22
Upper Colorado		BEI02	590.6	0.08	0.07	18.1	7.2E-21	2.6E-21
Upper Colorado		HP5	616.9	0.32	0.19	24.2	3.2E-20	1.1E-20
Upper Colorado		PFV01	620.55	0.19	0.18	31.0	3.6E-20	1.5E-20
Upper Colorado		HP14	1204	0.05	0.05	31.7	8.7E-21	3.1E-21
Upper Colorado		TRB01	2284.3	0.07	0.06	45.3	1.7E-20	6.0E-21
Upper Colorado		SAF02	2510.87	0.08	0.07	4.7	1.6E-21	5.9E-22

Fish Scale Formation exhibits similar porosity to the Westgate Formation with an average value of 16.0%, although with a lower range (3.0 -23.0%). Measured mean pore radius varies from 6.3 – 35.6nm, with an average value of 19.9nm. The pore size distributions pattern exhibited is also similar to the Westgate Formation; however, grain size appears to be the dominant control on pore size distributions. For example, the grain size distribution data (Table 4.5) show that sample CR30 which has total porosity of 18%, is characterised by tight pore size distributions (mean pore size of 12.8nm) and clay fractions of 62.2%. On the other hand, sample AER9 with total porosity of 21% has broader GSDs with a mean pore size of 20.8nm due to higher contribution of sortable silt content (37.8%). Both samples have similar porosities but different pore size distributions due to differences in grain size compositions.

The Belle Fourche Formation exhibits the broadest and highest mean pore radius (7.6 – 953.1nm) with an average value of 127.9nm. Porosity values range between 4 – 31% and average value of 21% (Table 4.7). Like the Westgate and Fish Scales Formations, the Belle Fourche Formation shows that tight grain size distributions are associated with clay rich samples, while silty and sandy rich samples results in broader PSDs. The Crooked River core CR35 with PSDs <10nm contain 60.3% clay content is another typical example. The Anderson et al Ribson core which is located at the Alberta/Saskatchewan border show distinct PSDs in all the Westgate, Fish Scales and Belle Fourche Formations. Samples (AER3, AER9 & AER17) are characterised by a bimodal PSDs. The pore space networks of mudstones tend to be either unimodal signifying single-scale porosity, (i.e. either dominantly microporosity or nanoporosity) or bimodal signifying both micro-porosity and nano-porosity are present (Javadpour et al. 2007). The grain size distribution for sample AER9 indicates that it contain a significant range of clay-sized, silt-sized and sand-sized sediments, while sample AER3 though rich in clay content (53%) has significant sand fractions (12%). Javadpour et al. (2007) report that samples containing a significant range of clay-sized, silt-sized and sand-sized sediments have characteristic bimodal pore size distribution with significant implications on gas capacities as both micrometer and nanometer-scale pores may be present within a shale interval.

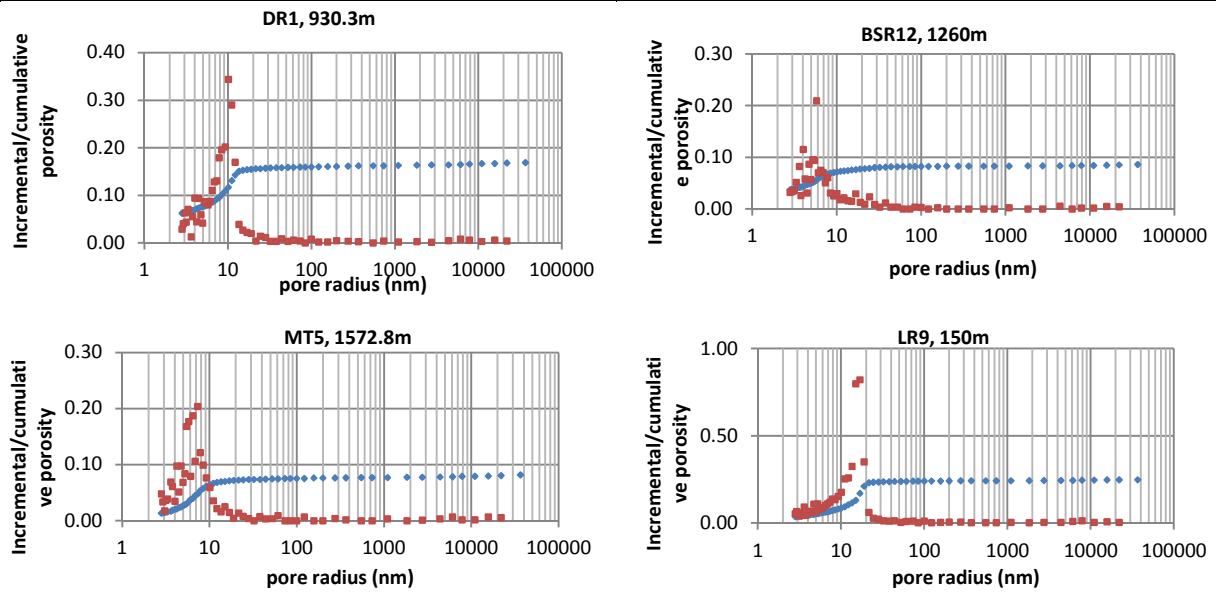


Figure 4.15: PSDs of the Westgate Formation. Samples characterised by tight pore size distributions between 10 – 70nm, associated with low porosity values (0 -15%) due to increased level of compaction

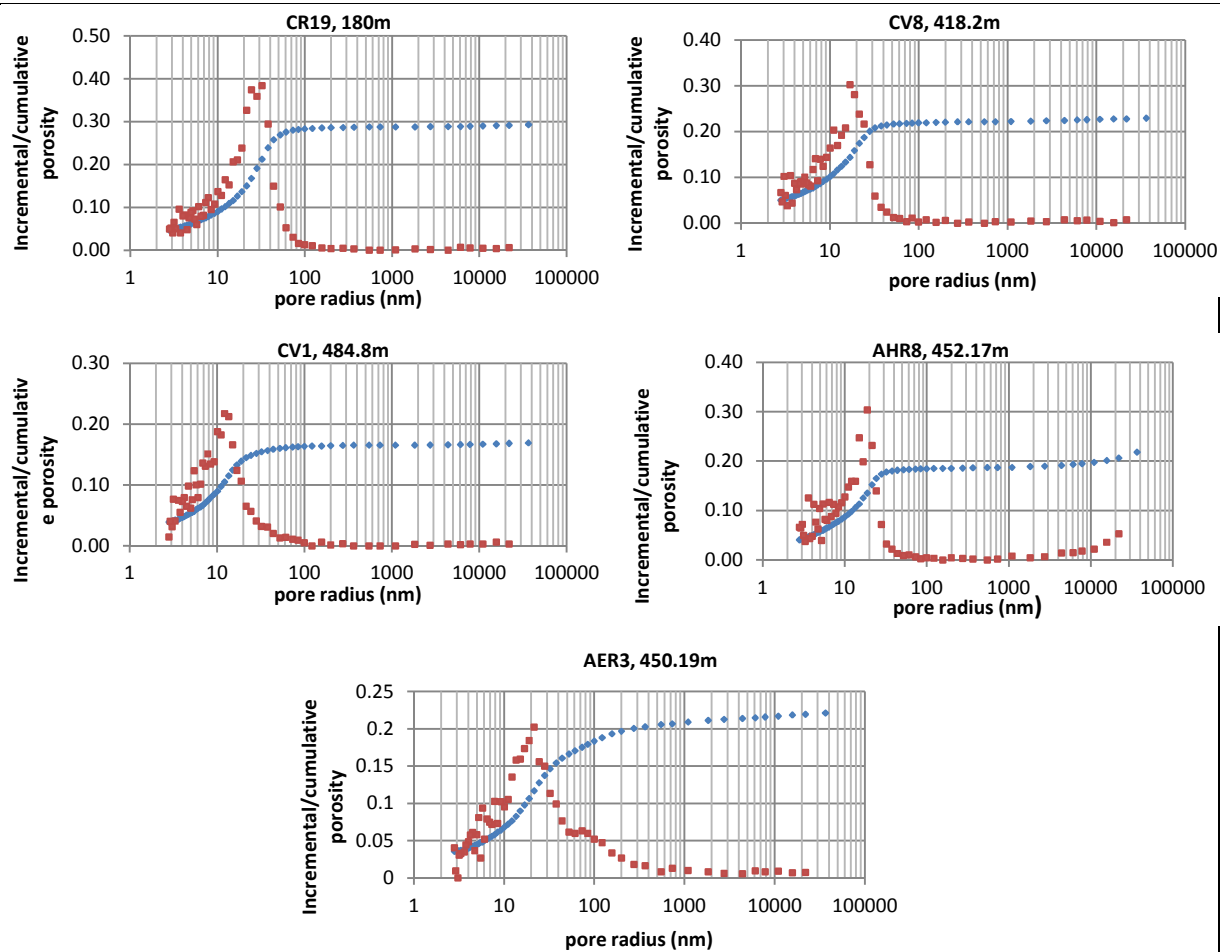


Figure 4.16: PSDs of the Westgate Formation. Samples characterised by broader pore size distributions between >10nm, associated with higher porosity values (19-29%) due to low level of compaction. Note that sample AER3 has the broadest PSD and also bimodal due to sand fractions of ~10%.

Javadpour et al. (2007) indicates that nanopores actually contain a greater surface area than micropores therefore, the greatest potential for gas adsorption lies within intervals of dominantly unimodal nanoporosity.

The Second White Specks Formation has porosities ranging from 7 – 35% (average 22%), representing the highest range of porosity of any of the lower Colorado Group Formations. Mean pore radius of the Second White Specks Formation is also highly variable ranging between 2.7– 315.0nm (average of 61.2%). The Second White Specks show a more variable pore size distributions comprising a unimodal tight pore size distributions rich in clay content, bimodal distributions consisting of both clay sized and silt sized materials and a third pore size distribution that is broader and rich in carbonate content (Fig.4.21-4.22).

The Upper Colorado samples analysed here-in show lower porosities with an average value of 12% (7 – 24%); and mean pore radius of (3.2 – 45.3nm, average 22.2nm) compared to the lower Colorado Group Formations.

Porosimetry indicates that calculated permeabilities for the entire data set range between 9.0×10^{-7} to 1.9×10^{-3} mD, spanning 4 orders of magnitude and generally within the range of 10 – 100nD. The relationship between porosity and permeability shows a fairly good correlation for all the formations (Fig. 4.24). Correlations are fairly good with higher permeability values generally associated with more porous sediments. The Fish Scales Formation show the most restricted range of permeability with values within one order of magnitude (1.1×10^{-5} – 3.0×10^{-5} mD). The Viking, Westgate and Upper Colorado samples have permeability values spanning two orders of magnitude (1.3×10^{-5} – 3.0×10^{-4} mD; 1.8×10^{-6} – 5.5×10^{-5} mD; 1.1×10^{-5} – 3.0×10^{-5} mD) respectively. The Belle Fourche and Second White Specks Formations exhibit broader and higher range of permeabilities (3-4 orders of magnitude) with values ranging between 1.3×10^{-5} – 1.9×10^{-3} mD and 9.0×10^{-7} – 2.9×10^{-4} mD respectively.

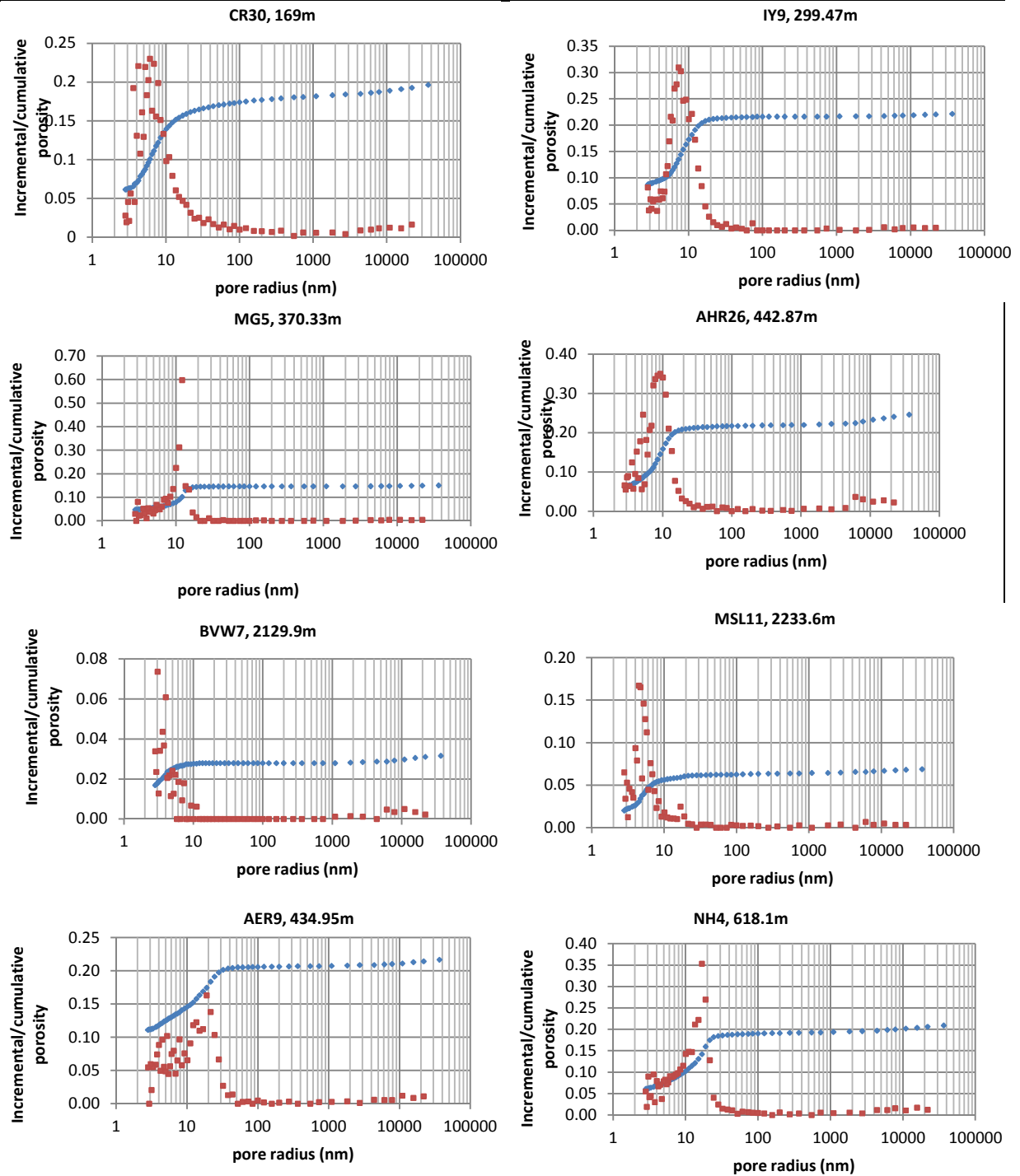


Figure 4.17: PSDs for the Fish Scales Formation similar to the PSD's observed in the Westgate Formation. Note the broader PSDs in sample AER 9 due to a significant range of clay-sized, silt-sized and sand-sized sediments.

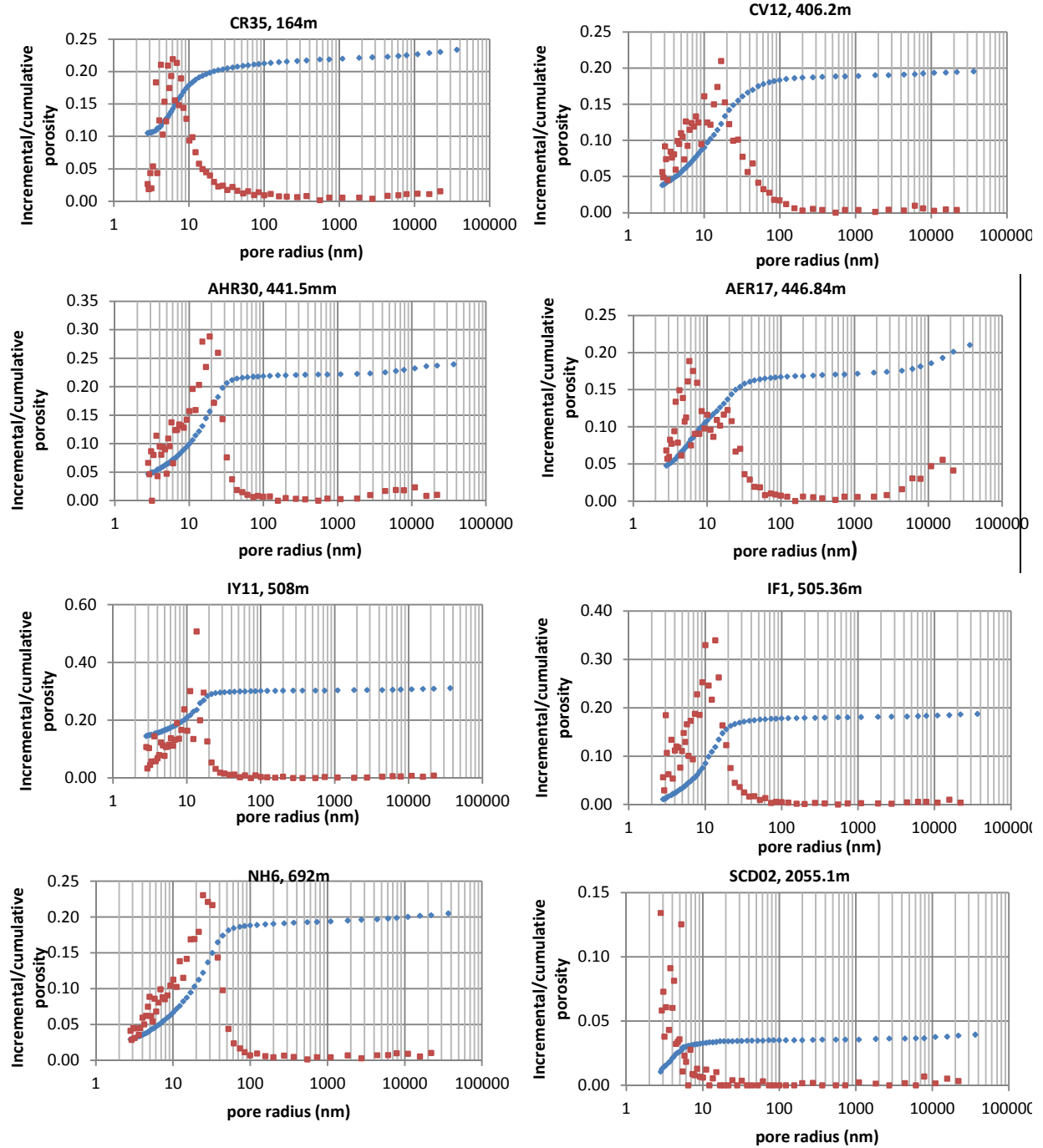


Figure 4.18: PSDs of the Belle Fourche. Clay rich samples tend to results in tighter PSDs, while silty and sandy rich samples results in broader PSDs

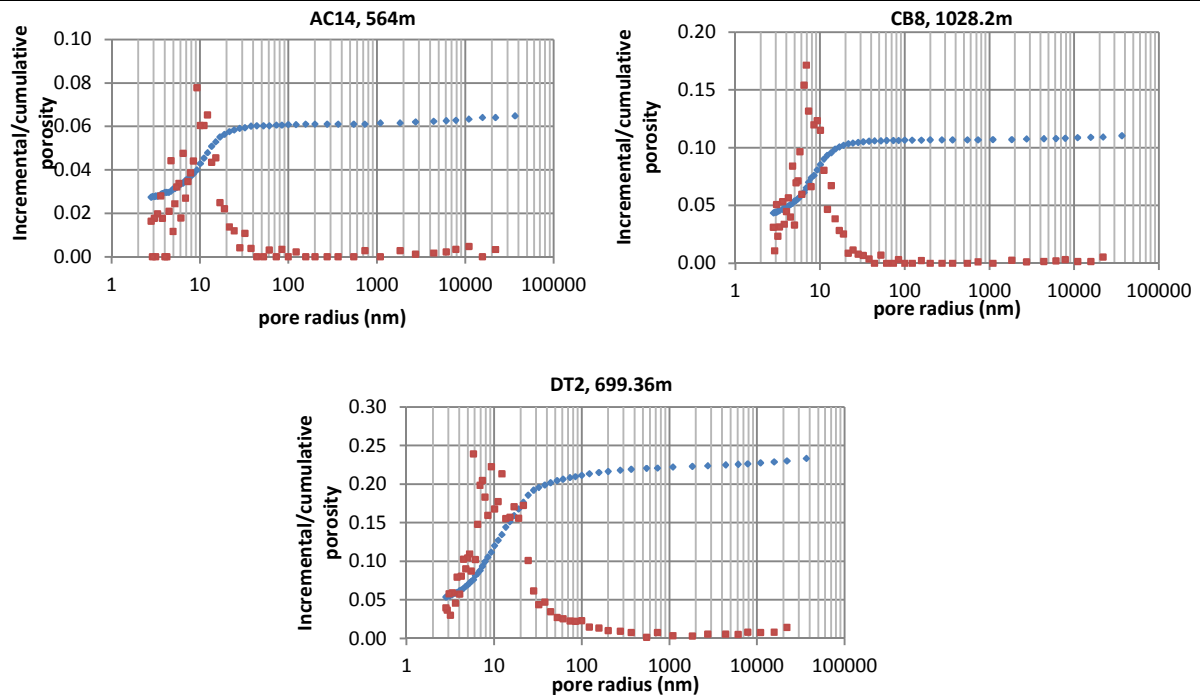


Figure 4.19: PSDs of the SWS. Samples characterised by tight pore size distributions between 10 – 70nm, associated with low porosity values (0 -11%) due to increased level of compaction. Sample DT2 has higher porosity but the PSD is still relatively tight due to high clay fractions of ~56%.

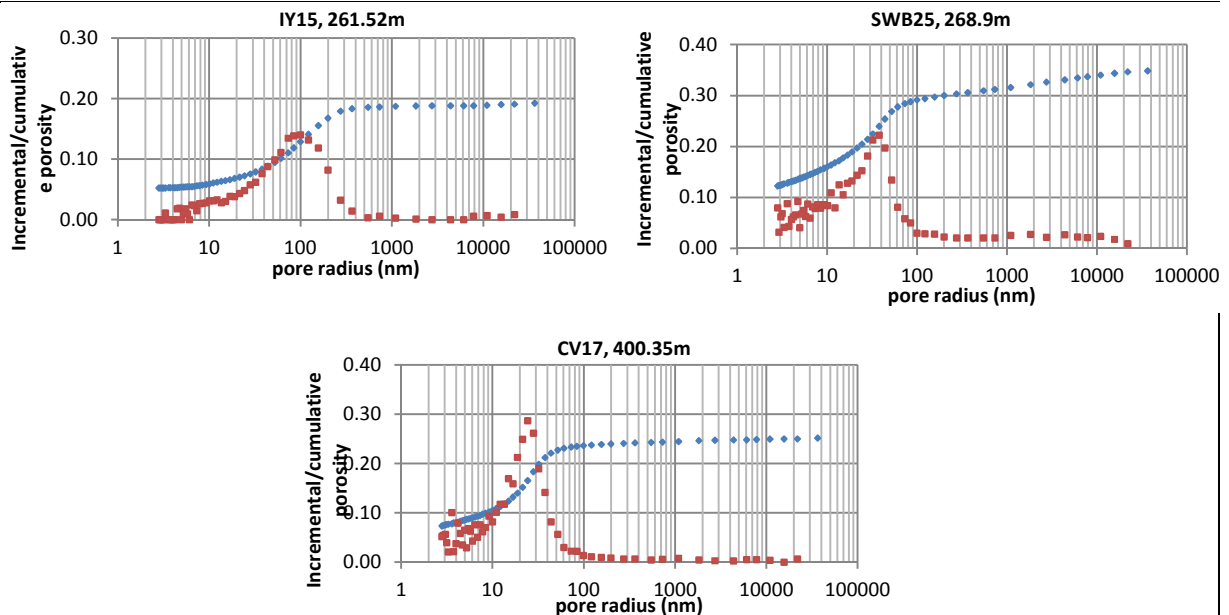


Figure 4.20: PSDs of the SWS Formation. Samples characterised by very broad pore size distributions associated with high porosity values (19-32%). Samples IY15 and SWB25 have carbonate contents of 84% and 35.6% respectively while CV17 has only 6.8%

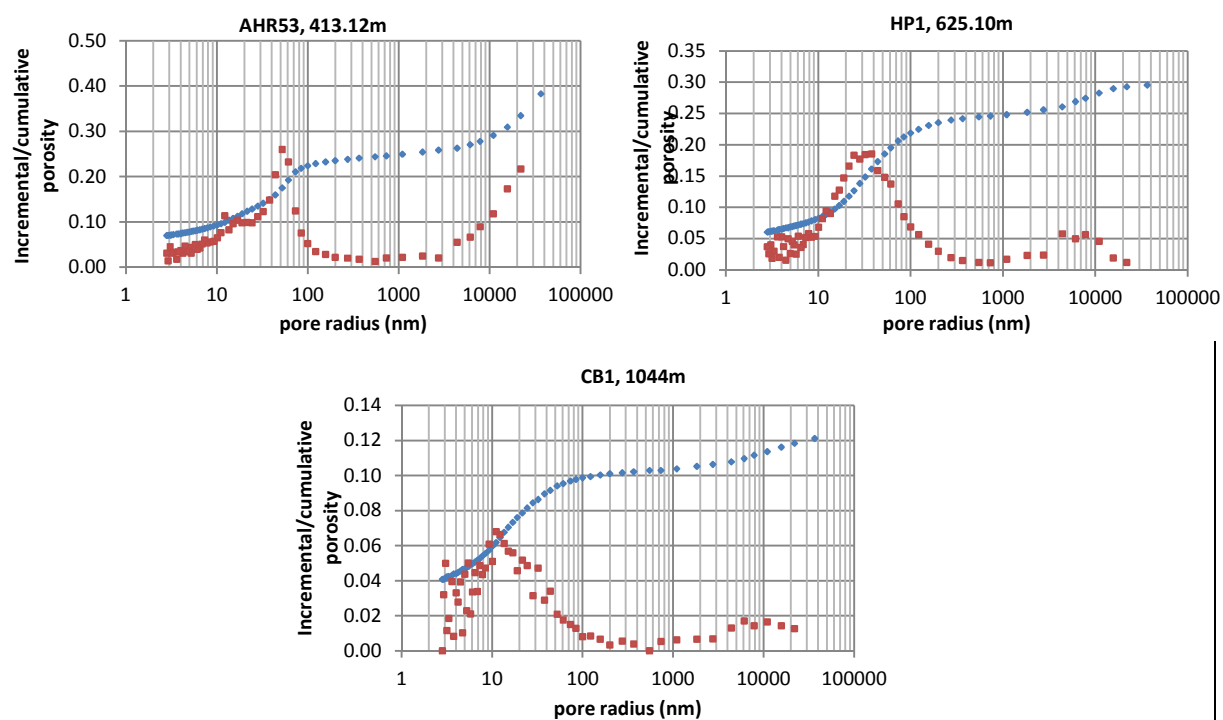


Figure 4.21: PSDs of the SWS Formation. Samples characterised by broad and bimodal PSDs due to significant range of clay-sized, silt-sized and sand-sized grains.

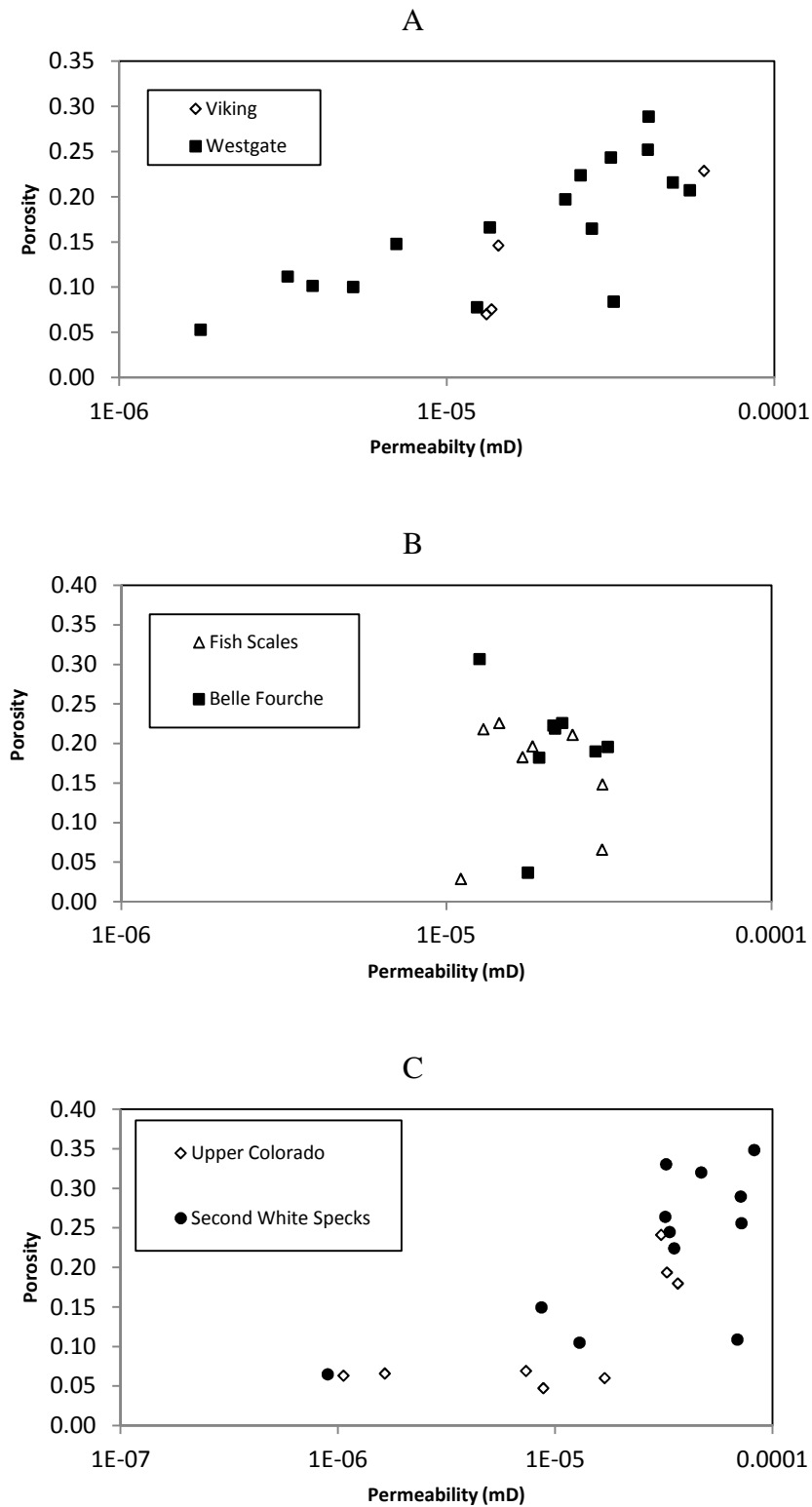


Figure 4.22: Relationship between porosity and permeability for (A) Viking and Westgate Formations (B) Belle Fourche and Fish Scales Formation and (C) SWS Formation and Upper Colorado samples

4.6 Summary

The mineralogical composition of the Westgate formation is dominated by quartz (5-50%) and clays (25-70%) with very low feldspar and carbonate contents. The Fish Scales Formation mineralogy is similar to the Westgate Formation. Quartz ranges between 4-61% (mean 35%), while, clays varies between 11- 67% (mean 38%). However, the Fish Scales contains some carbonate rich samples (3 – 40%) in the lower section of the formation. The Belle Fourche Formation exhibits a broader range of mineralogy than the underlying Fish Scales Formation, with a relative increase in the proportion of carbonates. Carbonates peak at 52% at the upper part of the formation but with a mean of 6.7%. The clays vary from 8.7- 64.1% (mean 44%) significantly higher than quartz 6.6-48.8% (mean 25%). The mineralogy of the Second White Specks Formation is quite distinct from the other Colorado Group shales exhibiting the greatest variation and the greatest carbonate contents. Calcite occurs in concentrations ranges from 3.1-74% as a common feature of the Second White Specks, and is clearly visible as *Inoceramus* shells, and coccoliths on thin sections. However, quartz (0-56%) and clays (0-65%) do occur in high concentrations in some samples, indicating that the Second White Specks formation is composed of calcareous limestone to mudstone.

Grain size analysis shows that the Colorado group is dominated by fine grain clay size sediments but generally consists of heterogeneous mixture of mudstones and silty shales. The Westgate Formation is characterised by a dominant flocculated grain size distribution when fitted with Kranck model (1996) indicative of deposition in a quiet energy setting, although some samples exhibit a flocculated-silt distribution indicative of slow deposition at the distal end of sediment transport path in relatively high energy environments. Similarly, the Fish Scales Formation contain both flocculated materials characteristic of low energy environment and flocculated-silt mixture materials assumed to be deposited from static water columns or from dilute flows.

The Belle Fourche Formation is characterised by silt-size grains supported in a clay/mudstone matrix deposited as flocculated and silt dominated floc-silt mixture materials. The Second White Specks show grain size distribution characteristic of different types of mudstones including flocculated, floc-silt mixture, and silt-dominated distribution types representing different depositional environments (high energy to low energy).

About half of the samples could not be disaggregated because of the high abundance of fossil (specks) materials and therefore fitting the data to the Kranck model (1996) was problematic which could have affected the quality of the result due to poor sorting due to poor data quality.

The measured MICP porosity for the Colorado Group ranges from 3- 35%, with an average porosity value of 18%. Pore size distributions are predominantly unimodal with an average mean pore radius (r_{mean}) value of 50.5nm, although some samples exhibit bimodal pore size distributions reflecting mixture of mudstones and silt size materials. Porosity data obtained from the Westgate ranges from 5.0 – 29.9% total porosity (the majority of samples have porosity values <20%), whereas values from the Fish Scales range from 3.0-22.0% (Table 4.5 -4.6). The Second White Specks and Belle Fourche Formations appear to be the most porous with average porosities and mean pore radii of (22%; 61.1nm, 21%; 127.9nm) respectively.

5 CHAPTER FIVE: SPATIAL AND STRATIGRAPHIC VARIATIONS OF THE COLORADO GROUP

5.1 Introduction

The main aim of this chapter is to integrate the mineralogy, grain size, pore size data and organic facies data in order to interpret and discuss (a) spatial and temporal variations in mineralogy, grain size and TOC, (b) the main controls on organic richness of the Colorado Group and (c) influence of grain size and porosity on the pore size distributions and the implications for shale gas prospects.

Mineralogy, palynofacies and grain size data were integrated in order to investigate if there is any relationship that can be linked to sediment source, transport pathways, as well as energy of the water column and locations of sedimentation. Palynofacies and geochemical data were obtained from Buckley's (2004) study. Palynofacies analysis is the transmitted white light analysis of the microscopic particulate organic-matter assemblage within sediments, after any mineral constituents have been chemically broken down and removed. Palynofacies thus provides information on the nature of the depositional environment and source rock potential. Integration of mineralogical data with palynofacies and their correlations with grain size data is hypothesised to show some relationships via common supply, transport processes and depositional cycles. This in turn can be useful in correlating and understanding the sequence stratigraphy of organic-rich sections as well as predicting source rock and shale gas reservoir potential.

Colorado Group isopach data (Leckie et al. 1994; Schröder-Adams et al. 1996) have shown the deformation edge of the Western Cordillera in north-western Alberta as the main source of detritus input into the basin (Fig. 5.1). Isopachs of the Westgate Formation are thickest in north-eastern British Columbia (up to 400 m) thinning towards the southeast (Schröder-Adams et al. 1996). The isopach from the base of the Fish Scales Formation to the base of the Dunvegan Formation (Fish Scales and lowest Belle Fourche Formations) shows a similar south-eastwards thinning with maximum thicknesses over the Peace River Arch in north-eastern British Columbia and north-western Alberta (Schröder-Adams et al. 1996). The isopach from Dunvegan (Belle Fourche Formation) to Second White Specks Formation shows a thick area on the Peace River Arch but the thinning trend has shifted and is north-

eastwards. Isopachs of Fish Scales and Belle Fourche Formations show a general eastwards thinning. Isopach maps from above the Second White Specks Formation (Schröder-Adams et al. 1996) show a general southwards shift of the depocentre and basin, with thinning towards the northeast. However, sediment isopachs for the Colorado Group are not parallel to the palaeo-coastline and therefore, the coastline cannot be used as the point of terrestrial input. Buckley, (2004) previously calculated the distance from source based upon isopachs with an E-W transect from a point in the Peace River area (55° 15' N 120° 00' W; Fig. 5.2). Well locations were plotted along this transect since same sample as Buckley (2004) sets were used in this study.

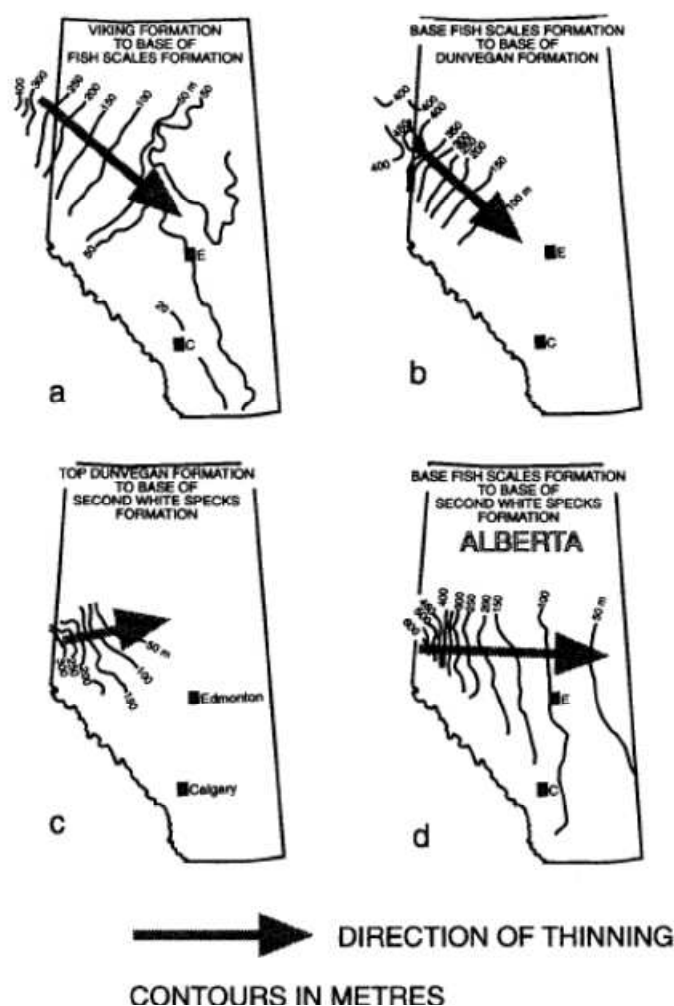


Figure 5.1: Isopach maps of four time slices within the upper Albian Viking Formation to uppermost Cenomanian base Second White Specks Formation (after Schröder-Adams et al. 1996)

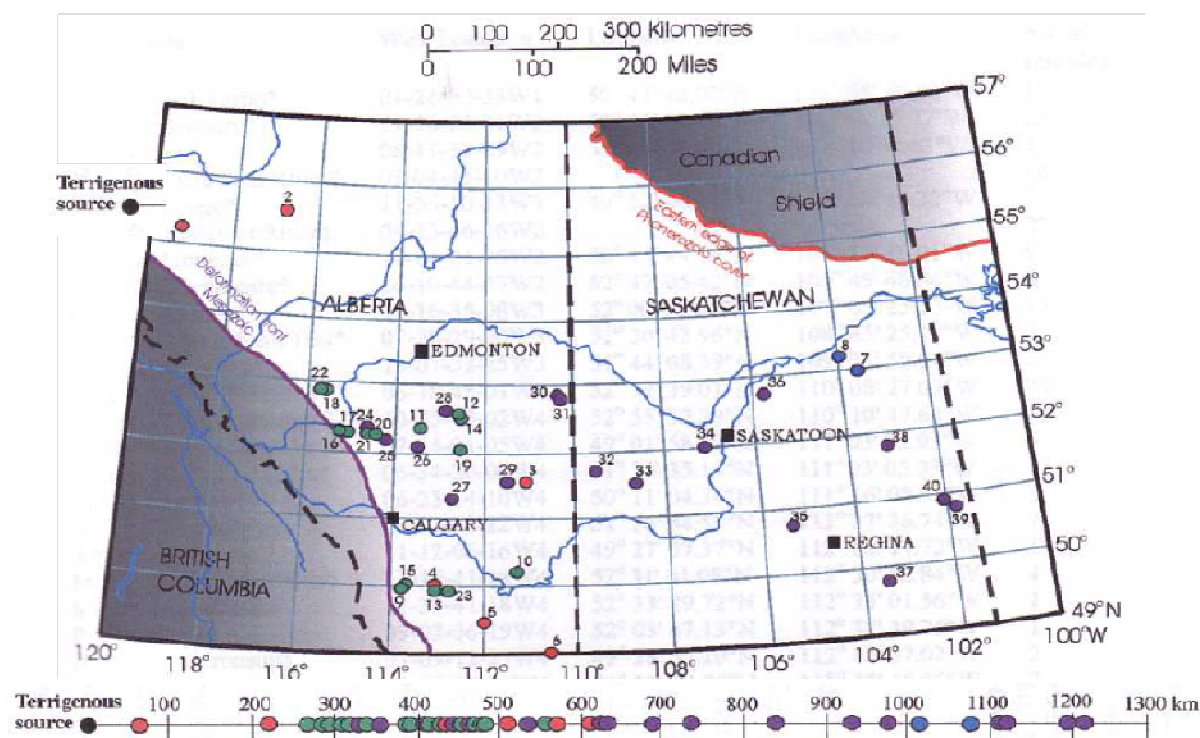


Figure 5.2: Map of the Colorado Group with study wells and transect (after Buckley, 2004). The line of section onto which the wells are projected runs east-west from the terrigenous source in north-west Alberta

Various studies (Buckley, 2004; McNeil and Gilboy, 1999; White et al. 1999; Schröder-Adams et al. 1996; Bloch et al. 1993) have produced sequence stratigraphic interpretations of the WCSB's Colorado Group based on high resolution micropalaeontological, geochemical and palynofacies data. Similarly, the study of organic facies has also been utilised (Tyson, 1996) to produce an overview of organic facies variations within a sequence stratigraphic framework in marine siliclastic systems. Tyson (1996) produced mappable suites which correspond with sea level fluctuations and sediments input based on geochemical data such as HI, TOC and carbonate content of the onshore Kimmeridge Clay Formation of the UK. The study shows that highest TOC values are associated with condensed sections, especially the maximum flooding surface (MFS), where siliciclastic input is at minimum.

Schröder-Adams et al. (1996) provide a general overview of the paleoenvironmental changes in the Cretaceous Colorado Group (Fig 5.3). The upper Albian Westgate Formation was deposited during a general transgression and it is characterised by up to three coarsening upward cycles (Schröder-Adams et al. 1996) due to changes in sea-levels and sediments

supply. Leckie et al. (2000) noted that the Westgate Formation is absent from the southern Alberta Foothills as a result of non-deposition or subsequent erosion.

The base of the early Cenomanian Fish Scales Formation is described as ‘either a wave-winnowed lag formed during a relative sea-fall and subsequent rise, or a current-winnowed lag in deep water’ (Schröder-Adams et al. 1996). Leckie et al. (1992) suggest that the base of the Fish Scale Zone also represents a major hiatus in Saskatchewan and Manitoba, with several substages missing below it. Deposition under a stratified water column with anoxic bottom waters has been interpreted to form a condensed section of well laminated shales that constitute the rest part of the formation (Schröder-Adams et al. 1996).

The middle to upper Cenomanian Belle Fourche Formation comprises lower sandstones and an upper series of prograding sandy wedges (Leckie et al. 1992). The lower part is characterised by marine shales and sandstones deposited on a shelf under low to moderate energy conditions (Leckie et al. 1992). Schröder-Adams et al. (1996) suggest a sea-level fall during the middle Belle Fourche in north-western Alberta associated with a relative increase in detrital input due to the progradation of the Dunvegan Delta, followed by a relative sea level rise.

The Second White Specks (Late Cenomanian – early Turonian) Formation is thought to have been deposited during a maximum transgression period associated with high productivity in the upper water column and an anoxic bottom water conditions. The Second White Specks Formation is absent in northwest British Columbia, where there is an established hiatus from the Upper Cenomanian to the Coniacian (Stott, 1993).

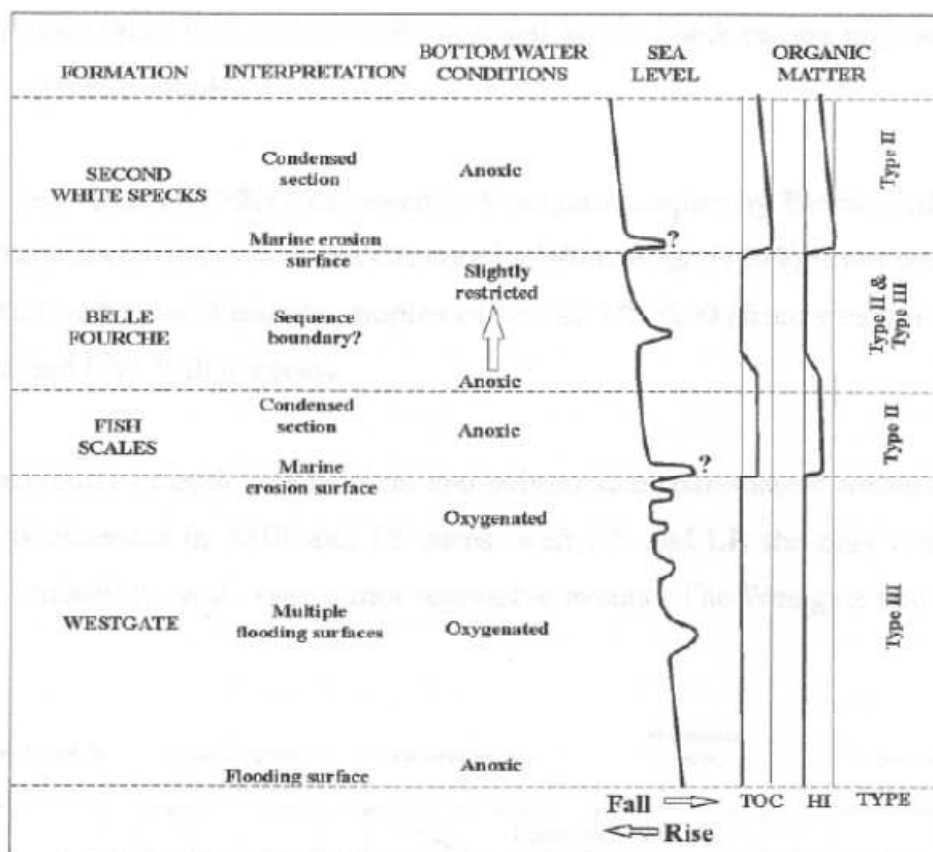


Figure 5.3: Characteristic features of the lower Colorado Group Formation related to fluctuations in sea level (after (Schröder-Adams et al., 1996).

5.2 Spatial trends in Mineralogy, Grain Size and Palynofacies

Clastic minerals (quartz and clays) and phytoclasts (microphyte higher plant material; Tyson, 1995) all of which are derived from the continent were cross plotted. Amorphous organic matter (AOM), described as a “heterogeneous amorphous matrix derived from planktonic algae and bacteria” (Tyson, 1995) was cross plotted against carbonate, since both are produced within the water column and might be in high concentrations where terrigenous input is minimal. Additionally, mineralogy and lithology were correlated with increasing distance from the shoreface (source of clastic input) to investigate spatial variations. Sediment input into the WCSB is generally derived from the Cordillera to the west and also from the stable craton of the Canadian Shield to the east (Leckie et al. 2008; Schröder-Adams et al. 1996).

5.2.1 Westgate Formation

The relationships between mineralogy and palynofacies and between mineralogy and grain size distributions for the Westgate Formation are shown in Figure 5.4 and 5.5 respectively. The formation does not show any correlation between (a) quartz and phytoclast and (b) clays and phytoclasts. Similarly, the correlations between carbonate and %AOM and mineralogy vs grain size are poor. Cross plots of quartz and clays with increasing distance from the shore face shows that the input of the clastic minerals are quite variable throughout the basin and also at any single location. Carbonate is consistently low in the Westgate Formation across the entire basin, with values generally less than 10% within a wide range of phytoclasts plus AOM inputs.

The lack of correlations may be due to high sedimentation rate in relatively shallow water. Sedimentation rates during the Westgate varies between 1-6cm/100y (Schröder-Adams et al. 1996) forming an easterly tapering wedge which ranges from less than 20m in south west Alberta and thickens from 20m at the Manitoba-Saskatchewan border to 120m in north western Alberta (Bloch et al. 1999). The presence of moderately to well oxygenated waters, based on a high degree of bioturbation, has been suggested to indicate deposition in shallow, wave influenced sea water (Leckie et al. 2008; Schröder-Adams et al. 1996).

Thin section and photomicrograph of sample within the Westgate in this study also indicate relatively coarse sediment, with evidence of very highly burrowed, medium grey mudstones and silt-size laminae (Fig. 5.6 & 5.7). Similarly, grain size distribution spectra for the Westgate formation are generally dominated by flocculated settled materials indicative of low energy environment. The silty laminae observed within the mudstones however show that occasional periods of high energy activity occurred.

The low carbonate and high clastic mineral content indicate that the bulk of the sediment input during deposition of the Westgate formation is of continental origin; however, the Westgate also contains significant AOM. This has been noted by other authors (Buckley, 2004; Bloch, 1995) who describe the Westgate Formation as comprising non-calcareous mudstones and siltstones and generally has the lowest HI (19 -256mgHC/gOC) and consistently lower TOC values (~2wt. %) of all the lower Colorado Group units. Tmax values ranges from 402 to 459°C (mean 430°C), and increases with depth suggestive of Type III organic matter consistent with significant terrestrial input or degradation of AOM at the sediment-water interface.

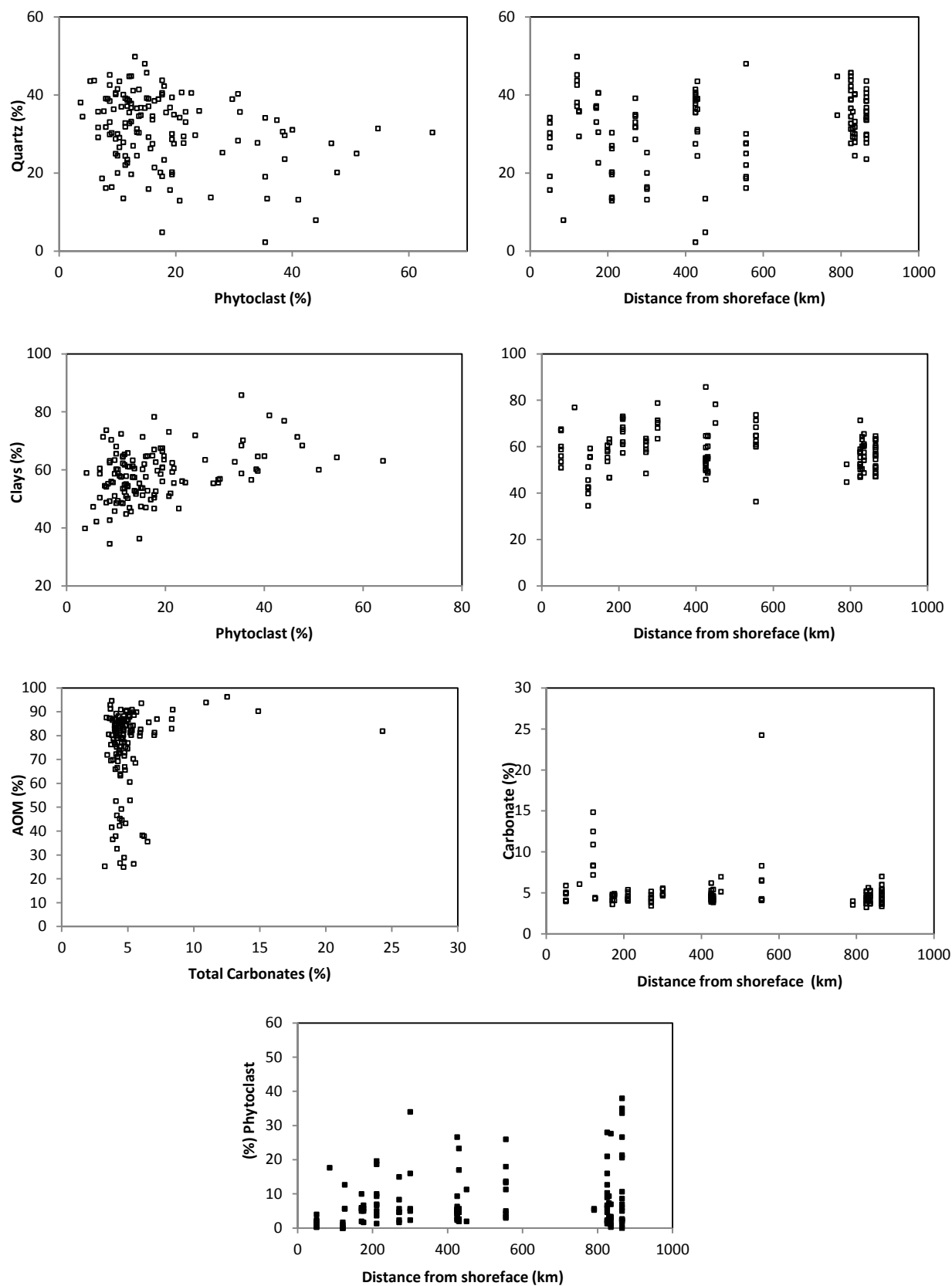


Figure 5.4: Cross plots of mineralogy against palynofacies and its variations throughout the basin within the Westgate Formation

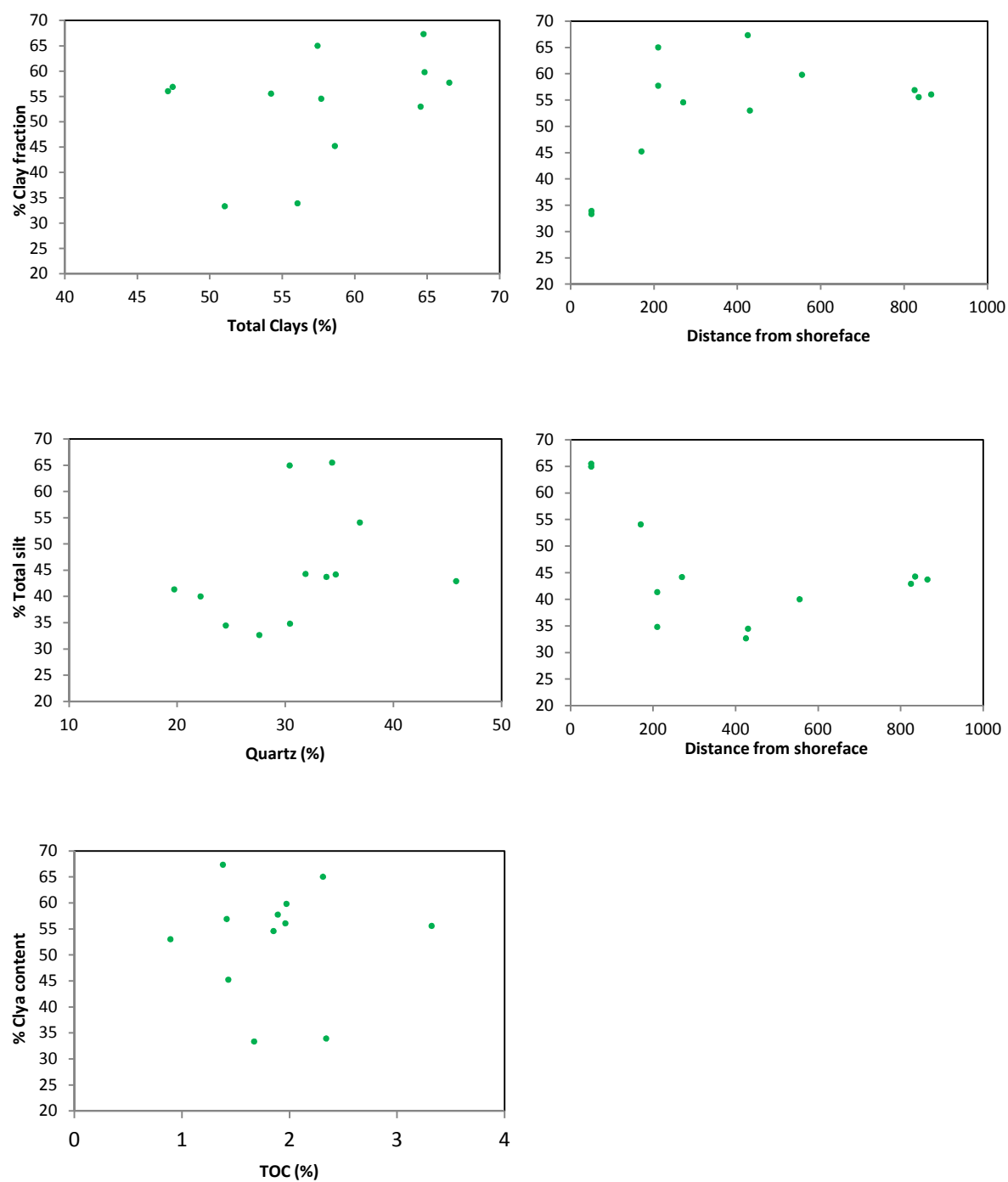


Figure 5.5: Cross plots of mineralogy against Grain size and its variations throughout the basin within the Westgate Formation

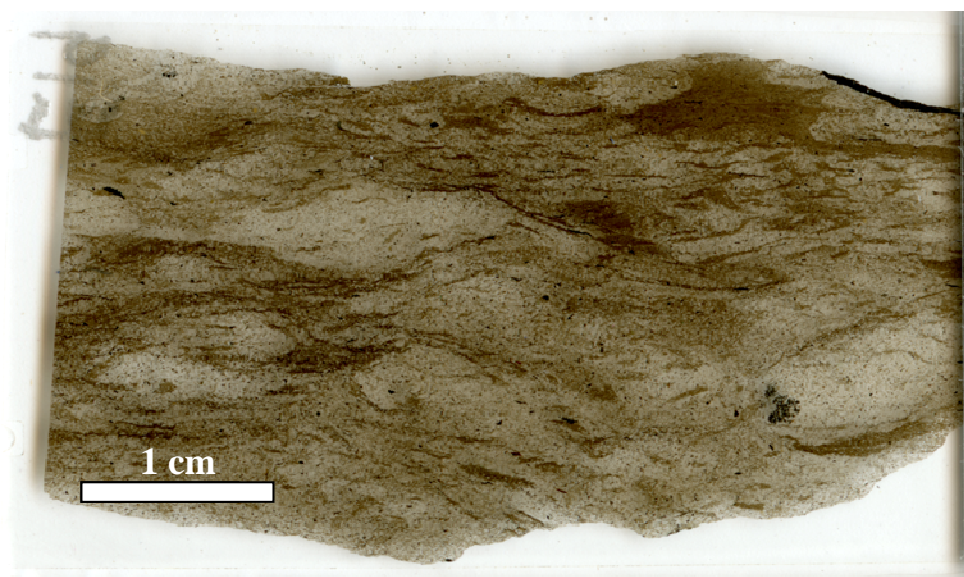


Figure 5.6: Thin Section a sample observed within the Westgate Formation, showing evidence of severe bioturbation

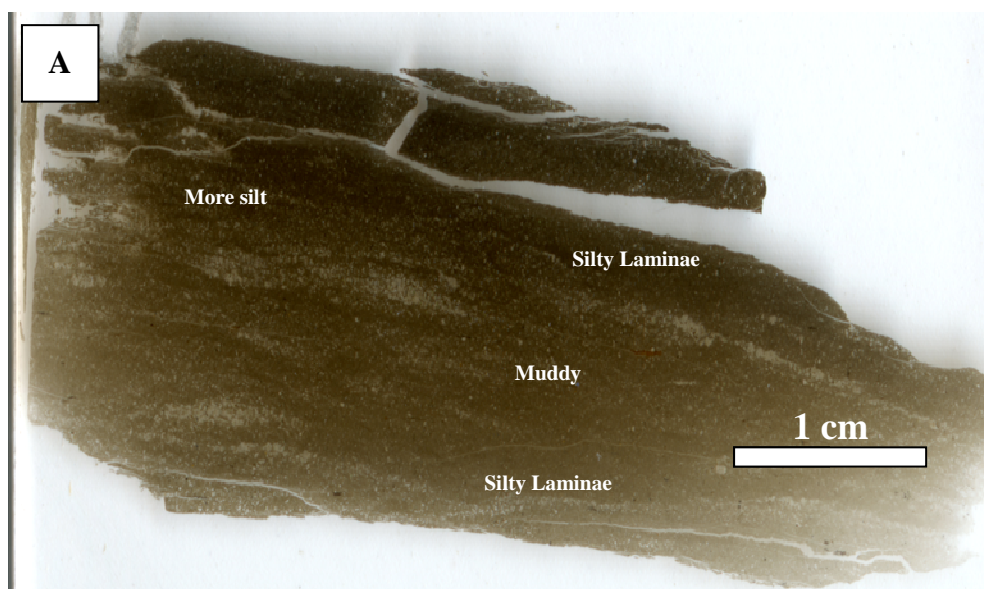


Figure 5.7: (A) Thin Section and SEM image of a sample observed within the Westgate Formation, at a depth of 1238m in the PH core consisting of medium grey mudstones with lenticular silty laminae.

5.2.2 Fish Scales Formation

The Fish Scales Formation exhibits a similar relationship to the Westgate Formation between mineralogy and palynofacies. The plots between quartz vs. phytoclast, clays vs. phytoclasts, carbonate vs %AOM and mineralogy vs grain size do not show any trend (Fig. 5.8). Cross plots of quartz and clays with increasing distance from the shore-face shows that the input of the quartz and clays are quite variable throughout the basin and also at any single location (Fig.5.8). Variation in siliciclastic minerals is highest at the centre of the basin ~400km from the shoreface. Carbonate content is occasionally up to 40% but is generally low (0-15%) across the entire basin.

Sedimentation rate during the Fish Scales is generally low (1-2cm/100y; Schröder-Adams et al. 1996) with a maximum thickness of only 20m. It is present in strata from British Columbia to Manitoba, although locally absent in parts of central Saskatchewan (Leckie et al., 1992). Bloch et al. (1999) describes the formation as a bioclastic conglomerate with the base of the Fish Scale regarded as a basinwide marker due to a pronounced gamma response (Leckie et al. 1992). Different deposition mechanisms have been suggested for the Fish Scales (Leckie et al. 1992). One of the mechanisms suggests that deposition occurred during a continued sea-level rise and joining of the Tethyan and Boreal water masses, thereby generating vigorous bottom currents responsible for winnowing the bioclastic debris. This may have favoured the deposition of silt-sized materials and the destruction of flocs formation. However, grain size spectra suggests both floc and silt sized deposition occurred and therefore perturbations in energy conditions. It may also be possible that the bottom currents transported both the flocs and silt materials from their primary points of deposition since flocs are capable of basin-wide ripple migration just like the silt components (Schieber and Southard, 2009). The lack of correlation between mineralogy and palynofacies may also indicate that perhaps the transport pathway is not perpendicular to the shoreface.

The Fish Scales Formation is characterised by mixed Type II and Type III kerogen and therefore the influence of both terrestrial and marine sources. It has a higher TOC content of up to 8wt. % (average of 3.2wt.%), HI (28 – 438mgHC/gOC) and mean Tmax value of (419°C) than the Westgate Formation (Buckley, 2004b). Also note that the AOM dominance which may reflect more production and preservation, or cut-off of phytoclast supply.

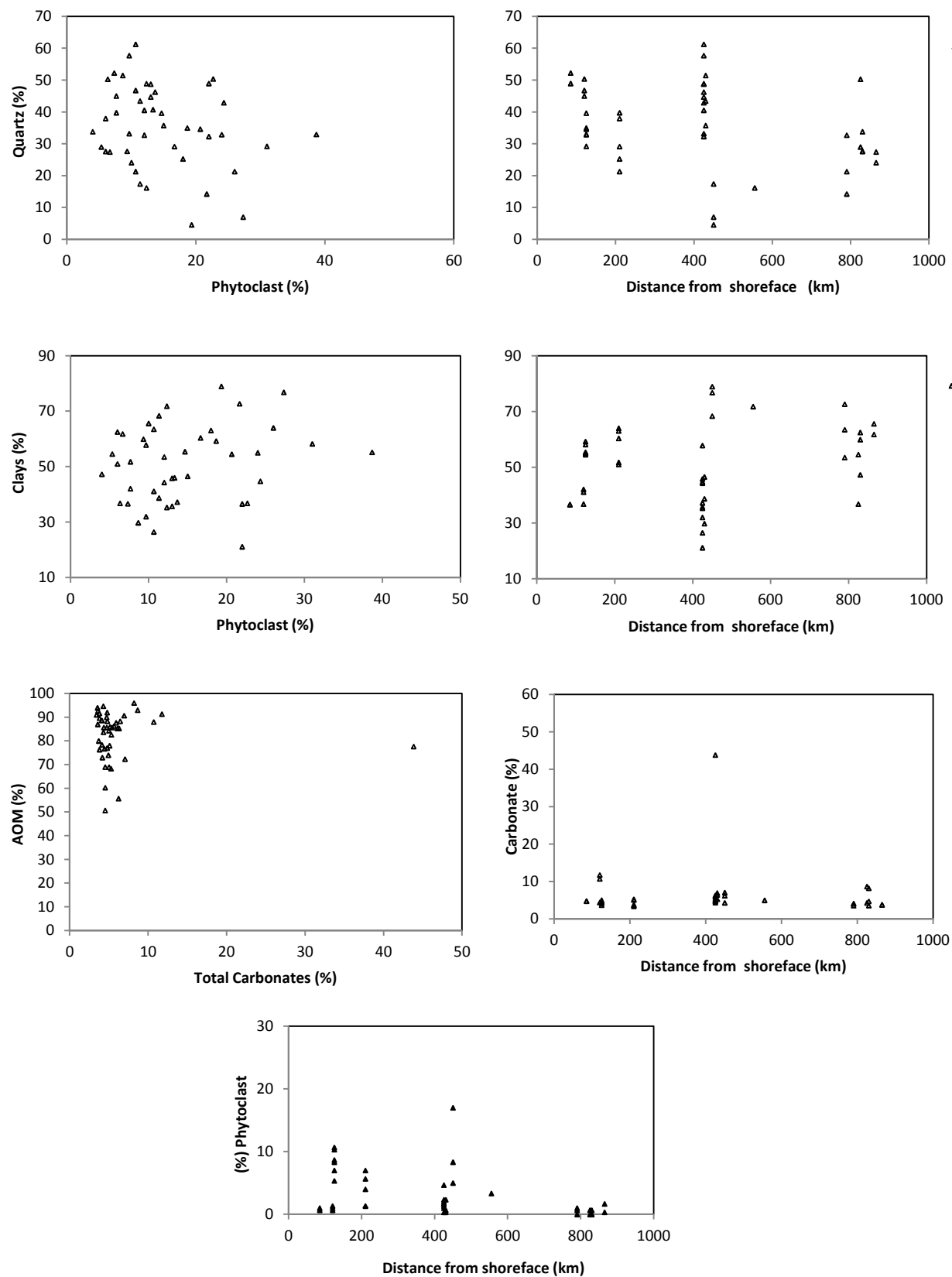


Figure 5.8 Cross plots of mineralogy against palynofacies and its variations throughout the basin within the Fish Scales Formation

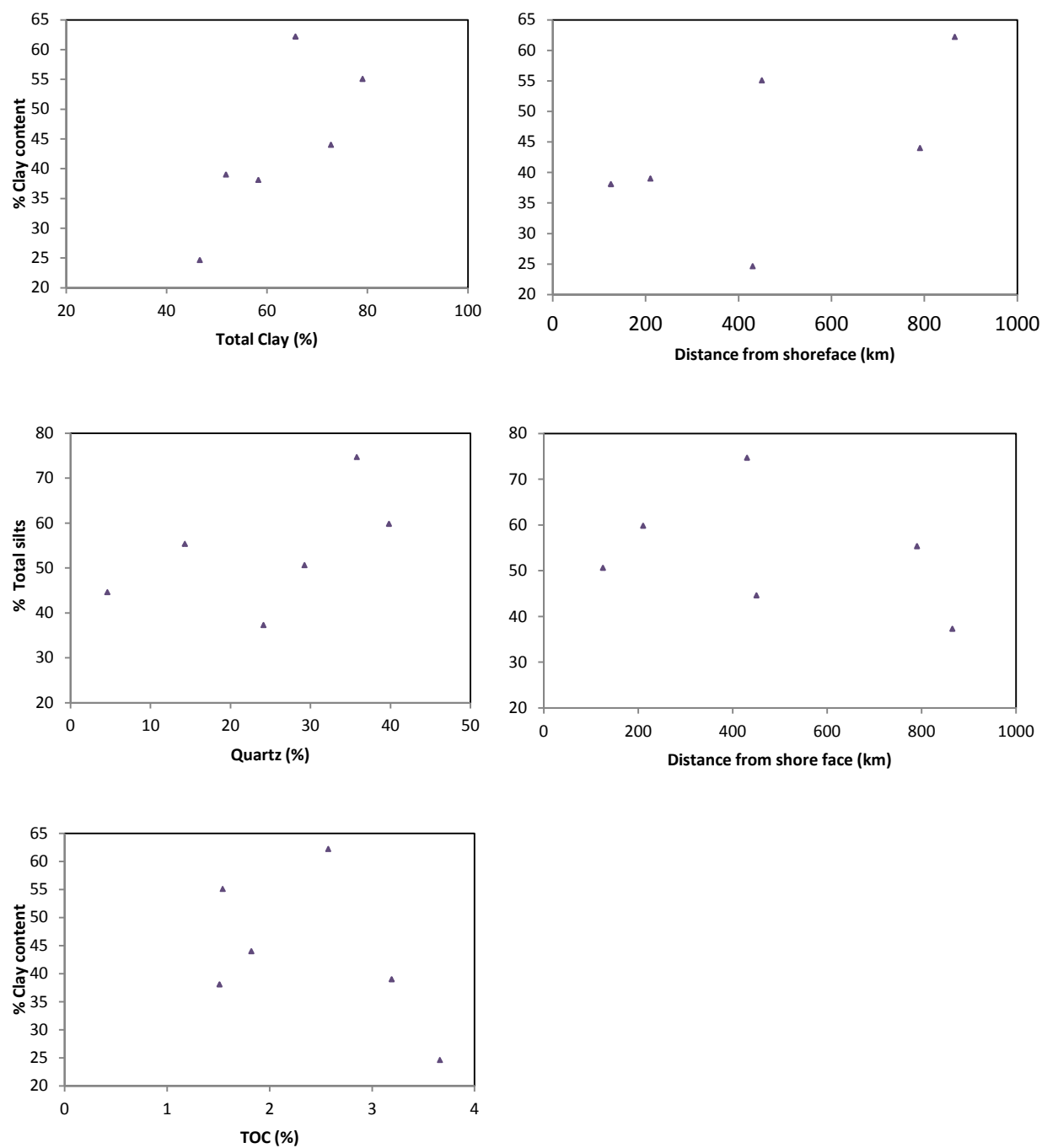


Figure 5.9: Cross plots of mineralogy against Grain size and its variations throughout the basin within the Fish Scales Formation

5.2.3 Belle Fourche Formation

The correlations between mineralogy and palynofacies did not show any relationships for the Belle Fourche and Second White Specks Formations. The carbonate concentration displays steady increase in both the Belle Fourche and Second White Specks Formations with increasing distance from shoreface but still highly variable at any single location, while the concentrations of quartz and clays show little to no variation across the basin (Fig 5.10 -5.11).

The concentration of carbonate in Belle Fourche Formation displays no increase up to 400km distance from the shoreface after which it slightly increases and remains steady up to 700km and then increases sharply beyond 800km. Carbonate-rich facies have been reported to be well developed within the east-central portion of the Western Interior Seaway (WIS) during the Cenomanian, which later become well established in the east, and migrated to the west where carbonate is consistently lower (Buckley, 2004). The thickness of the Belle Fourche Formation is quite variable ranging from 150m in the northwest Alberta foothills to just 20m along the Manitoba escarpment due to high variation in sedimentation rates (0.7 – 5cm/100y) (Schröder-Adams et al. 1996). Leckie et al. (2008) and Leckie et al. (1992) describe the Belle Fourche Formation as comprising lower sandstones characterised by marine shales and sandstones deposited on a shelf under low to moderate energy conditions and upper prograding sandy wedges. The shales are sparsely bioturbated, non-calcareous to slightly calcareous mudstones and siltstones. These descriptions agree with the mineralogy and grain size data generated in this study; carbonate content is highly variable (2 – 74%), while grain size spectra consists of flocculated settled materials deposited under low energy conditions as well as relatively high energy deposited silt components. The formation is characterised by Type II and III kerogen, HI (5-489mgHC/gOC), mean Tmax value of 426°C and consists of TOC values below 2wt. % (Bloch, 1995), although (Buckley, 2004) measured TOC content up to 11wt. % largely reflecting both marine and terrestrial influences.

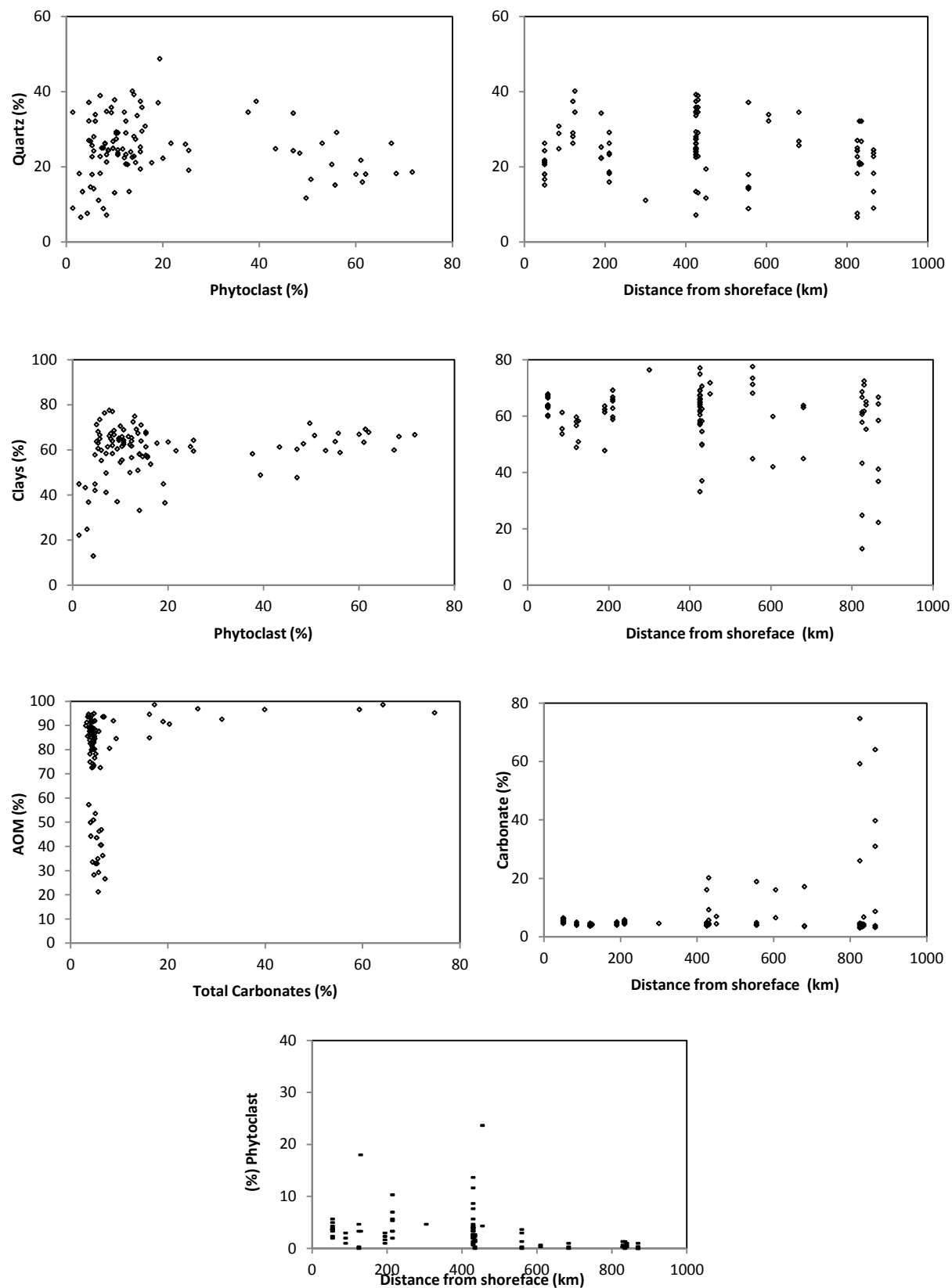


Figure 5.10 Cross plots of mineralogy against palynofacies and its variations throughout the basin within the Belle Fourche Formation

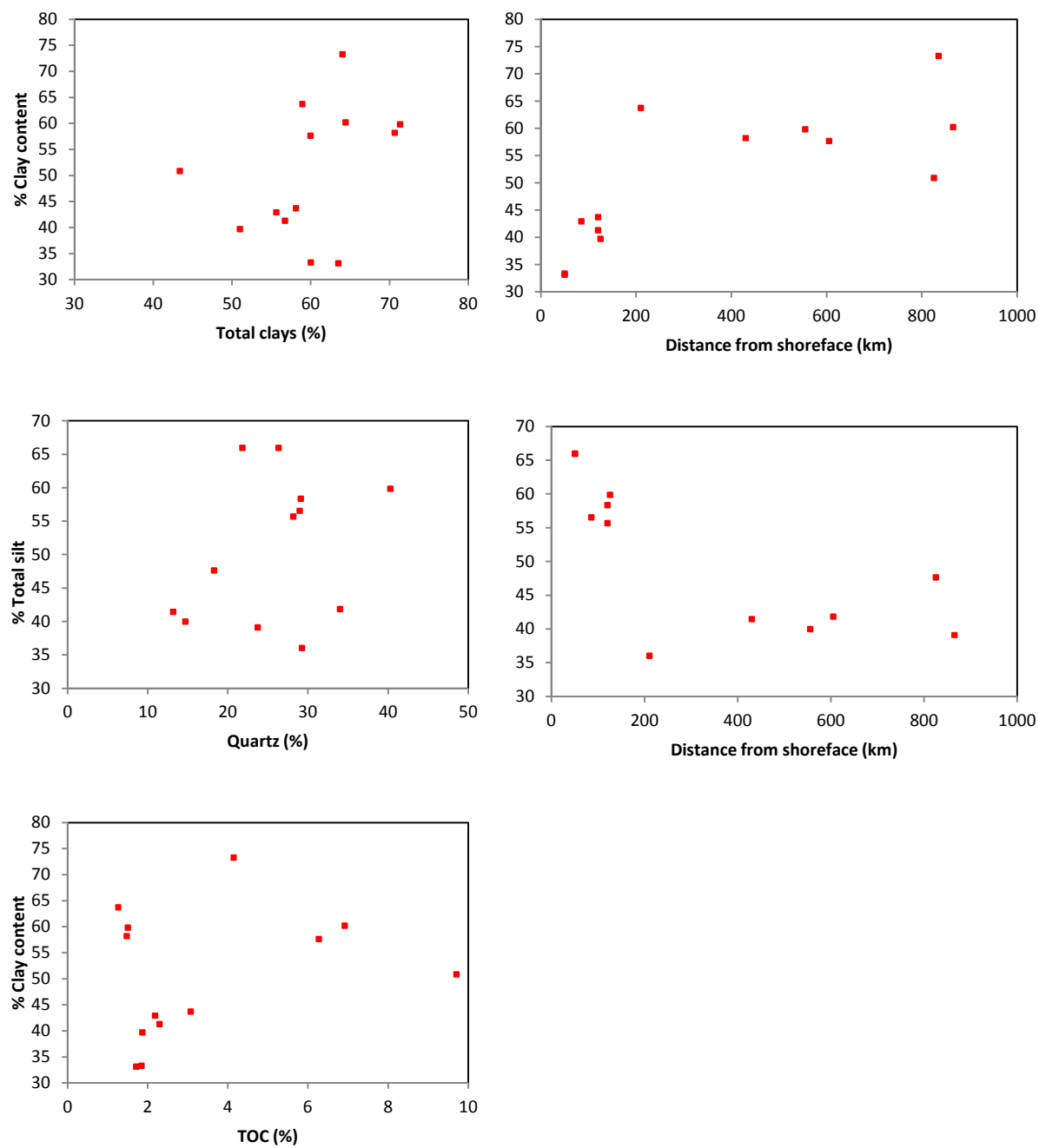


Figure 5.11: Crossplots of mineralogy against Grain size and its variations throughout the basin within the Belle Fourche Formation

5.2.4 Second White Specks Formation

The shales of the Second White Specks are characterised by a high total organic carbon content (5-11wt. %), high hydrogen indices (100 – 620mgHC/gOC) (Buckley, 2004; White et al. 1999; Bloch, 1995) and high gamma values on well logs. These characteristics have been attributed to increased productivity in the upper water column and anoxic bottom waters which preserved abundant Type II organic matter (Schröder-Adams et al. 1996). Tmax, ranges between 398 - 437°C (mean 418°C).

There appear to be some correlations between mineralogy and grain size in the Second White Specks Formation (Fig. 1.13). The evidence of increased productivity and preservation of AOM is pronounced in the Second White Specks Formation where high AOM occur across all ranges of carbonate content and which suggests that the sediments were deposited within a distal basin with reduced detrital supply. The Second White Specks Formation exhibits the highest concentrations in carbonate content and is laterally variable, increasing steadily towards the eastern margin. The sequence vary from 90m thickness in north western Alberta to 25m in the east (Bloch et al., 1993) and from 63m in the southwestern Saskatchewan to 13m in the north (Gilboy, 1988) with sedimentation varying from 1.25-4cm/100y (Schröder-Adams et al. 1996). The formation represents a basin wide marker due to its unusual calcareous, organic rich claystones and siltstones (Bloch 1993). Grain size data in this work show that the Second White Specks have the highest percentage of silt size materials. Similarly, the grain size spectra of samples showed a significant increase in silt size deposited materials indicative of high energy activity.

Thin sections of samples from the Second White Specks show the presence of clay clasts (Fig 5.14) implying that the formation was deposited under relatively high-energy conditions, as this would be necessary to erode compacted sediments from the seafloor and transport them. The association of clay clasts with relatively coarser sediments and sand-sized organic matter fragments also indicates that the clay clasts relate to higher energy depositional events, as suggested by Schieber et al. (2010).

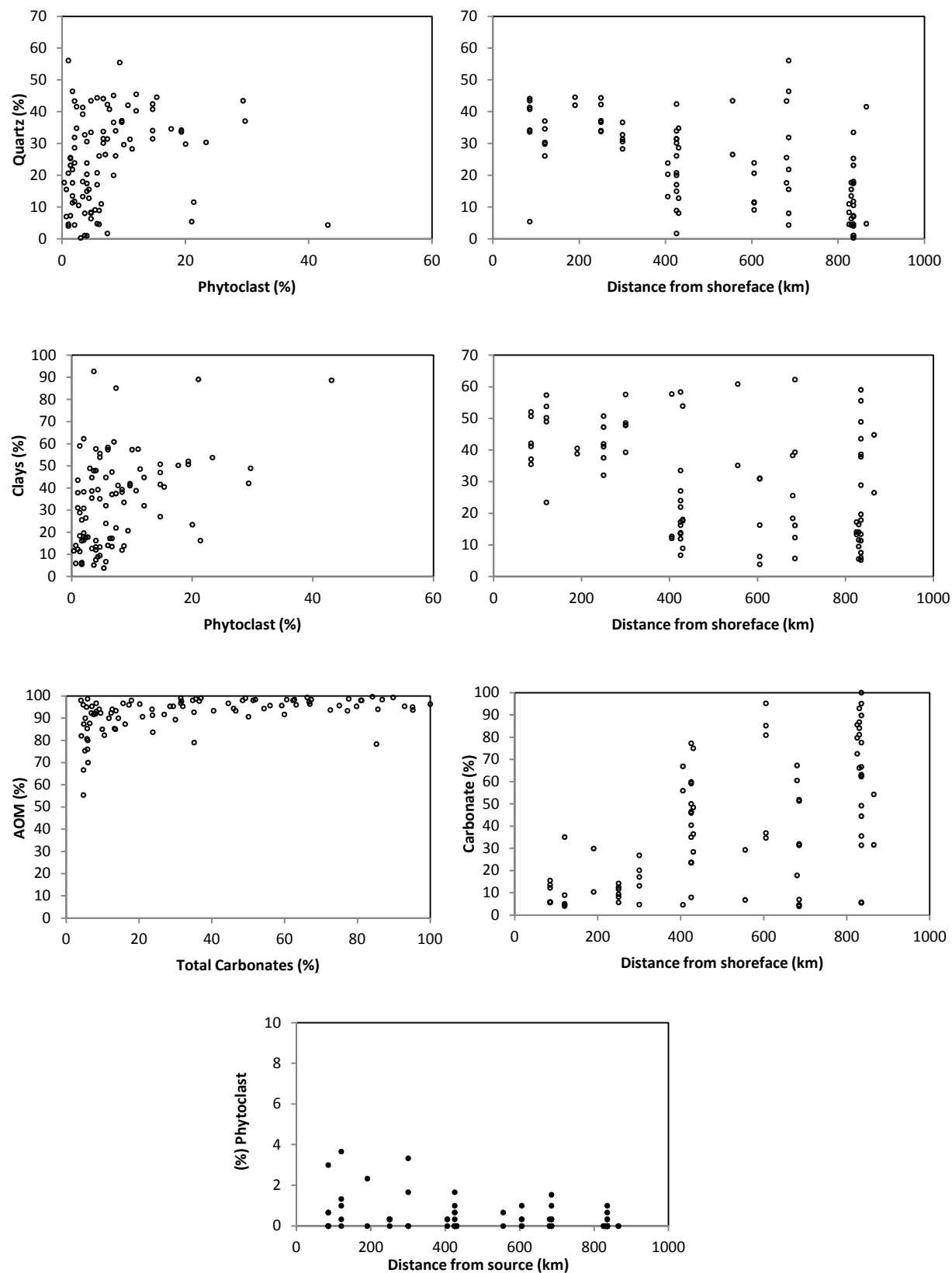


Figure 5.12: Crossplots of mineralogy against palynofacies and its variations throughout the basin within the Second White Formation

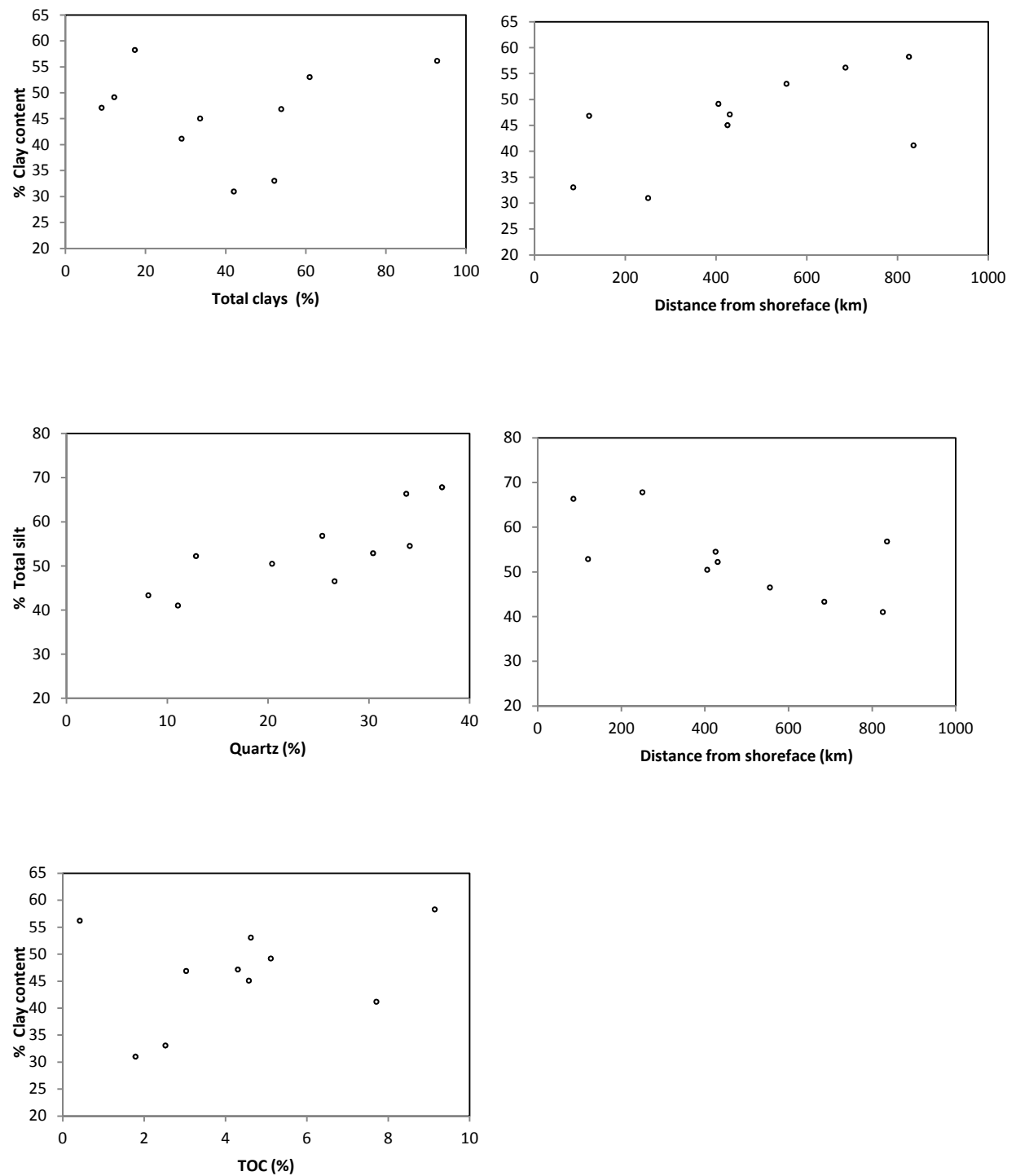


Figure 5.13: Crossplots of Mineralogy against Grain size and its variations throughout the basin within the Second White Specks

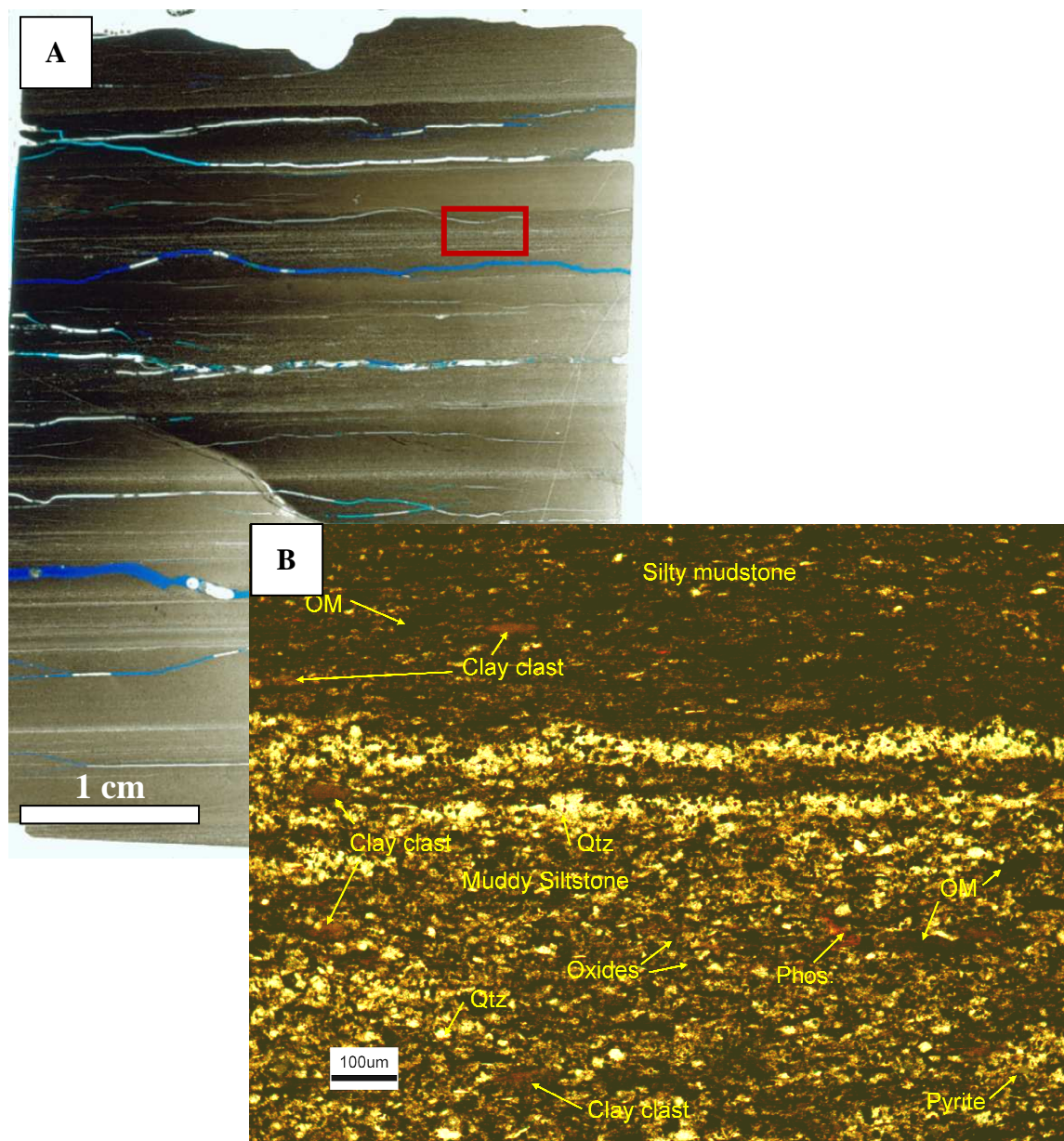


Figure 5.14:(A) Thin section of a sample within the Second White Specks Formation, at a depth of 655.65 containing clay clasts. The red rectangle denotes the view of the area within which the petrographic microscope image is taken. **(B)** Clay clasts within muddy siltstone and silty mudstone beds

The relationship between grain size and TOC for the lower Colorado Group formations was also examined. Sediment grain size has been shown to exert a major control on TOC, determining if and where organic matter can be deposited (Tyson, 1995). The Second White Specks is the only formation exhibiting correlations between grain size and TOC. TOC increases with increasing clay contents ($<2\mu\text{m}$), and decreases with increase in sortable silt contents ($>10\mu\text{m}$). A decrease in % sortable silt is an indication of decreased current speed (Curran et al, 2004) which can result in the deposition of finer grained sediment which, in distal environments, can lead to an increase in TOC due to reduced siliciclastic dilution. TOC also increases, partly due to the relative increase in marine organic matter, and the increased likelihood of dysoxic-anoxic conditions (Tyson, 1995). The low TOC values associated with more coarse grained sediments can be attributed to deposition in near-shore, oxic environments where degradation of organic matter is enhanced. Results from the Kranck model (1996) show that the Colorado Group sediments are dominated by flocc distributions deposited from flow or water column with a high suspended sediment concentration (chapter 4). However, the grain size distributions of the Second White Specks Formation show an increased contribution of unflocculated silt. This is ironic as the Second White Specks has the highest TOC and more silt indicate more current activity. This may then suggest that productivity is the key control on TOC.

A similar but less apparent trend is exhibited by the Belle Fourche Formation where higher TOC values are generally associated with finer fractions. The Fish Scales and Westgate formations did not show any systematic variation with grain size data.

In general, there are no clear relationships between mineralogy and palynofacies for the Westgate, Fish Scales and Belle Fourche Formations. The input of the siliclastic minerals in the Westgate is quite variable throughout the basin and also at any single location. Carbonate content of the Westgate Formation is consistently low across the entire basin, with values generally less than 10%. Quartz and clays are quite variable throughout the basin and also at any single location within the Fish Scales. Variation in siliclastic minerals is highest at the centre of the basin ~400km from the shoreface, while carbonate input also increases within the centre of the basin (up to 30%) but generally remains low (0-15%) across the entire basin.

The carbonate concentration displays steady increase in both the Belle Fourche and Second White Specks Formations with increasing distance from shoreface but is still highly variable at any single location, while the concentrations of quartz and clays show little to no variation across the basin. The Second White Specks Formation is the only unit that appears to show some correlation between mineralogy and grain size. Total silt (2-63 μ m) correlates positively with %quartz. Similarly, clay content (<2 μ m) increases steadily with increasing distance from the shoreface, while silt content decreases laterally across the basin from the sediment input source.

5.3 Stratigraphic Variations

This section attempts to investigate the stratigraphic variations of the lower Colorado Group shales based on the FTIR derived mineralogy. The mineralogy data are correlated with palynofacies and geochemical data from Buckley, (2004b) study and compared with the stratigraphic studies mentioned above using five wells within Alberta and Saskatchewan with continuous cores covering Westgate to Second White Specks Formations. The core sections include two central WCSB wells - 10-35-45-02W4; 06-18-45-01W4- located close to the Alberta-Saskatchewan border and three wells from the Saskatchewan eastern margins - 04-23-46-16W2, 01-24-20-33W1, 01-04-45-10W2- within the lower Colorado Group formations (Fig. 5.13)



Figure 5.15: Map of the Western Canada Sedimentary Basin with location of studied wells in rectangles

30 - (10-35-45-02W4) AHR

29- (06-18-45-01W4) AER

36- (04-23-46-16W2) LR

38 - (01-24-20-33W1) IY

40- (01-04-45-10W2) CR

The Westgate Formation exhibits little mineralogical variation in all the wells. Appreciable variability occurs only within the 40 and 36 (Figs. 5.16 & 5.17) cores. The events are represented by localised decrease in quartz content at 194m and 178m in the 40 core (Fig. 5.16) corresponding to two minima on the log AOM:Phytoclast ratio. This corresponds to a maximum flooding surface at 194m suggested by McNeil and Gilboy (1999) based on biostratigraphy and associated with an increase in HI which correlates with a reduction in quartz concentration. Within the 36 core (Fig. 5.17) a localised decrease in quartz content at 142m is characterised with a decrease in marine organic matter (AOM). The quartz distribution within both wells appear to reflect the coarsening-up sequence described by Schröder-Adams et al. (1996). TOC and carbonate content remain relatively low and constant throughout the formation.

The mineralogy of the Fish Scales Formation show a striking decrease in quartz content upsection in all the wells considered. A sharp increase in carbonate content occurs at the base of the Fish Scales within the 30 (Fig. 5.14), and relatively small increase in the 04-23-46-16W2 (Fig. 5.16) cores. Carbonates values increase from less than 5% to ~ 30% within the 30 core corresponding to interval of increased TOC which suggests increased production/preservation state of the organic matter assemblage (Fig. 5.14). Leckie et al. (1992); Bloch et al. (1993); White et al. (1999) and McNeil and Gilboy, (1999) all describe the base of Fish Scales Formation as a transgressive surface.

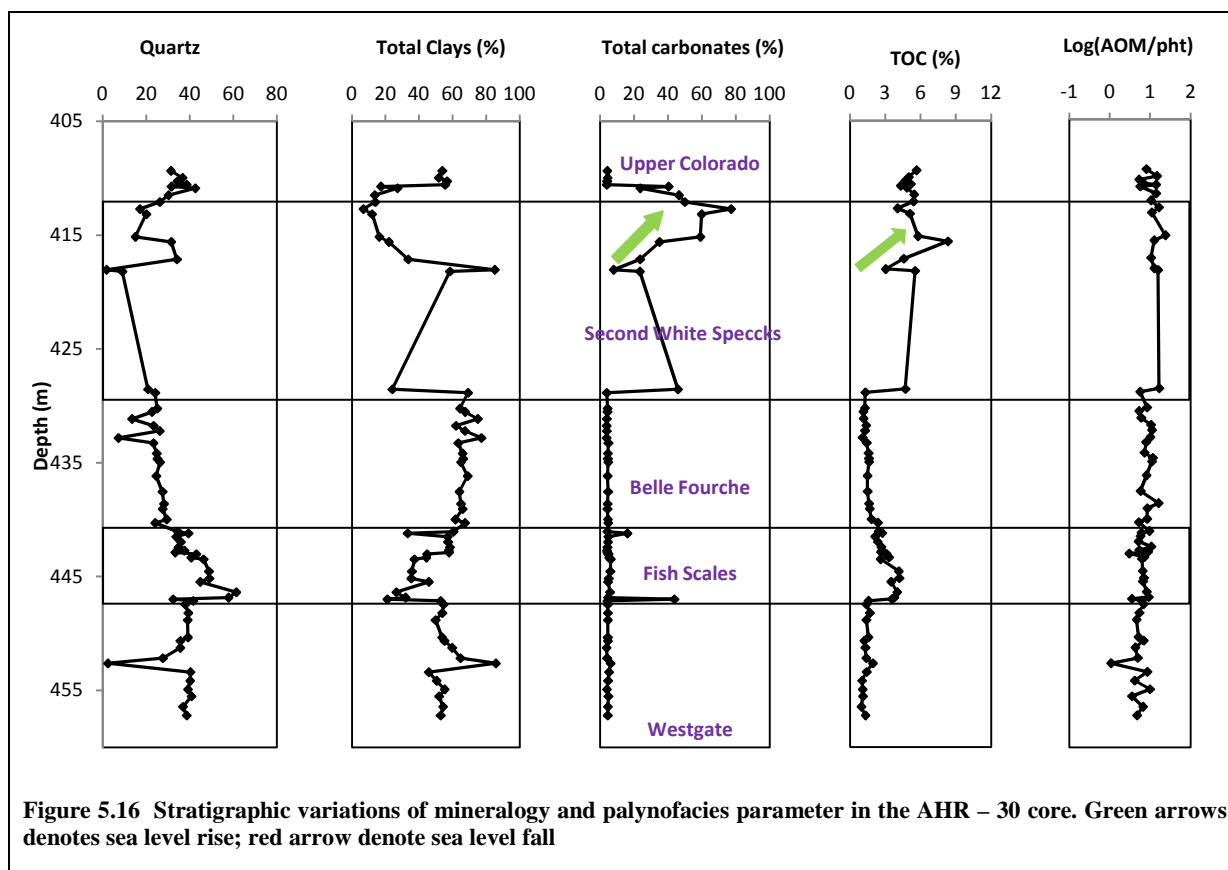


Figure 5.16 Stratigraphic variations of mineralogy and palynofacies parameter in the AHR – 30 core. Green arrows denotes sea level rise; red arrow denote sea level fall

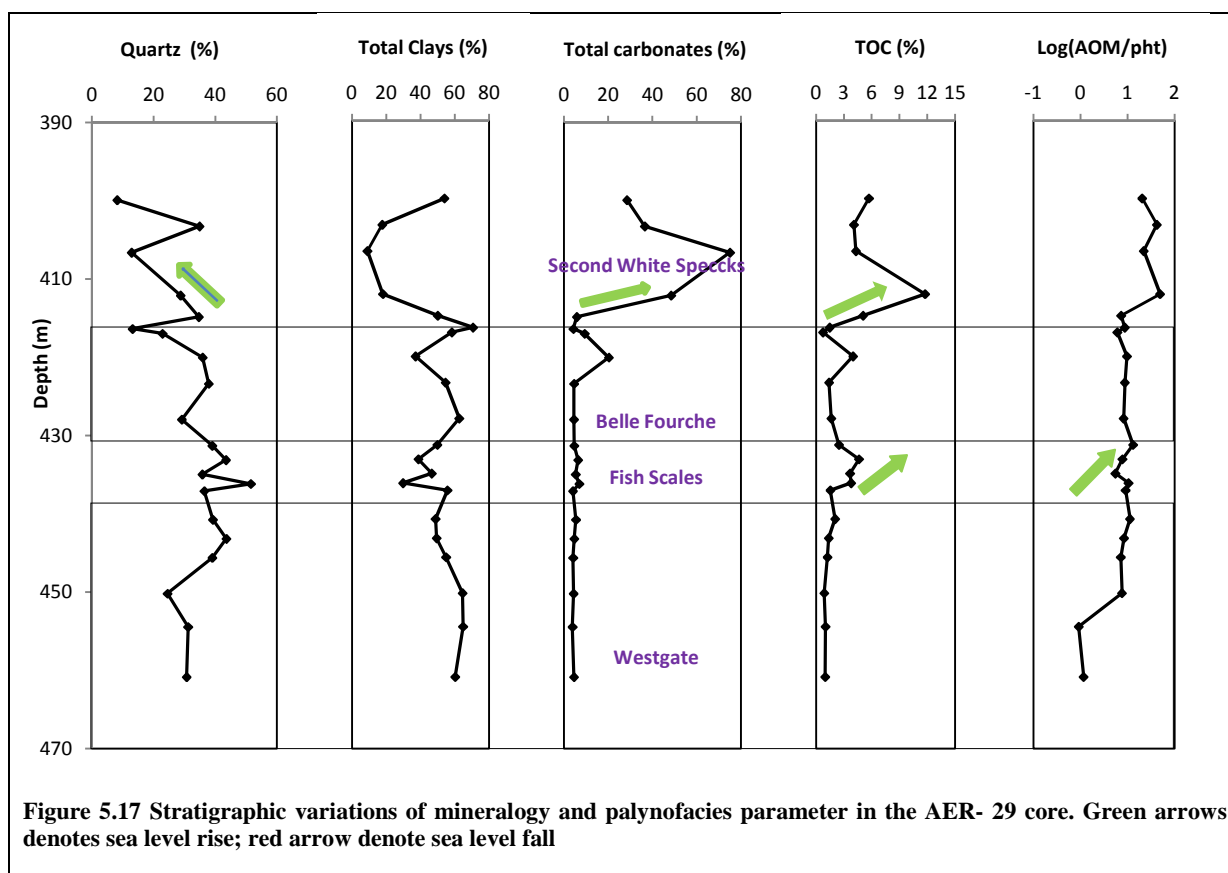
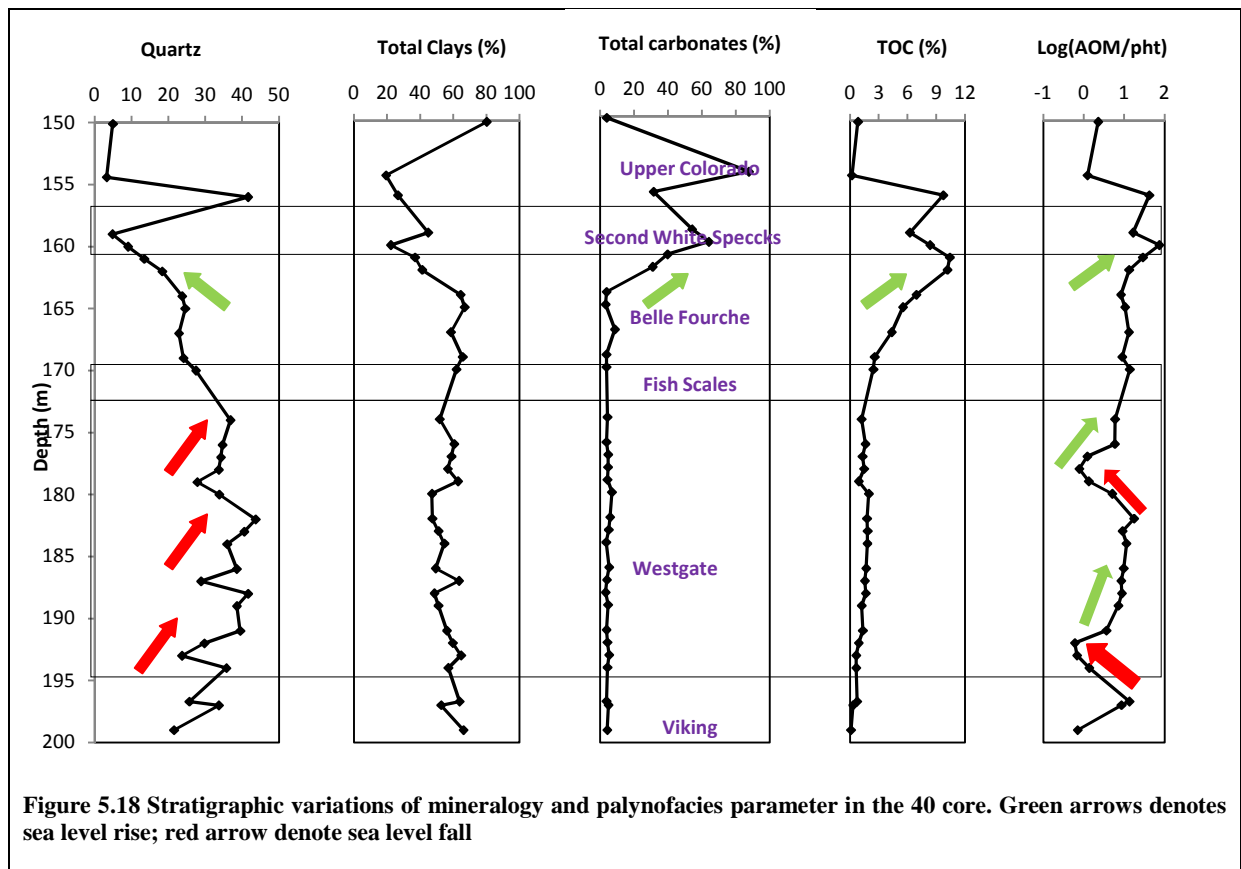


Figure 5.17 Stratigraphic variations of mineralogy and palynofacies parameter in the AER- 29 core. Green arrows denotes sea level rise; red arrow denote sea level fall



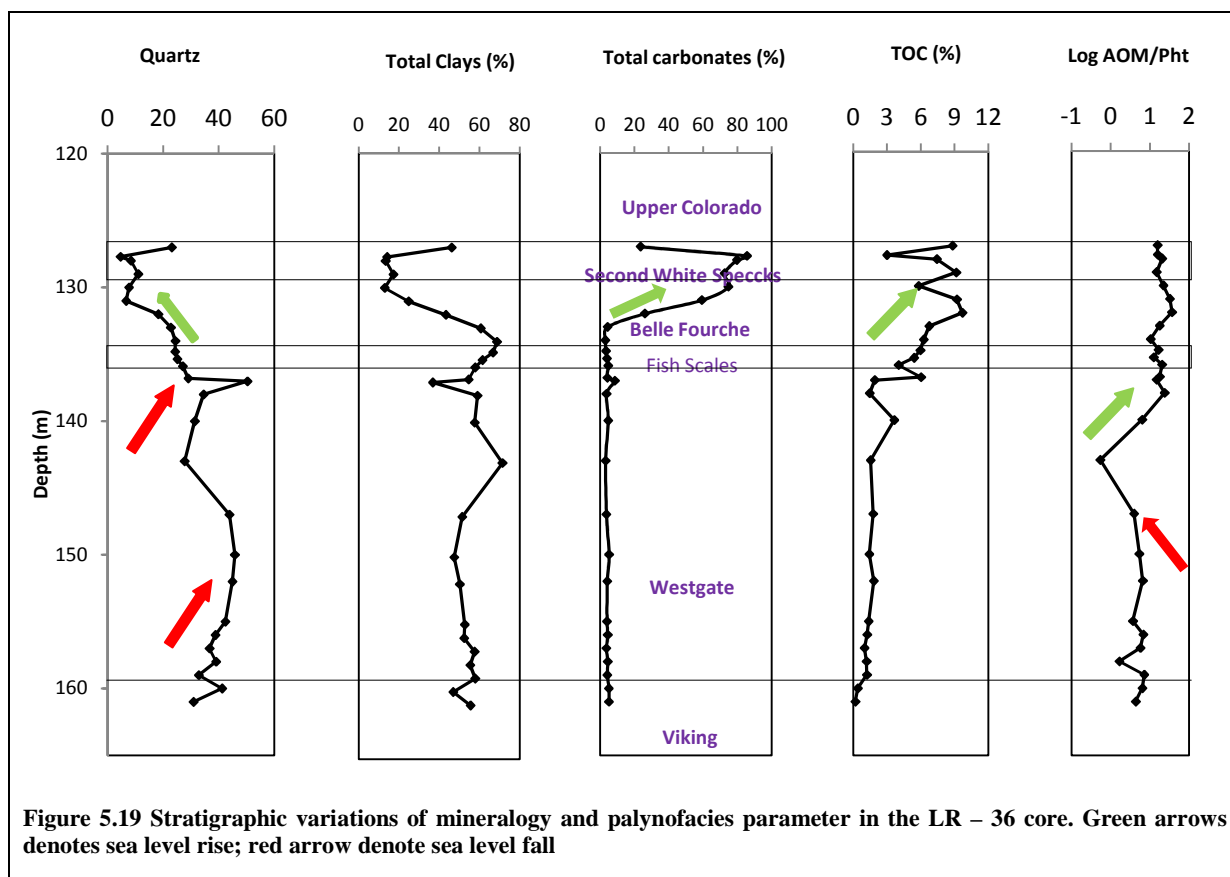


Figure 5.19 Stratigraphic variations of mineralogy and palynofacies parameter in the LR – 36 core. Green arrows denotes sea level rise; red arrow denote sea level fall

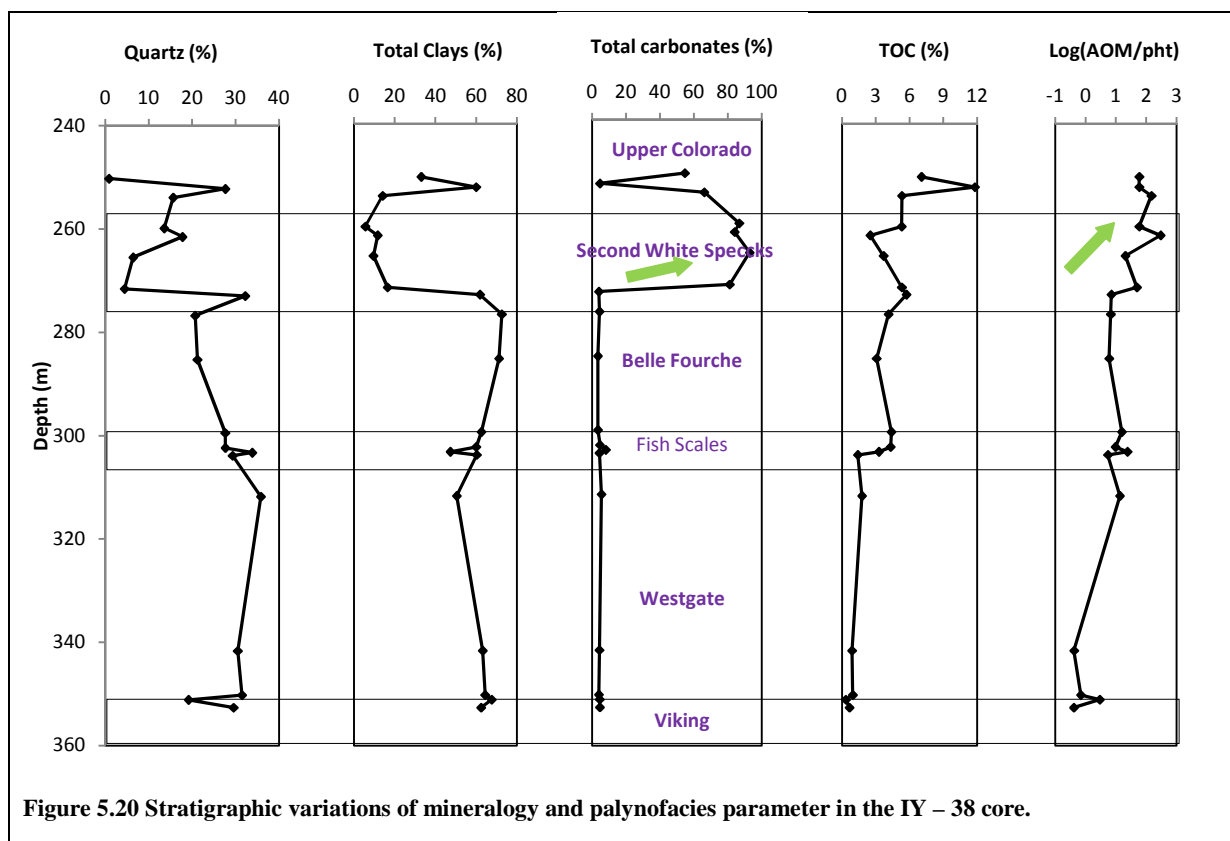


Figure 5.20 Stratigraphic variations of mineralogy and palynofacies parameter in the IY – 38 core.

The transgressive trend seems to appear at the base of the Fish Scales in all of the stratigraphic cores showing a relative increase in carbonate content except the 40 core (Fig. 5.16) but it may be due to low sampling density.

The Belle Fourche Formation within all the wells, except the 30 are characterised by an overall decrease in quartz content and increase in carbonate up section. The sequence above 164m in the 40 core is characterised by increasing carbonate content, AOM and TOC values consistent with a transgressive episode. The lower section of the Belle Fourche between (165-170m) is characterised by relatively low carbonate and TOC values indicative of regressive event. The regressive event manifest as gradual increase in clastic minerals of up to 80%, low carbonate and TOC contents within the central cores of 29 (5.15) and 30 (Fig. 5.14), although, the mineralogy within the 30 core does not exhibit a strong variation compared to the 29 core. The middle of the 06-18-45-01W4 well is characterised by a peak in carbonate associated with an increase in TOC at 420m which gradually reduced as carbonate input decreases upsection. Similar trend is observed in the 36 core at 133m (Fig. 5.17): the sequence above 133m is characterised by increasing carbonate and TOC contents compared to the sequence below it. These are consistent with transgressive trends reported by Buckley, (2004) and White et al. (1999), describing the upper Belle Fourche as containing TOC greater than 10%, HI of approximately 400 and low to moderate organic matter preservation. The 38 (Fig. 6.18) core exhibits less variation compared to both the 40 and 26 cores although fewer samples were analysed within the 38 section to make any inter core comparison. The varying profiles exhibited within the central and eastern margin Belle Fourche cores may be due to unconformity caused by depositional hiatus between the upper Fish Scale and lower Belle Fourche reported by McNeil & Gilboy (2000).

The Second White Specks interval show significant rise in carbonate content within all the wells but the increase is relatively more in the 30 and 38 cores at the Belle Fourche – Second White Specks boundary. Although the unavailability of samples between 428 – 418m in the 30 cores creates a gap in the trend the upper section is marked by an overall increase in carbonate content from 8% at 415m to 77% at 412m accompanied, by a sharp drop in clay contents. The increase in carbonate content within the upper interval in the 30 cores is associated with increase in log AOM:Phy ratio and TOC values from 3.03% at 418 to 8.32%

at 415m indicative of a transgressive trend. Similarly, the 06-18-45-01W4 core show marked increase in carbonate content at the base of the Second White Specks increasing from 5.8% at the boundary with the Belle Fourche to 75% at 406.6m and then drop sharply between 406-399m interval from 75 to 28% (Fig.5.14)). The 01-04-45-10W2 and 04-23-46-16W2 show more subtle increase in carbonate content. It appears that the carbonates content is associated with good organic matter preservation showing increase in TOC. Schröder-Adams et al. (1996) attribute this with a maximum transgression that occurred within the basal Second White Specks Formation.

General trends indicate that AOM/phytoclast ratio increases within the upper Westgate, then remains constant, and then increases again into the Second White Specks in all the wells. AOM/Phytoclasts ratio also increases within the upper Belle Fourche in the 01-04-45-10W2 and 04-23-46-16W2 wells. AOM/phytoclast ratio also show a positive correlation with TOC content for values >3%, but do not correlate when TOC is <3%.

5.3.1 Controls on Colorado Group Sediment Deposition

Previous studies have shown that the main controls on the deposition of the Colorado Group include changes in eustatic sea level, sediment flux, and tectonic influences (Caldwell, 1984; Bhattacharya and Walker, 1991; Varban and Plint, 2008). The lower Colorado data in this study shows that the formations are similar based on grain size analysis, pore size distributions, bulk mineralogy and TOC; however, the Second White Specks is different based on its calcareous nature and more abundant organic matter.

The organic matter assemblage of the Colorado Group is generally dominated by AOM; however, the AOM is predominantly poorly preserved. The Westgate and Belle Fourche formations exhibit greater phytoclast content, and typified by Type III kerogen compositions indicative of more proximal environments than the Fish Scales and Second White Specks formations, which are characterised by mixed Type II/III kerogen. Since, one of the most effective ways of enhancing organic matter preservation was to reduce the exposure time of organic matter to oxygen. Anoxic (low oxygen) waters and/or intermittently anoxic bottom waters are required in order to reduce the rapid addition of oxygen and sulphate through biological irrigation by macrobenthos (Bohacs et al. 2005). This means that the Fish Scales and Second White Specks formations with higher contents of organic matter are most likely associated with oceanic realms where primary productivity is high, water columns are shallow or moderate and sediments in which the addition of oxidants is minimized either by moderately high sedimentation rates or restricted biological stirring (Bohacs et al. 2005).

The lack of bioturbation within the Second White Specks Formation suggests widespread persistent anoxia, compared to the Westgate and Belle Fourche Formations. Oxic conditions, indicated by moderate to intense bioturbation are observed within the Westgate Formation, ultimately reducing the preservation of the organic matter. Bioturbation is observed in thin section and photomicrograph of some samples indicating moderately to well oxygenated waters suggesting deposition in relatively shallow water depths (Schröder-Adams et al. 1996).

The calcareous nature of the Second White Specks is likely a reflection of a strong influence of Tethyan waters, as these nutrient-rich waters would promote the proliferation of planktic

taxa and the deposition of biogenic calcite from their remains. Planktic foraminifers were noted as an indicator of seaway connectivity with the Gulf of Mexico, which promoted the circulation of warm, nutrient-rich Tethyan waters in the seaway (Schröder-Adams et al. 1996). Therefore, it is most likely that the absence or presence of Tethyan-derived waters is responsible for the change in the abundance of biogenic carbonate content within the Colorado Group.

The grain size data in this study indicate that the Colorado group is dominated by fine grained clay materials ($<2\mu\text{m}$), suggesting deposition in quiet, low energy environment (Curran et al. 2004). However, the presence of clay clasts signifies deposition under relatively high-energy conditions, since higher energy is necessary to erode compacted sediments from the seafloor and transport them. Previous studies of the Colorado Group have interpreted its depositional setting within the foreland basin to be representative of either a distal shallow shelf setting or a prodeltaic setting (Nielsen et al. 2003). Either depositional setting has relatively low accommodation space, which promotes sediment bypass further from the paleoshoreface (Varban and Plint, 2008). This suggests that the Colorado Group consists of a complex dynamic depositional system and either deposition was dominantly controlled by eustatic or tectonic parameters changes in the geologic record will be affected similarly.

It is probable that deposition of the Colorado Group occurred at such a distance from the shoreface that the paleodepositional setting can only be identified as a non-distinct, distal expression. AOM was likely deposited out of suspension, and then reworked by relatively high-energy events that were also capable of transporting terrestrial organic matter, as well as eroding and transporting clay clasts.

The TOC content and kerogen type will affect shale gas prospects since organic matter is targeted by anaerobic bacteria and converted to methane gas during methanogenesis (Rice, 1993) within a biogenic shale gas reservoir. Therefore, rocks with high organic matter content have a greater capacity for methane gas generation since there is more organic matter to be converted to gas. It can be assumed that rocks with consistently moderate or high percentages of total organic carbon would be the most favorable gas target over rocks with highly variable total organic carbon content. Based on this, the Second White Specks and Fish Scales formations display the highest total organic content, ranging from 0.1 – 11.4 wt. %

and 1.2 – 8.0 wt.%, respectively. Both of these units appear to contain abundant type II kerogen, which is sourced from bacterial, planktonic and marine plant remains. This particular kerogen type is ideal for methanogenesis, as anaerobic bacteria preferentially degrade marine organic matter prior to terrestrially source organic matter (Type III kerogen) (Rice and Claypool, 1981). On the other hand, the Westgate and Belle Fourche formations display organic carbon contents ranging between 0.4 – 4.6 wt.% and 0.4 – 11.4 wt.% and have abundant Type III organic matter which is gas prone so can be considered potential source rocks.

The low porosity and permeability of the Colorado Group shales can be attributed to the abundance of clay minerals. Studies (Passey et al. 2010) from previous plays have shown that production is optimal when clay minerals are less than 50%. The low permeabilities mean that fractures are required for economic production which in turn requires brittle behaviour. Historical gas productions within the Colorado Group come from the Belle Fourche and Second White Specks formations (Bloch, 1995). The second White Specks Formation is the only interval with considerable amounts of carbonate to influence fracture stimulation. However, most of the production within the Belle Fourche and Second White Specks comes from siltstone intervals (Bloch, 1995) and it is not known if the shales contain sufficient brittleness, although evidence of recrystallised calcite are seen on thin sections but generally, the carbonate are seen as biogenic specks materials (coccoliths).

5.3.2 Summary

The integration of the various data shows that simple correlations between minerals, grain size and phytoclasts and their spatial variation from the shore are not apparent. AOM constitutes the dominant organic matter in all the formations, however, the Westgate formation contains significant amount of phytoclasts throughout the basin. Mineralogy (quartz and clay) is variable but not related to location within the basin. Carbonate shows a spatial increase in the Belle Fourche and Second White Specks Formations with increasing distance from siliciclastic source.

Grain size data indicate that the Colorado Group consists of substantial amount of clay-grade plus fine silt materials dominated by flocculated grain size spectra. Thin sections show presence of silt laminae and clay clast indicating current activities capable of transporting both flocs and silts. The lack of correlation between mineralogy and palynofacies may suggest that the dominant sediment processes are lateral transport across a very wide, shallow sea, with flocs, silts and phytoclasts all behaving similarly. Schieber et al. (2010) demonstrate that the ability of clays to flocculate makes them hydrodynamically equivalent to coarser materials; therefore both the clays and quartz can be transported as bed load and be re-deposited separately from phytoclasts. Furthermore, a lack of space to accommodate the sediments may lead to deposition 'bypass' and the sediment transport pathways may not be perpendicular to the shoreline (sediment source) (Varban and Plint, 2008). The lack of clear correlations can also be tied to the supply of materials to the sea, as well as to hydrodynamic differences and locations of sedimentation. The supply of different components to the sea is relative, so that an increase in supply of one component can reduce the concentration of a second component, even if the supply of the second remains constant.

The Colorado Group is characterised by moderate to high TOC; TOC does not correlate to grain size or to distance from the shore. However, AOM dominated intervals are associated with high TOC values.

TOC content is highest in the Second White Specks where AOM and carbonate are also highest. This may suggest that the dominant control on TOC is productivity (Bohacs et al. 2005) and perhaps preservation, although preservation may be limited due to the presence of current activity.

Stratigraphic variations in selected wells show that carbonate rich intervals generally correspond with transgressive sequences and are associated with increases in marine organic matter, HI and TOC. On the other hand, increase in siliciclastic minerals correlates with regressive intervals associated with drop in sea – level and increases in terrestrial organic matter. The Second White Specks Formation also exhibits positive correlation between TOC and clay contents ($<2\mu\text{m}$).

The pore size distributions of the lower Colorado Group formations are generally affected by the relative percentages of clay fractions and silt fractions as well as by the level of compaction consistent with the behaviour of pore size distributions of mudstones reported by Yang and Aplin, (1998). Clay rich sediments tend to be unimodal with tight pore size distributions while sediments with both clay-sized and silt materials tend to have broader and occasionally bimodal pore size distributions. Porosity appears to be the dominant control for the pore size distributions in the Westgate Formation, possibly because it is relatively deeper than the rest of the formations. A combination of lithology and porosity is likely to have influenced the pore size distributions in the Fish Scales, Belle Fourche and Second White Specks formations. The unimodal porosity typical of the lower Colorado group formations, and the dominance of clay-sized and silt-sized sediments as indicated by grain size data promotes the adhesion of gas molecules, which makes these sediments optimal for gas adsorption (Javadpour et al. 2007).

The complex nature of the WCSB and lack of adequate continuous core makes the interpretation of the shale gas potential difficult and therefore comments are general. Chapter six considers the shale gas potential of the Upper Colorado Group from a single well with continuous core samples over a 200m interval.

6 CHAPTER SIX: SHALE GAS POTENTIAL OF THE UPPER COLORADO GROUP, SOUTHWESTERN SASKATCHEWAN (12-19-013-28W3 WELL)

6.1 Introduction

The aim of this chapter is to conduct a detailed study of a single well (12-19-013-28W3) within the Bigstick Field located in southeastern Alberta and southwestern Saskatchewan (Fig 6.1). This study area will be used for the shale gas characterisation of the Upper Colorado Group shales integrating geochemistry, mineralogy, grain size, thin sections, porosity and permeability data. Pore size distributions, porosity and permeability of the Upper Colorado shales are determined with the purpose of identifying the gas capacity and producibility of the shales. In addition to this, geochemical (TOC and Rock-Eval) data are also observed with the purpose of identifying organic rich intervals and establishing organic matter type within the formations.

6.2 Background to the Upper Colorado Group

Figure 6.2 shows a generalised composite stratigraphic section of the Upper Colorado summarised from multidisciplinary data (Nielsen et al. 2003). The Upper Colorado Formations incorporate the Carlile to Niobrara Formations (Fig. 6.3) according to Nielsen et al. (2003) nomenclature. The Carlile Formation is a 30 m (east) to 160 m (west) thick non-calcareous, dark grey shaly interval with only minor sand partings that is informally subdivided into lower, middle and upper units. The lower unit of the Carlile Formation is 35 to 40 m thick, homogenous grey shale with occasional non-bioturbated sand partings, no microfossils and average TOC value of 2.2%. The boundary between the Carlile Formation and the underlying Second White Specks Formation is conformable and is easily recognised by a change from a calcareous, highly organic (>3%) shale with common macrofossils to a non-calcareous shale with an organic content generally <2% and rare macrofossils (Nielsen et al. 2003). The middle unit is an approximately 30 meter dark grey, slightly bioturbated, silty shale. The average TOC value is 1.4%. The upper unit is the sandiest of the three units with some macrofossils and bioturbation and TOC in the range of 0.5 and 2.5% (Nielsen et al. 2003).

The boundary between the Carlile and Niobrara formations is unconformable and the thickness of the Niobrara Formation varies from 80 m in the northeast to 240 m in the southwest. It is subdivided into three members: the lower shaly Verger, the sand-rich Medicine Hat, and the uppermost calcareous First White Specks (Nielsen et al. 2003). In general, the Niobrara Formation is composed of dark grey marine shales, siltstones and very fine, grey sandstones and a few layers of chert pebbles.

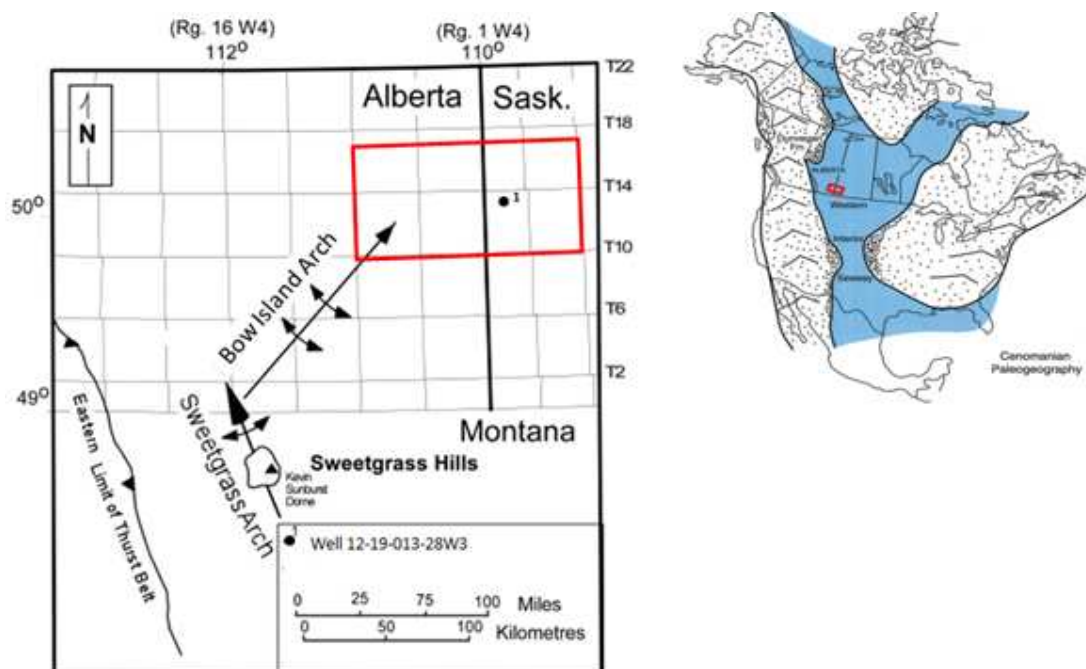


Figure 6.1: Map of the study area, outlined area Indicates location of studied core, 12-19-013-28W3 in the Bigstick modified from Nielsen et al. (2003). The study area overlies the southern Alberta-Saskatchewan border inset outlined in red, within the Western Interior Seaway during Cenomanian age (early Upper Colorado Group deposition).

The Verger Member is a 20 m (in the northeast) to 120 m (in the southwest) thick shaly interval, slightly bioturbated and with only minor sand partings. The TOC values range from 1.5 to 1.9%, and both macro- and microfossils are abundant. The age of this lower member of the Niobrara Formation is Coniacian. The Medicine Hat Member is relatively uniform with a thickness between 40 and 65 m. The member consists of numerous, fine-grained sandstones separated by shale and siltstone. The First White Specks Member is the youngest in the Niobrara Formation, and is a dark grey calcareous shale with thickness from 75 m in the west to 20 m in the east (Nielsen et al. 2003).

The Milk River Formation is one of numerous units deposited in the Western Interior Seaway during the Late Cretaceous. Seven distinct marine lithofacies have been identified (Ridgley, 2000), each having sandstone, siltstone, and mudstone or shale lithologies present. The lithofacies correspond to various depositional environments including delta front, shoreface, and inner and outer shelf. Overall, deposition of the Milk River spanned at least two episodes of sea-level fall, which prompted basinward shifts of facies. These basinward shifts of facies were followed by marine transgressions (Ridgley, 2000). The two sea-level falls are seen in the rock record as major erosional surfaces (Ridgley, 2000)

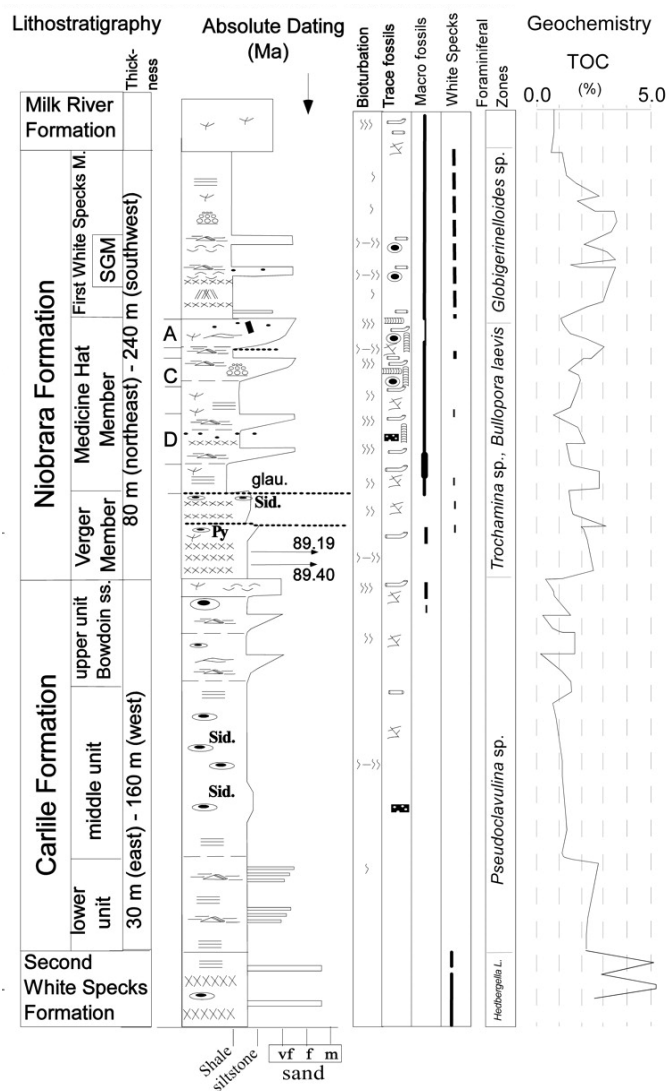


Figure 6.2: Schematic section of the Carlile and Niobrara formations after Nielsen et al. (2003)

				Alberta, Canada	Saskatchewan, Canada	Montana, USA			
CRETACEOUS	Upper	Campanian	MONTANA GROUP	Belly River Formation *	Belly River Formation *	Judith River Formation *			
				Pakowki and Lea Park formations	Pakowki and Lea Park formations	Claggett Shale			
				Milk River Formation *	Milk River Formation *	Eagle Sandstone and Gammon Shale *			
		Santonian	COLORADO GROUP	Niobrara Formation	Medicine Hat Sandstone *	Medicine Hat Sandstone *	Niobrara Formation	Martin sandy zone *	
				Coniacian				Niobrara Formation	
		Turonian		Cardium Sandstone	Carlile Shale	Carlile Shale	Bowdoin sandstone *	Carlile Shale	Bowdoin sandstone *
				Second White Specks Formation *	Second White Specks Formation	Second White Specks Formation	Greenhorn Limestone *		
		Cenomanian		Belle Fourche Formation *	Belle Fourche Formation *	Belle Fourche Formation *	* Phillips sandstone	* Mosby Sandstone	
							Belle Fourche Shale *		
					Fish Scales Zone	* Barons Siltstone	Fish Scales Formation	Mowry Shale	

Figure 6.3: Correlation chart showing selected Cretaceous rock units from south-eastern Alberta, south-western Saskatchewan, and Montana. Asterisks mark gas-producing formations (Ridgley, 2002).

A total of 126 samples over a 200m thick interval were taken from the core of well 12-19-013-28W3 and covering Belle Fourche through to the First White Specks Member for the various analyses. However, emphases were focussed on the Upper Colorado Formations and members (Carlile – First White Specks) intervals only.

6.3 Bulk mineralogical results of 12-19-013-28W3 well

Bulk mineralogical analysis was conducted on all the 126 samples using the FTIR spectroscopy model developed in this study. The mineralogy percentages for the Upper Colorado Group shales from the Bigstick 12-19-013-28W3 well show that clay minerals dominate the composition of each formation and member, followed by quartz (Table 6.1, Appendix III). Minor amounts of dolomite, calcite, and feldspar are also present. The Upper Colorado samples have the following ranges: quartz: 3.9-51.5%, calcite: 0.9-59.7%, dolomite: 0.1-1.7%, kaolinite: 0.6-27%, illite-smectite: 15-43.1%, and total clay: 15.4-48.5%. Average percentages for the minerals present differ as follows: quartz: 34.7%, calcite: 11.2%, dolomite: ~1%, kaolinite: 8%, and illite-smectite: 34%.

Quartz content is highest within the Verger member of the Niobrara Formation (30.3-49.7%; mean 40%), but is still comparatively high within the Medicine Hat Member (24.9-48.7%, mean 39.2%). The greatest percentage of total clays is within the Carlile Formation (62.1%). It is surprising that the Carlile Formation have a broader range of carbonate content (1.1 – 61.4%) than the First and Second White Specks Formations (6.0 – 28.3% and 4.1 – 58.3% respectively), but overall, the First and Second White Specks Formations are the most calcareous shales within the Upper Colorado Group with an average carbonate contents of 17.7% and 23.9% respectively, while the average carbonate content of the Carlile Formation is 8.4%.

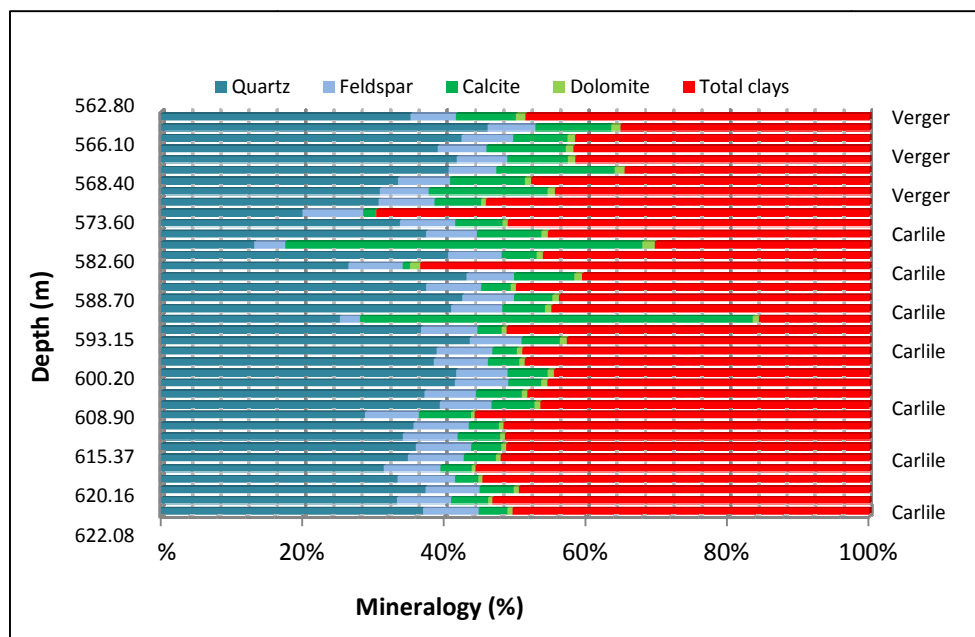


Figure 6.4: Semi-quantitative mineralogy of the Verger Member of the Niobrara Formation and Carlile Formation. Clay minerals dominate the composition of each sample, followed by quartz. Minor amounts of dolomite, calcite, and feldspar are also present. The Carlile Formation shows sections of increased carbonate content. Verger Member shows the highest amount of quartz percentage.

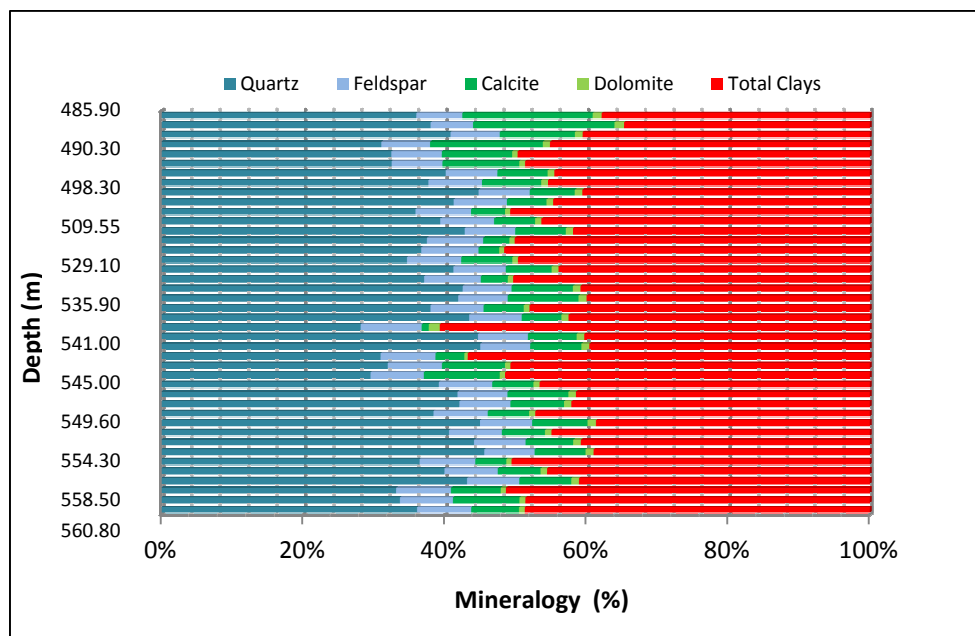


Figure 6.5: Semi-quantitative mineralogical analysis of the Medicine Hat Member, showing increased amount of quartz compared to the Carlile Members and the First White Specks Member

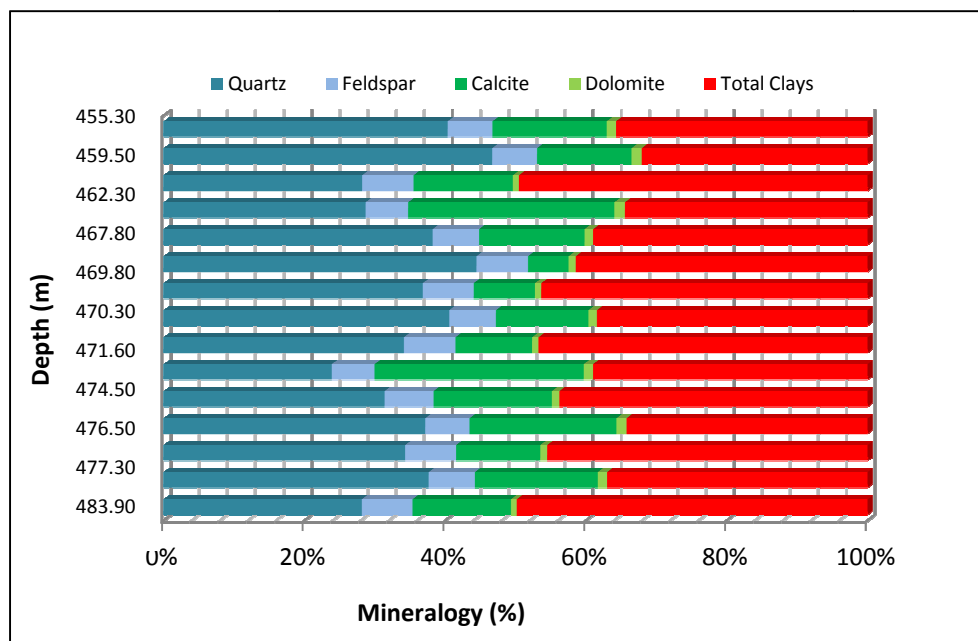


Figure 6.6: Semi-quantitative mineralogical analysis of the First White Specks Members of the Niobrara Formation. The First White Specks Member is the most calcareous on average within the Upper Colorado with average carbonate content of 17.7% (Calcite + dolomite)

Table 6.1: Mineralogical Composition of 12-19-013-28W3

Mineral	N	Mean	StDev	Minimum	Maximum
First White Specks					
%Quartz	15	36.1	8.1	22.8	51.5
%Calcite	15	15.9	6.3	6.0	28.3
%Dolomite	15	1.8	0.3	0.8	1.6
%Kaolinite	15	5.9	2.8	0.6	10.9
%Illite-smectite	15	31.9	2.8	26.5	35.9
Medicine Hat					
%Quartz	42	39.2	6.0	24.9	48.7
%Calcite	42	7.8	3.8	0.9	21.4
%Dolomite	42	1.0	0.2	0.5	1.5
%Kaolinite	42	6.3	2.7	0.6	14.2
%Illite-smectite	42	35.6	2.1	28.9	43.1
Vergers					
%Quartz	8	40.0	6.2	30.3	49.7
%Calcite	8	11.6	3.4	7.9	16.9
%Dolomite	8	1.2	0.2	0.9	1.5
%Kaolinite	8	5.0	3.0	0.7	8.5
%Illite-smectite	8	34.3	2.7	31.0	40.1
Carlie					
%Quartz	30	35.4	7.9	12.3	47.8
%Calcite	30	8.4	12.5	1.0	59.7
%Dolomite	30	0.8	0.3	0.1	1.7
%Kaolinite	30	8.7	3.1	2.0	19.0
%Illite-smectite	30	35.7	5.4	14.9	43.1
Second White Specks					
%Quartz	21	25.3	11.5	3.9	46.2
%Calcite	21	22.9	19.5	4.0	56.6
%Dolomite	21	1.0	0.4	0.1	1.7
%Kaolinite	21	10.7	6.7	4.4	37.0
%Illite-smectite	21	29.7	8.2	15.1	40.2
Belle Fourche					
%Quartz	12	28.8	6.3	21.5	43.0
%Calcite	12	4.1	1.9	2.5	8.7
%Dolomite	12	0.5	0.2	0.2	1.0
%Kaolinite	12	13.5	3.1	7.2	17.8
%Illite-smectite	12	37.9	1.2	34.9	38.9

6.4 Grain size distributions and thin sections of 12-19-013-28W3 well

Grain size distributions and thin sections for samples taken from the Upper Colorado Group were conducted by Dr. Ron Spencer at the University of Calgary, Canada. Grain size analysis was conducted using the laser diffractometry technique on a suite of 60 samples; described by Beuselink et al. (1998) and classified according to the Udden-Wentworth. The grain size distributions for the Upper Colorado shales are dominated by combined silt and clay fractions accounting for between 50-90% (Table 6.2) and generally exhibit upward-coarsening trends in all formations and members except in the Verger member and First White Specks Formation which show no apparent trend.

6.4.1 Carlile Formation

Grain size distributions appear to be overall upward-coarsening in the Carlile. Grain size in the Lower and Middle Carlile members, as well as into the Upper Carlile member is upward-coarsening. An upward-fining (U-F) is however, observed at approximately 575 m depth until the top of the Carlile Formation (Fig. 6.7). The change between ‘upward-coarsening’ and ‘upward-fining’ is interpreted to represent a transgressive surface (‘TS’) within the Upper Carlile member.

The Upper Carlile member is comprised of very fine-grained sand and fine-grained sand. Thin section of samples from the Lower Carlile member is shown in Figure. 6.8 at a depth of 606.5m) comprising of silty mudstone, rare quartz grains and organic matter (OM). SEM analyses angular pieces of red phosphate are present throughout Carlile Formation mudstones. The mudstone show signs of moderate to intense bioturbation and trace fossils are typically filled with mud-rich or clay-rich sediments.

The Middle Carlile Member comprise of clayey siltstones and muddy siltstones (Fig. 6.7). The siltstone contains quartz grains, organic matter (OM), and phosphate (Phos) while the muddy siltstones contain organic matter (OM), phosphate (Phos) and pyrite, which are present throughout the sediments, with signs of intense bioturbation (Fig. 6.9). Trace fossils within the Middle Carlile member tend to be filled with relatively finer-grained, well sorted sediments and areas not cemented with mud or clay are stained with blue epoxy (Fig. 6.9A).

The presence of flattened and distorted burrows suggests that the sediments have undergone some level of compaction.

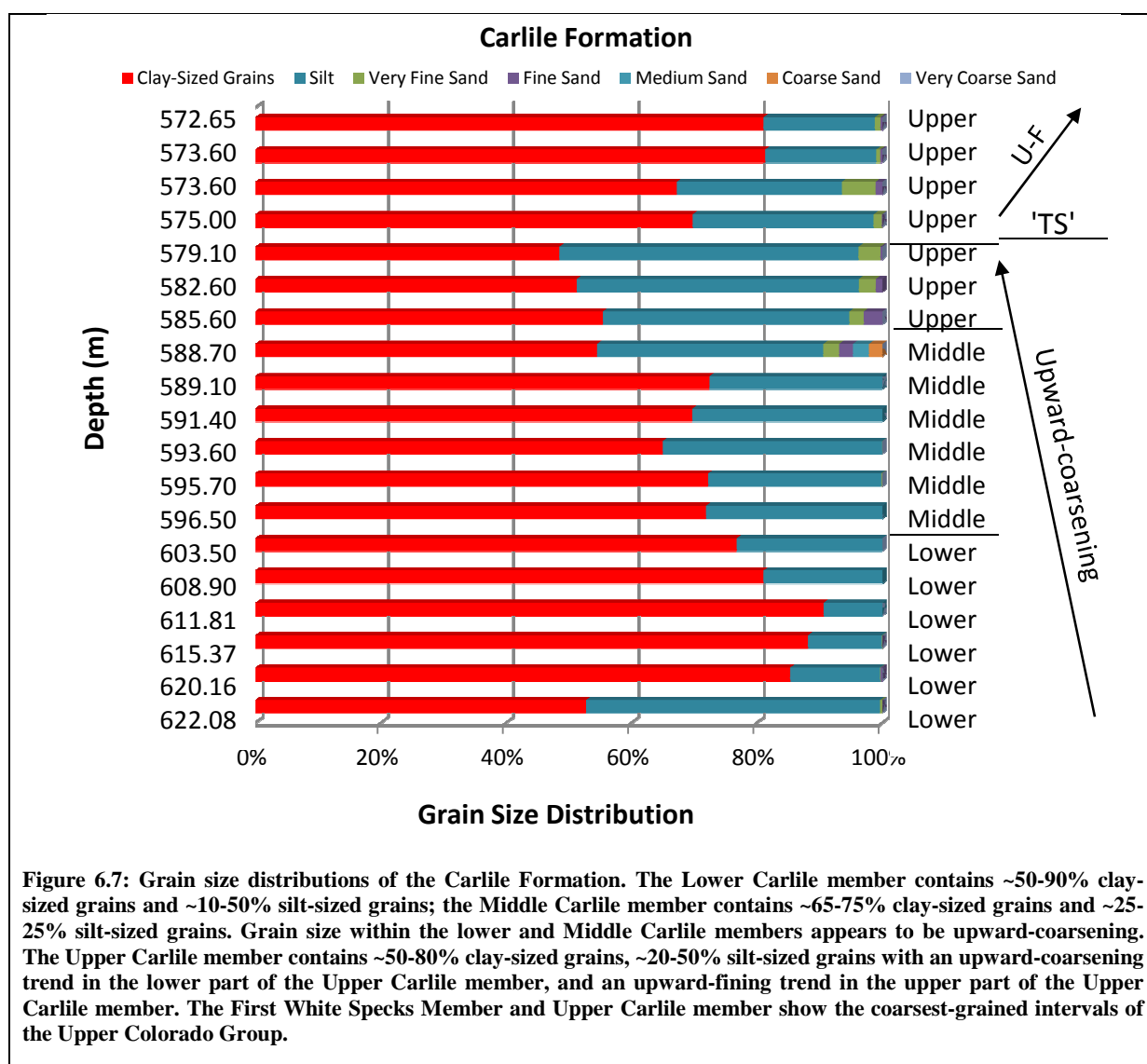
Table 6.2: Grain size distributions for 12-19-13-28/W3 Well (Lower, Middle, Upper Carlile and Verger Members)

Depth (m)	Formation/member	Clay % (< 4µm)	Silt % (4-62.5µm)	Very Fine Sand % (62.5-125µm)	Fine Sand % (125-250 µm)	Medium Sand % (250-500µm)	Coarse Sand % (500-1000µm)	Very Coarse Sand % (1000-2000µm)
622.08	L. Carlile	52.76	46.86	0.37	0.01	0	0	0
620.16	L. Carlile	85.29	14.33	0.1	0.29	0	0	0
615.37	L. Carlile	88.12	11.77	0.09	0.02	0	0	0
611.81	L. Carlile	90.62	9.38	0	0	0	0	0
608.9	L. Carlile	81.04	18.98	0	0	0	0	0
603.5	L. Carlile	76.76	23.24	0	0	0	0	0
596.5	M. Carlile	71.87	28.13	0	0	0	0	0
595.7	M. Carlile	72.22	27.6	0.14	0.04	0	0	0
593.6	M. Carlile	64.99	34.99	0.03	0.02	0	0	0
591.4	M. Carlile	69.69	30.32	0	0	0	0	0
589.1	M. Carlile	72.43	27.57	0	0	0	0	0
588.7	M. Carlile	54.55	36.08	2.54	2.21	2.5	2.15	0
585.6	U. Carlile	55.37	39.24	2.29	2.99	0.12	0	0
582.6	U. Carlile	51.27	44.98	2.69	1.05	0	0	0
579.1	U. Carlile	48.49	47.7	3.51	0.31	0	0	0
575	U. Carlile	69.87	28.89	1.33	0.09	0	0	0
573.6	U. Carlile	67.22	26.32	5.38	1.09	0	0	0
573.6	U. Carlile	81.3	17.7	0.65	0.34	0	0	0
572.65	U. Carlile	81.03	17.76	0.9	0.31	0	0	0
569.8	Verger	86.88	13.12	0	0	0	0	0
568.4	Verger	60.1	34.17	5.36	0.37	0	0	0
567.1	Verger	49.85	40.29	8.51	1.35	0	0	0
566.1	Verger	64.95	31.89	2.81	0.36	0	0	0
565.2	Verger	57.29	39.23	3.83	0.59	0	0	0
563.8	Verger	70.77	26.25	2.8	0.18	0	0	0
562.8	Verger	77.51	17.68	0.8	2.89	1.12	0	0
562.3	Verger	71.02	24.34	4.07	0.58	0	0	0
561.5	Verger	67.62	32.34	0	0	0	0	0

Table 6.3: Grain size distributions for 12-19-13-28/W3 Well (Med. Hat and 1SW Members)

Depth (m)	Formation/member	Clay % (< 4um)	Silt % (4-62.5um)	Very Fine Sand % (62.5-125um)	Fine Sand % (125-250 um)	Medium Sand % (250-500um)	Coarse Sand % (500-1000um)	Very Coarse Sand % (1000-2000um)
560.8	Med Hat	86.51	13.49	0	0	0	0	0
560.25	Med Hat	72.91	26.26	0.51	0.31	0	0	0
558.8	Med Hat	76.55	23.27	0.15	0.04	0	0	0
557.85	Med Hat	81.68	18.32	0	0	0	0	0
557.1	Med Hat	87.65	12.44	0	0	0	0	0
555.1	Med Hat	81.47	18.53	0	0	0	0	0
554.3	Med Hat	86.92	12.97	0.07	0.04	0	0	0
553	Med Hat	83.14	16	0	0	0	0	0
550.9	Med Hat	99.86	0.14	0	0	0	0	0
549.6	Med Hat	87.88	12.12	0	0	0	0	0
546.3	Med Hat	88.06	11.94	0	0	0	0	0
545.55	Med Hat	73.51	25.84	0.63	0.06	0	0	0
540	Med Hat	99.32	0.72	0	0	0	0	0
535.9	Med Hat	84.89	15	0.07	0.04	0	0	0
530.2	Med Hat	82.75	17.25	0	0	0	0	0
527.26	Med Hat	77.58	22.43	0	0	0	0	0
513.45	Med Hat	75.84	23.91	0.05	0.21	0	0	0
508	Med Hat	69.21	30.9	0	0	0	0	0
503.6	Med Hat	81.59	18.24	0.15	0.03	0	0	0
498.3	Med Hat	76.07	23.52	0.36	0.05	0	0	0
496.8	Med Hat	76.38	23.16	0.42	0.04	0	0	0
492.9	Med Hat	61.5	38.5	0	0	0	0	0
487.7	Med Hat	66.63	32.74	0.57	0.03	0	0	0
485.3	1WS	76.87	21.7	1.33	0.1	0	0	0
481.1	1WS	69.06	30.65	0.27	0.02	0	0	0
477.3	1WS	49.96	41.93	7.06	1.05	0	0	0
475.5	1WS	51.22	41.77	6.21	0.8	0	0	0
471.6	1WS	66.82	31.16	1.69	0.3	0.03	0	0
467.8	1WS	61.5	34.23	3.7	0.57	0	0	0
463.2	1WS	55.94	42.16	1.83	0.07	0	0	0
462.5	1WS	54.72	37.57	6.62	1.09	0	0	0
458	1WS	69.18	29.81	0.95	0.06	0	0	0

Samples from the upper Carlile member show a dominant clay-rich mudstone containing dark brown, angular and ellipsoid clay clasts interval. Organic matter (OM) and phosphate fragments (Phos) are similarly angular in shape (Fig. 6.10). This change in appearance of clay clasts is distinct to only the Upper Carlile and may indicate significant changes in the environmental conditions during deposition. This is likely a combination of decreased sediment supply and increased sediment consolidation. These changes likely coincide with the occurrence of a transgressive surface in the Upper Carlile member that was identified in the grain size data.



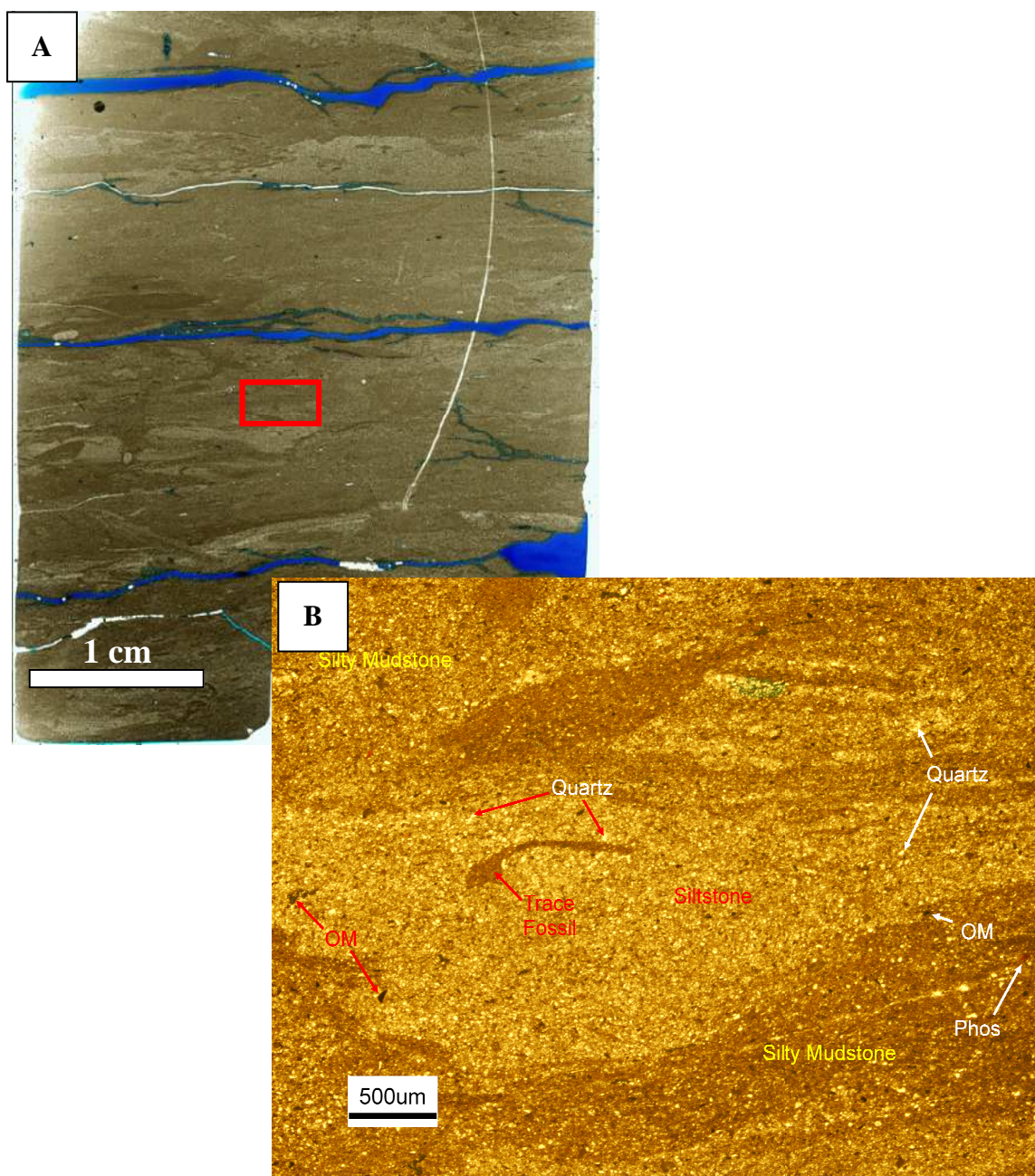
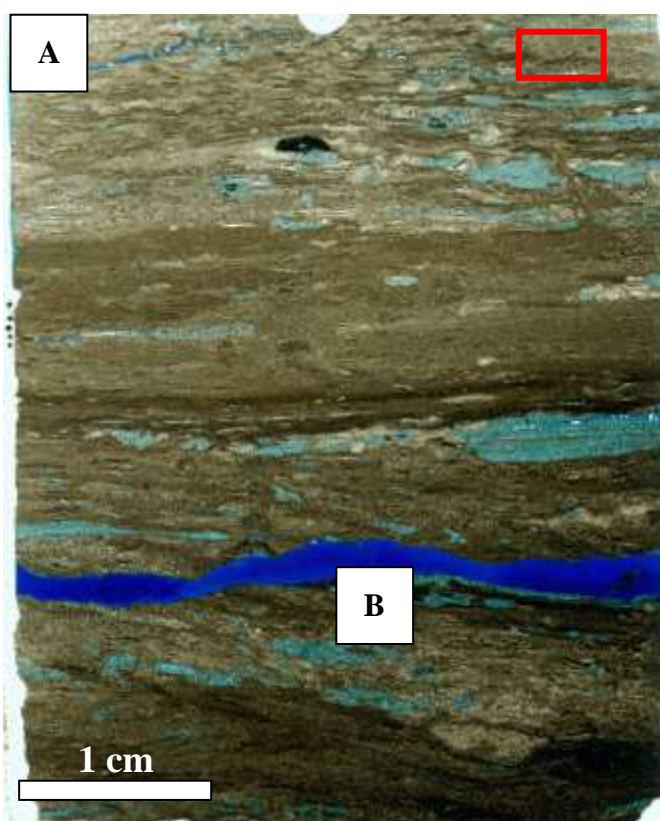


Figure 6.8: A) Scanned thin section of a sample within the Lower Carlile Member at a depth of 606.5 m showing moderately to intensely bioturbated silty mudstone. The red rectangle represents the view of the petrographic microscope image in (B) showing the bioturbated siltstone lamination with trace fossil. Trace fossils are filled with mud-rich or clay-rich sediments.



C

Figure 6.9: A) Scanned thin section of a sample within the Middle Carlile Member showing a muddy siltstone at a depth of 600.2m with intense bioturbation. The red rectangle denotes the view of the petrographic microscope image in (B) Mud and clay-filled burrows within muddy siltstone. Flattened, distorted burrows indicate compaction of the sediments. Resin impregnation suggests significant large and accessible pores in parts of the sediment. (C) Flattened, distorted burrows indicate compaction of the sediments. Petrographic image of a sample within the Middle Carlile member, at a depth of 600.2m containing muddy siltstone, organic matter (OM), phosphate (Phos) and pyrite. Also present is a foraminifer (foram) filled with framboidal pyrite.

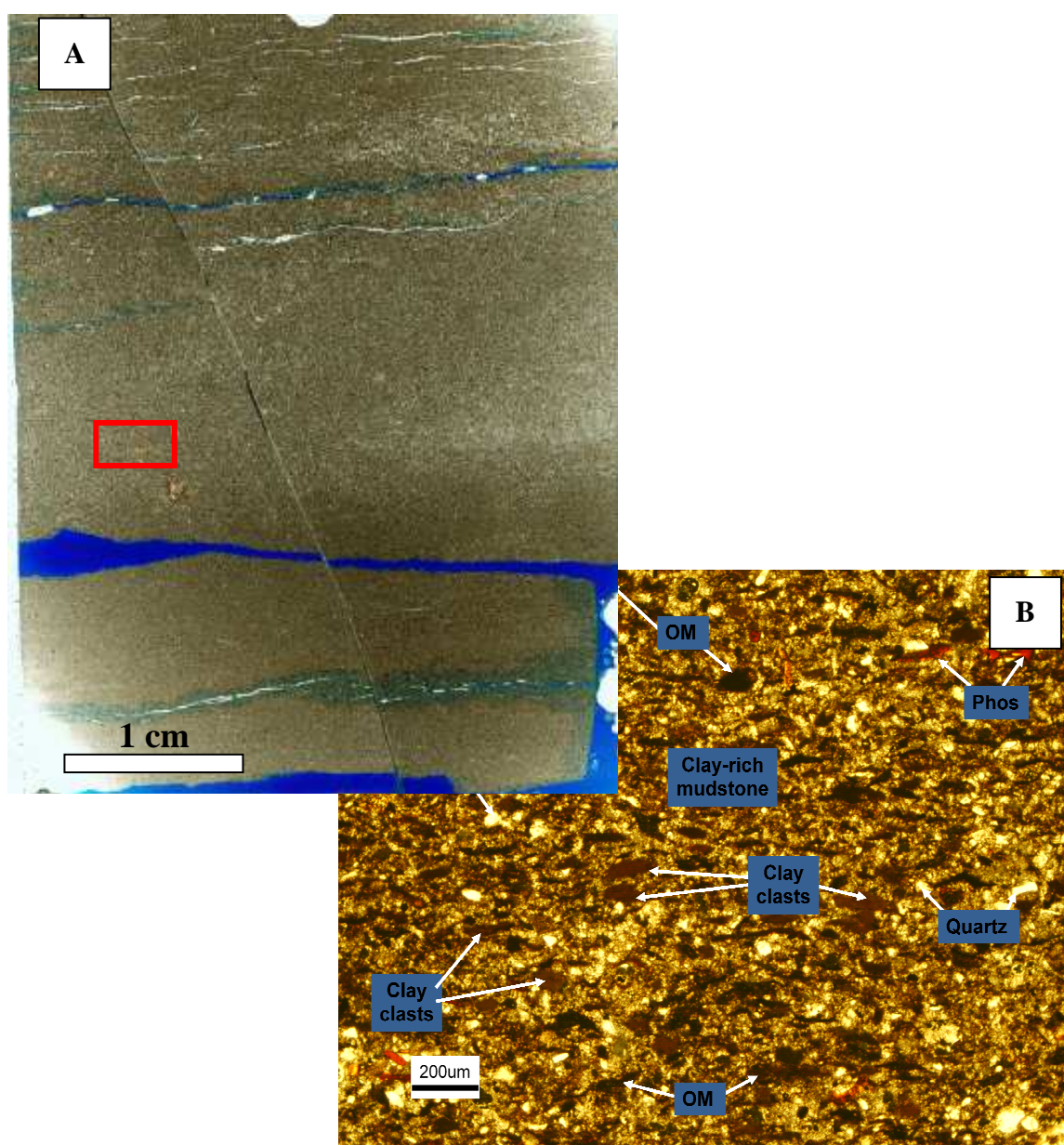
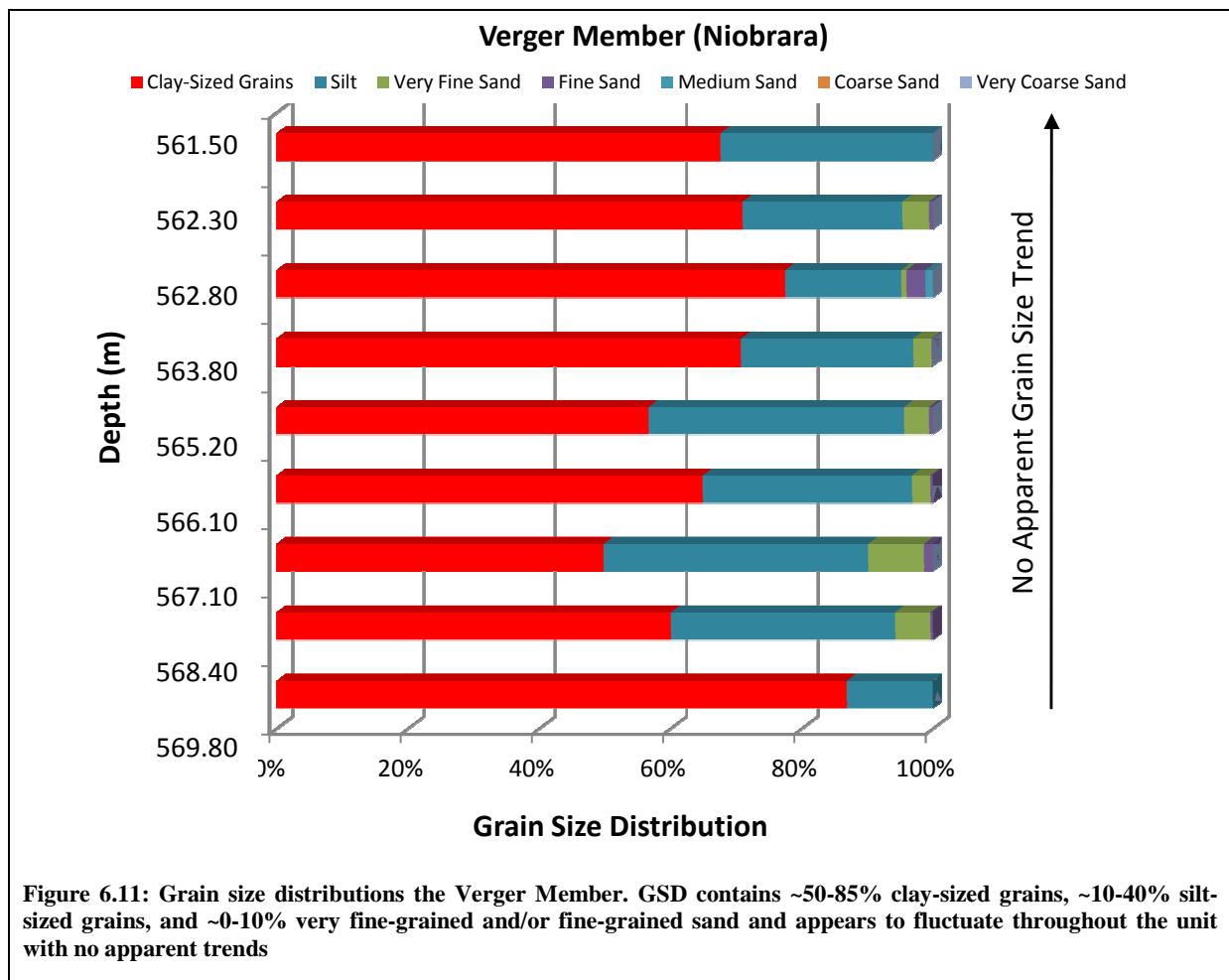


Figure 6.10: (A) Scanned thin section of a sample within the Upper Carlile member, at a depth of 580 m showing a clay-rich mudstone. The red rectangle denotes the view of the petrographic microscope image in (B) containing dark brown, angular clay clasts, organic matter (OM) and phosphate fragments (Phos)

6.4.2 Niobrara Formation

Grain size does not appear to exhibit any visible trend throughout the Verger Member (Fig.6.11). The thin section of sample within the Verger member appears homogeneous with no bedforms (Fig. 6.12). The Verger Member is dominated by clay-rich mudstone with lenticular clay clasts and organic matter (OM) within the mudstone (Fig. 6.12). Quartz grains are also present and appear as individual floating grains.



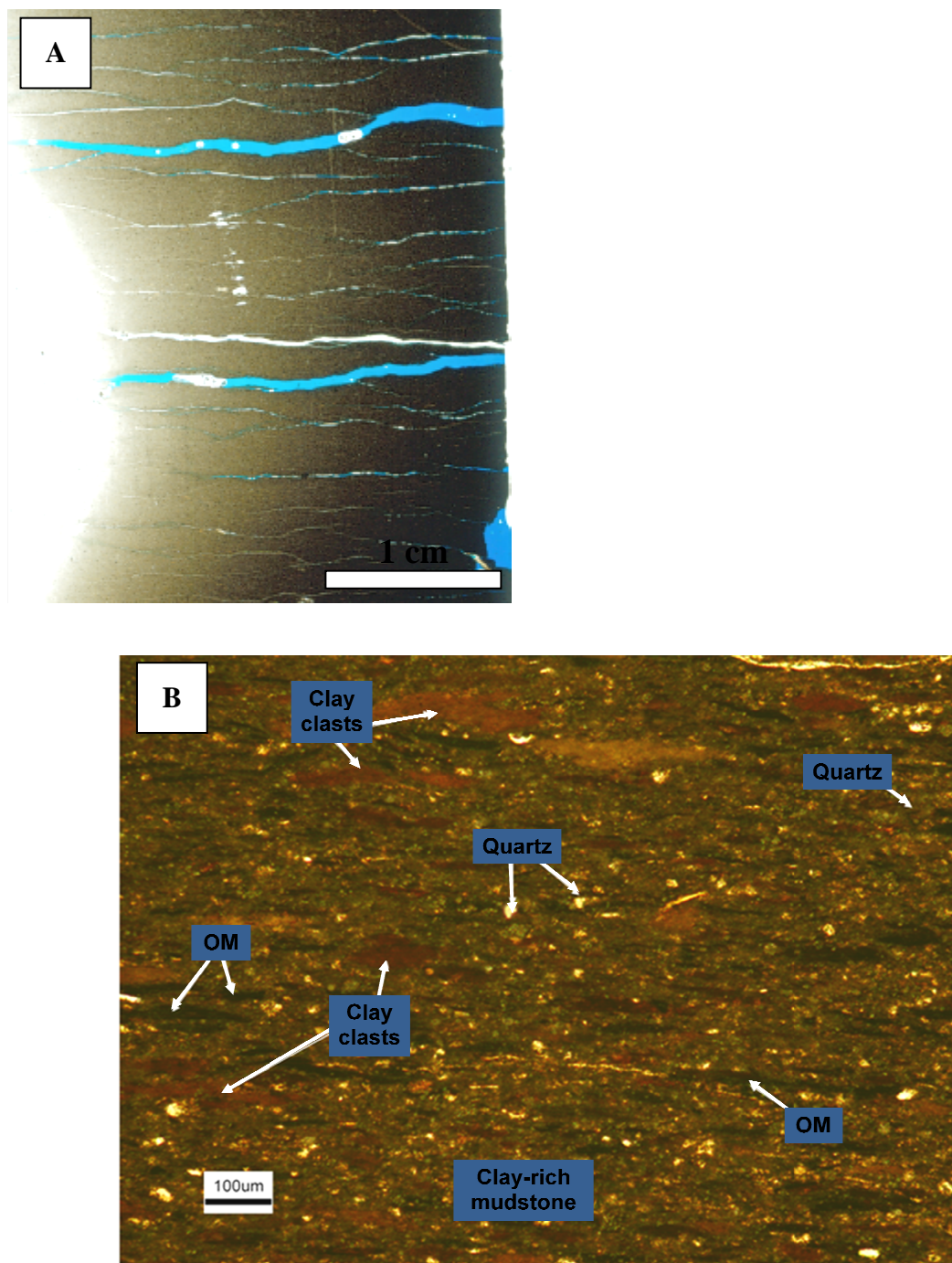
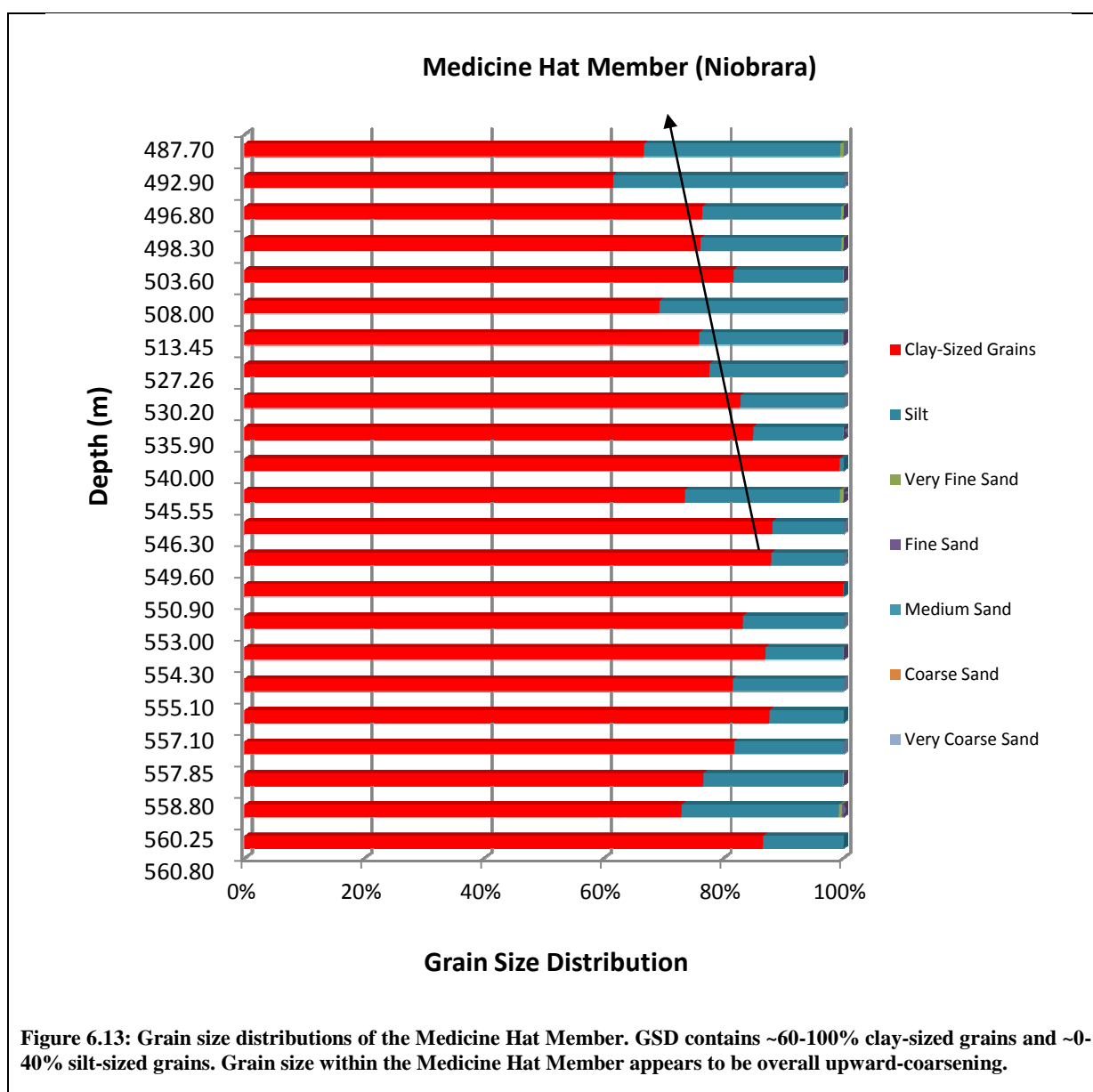


Figure 6.12: (A) Scanned thin section of a sample, within the Verger Member, at a depth of 568.4m showing a homogeneous clay-rich mudstone with no bedforms. (B) Show a petrographic view of lenticular clay clasts and abundant organic matter (OM) within the Verger Member.

Grain size distributions are overall upward-coarsening in the Medicine Hat Member (Figs 6.13). Thin sections show that the Medicine Hat Member comprises clay-rich siltstone, lenticular clay clasts within silty organic-rich mudstone and fine-grained sandstone laminae. The clay-rich siltstone contains quartz grains, organic matter (OM), phosphate (Phos) and fish bones. Clay clasts in the Medicine Hat Member are accompanied by elongated stringers of black organic matter (OM) and phosphate (Phos). The clay clasts look very similar in appearance to those observed in the Verger Member, which implies that the sediments have been eroded. The muddy siltstones contain calcite overgrowths, pyrite, organic matter (OM), quartz grains and calcite grains (Figs 6.14 – 6.16).



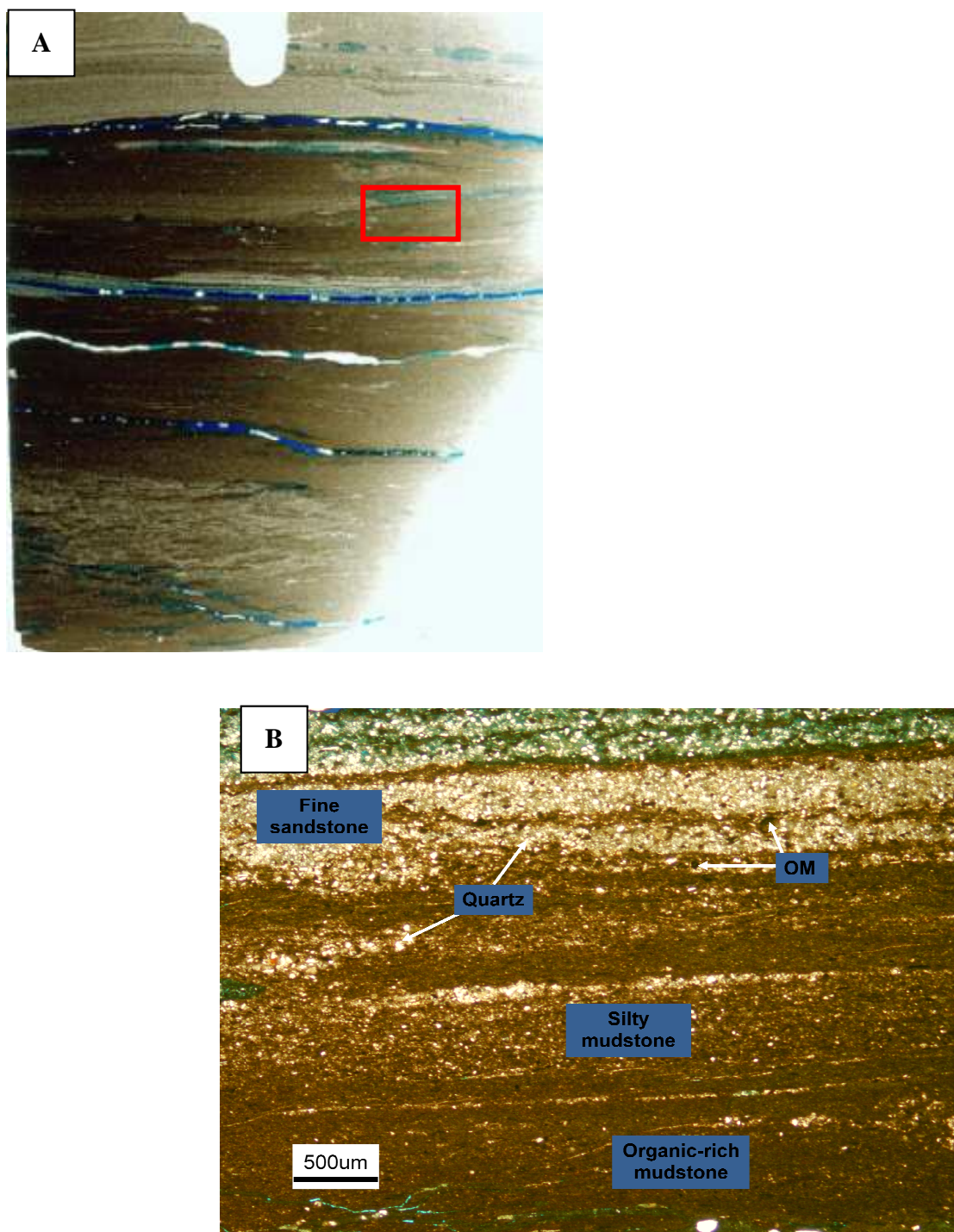


Figure 6.14: A) Scanned thin section of a sample within the Medicine Hat Member at a depth of 527.25 m, showing organic-rich mudstone and fine-grained sandstone laminae. The red rectangle denotes the view of the petrographic microscope image in (B) containing organic-rich and silty mudstone laminations overlain by a fine sandstone lamination.

The overgrowth may represent burrow fill that has been occluded by calcite cement. Multiple carbonate cements including dolomite cements are most abundant, with minor calcite cement within the Medicine Hat Member (Fig. 6.16).

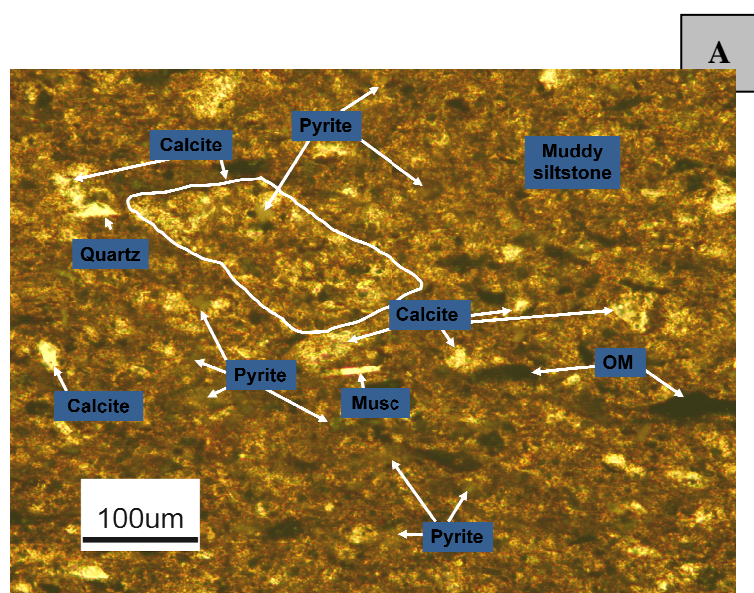


Figure 6.15: A) Petrographic image of a thin section of a sample within the Medicine Hat Member, at a depth of 519.25 m. Pyrite, organic matter (OM), calcite grains are present throughout the sediments.

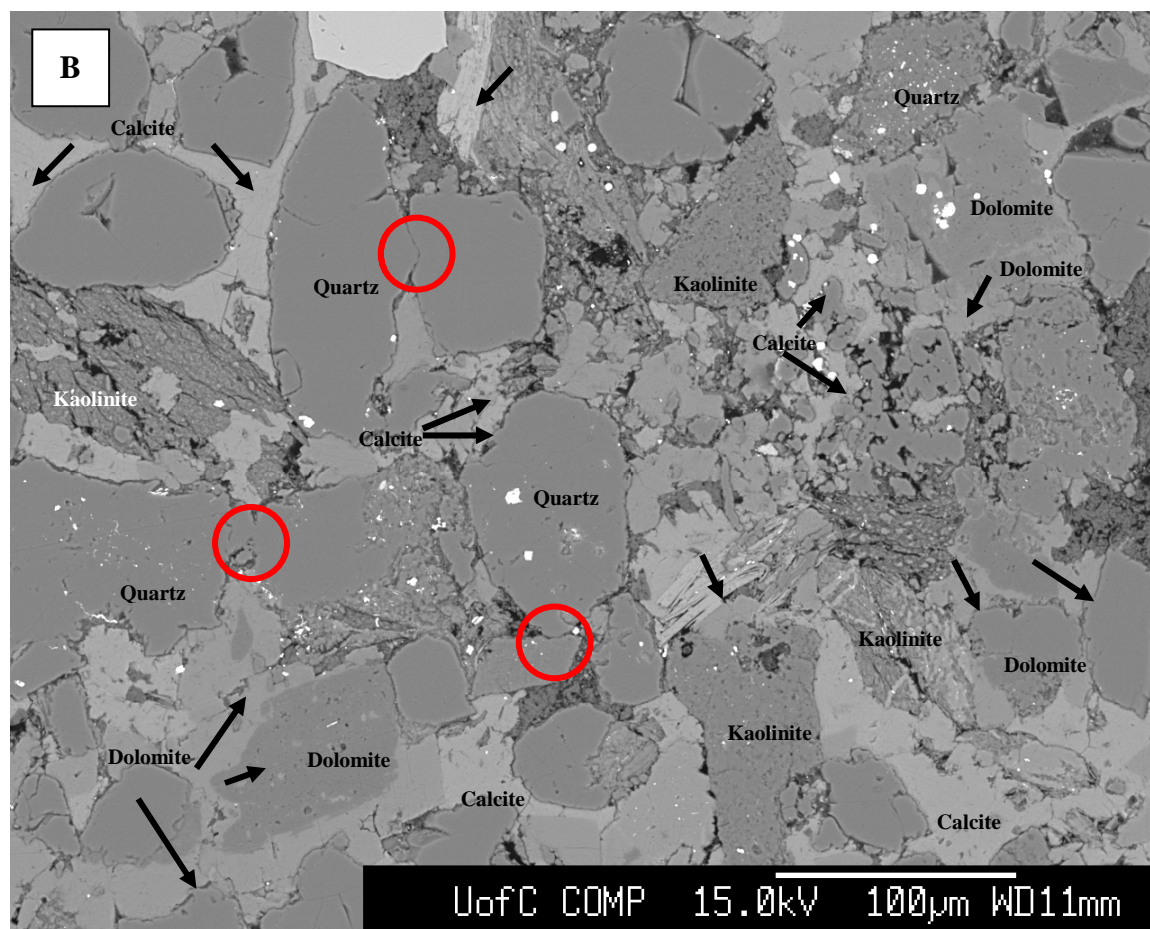
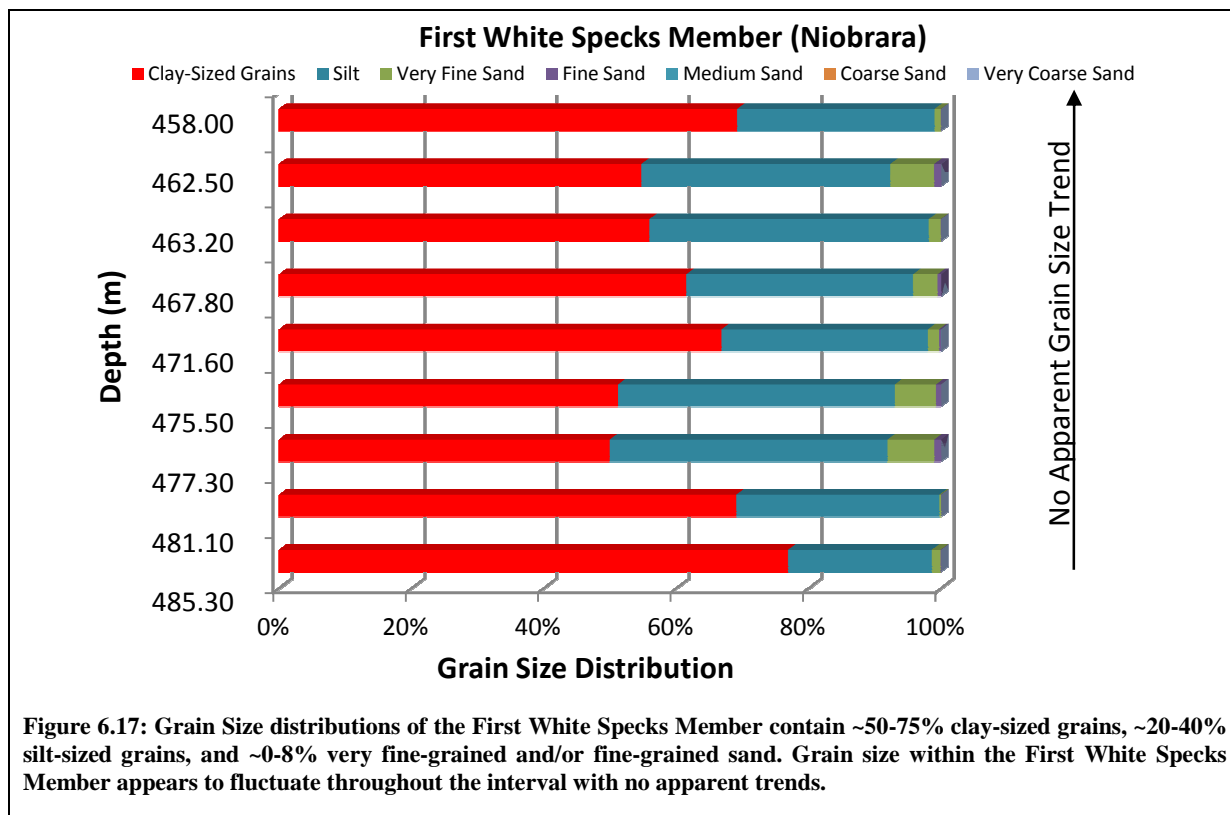


Figure 6.16: (B) SEM image within the Medicine Hat Member, at a depth of 530.2m showing multiple carbonate cements - dolomite are most abundant, with minor calcite cement. Compaction is apparent within this interval, as several quartz grains display point contact (circled in red).

Grain Size distributions remain relatively stable throughout the First White Specks Formation (6.17). The results suggest that the First White Specks Member is coarser than the Medicine Hat Member. However, it is possible that the coarse sediment fraction is actually comprised of calcareous cemented clay aggregates, which are being misinterpreted as sand by the grain size analyzer. Thin sections (Fig. 6.18) show that the First White Specks Member comprises clay-rich, organic-rich mudstone and calcareous and siliciclastic sandstone laminations. Stringers of black organic matter (OM) occur throughout the mudstone. Siltstone laminations and beds are comprised of calcite and occasional quartz grains. Permeability along some laminations is indicated by the presence of blue epoxy. Some laminations are cemented with a combination of calcite and mud. Organic matter (OM), phosphate (Phos) and abundant clay clasts are present throughout organic-rich, clay-rich beds and laminations (Fig 6.18).



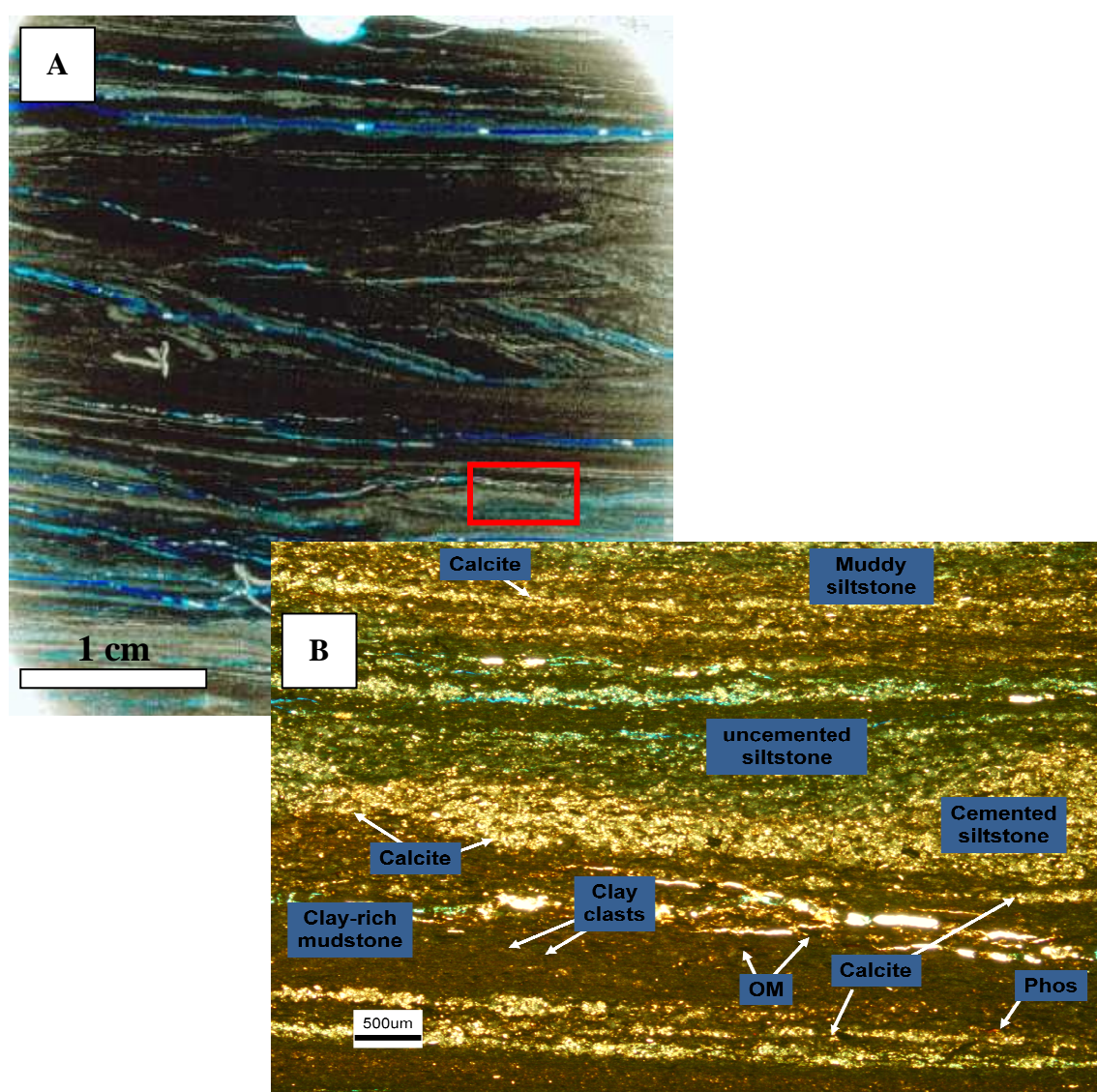


Figure 6.18: First White Specks A) Scanned thin section of the sample within the First White Specks Member, at a depth of 471.6 m showing calcareous and siliciclastic siltstone laminations. The red rectangle denotes the view of the petrographic microscope image in (B) Siltstone laminations and beds are comprised of calcite and occasional quartz grains. Organic matter (OM), phosphate (Phos) and abundant clay clasts are present throughout organic-rich, clay-rich beds and laminations.

6.5 PSD, porosity and permeability of 12-19-013-28W3

A total of 20 samples within the 12-19-013-28W3 were measured for PSD, porosity and permeability. The results from mercury injection analyses for the Upper Colorado Group are presented in Table 6.2 and Figures 6.16 – 6.21 showing total porosities and permeability values. Total porosities within the samples range from 10.32-19.76%, and display largely unimodal porosity distribution between (10-20nm).

Measured porosity within the Carlile Members varies between 10.3- 19.3%, with tight mean pore throat sizes between 8.27-28.9nm. Grain size data and thin sections show that the Members consist of a dominant clay-rich mudstone, clayey siltstones and muddy siltstones. Clay fractions constitute 50 – 90% of the total fractions typical of matrix supported sediments (Yang and Aplin, 1998b). Similarly, the lower parts of the Medicine Hat Member and Verger Member all have unimodal porosity characterised by clay fraction >50%. Total porosities for Medicine Hat Member range between 14.5-18.7%, while mean pore throat size range between 13.9-23.3nm

Bimodal pore size distributions are seen within the First White Specks Formation, the upper part of the Medicine Hat Member, and Second White Specks Formation. These intervals correspond to sections with increased fractions of coarser silt and sand grains. The highest porosity was recorded within the First White Specks Member (19.8%; 35nm), while the lowest values were recorded within the Middle Carlile Member (10.3%; 28.9nm).

It is likely that the true porosity is much higher than the total porosity measured in the Upper Colorado Group, as the abundant mud and clay within these formations/members would probably cement up much of the pore space network. Permeability values computed from the mercury injection dataset show that the Upper Colorado Group ranges from 3.27-151 nD, with an average of 14.4 nD.

Table 6.4: Porosity data for 12-19-013-28W3

Depth (m)	Formation/Member	Average Permeability (nD)	Total Porosity (%)	Mean Pore Throat Radius (nm)
471.6	1 st White Specks	151	19.8	35
496.8	Medicine Hat	6	18.0	23
508	Medicine Hat	8	18.0	21
519.25	Medicine Hat	3	18.7	18
530.5	Medicine Hat	5	17.7	16
539.35	Medicine Hat	4	14.5	14
545.85	Medicine Hat	5	17.3	17
552	Medicine Hat	7	16.0	18
562.8	Verger	5	19.8	21
572.65	Upper Carlile	8	16.0	19
582.6	Upper Carlile	5	19.3	18
589.5	Middle Carlile	11	14.6	16
595.7	Middle Carlile	7	10.3	29
603.5	Lower Carlile	7	14.9	13
611.31	Lower Carlile	5	14.6	12
619	Lower Carlile	7	15.0	15
625	Lower Carlile	8	16.9	9
644.8	2 nd White Specks	10	19.9	20
650.81	2 nd White Specks	10	16.9	17
667.34	2 nd White Specks	17	17.5	310

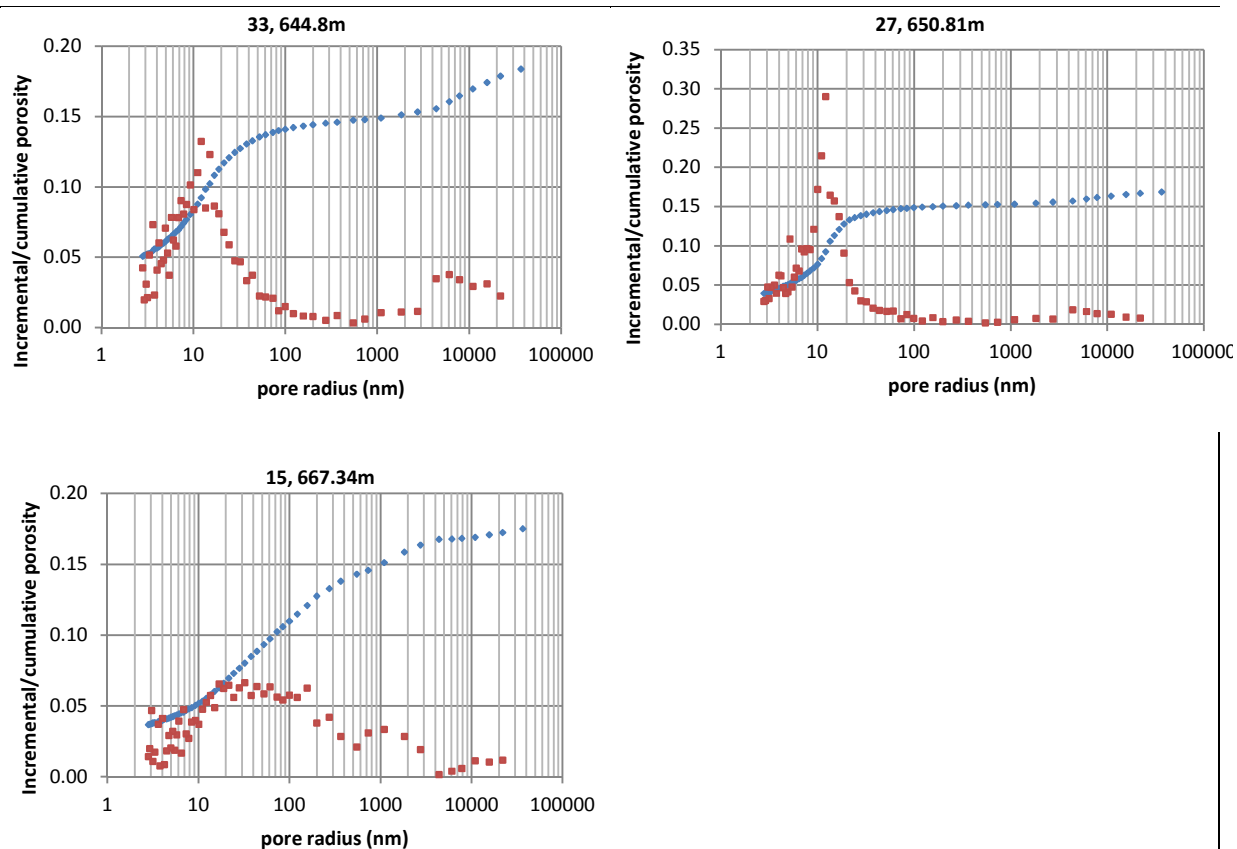


Figure 6.19: Pore size distribution plots at various depths in the Second White Specks Formation. Samples at 644.4m and 667.34m have bimodal PSD and mean pore sizes of 19.5nm and 310nm respectively, while sample at 650.18m has a unimodal PSD and a mean pore size of 16.9nm.

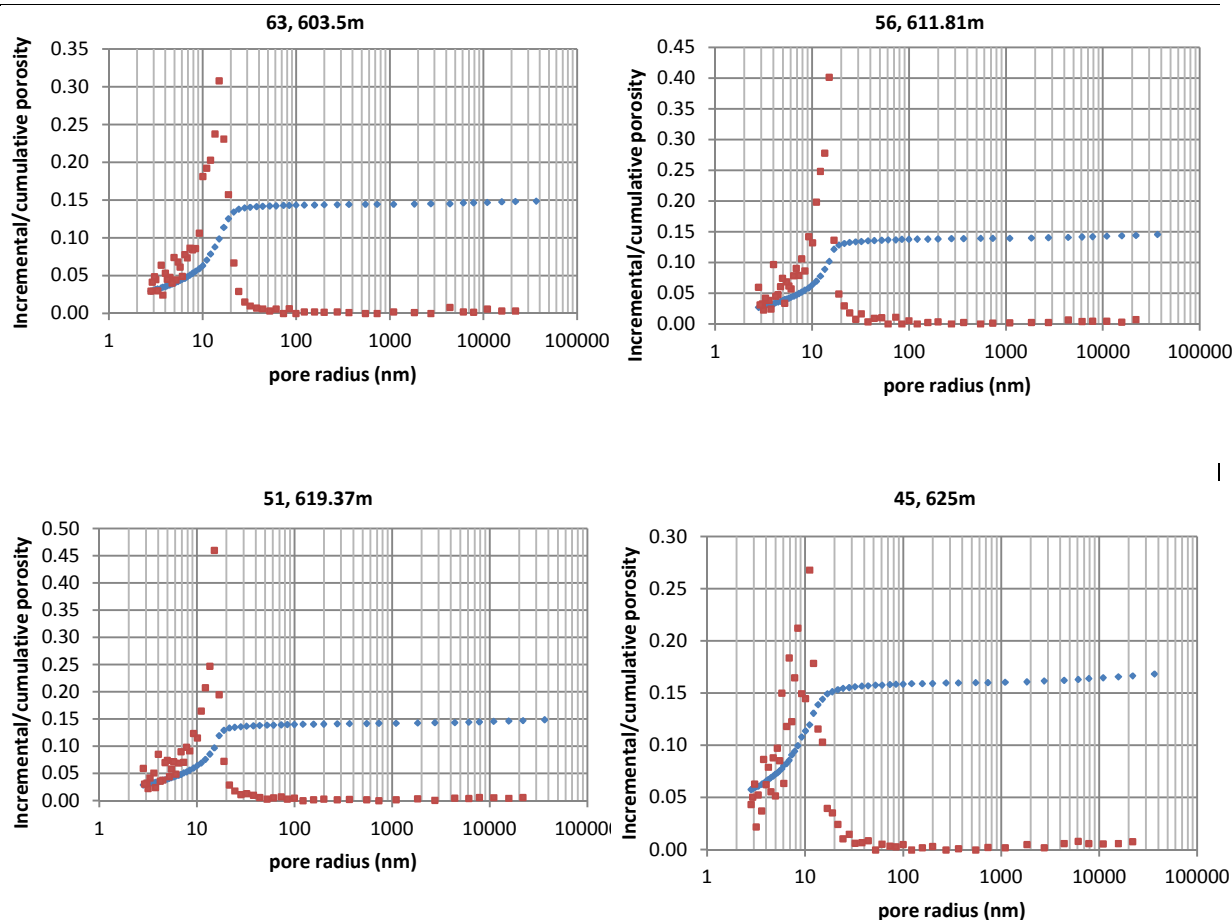


Figure 6.20: Pore size distribution plots at various depths within the Lower Carlile Member. All the samples are characterized by a unimodal PSD optimal gas adsorption (Javadpour et al., 2007)

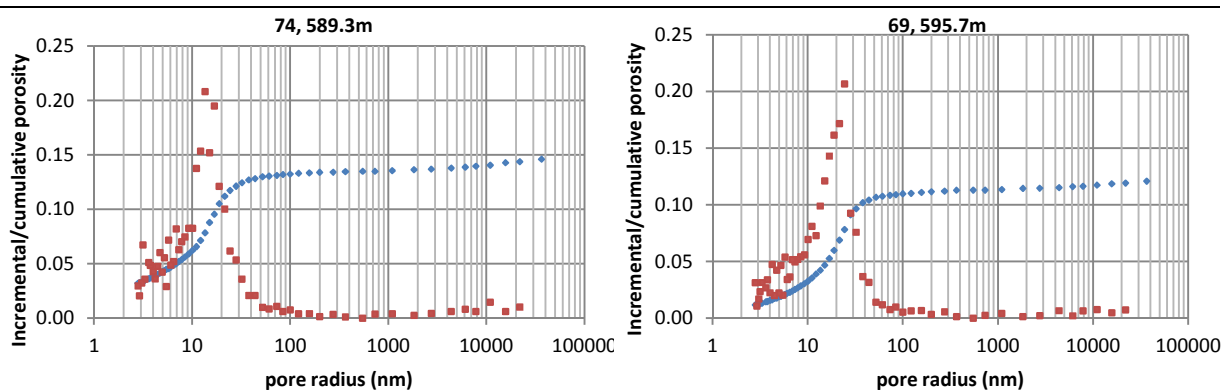


Figure 6.21: Pore size distribution plots at various depths within the Middle Carlile Member. All the samples are characterized by a unimodal PSD

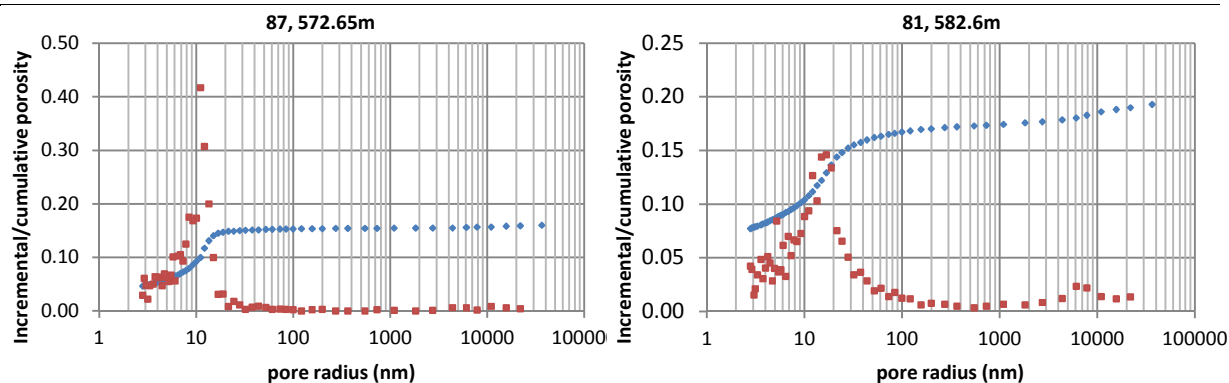


Figure 6.22: Pore size distribution plots at various depths within the Upper Carlile Member. All the samples are characterized by a unimodal PSD

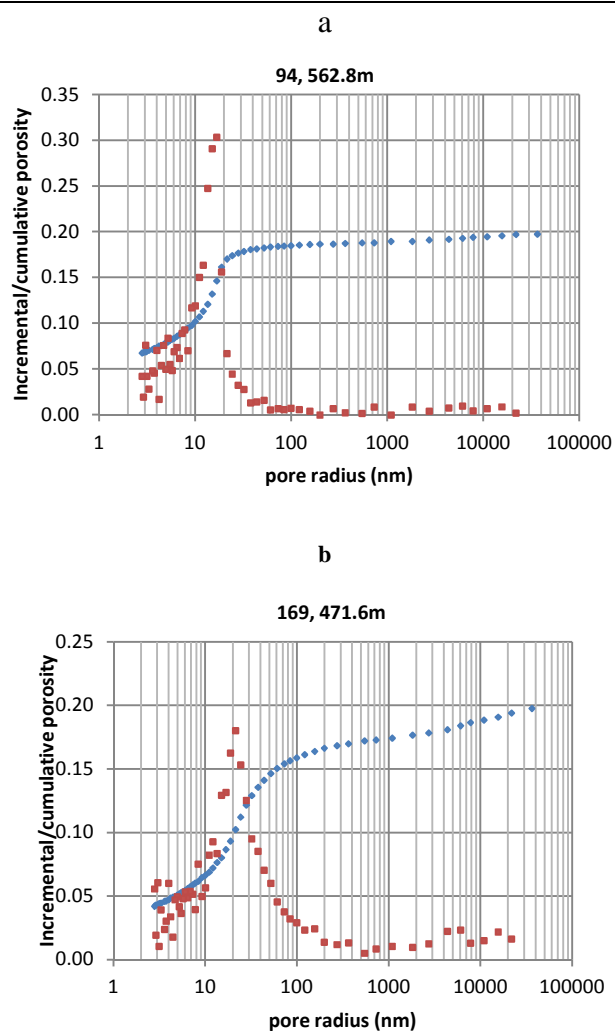


Figure 6.23: Pore size distribution plot of (a) sample at a depth of 562.8m within the Verger Member and (b) First White Specks at a depth of 471.6m, all characterized by a unimodal PSD

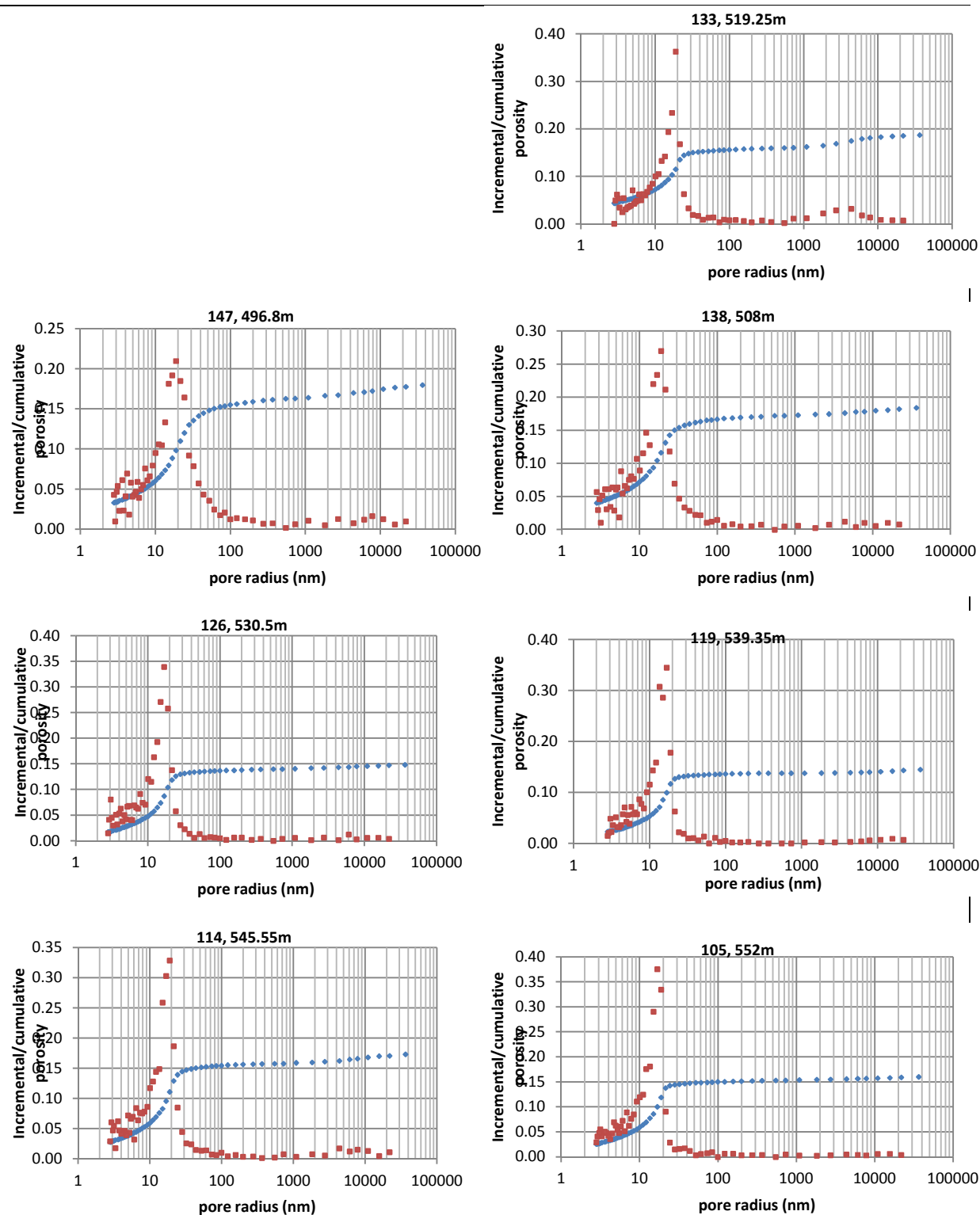


Figure 6.24: Pore size distribution plots at various depths within the Medicine Hat Formation. Only sample at depth of 519.25m exhibit bimodal PSD

6.6 Total Organic Carbon (TOC) distribution within the 12-19-013-28W3

A total of 48 samples covering the Belle Fourche to the First White Specks within 12-19-013-28W3 well were selected for TOC and Rock-Eval analyses. Details of procedures followed are described in chapter two. Appendix II shows the distribution of TOC within the upper Colorado group determined from LECO analysis, while figure 6.25 display TOC trends with relation to depth. Generally, TOC values within the Upper Colorado Group range from 0.77-7.06 wt. %, with an average of 2.67 wt. %. The top of the Belle Fourche Formation exhibits relatively high TOC values increasing from 2.22 to 4.40 wt. %. However, these values may not be representative of TOC values throughout the entire formation as only a small interval of the formation was sampled. The Second White Specks Formation contain variable TOC values throughout the interval, ranging between 1.87 wt. % and 7.06 wt. %. Apart from the fact that the lowest value is recorded at the top of the formation, there does not appear to be any clear trend within the entire formation.

The Lower Carlile member continues with the low TOC values initiated in the upper part of the Second White Specks. TOC values remain quite uniform throughout this interval, ranging between 1.49-1.68 wt. %. The upper part of the Lower Carlile member records the lowest TOC values recorded in the Upper Colorado Group dataset with values ranging between 0.77-1.08 wt.%. Slight upwards-decreasing trend in TOC values occur within the Middle Carlile member from 4.35-3.78 wt. %. The Upper Carlile member does not appear to show any TOC trend containing values that vary between 2.22-3.68 wt.%.

Verger Member TOC values show an upwards-decreasing trend, but this again may not be representative of the entire interval because only two data points were recorded with values of 2.20 wt.% and 1.49 wt.%. The Medicine Hat Member displays no apparent TOC trend; values throughout vary between 1.09-4.27 wt. %, but most samples have TOC values under 2.20 wt. %. Higher TOC peaks occur throughout the Medicine Hat Member with irregularity. The highest TOC is recorded at the top of the interval, perhaps corresponding to the transgressive surface that precludes First White Specks deposition. Relatively uniform TOC values are present within the First White Specks Member, with upwards-decreasing values between 3.47 wt. % and 1.10 wt. %.

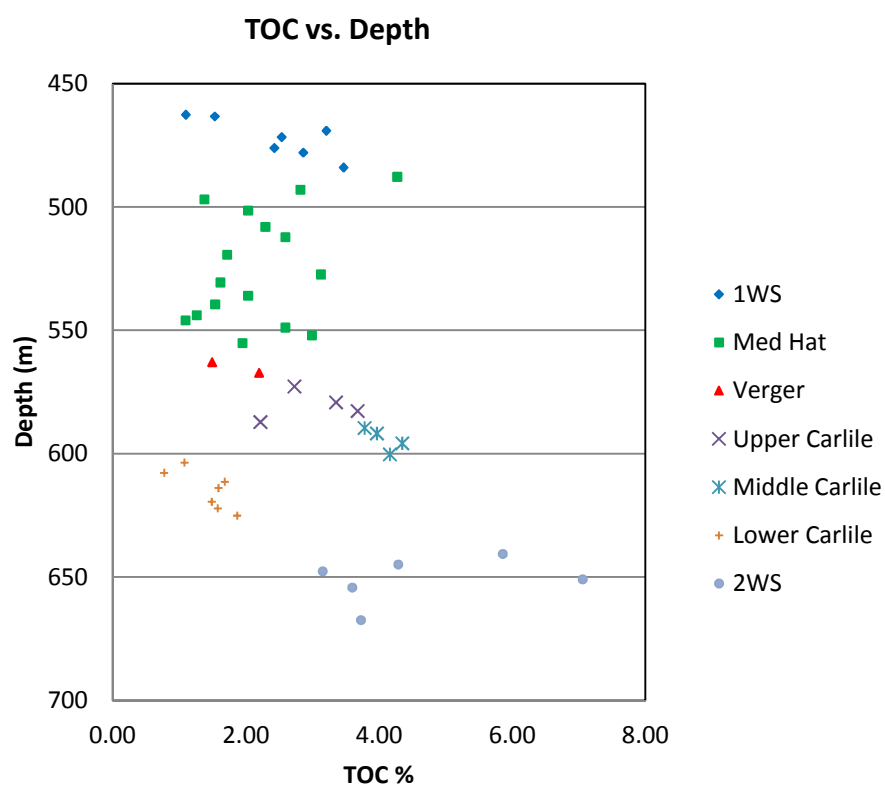
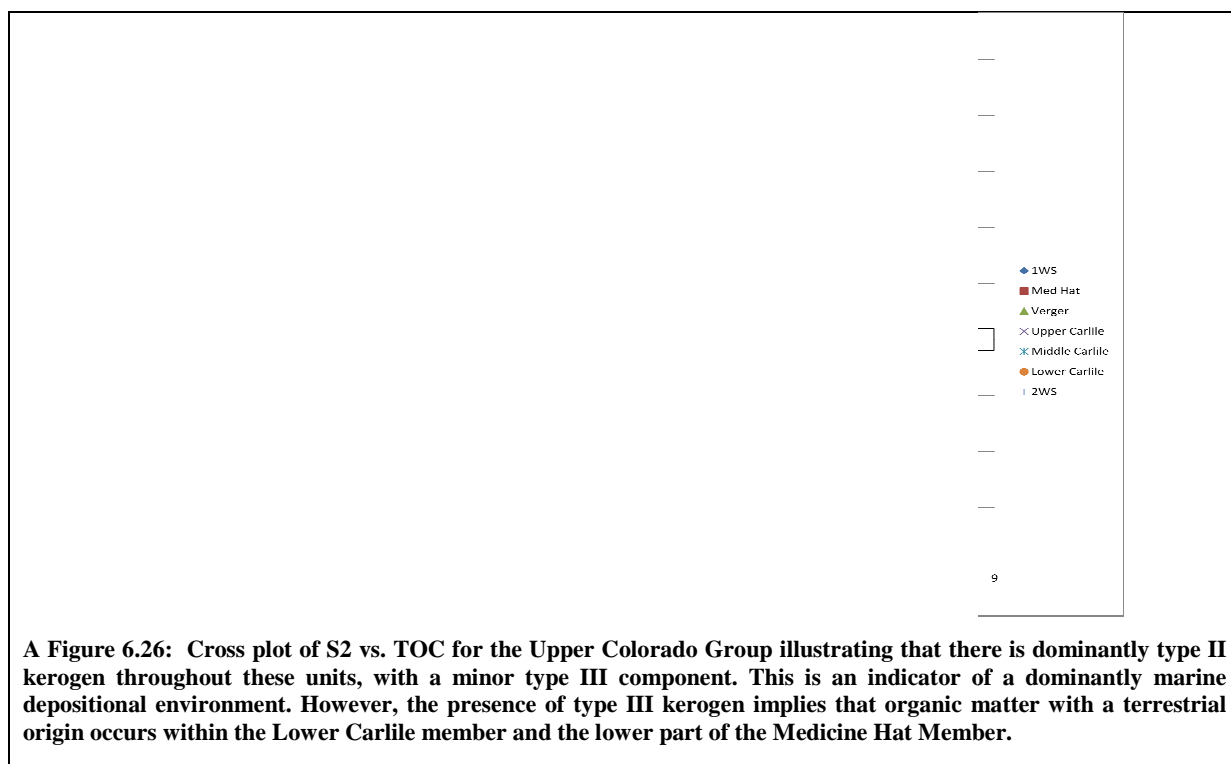


Figure 6.25: TOC variation in the Upper Colorado Group with depth



6.7 Rock-Eval Analyses of 12-19-013-28W3

Rock-Eval results are displayed in Table 6.5. Cross plot of S2 vs. TOC is shown in (Figure 6.26) indicating kerogen type for the Upper Colorado Group. There is dominantly type II kerogen throughout these units, with a minor type III component. This is an indicator of a dominantly marine depositional environment. However, the presence of type III kerogen implies that organic matter with a terrestrial origin occurs within the Lower Carlile member and the lower part of the Medicine Hat Member. It appears that the Second White Specks Formation and Lower Carlile member contain terrestrially influenced organic matter, as most samples from these shales contain only type III kerogen. The Middle Carlile member, Upper Carlile member, Verger Member, upper part of the Medicine Hat Member and First White Specks Member appear to contain mostly marine plant material, such as algae and bacteria. A mixture of type II and type III kerogen is observed in the Medicine Hat Member; Type II kerogen is present in samples from the lower half of the Medicine Hat Member, and type III kerogen is typically present in samples from the upper half of the Medicine Hat Member. Thus, terrestrial influence appears to be overall decreasing upwards through the Medicine Hat Member as grain size increases upwards.

Table 6.5 and figure 6.27 show Production index values within the Upper Colorado Group. Values range from 0.0638 to 0.6131. The majority of these values fall within a typical zone of oil generation ($PI = 0.1-0.4$; (Peters, 1986; Tissot and Welte, 1984), while few PI values even surpass the zone of oil generation ($PI = >0.4$).

Figure 6.27 and 6.28, show cross plots of production index with depth and maximum temperature values with production index for the Upper Colorado Group respectively. The Maximum temperatures (T_{max}) for the formations fall between 389.0 °C and 432.5 °C; and therefore generally immature. They fall below the oil zone threshold for a mixture of type II and type III kerogen (430°C-435°C; (Espitalie et al., 1985), and considerably below the oil zone thresholds for only type II kerogen or only type III kerogen (450°C-455°C and 465°C-470°C, respectively; (Espitalie et al., 1985). Every formation within the Upper Colorado Group is indicated to be thermally immature with regards to the oil window (Fig 6.28).

Table 6.5: Rock-Eval results for 12-19-13-28/W3

Depth (m)	Formation	S1 Avg.	S2 Avg.	TOC Avg.	Tmax Avg.	PI	HI
462.5	1WS	0.2	0.82	1.1	431	0.20	74.89
463.2	1WS	1.18	1.4	1.53	419.5	0.46	91.18
469	1WS	1.31	9.53	3.21	413.5	0.12	297.19
471.6	1WS	1.04	7.5	2.54	419.5	0.12	295.66
476	1WS	1.07	5.75	2.43	420	0.16	237.11
477.9	1WS	1.46	8.56	2.86	416	0.15	299.13
483.9	1WS	1.64	12.53	3.47	416	0.12	361.47
487.7	Med Hat	1.64	17.77	4.27	411.5	0.08	416.04
492.9	Med Hat	1.79	10.41	2.82	413	0.15	369.63
496.8	Med Hat	3.78	2.39	1.38	417	0.61	173.45
501.4	Med Hat	2.97	4.53	2.03	415	0.40	223.15
508	Med Hat	1.71	5.63	2.29	417.5	0.23	245.85
512.15	Med Hat	1.37	6.66	2.59	411.5	0.17	257.14
519.25	Med Hat	1.11	4.38	1.72	420	0.20	255.1
527.26	Med Hat	1.07	8.6	3.13	415.5	0.11	275.2
530.5	Med Hat	0.45	1.98	1.62	423	0.19	122.29
535.9	Med Hat	1.13	4.08	2.03	421	0.22	200.99
539.35	Med Hat	0.98	3.19	1.54	419	0.24	207.82
543.75	Med Hat	0.59	1.55	1.26	425.5	0.27	123.02
545.85	Med Hat	0.79	1.17	1.09	421	0.40	107.34
548.8	Med Hat	0.56	4.45	2.59	389	0.11	171.62
552	Med Hat	1.26	11.33	2.99	416	0.10	378.93
555.1	Med Hat	1.03	3.94	1.95	427	0.21	202.31
562.8	Verger	1.13	1.9	1.49	432.5	0.37	127.52
567.1	Verger	0.91	5.52	2.2	430	0.14	251.48
572.65	Upper	1.03	8.33	2.73	420	0.11	305.69
579.1	Upper	1.21	9.32	3.35	423	0.11	278.21
582.6	Upper	1.22	12.37	3.68	415.5	0.09	336.46
587.1	Upper	0.49	7.12	2.22	418.5	0.06	321.22
589.5	Middle	1.6	14.44	3.78	412	0.10	382.01
591.7	Middle	1.45	12.38	3.97	404	0.10	312.11
595.7	Middle	1.27	11.3	4.35	402	0.10	259.95
600.2	Middle	1.23	11.31	4.16	403	0.10	271.75
603.5	Lower	0.64	0.85	1.08	417	0.43	79.07
607.65	Lower	0.44	0.49	0.77	419	0.47	62.99
611.31	Lower	1.26	2.61	1.68	421	0.33	155.06
613.82	Lower	0.67	2.01	1.59	425	0.25	126.81
619.37	Lower	0.72	1.68	1.49	425.5	0.30	112.79
622.08	Lower	1.07	2	1.58	426	0.35	126.98
625	2WS	0.77	2.5	1.87	423	0.24	133.78
640.52	2WS	0.78	9.01	5.86	390	0.08	153.8
644.8	2WS	1.5	13.85	4.29	412.5	0.10	323.1
647.57	2WS	1.51	12.13	3.15	418.5	0.11	384.92
650.81	2WS	1.3	16.83	7.06	412.5	0.07	238.55
654.14	2WS	1.09	6.55	3.6	402.5	0.14	182.06
667.34	2WS	0.89	7.13	3.73	414.5	0.11	191.28
670.26	Belle	2.01	15.01	4.4	413	0.12	341.02
673.8	Belle	0.48	5.35	2.27	430.5	0.08	236.2
677.12	Belle	0.47	5.13	2.22	431.5	0.08	230.86

As the Upper Colorado Group is locally immature, it appears that Rock-Eval data from well 12-19-013-28W3 displays abnormally high production index (PI) values for an immature source rock. Production index values are mainly above 0.1, in the range typically seen within mature marine shales within the oil window (Tissot and Welte, 1984). Uncontaminated, immature source rock has characteristic production index values of less than 0.1; if PI values are higher, it is likely that mature hydrocarbons have migrated from another stratigraphic unit, or that the immature rock has been contaminated by oil-based drilling fluids (Tissot and Welte, 1984; Bloch et al. 1999). Therefore, it is likely that all formations within the Upper Colorado Group contain migrated hydrocarbons from a mature source rock, or that these mudstones have been contaminated by drilling fluids.

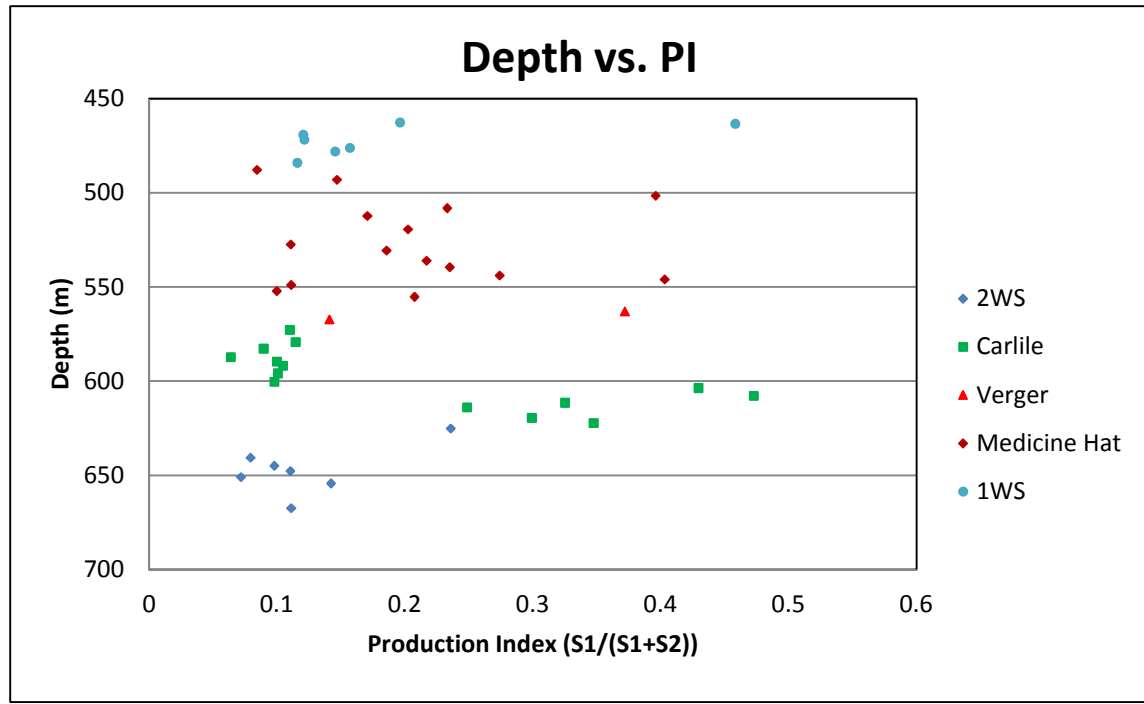


Figure 6.27: Plot of Depth vs. PI for the Upper Colorado Group

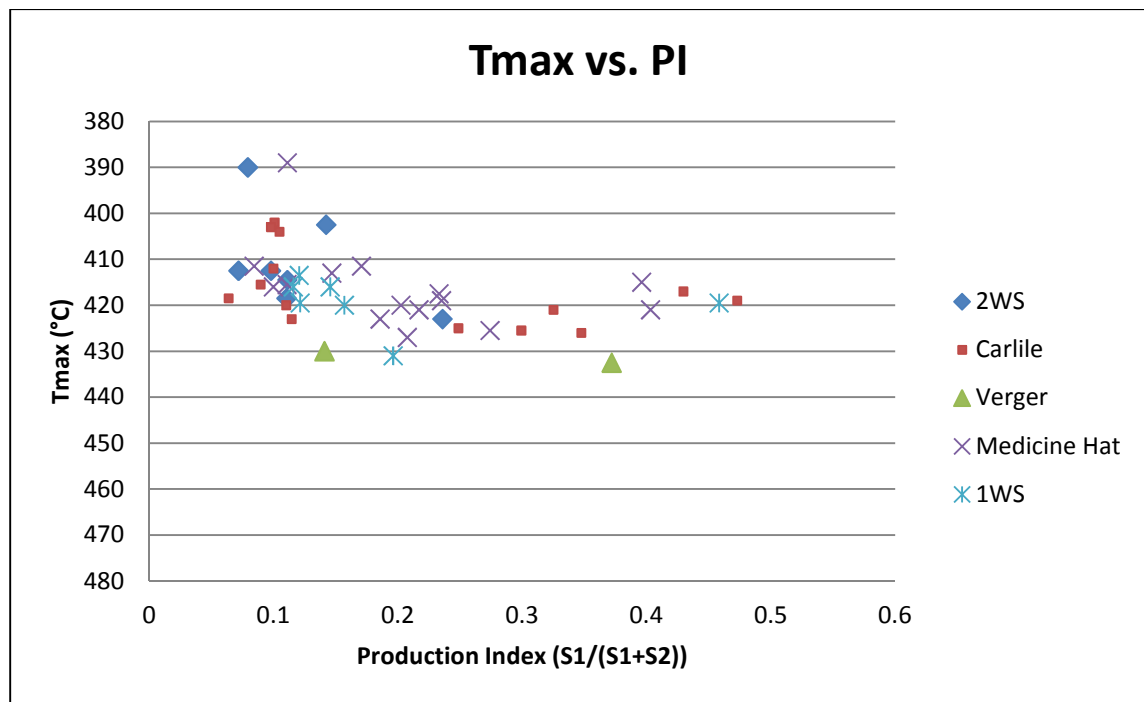


Figure 6.28: Plot of Tmax vs. PI for the Upper Colorado Group.

6.8 Shale gas reservoir properties of the Upper Colorado Group

Shallow gas of biogenic (microbial) origin in Upper Cretaceous reservoirs has been previously reported to form an important source of produced natural gas in Saskatchewan and Alberta, Canada and Montana, USA (Ridgley, 2002; Rice and Spencer, 1996; Rice and Claypool, 1981). Recent studies by Shurr and Ridgley (2002) have also demonstrated that early-generation biogenic gas is dominant within the Cretaceous Colorado Group rocks throughout eastern Alberta and Saskatchewan. Source beds in such reservoirs are typified by their fine-grained nature, low porosity and low permeability (Shurr and Ridgley, 2002). Maturity (T_{max}) generally increases westward across the Western Canadian Sedimentary Basin, which should correspond with increasing thermogenic gas content (Bloch, 1995)

TOC values within the Upper Colorado Group range from 0.77-7.06 wt. %, with an overall average of 2.67 wt.%, and therefore, can be considered as having good source rock potential (Tissot and Welte, 1984). Average TOC values of members and formations within the Upper Colorado Group in this study range from 1.37-4.22 wt.%. TOC values are consistently highest within the Middle and Upper Carlile members; but values here are fairly variable. All the formations appear to be thermally immature with respect to the oil window. Maximum temperatures for the Upper Colorado range between 389.0 °C and 432.5 °C which is below the T_{max} value of 435°C generally considered as the onset of oil generation (Tissot and Welte, 1984). However, production index values throughout the Upper Colorado Group are quite high, ranging from 0.06 to 0.61. The zone of oil generation is generally defined by PI values of between 0.1 – 0.4, while immature samples are defined by PI values of <1 (Tissot and Welte, 1984). As values over 0.1 are not typical for immature source rocks, it is probable that the Upper Colorado Group contains migrated hydrocarbons from a mature source rock or has been contaminated by oil-based mud.

The Upper Colorado Group contains dominantly type II kerogen, with minor amounts of type III kerogen. This mixture of kerogen types suggests that the Upper Colorado Group was generally deposited in a marine depositional setting with occasional higher terrestrial influence. Type III kerogen is present within the Lower Carlile member and towards the base of the Medicine Hat Member. The occasional input of type III kerogen means that higher plant materials have been incorporated into the Upper Colorado shales and/or there were periods of oxidizing marine conditions that degraded marine organic matter.

This indicates that relatively high amounts of terrigenous (Type III) organic matter within the Lower Carlile member and lower part of the Medicine Hat Member may affect their capacities for biogenic gas potentials (methanogenesis). It is shown that anaerobic bacteria will preferentially consume particular organic compounds in a certain order during the early stages of diagenesis. Organic matter sourced from marine environments will be preferentially biodegraded first, and terrestrial organic matter is generally biodegraded at a relatively later time (Tissot and Welte, 1984). Therefore, methanogen-producing anaerobic bacteria will target shales that are rich in kerogen type II before shales that are rich in kerogen type III. Increased terrestrial input (type III content) observed within the Lower Carlile member or lower part of the Medicine Hat Member is likely to reduce the capacity of these sediments to be methanogenic gas producers. In contrast, shales within the Middle or Upper Carlile Member or upper part of the Medicine Hat Member would likely contain the most desirable organic matter types for biodegradation and methanogenesis.

The Rock-Eval pyrolysis data from the well in this study is consistent with data reported by Shurr and Ridgley, (2002) who show that the Upper Colorado Group source rocks have total organic carbon (TOC) values up to 4% and hydrogen index (HI) values up to 420 mg hydrocarbon/g TOC. The low HI values (89 to 152 mg hydrocarbons/g TOC) for the Niobrara/Medicine Hat are consistent with the unit containing predominantly terrestrial organic matter (Shurr and Ridgley, 2002). Similarly, Nielsen et al. (2003) reported source rock geochemistry characteristics for each formation unit within the Colorado Group (Table 6.6) with present TOC levels above 1% in all mudstones.

Table 6.6: Source rock geochemistry of the Upper Colorado Group (Nielsen et al., 2003).

Formation	Member	TOC (%)	HI (mg/g)	Tmax (°C)	Kerogen Type
SWS FM		5.1	200		
Carlile FM	Lower	2.1	74	446	III
	Middle	1.4	42.4	454	III
	Upper	1.5	58	440	
Niobrara FM	Verger	1.5-1.9		420	II-III
	Medicine Hat	1.2-1.5			
	1st WS	1.72	283	410-431	

Previous studies have also demonstrated that shales within the Colorado Group typically have poor reservoir properties, due to the abundance of clay minerals and readily compactable matrix-supported fabrics (Bloch et al.1999). Abundant clay minerals increase fluid sensitivity hindering drilling, completion and production. Clay and mud within the Upper Colorado Group are also effective cements, which can create laterally extensive impermeable barriers and reduce permeability within the mudstones. However, there is long production history of biogenic gas from the sandstone units within the Medicine Hat Member signifying that some intervals within the Upper Colorado Group possess better shale gas reservoir properties than others; which is also likely true of finer-grained mudstone intervals. It is not only lateral variations that control the location of gas production ‘sweet spots’, as mudstones within the same stratigraphic unit could produce commercial shale gas simultaneously, and this could give the appearance of lateral ‘sweet spots’ (Shurr and Ridgley, 2002). Lateral facies changes could produce similar shale gas production patterns (Shurr, 2002). Therefore, it is not unusual for a single shale unit to have commercial gas production in some localities, but have no gas production in nearby locations

The Upper Colorado Group within the Bigstick Field has experienced relatively shallow burial depth and low maximum temperatures, which has resulted in an immature, unlithified source rock. Shallow biogenic shale gas reservoir properties of formations and members within the Upper Colorado Group are shown in Table 6.7. Mudstones within all formations and members display moderate to high fluid sensitivity, have poor fraccability and contain clay and mud cements, but the Carlile Formation and Verger Member do not contain calcareous cements. This implies that while the Carlile Formation and Verger Member may

be more difficult to fracture than the Medicine Hat Member, for instance, comprised of relatively softer sediments, the Carlile Formation and Verger Member also appear to have the highest sorption capacity. All samples within the Carlile Formation and Verger Member display unimodal porosity, which maximizes the grain surface area for gas adhesion (Javadpour et al. 2007).

TOC content and kerogen type will also affect shale gas reservoir qualities. Within a biogenic shale gas reservoir, organic matter is targeted by anaerobic bacteria and converted to methane gas during methanogenesis. Rocks with high organic matter content have a greater capacity for methane gas generation, as there is more organic matter to be converted to gas. Therefore, rocks with consistently moderate or high percentages of total organic carbon would be the most favorable gas target over rocks with highly variable total organic carbon content. The Middle and Upper Carlile members contain the most ideal total organic content ranging from 3.78-4.35 wt. % and 2.22-3.68 wt. %., respectively. Both of these members appear to contain only type II kerogen, which is sourced from bacterial, planktonic and marine plant remains, and which is ideal for methanogenesis, as anaerobic bacteria preferentially degrade marine organic matter prior to terrestrially sourced organic matter.

Table 6.7: shale gas reservoir properties of formations and members within the Upper Colorado Group.

Fm./Mbr.	Fluid Sensitivity	Fracca-bility	Mud/Clay Cements	Calcareous Cements	Sorption Capacity	TOC (wt.%)	Kerogen
1 st White Specks	Mod./High	Poor	Yes	Yes	Low -Mod.	1.10-3.47	Dominant type III
Medicine Hat	Mod./High	Poor	Yes	Yes	Mod.-High	1.09-4.27	Type II/III
Verger	Mod./High	Poor	Yes	No	High	1.49-2.20	Type II/III
Upper Carlile	Mod./High	Poor	Yes	No	High	2.22-3.68	Type II
Middle Carlile	Mod./High	Poor	Yes	No	High	3.78-4.35	Type II
Lower Carlile	Mod./High	Poor	Yes	No	High	0.77-1.68	Dominant type III
2 nd White Specks	Mod./High	Poor	Yes	Yes	Mod. - High	1.87-7.06	Type II/III

The Middle Carlile member is likely the best shale gas target within the Upper Colorado Group. As the Middle Carlile member has a high potential for gas adsorption, it is possible that horizontal drilling within this interval may make the muddy siltstone a viable gas target. Another possible shale gas target within the Upper Colorado Group, based on the properties in Table, is within the lower part of the Medicine Hat Member. This interval appears to be less calcareous cemented than towards the top of the Medicine Hat Member, and contains more clay-sized sediments based. These qualities imply that the lower part of the Medicine Hat Member has a higher sorption capacity than the upper part of the Medicine Hat Member, and also indicate that the interval may contain enough calcareous sediment to increase the strength of the rock, making it more fraccable. However, the lower part of the Medicine Hat Member also contains dominantly type III kerogen, as opposed to the upper Medicine Hat Member, which contains dominantly type II kerogen. Moderate TOC values towards the base of the Medicine Hat Member (1.95-2.99 wt.%) and intervals of moderate bioturbation, in combination with the lower Medicine Hat Member's aforementioned qualities, may serve to make this interval a viable shale gas target.

6.9 Summary

- 1) The Upper Colorado Group has moderate to excellent source rock potential within the study area (12-19-013-28W3) with TOC values ranging from 0.77-7.06 wt.%, and general average of 2.67 wt.% which is above the minimum TOC guideline of 0.5 wt.% to determine economic natural gas generation (Tissot and Welte 1984).
- 2) A bivariate plot of kerogen types shows that the Upper Colorado Group contains an abundance of type II kerogen, with a lesser presence of type III kerogen. These kerogen types are indicative of a dominantly open-marine environment, with minor terrestrial input. A slightly greater appearance of type III kerogen within the Medicine Hat and Lower Carlile Members likely signifies a somewhat higher input of terrestrial organic matter (i.e. woody material, land plants). The slight difference in kerogen types indicates that different organic material ratios likely comprise the total organic carbon in the Upper Colorado.
- 3) It appears that the Middle Carlile member, Upper Carlile member, Verger Member, upper part of the Medicine Hat Member and First White Specks Member would be optimal for methanogenesis because they contain mostly Type II kerogen derived from marine plant material, such as algae and bacteria. Biogenic gas potential is likely to be less within the Second White Specks Formation and Lower Carlile member as they contain mostly terrestrially influenced organic matter (type III kerogen).
- 4) The Upper Colorado Group is immature, within the study area (12-19-013-28W3). Tmax for the formations fall between 389 °C and 432°C; it therefore appears that Rock-Eval data displays abnormally high production index (PI > 0.1) values for an immature source rock. This suggests that the shales either contain migrated hydrocarbons or have been contaminated with oil-based drilling mud.

- 5) All samples taken for laser grain size analysis from well 12-19-013-28W3 showed that the Upper Colorado Group is comprised almost entirely of clay-sized and silt-sized grains.
- 6) Total porosity values within the Upper Colorado Group range from 7.4-19.7%, with samples largely displaying tight pore size distribution (10-20nm), and unimodal pore size distribution due to the dominance of clay sized sediments. Unimodal porosity distribution dominated by clay size sediments is ideal for gas adsorption, as it provides maximum sediment surface area for the adhesion of gas molecules (Javadpour et al. 2007). The Carlile Formation appears to contain only unimodal porosity, and it is possible that this interval has the highest sorption capacity within the Upper Colorado Group. Permeability values obtained using mercury injection techniques range from 3-151 nD, with an average of 14.4 nD.
- 7) The Middle Carlile member is likely the best shale gas target within the Upper Colorado Group. As the Middle Carlile member has a high potential for gas adsorption, it is possible that horizontal drilling within this interval may make the muddy siltstone a viable gas target

7 CHAPTER SEVEN: CONCLUSIONS & FUTURE WORK

7.1 GENERAL CONCLUSIONS

The Colorado Group mudstone's shale gas characteristics have been studied utilising a range of techniques including mineralogy, grain size distributions, thin section analysis, pore size distributions, permeability and porosity calculations and organic matter content.

The use of Attenuated Total Reflectance Fourier Transform Infrared Spectroscopy (ATR-FTIR) has been tested as a method to rapidly quantify the mineralogy of mg quantities of shales. Multivariate statistical models based on Partial Least Squares (PLS) was applied to the mid-infrared attenuated total reflectance spectra (ATR) in order to provide a rapid chemometric method to generate a semi-quantitative mineralogy. Calibrations were constructed using (a) pure minerals, (b) natural shales and (c) natural shales which were amended with pure minerals, to give a broader compositional spectrum. Quartz, total clay and total carbonate can generally be estimated to within 5% absolute of true value. Predictions of the abundance of individual clays (kaolinite, chlorite, illite-smectite) are less good but are usable for some applications, where relative abundance is sufficient. Calcite and dolomite are difficult to separate by ATR. Given the different grain densities of calcite and dolomite, this is relevant for porosity estimates from density logs. DRIFTS spectra for carbonates contain more spectra features (peaks) than ATR spectra so that calcite and dolomite are more likely to be separated by DRIFTS. Calibration is absolutely critical to achieve accurate results. This work suggests that semi-artificial shales rather than pure minerals may be the best calibrants, but the use of models in new strata must be undertaken with care. As the range of minerals increases, quantification is more difficult. 30-50 samples per day can be analysed. Given its rapidity, ATR-FTIR spectroscopy allows high sample throughput and thus high density sampling strategies, for example: ultra-high resolution single well studies, multi-well studies. Therefore, this study shows that ATR technique has great potentials for quantitative mineralogy.

Analysis of the lower Colorado Group (Albian to Turonian) show that the depositional system is complex with widely changing seaway conditions reflected in the geochemistry and thin sections (fabrics) of the sediments without affecting the mineralogy significantly. These changes are likely the result of fluctuations in relative sea level and in the connectivity of the

seaway with the Boreal and Tethys seas (Leckie et al. 2008; Schröder-Adams et al. 1996). Clay clasts were identified within the Second White Specks Formation in thin section. The presence of clay clasts is significant, as it indicates the advective deposition of fine-grained sediments in this widely varying paleodepositional setting. It is likely that the clay clasts are rip-up clasts that were generated during high-energy storm events.

All the formations within the lower Colorado Group display moderate to excellent source rock potential with TOC values consistently > 2wt.%. However, the formations are dominated by clay sized grains, low porosities and permeabilities making them poor shale gas reservoir. The Belle Fourche and Second White specks contained intervals with silt-sized grains and increased porosities that can act as 'sweet spots'.

Authigenic cements and clay-sized grains as well as siltstone laminations are observed throughout the Upper Colorado Group; whereas calcareous cements are present only within the Medicine Hat Member and First White Specks Member. Calcite overgrowths are also observed within mudstones in the basal part of the Medicine Hat Member. This may influence the reservoir property as shale gas plays with significant recrystallised carbonate are more brittle and responds well to stimulations (Passey et al. 2010), although they are also likely to fill in pores and reduce the porosity and thus the storage sites for free gas in the reservoir. The presence of sands/siltstone laminae is indicative of dominantly advective transport of sediments within the study area. It is probable that the clay-sized and mud-sized sediments were transported as sand-sized floccules, held together by Van der Waals forces within a bottom boundary current, in a manner analogous to sand transport (Schieber and Southard, 2009).

The Upper Colorado Group within the Bigstick Field has experienced relatively shallow burial depth, which has resulted in an unlithified source rock. Mudstones within all formations and members display moderate to high clay and mud cements, this implies that the Upper Colorado Group comprised of relatively softer sediments that are not suitable for fracture stimulation. High clay content is likely to contribute to the adsorption capacities of the shales due to increased micropores suitable for gas adsorption (Ross and Bustin, 2008).

The Middle Carlile member is likely the best shale gas target within the Upper Colorado Group in the study area. This unit does not contain any calcareous cement, is believed to have a high sorption capacity due high clay fractions, contains only type II kerogen, and has consistently high TOC values throughout. The lower part of the Medicine Hat Member is also a possible shale gas target, as mudstones within this interval have relatively high clay size sediments and thus high sorption capacity, contains consistently moderate to high TOC values throughout, and contains minor calcareous cements. Calcareous cements should not significantly impede porosity or permeability within the mudstone, but will likely strengthen the rock and increase its brittle behaviour.

7.2 FUTURE WORK

The application of Attenuated Total Reflectance Fourier Transform Infrared spectroscopy in this study has shown good potential for rapid semi-quantitative mineralogy for high data resolution building and routine studies. However, TOC is another important parameter that must be quantified routinely. Previous studies (Leach et al. 2008) has shown that TOC can be estimated rapidly using Near Infrared Spectroscopy. Future studies should consider the feasibility of combining Mid-infrared (for minerals) and Near Infrared (TOC) for estimating the major minerals and TOC content of shales using a single calibration. It is also proposed that the FTIR spectroscopy can be used to build a Mineralogy Log which can then be calibrated against major downhole wireline log data to investigate field characteristics.

The techniques utilised to characterise the Colorado Group in this study did not consider the potential gas capacity of the shales. Potential gas capacity is a very important parameter for a shale gas characterisation (Ross and Bustin, 2008). The high TOC content (>1.5 wt. %) of the Colorado Group might provide micropores for maximum methane adsorption. Organic matter is microporous, with a large internal surface area favouring the storage of significant amount of gas (Ross and Bustin, 2008). Therefore, adsorption analysis is necessary for the Colorado Group shales in order to identify the maximum amount of gas the shales sample can hold.

Geochemical techniques used in this study suggest that the Upper Colorado Group contains a mixture of kerogen types and general deposition in a marine depositional setting with occasional higher terrestrial influence. However, additional geochemical analyses (GC and GCMS) are required to support this. C_{28}/C_{29} sterane values can be used as an indicator of land plant materials, as terrestrial hydrocarbons are often enriched in C_{28} steranes (Grantham and Wakefield, 1988), and thus, terrestrially influenced shales should have a high C_{28}/C_{29} sterane ratio. Similarly, a ratio of sterane/pentacyclic terpanes (St/PT) can also be used as an indicator for organic input, as terrestrially derived organic matter contains relatively high amounts of pentacyclic terpanes (DeGrande et al. 1993).

7.3 REFERENCES

- Aplin, A. C. and Macquaker, J. H. (2012) 'Getting Started in Shales', *AAPG/Datapages - Getting Started Series*, 95 (12), pp. 2031-2059.
- Aplin, A. C., Matenaar, I. F., McCarty, D. K. and Pluijm, B. A. v. d. (2006) 'Influence of mechanical compaction and clay mineral diagenesis on the microfabric and pore-scale properties of deep-water Gulf of Mexico mudstones', *Clays and Clay Minerals*, 54, pp. 500-514.
- Beebe, K. R. and Kowalski, B. R. (1987) 'An introduction to multivariate calibration and analysis', *Anal. Chem.*, 59, pp. 1007-1017A.
- Beuselinck, G. G., Poesen, J., Daguier, G. and Froyen, L. (1998) 'Grain-size analysis by laser diffractometry - comparison with the sieve-pipette method ', *Catena*, 32, (3-4), pp. 193-208.
- Bhargava, S., Awaja, F. and Subasinghe, N. D. (2005) 'Characterisation of some Australian oil shale using thermal, X-ray and IR techniques', *Fuel*, 84, (6), pp. 707-715.
- Bhattacharya, J. P. and R.G. Walker. (1991) 'River- and wave-dominated depositional systems of the Upper Cretaceous Dunvegan Formation, northwest Alberta', *Bulletin of Canadian Petroleum Geology*, 39, pp. 69-191.
- Bjorsvik, H. R. and Martens, H. (2000) *Data analysis: calibration of NIR instruments by PLS regression.*: In Burns, D.A., Ciurczak, E.W. (Eds.), Dekker, Newyork.
- Bloch, J. (1995) 'Source rock potential and reservoir characteristics of the lower Colorado (Albian-Turonian) Colorado Group, Western Canada Sedimentary Basin', *Geological Survey of Canada Open File Report*, 3036, pp. 71p.
- Bloch, J., Schröder-Adams, C. J., Leckie, D. A., Craig, J. and McIntyre, D. J. (1999) 'Sedimentology, micropaleontology, geochemistry, and hydrocarbon potential of shale from the Cretaceous Lower Colorado Group in Western Canada', *Geological Survey of Canada Bulletin*, 531, (185p).
- Bloch, J., Schröder-Adams, C. J., Leckie, D. A., McIntyre, D. J., Craig, J. and Staniland, M. (1993) 'Revised stratigraphy of the lower Colorado Group (Albian-Turonian), Western Canada ', *Bulletin of Canadian Petroleum Geology*, 41, pp. 325-348.
- Bohacs, K. M., Grabowski, G.J., Carroll, A.R., Mankiewicz, P.J., Kimberlee, J. M.-G., Jon.R. S., Wenger, M.B., and Simo, J.A. (2005) 'Production, destruction, and dilution—the many paths to source-rock development: in Harris, N.B., editor, The Deposition Of Organic-Carbon-Rich Sediments: Models, Mechanisms, And Consequences: ' *Society for Sedimentary Geology Special Publication*, No. 82, pp. 61–101.

- Breen, C., Clegg, F., Herron, M. M., Hild, G. P., Hillier, S., Hughes, T. L., Jones, T. G. J., Matteson, A. and Yarwood, J. (2008) 'Bulk mineralogical characterisation of oilfield reservoir rocks and sandstones using Diffuse Reflectance Infrared Fourier Transform Spectroscopy and Partial Least Squares analysis', *Journal of Petroleum Science and Engineering*, 60, (1), pp. 1-17.
- Breen, C., Illés, J., Yarwood, J. and Skuse, D. R. (2007) 'Variable temperature diffuse reflectance infrared Fourier transform spectroscopic investigation of the effect of ball milling on the water sorbed to kaolin', *Vibrational Spectroscopy*, 43, (2), pp. 366-379.
- Buckley, L. (2004) *Organic Facies of the Cretaceous Colorado Group, Western Canada Sedimentary Basin*. Thesis thesis. Newcastle University.
- Buckley, L. and Tyson, R. V. (2003) 'Organic Facies Analysis of the Cretaceous Lower and Basal Colorado Group (Cretaceous), Western Canada Sedimentary Basin - A preliminary Report in; summary of investigations', *Saskatchewan Geological Survey, Saskatchewan Industry Resources, Miscellaneous Report*, 1, (A-10), pp. 13.
- Bustin, R. M., Bustin, A., Ross, D., Chalmers, G., Murthy, V., Laxmi, C. and Cui, X. (2008) *Search and Discovery Articles #40382 at AAPG Annual Convention*. San Antonio, Texas, April 20-23.
- Caldwell, W. G. E. (1984) 'Early Cretaceous transgressions and regressions in the southern Interior Plains. In: The Mesozoic of Middle North America. Stott, D.F. and D.J. Glass (eds.)', *Canadian Society of Petroleum Geologists Memoir* 9, pp. 173-203.
- Canfield, D. E. and Raiswell, R. (1991a) 'Carbonate precipitation and dissolution. Its relevance to fossil preservation, in P. A. Allison, and D. E. G. Briggs, eds., Taphonomy: releasing the data locked in the fossil record. ', *Topics in Geobiology*, 9, pp. 411-453.
- Canfield, D. E., Thamdrup, B. and Hansen, J. W. (1993) 'The anaerobic degradation of organic-matter in Danish coastal sediments - iron reduction, manganese reduction, and sulfate reduction', *Geochimica et Cosmochimica Acta*, 57, pp. 3867-3883.
- Clark, R. N. (1999) *Spectroscopy of Rocks and Minerals, and Principles of Spectroscopy*. New York: John Wiley & Sons, Inc.
- Claypool, G. E. and Kaplan, I. R. (1974) 'The origin and distribution of methane in marine sediments', in *I. R. Kaplan, ed., Natural gas in marine sediments*. New York: Plenum Press, pp. 97-138.
- Coakley, J. P. and Syvitski, J. P. M. (1991) 'Sedigraph techniques. ', in J.P.M, S.(ed), *Principles, Methods, & Application of Particle Size Analysis*. In. New York: Cambridge University Press, pp. 129 - 142.
- Cranganu, C., Villa, M. A., Saramet, M. and Zakharova, N. (2009) 'Petrophysical Characterisation of Source and Reservoir Rocks in the Histria Basin, Western Black Sea', *Journal of Petroleum Geology*, 32, (4), pp. 357-372.

- Cronauer, D. C. (1982) 'Characterisation of oil shale by FTIR spectroscopy', *American Chemical Society Division of Fuel*, pp. 122-130.
- Crowley, J. K. and Vergo, N. (1988) 'Near-Infrared Reflectance Spectra of Mixtures of Kaolin-Group Minerals: Use in Clay Mineral Studies', *Clays and Clay Minerals*, 36, pp. 233-249.
- Curran, K. J., Hill, P. S., Schell, T. M., Milligan, T. G. and Piper, a. D. J. W. (2004) 'Inferring the mass fraction of flocc-deposited mud: application to fine-grained turbidites', *Sedimentology*, 51, pp. 927-944.
- Curtis, J. B. (2002) 'Fractured Shale-Gas Systems', *AAPG Bulletin* 86, (11), pp. 1921-1938.
- De Grande, S. M., Aquino Neto, F. R. and Mello, M. R. (1993) 'Extended tricyclic terpanes in sediments and petroleum', *Organic Geochemistry*, 20, (7), pp. 1039-1047.
- Dewhurst, D. N., Aplin, A. C., Sarda, J.-P. and Yang, Y. (1998) 'Compaction-driven evolution of porosity & permeability in natural mudstones: An experimental study', *Journal of Geophysical Research*, 103, (B1), pp. 651-661.
- Dewhurst, D. N., Aplin, A. C. and Sarda, J. P. (1999a) 'Influence of clay fraction on pore-scale properties and hydraulic conductivity of experimentally compacted mudstones', *Journal of Geophysical Research-Solid Earth*, 104, pp. 29261-29274.
- British Columbia Ministry of Energy and Mines and CBM Solutions (2005) 'Gas shale potential of Devonian strata, northeastern British Columbia; British Columbia Ministry of Energy, Mines and Petroleum Resources, Resource Development and Geoscience Branch', *Petroleum Geology Special Paper* 2005-1.
- Espitalie, J., Deroo, G. and Marquis, F. (1985) 'Rock Eval Pyrolysis and its applications', *Institute Francais du Petrol* 40, (563-579).
- Faraj, B., Williams, H., Addison, G. and McKinstry, B. (2004) 'Gas potential of selected shale formations in the Western Canadian Sedimentary Basin', *Houston, Hart Publications, Gas TIPS*, 10, (1), pp. 21-25.
- Farmer, V. C. and Russell, J. D. (1964) 'The infra-red spectra of layer silicates', *Spectrochimica Acta*, 20, (7), pp. 1149-1173.
- Geladi, P. and Kowalski, B. R. (1986) 'Partial least-squares regression: a tutorial', *Anal. Chim. Acta* 185, pp. 1-17
- Giesche, H. (2006) 'Mercury Porosimetry: a General (Practical) Overview', *Part.Part.Syst.Charact.*, 23, (9-19).
- Gilboy, C. F. (1988) 'Geology and natural gas production of the Upper Cretaceous Second White Speckled Shale, Southwestern Saskatchewan', *Summary of investigations 1988*,

- Saskatchewan Geological Survey, Saskatchewan Energy and Mines Miscellaneous Report*, 88-4, pp. 183-195.
- Grantham, P. J. and Wakefield, L. L. (1988) 'Variations in the sterane carbon number distributions of marine source rock derived crude oils through geologic time', *Organic Geochemistry*, 12, pp. 61-74.
- Griffiths, P. R. (1983) 'Fourier Transform Infrared Spectrometry', *Science*, 222, (4621), pp. 297-302.
- Hakuli, A., Kytokivi, A., Lakomaa, E.-L. and Krause, O. (1995) 'FT-IR in the Quantitative Analysis of Gaseous Hydrocarbon Mixtures', *Analytical Chemistry*, 67, (11), pp. 1881-1886.
- Harris, S. E., A.C., M. and Janecek, T. (1995) 'Estimating lithology from non-intrusive reflectance spectra,' *leg138*, *Proceedings of ODP Scientific Results* 138, pp. 413-428.
- Hedberg, H. D. (1936) 'Gravitational compaction of clays and shales', *American Journal of Science*, 31, pp. 241-287.
- Hildenbrand, A. and Urai, L. (2003) 'Investigations of the morphology of pore space in mudstones - first results', *Marine and Petroleum Geology*, 20, pp. 1185-1200.
- Hill, P. S., Voulgaris, G. and Trowbridge, a. J. H. (2001) 'Controls on flocc size in a continental shelf-bottom boundary layer', *Journal of Geophysical Research-Oceans*, 106, pp. 9543 - 9549.
- Hillier, S. (2003) 'Quantitative analysis of clay and other minerals in sandstones by X-ray powder diffraction (XRPD)', *Spec. Publi. Int. Assoc. Sedimentol*, 34, pp. 213-251.
- Holman, D. A., Thompson, A. W., Bennett, D. W. and Otvos, J. D. (1994) 'Quantitative Determination of Sulfur-Oxygen Anion Concentrations in Aqueous Solution: Multicomponent Analysis of Attenuated Total Reflectance Infrared Spectra', *Analytical Chemistry*, 66, (9), pp. 1378-1384.
- Hower, J., Eslinger, E. V., Hower, M. E. and Perry, E. A. (1976) 'Mechanism of burial metamorphism of argillaceous sediment. 1. Mineralogical and chemical evidence', *Geological Society of America Bulletin*, 87, pp. 725-737.
- Hughes, T. L., Methven, C. M., Jones, T. G. J., Pelham, S. E., Fletcher, P. and Hall, C. (1995) 'Determining cement composition by Fourier transform infrared spectroscopy', *Advanced Cement Based Materials*, 2, (3), pp. 91-104.
- Hunt, G. R. and Hall, R. B. (1981) 'Identification of Kaolins and Associated Minerals in Altered Volcanic Rocks by Infrared Spectroscopy', *Clays and Clay Minerals*, 29, pp. 76-78.
- Ishii, M., Shimanouchi, T. and Nakahira, M. (1967) 'Far infra-red absorption spectra of layer silicates', *Inorganica Chimica Acta*, 1, pp. 387-392.

- Janik, L. J. and Skjemstad, J. O. (1995) 'Characterization and analysis of soils using mid-infrared partial least-squares .2. Correlations with some laboratory data', *Australian Journal of Soil Research*, 33, (4), pp. 637-650.
- Janik, L. J., Skjemstad, J. O. and Raven, M. D. (1995) 'Characterization and analysis of soils using mid-infrared partial least-squares .1. Correlations with XRF-determined major-element composition', *Australian Journal of Soil Research*, 33, (4), pp. 621-636.
- Jarvie, D. M., Hill, R. J., Ruble, T. and Pollastro, R. M. (2007) 'Unconventional shale-gas systems: The Mississippian Barnett Shale of north central Texas as one model for thermogenic shale-gas assessment', *AAPG Bulletin*, 91, pp. 475-499.
- Javadpour, F., Fisher, D. and Unsworth, M. (2007) 'Nano-scale gas flow in shale sediments. ', *Journal of Canadian Petroleum Technology*, 46, (10), pp. 55-61.
- Karakassides, M. A., D., P. and D., G. (1997) 'Infrared Reflectance Study of Thermally Treated Li- and Cs-Montmorillonites', *Clays and Clay Minerals*, 45, pp. 649-658.
- Kranck, K. and Milligan, T. G. (1985) 'Origin of grain-size spectra of suspension deposited sediment:' *Geo-Marine Letters*, 5 pp. 61-66.
- Kranck, K. and Milligan, T. G. (1991a) *Grain size in oceanography*, In: Syvitski, J.P.M. (ed.) *Principles, Methods, & Application of Particle Size Analysis*. Newyork: Cambridge University Press, 332-345.
- Kranck, K. and Milligan, T. G. (1991b) *Grain size in oceanography*, In: Syvitski, J.P.M. (ed.) *Principles, Methods, & Application of Particle Size Analysis*, . New York, 332-345: Cambridge University Press.
- Kranck, K., Smith, P. C. and Milligan, a. T. G. (1996b) 'Grain-size characteristics of fine-grainedunflocculated sediments .2. 'Multi-round' distributions', *Sedimentology*, 43, (597-606).
- Kranck, K., Smith, P. C. and Milligan, T. G. (1996a) 'Grain-size characteristics of fine-grained unflocculated sediments .1. 'One-round' distributions', *Sedimentology*, 43, pp. 589-596.
- Landais, P. (1995) 'Statistical determination of geochemical parameters of coal and kerogen macerals from transmission micro-infrared spectroscopy data', *Organic Geochemistry*, 23, (8), pp. 711-720.
- Leach, C. J., Wagner, T., Jones, M., Juggins, S. and Stevenson, A. C. (2008) 'Rapid determination of total organic carbon concentration in marine sediments using fourier transform near-infrared spectroscopy (FT-NIRS)', *Organic Geochemistry*, 39, pp. 910-914.

- Leckie, D. A., Bhattacharya, J. P., Bloch, J., Gilboy, C. F. and Norris, B. (1994) 'Cretaceous Colorado/Alberta Group of the Western Canada Sedimentary Basin. In: Mossop, G. & Shetsen, I. (eds)', *Geological Atlas of the Western Canada Sedimentary Basin*, Canadian Society of Petroleum Geologists and the Alberta Research Council. , pp. 335-352.
- Leckie, D. A., Bhattacharya, J. P., Bloch, J., Gilboy, C. F. and Norris, B. (2008) 'Chapter 20: Cretaceous Colorado/Alberta Group of the Western Canada Sedimentary Basin. In: Geological Atlas of the Western Canada Sedimentary Basin. Mossop, G.D., and I. Shetsen (eds.)', *Canadian Society of Petroleum Geologists and Alberta Research Council, Special Report 4*.
- Leckie, D. A., C., S., Bloch, J., Wilson, M. and Wall, J. H. (1992) 'An anoxic event at the Albian-Cenomanian boundary: the Fish Scale Marker Bed, northern Alberta, Canada', *Palaeogeography, Palaeoclimatology, Palaeoecology*, 92, (139-166).
- Leckie, D. A., Schröder-Adams, C. J., Rosenthal, L. and Wall, J. H. (2000a) 'An outcrop of the Albian Viking Formation and a southerly extension of the Hulsberg/Harmon interval in west-central Alberta', *Bulletin of Canadian Petroleum Geology*, 48, pp. 30-42.
- Lis, G. P., Mastalerz, M., Schimmelmann, A., Lewan, M. D. and Stankiewicz, B. A. (2005) 'FTIR absorption indices for thermal maturity in comparison with vitrinite reflectance R₀ in type-II kerogens from Devonian black shales', *Organic Geochemistry*, 36, (11), pp. 1533-1552.
- Macquaker, J. H., Taylor, K. G. and Gawthorpe, R. L. (2007) 'High-resolution facies analyses of mudstones: Implications for paleoenvironmental and sequence stratigraphic interpretations of offshore ancient mud-dominated successions', *Journal of Sedimentary Research*, 77, pp. 324-339.
- Marko, P., Satu, H., Janne, P. and Lauri, N. (2000) 'Application of PLS multivariate calibration for the determination of the hydroxyl group content in calcined silica by DRIFTS', *Journal of Chemometrics*, 14, (5-6), pp. 501-512.
- Martens, H. and Naes, T. (1989.) *Multivariate Calibration*. Wiley, New York.
- Martini, A. M., Budai, J. M., Walter, L. M. and Schoell, M. (1996) 'Microbial generation of economic accumulations of methane within a shallow organic-rich shale', *Nature* 383, pp. 155-158.
- Martini, A. M., Walter, L. M., Budai, J. M., Ku, T. C. W., Kaiser, C. J. and Schoell, M. (1998) 'Genetic and temporal relations between formation waters and biogenic methane: Upper Devonian Antrim Shale, Michigan Basin, USA', *Geochimica et Cosmochimica Acta* 62, (10), pp. 1699-1720.
- Matteson, A. and Herron, M. M. (1993) 'Quantitative Mineral Analysis by Fourier Transform Infrared Spectroscopy', *SCA Conference Paper Number 9308*. pp.

- Matthews, H. L., Schein, G. and Malone, M. (2007) 'Stimulation of gas shales: they're all the same – right? ', *SPE 106070*, pp. 1-16.
- McCave, I. N. and Syvitski, J. P. M. (1995) 'sortable silt and fine sediment size/composition slicing: parameters for palaeocurrent speed and palaeoceanography', *Palaeoceanography*, 10, pp. 593-610.
- McKelvy, M. L., Britt, T. R., Davis, B. L., Gillie, J. K., Lentz, L. A., Leugers, A., Nyquist, R. A. and Putzig, C. L. (1996) 'Infrared Spectroscopy', *Analytical Chemistry*, 68, (12), pp. 93-160.
- McNeil, D. H. and Gilboy, C. F. (1999) 'High resolution Cretaceous biostratigraphy record from the Kennebec River and Leather River kimberlite cores, East-Central Saskatchewan- preliminary report', *Summary of investigations 1999, Volume 1, Saskatchewan Geological Survey, Saskatchewan Energy and Mines Miscellaneous Report*, 99-4.1, pp. 41-44.
- McNeil, D. H. and W.G.E. Caldwell. (1981) 'Cretaceous rocks and their foraminifera in the Manitoba Escarpment', *Special Paper – Geological Association of Canada*, 21, pp. 439
- Mondol, N. H., Bjorlykke, K., Jahren, J. and Hoeg, K. (2007) 'Experimental mechanical compaction of clay mineral aggregates - Changes in physical properties of mudstones during burial', *Marine and Petroleum Geology*, 24, pp. 289-311.
- Montgomery, S. L., Jarvie, D. M., Bowker, K. A. and Pollastro, R. M. (2005a) 'Mississippian Barnett Shale, Fort Worth basin, north-central Texas: Gas-shale play with multi-trillion cubic foot potential', *AAPG Bulletin* 89, (2), pp. 155-175.
- Montgomery, S. L., Jarvie, D. M., Bowker, K. A. and Pollastro, R. M. (2005b) 'Mississippian Barnett Shale, Fort Worth basin, north-central Texas: Gas-shale play with multi-trillion cubic foot potential', *American Association of Petroleum Geologist Bulletin* 89, (2), pp. 155-175.
- Moore, J. K. S. (2005) *Integration of the sedimentological and petrophysical properties of mudstone samples*. thesis. Newcastle University, 261 p.
- Naes, T., Isaksson, T. and Davies, T. (2004) *A user Friendly Guide to Multivariate Calibration and Classification* Chichester: NIR Publications.
- Nielsen, K. S., Schröder-Adams, C. J. and Leckie, D. A. (2003) 'A new stratigraphic framework for the Upper Colorado Group (Cretaceous) in southern Alberta and southwestern Saskatchewan, Canada', *Bulletin of Canadian Petroleum Geology*, 51, pp. 304-346.
- Painter, P. C., Rimmer, S. M., Snyder, R. W. and Davis, A. (1981) 'A Fourier Transform Infrared Study of Mineral Matter in Coal: The Application of a Least Squares Curve-Fitting Program', *Appl. Spectrosc.*, 35, (1), pp. 102-106.

- Passey, Q. R., Bohacs, K. M., Esch, W. L., Klimentidis, R. and Sinha, S. (2010) 'From Oil-Prone Source Rock to Gas-Producing Shale Reservoir - Geologic and Petrophysical Characterisation of Unconventional Shale-Gas Reservoirs', *CPS/SPE International Oil and Gas Conference and Exhibition*. 8-10 June, Beijing, China.
- Peltonen, C., Marcussen, Å., Bjorlykke, K. and Jahren, J. (2009) 'Clay mineral diagenesis and quartz cementation in mudstones: The effects of smectite to illite reaction on rock properties', *Marine and Petroleum Geology*, 26, pp. 887-898.
- Permanyer, A., Rebufa, C. and Kister, J. (2007) 'Reservoir compartmentalization assessment by using FTIR spectroscopy', *Journal of Petroleum Science and Engineering*, 58, (3-4), pp. 464-471.
- Peters, K. E. (1986) 'Guidelines for evaluating petroleum source rock using programmed pyrolysis', *American Association of Petroleum Geology Bulletin*, 70, pp. 318-329.
- Peussa, M., Harkonen, S., Puputti, J. and Niinisto, L. (2000) 'Application of PLS multivariate calibration for the determination of the hydroxyl group content in calcined silica by DRIFTS', *Journal of Chemom*, 14 pp. 501-512.
- Pollastro, R. M. (2003) 'Geologic and production characteristics utilized in assessing the Barnett Shale continuous (unconventional) gas accumulation, Barnett-Paleozoic total petroleum system, Fort Worth Basin, Texas', *Barnett Shale Symposium*. 1, 6 pp.
- Purcell, W. R. (1949) 'Capillary pressure- their measurements using mercury and the calculation of permeability therefrom ', *AIME Petroleum Trans*, 186, pp. 39-48.
- Ray, L. F. and Ursula, J. (1998) 'Combination Bands in the Infrared Spectroscopy of Kaolins-A DRIFT Spectroscopic Study', *Clays and Clay Minerals*, 46, (4), pp. 466-477.
- Rice, D. D. (1993) 'Biogenic gas: controls, habitats, and resource potential, in D.G. Howell, ed., *The Future of Energy Gases -* ', *U.S. Geological Survey Professional Paper 1570*, Washington, United States Government Printing Office, pp. 583-606.
- Rice, D. D. and Claypool, G. E. (1981) 'Generation, accumulation, and resource potential of biogenic gas', *American Association of Petroleum Geologists Bulletin*, 65, pp. 5-25.
- Rice, D. D. and Spencer, C. W. (1996) 'Northern Great Plains shallow biogenic gas. In: 1995 National Assessment of United States Oil and Gas Resources –Results, Methodology, and Supporting Data. D.L. Gautier, G.L. Dolton, K.I. Takahashi and K.L. Varnes (eds.).. Release 2', *U.S. Geological Survey Digital Data Series DDS-30*.
- Ridgley, J. L. (2000) 'Lithofacies architecture of the Milk River Formation (Alderson Member of the Lea Park Formation), Southwestern Saskatchewan and Southeastern Alberta – its relation to gas accumulation. In: *Summary of Investigations 2000*', *Saskatchewan Geological Survey*, 1, pp. 106–120.
- Ridgley, J. L. (2002) ' Regional geochemical study of the Upper Cretaceous shallow biogenic gas system in Saskatchewan, Alberta, and Montana; application of isotope and

- compositional systematics to understanding the distribution of gas resources. In Summary of investigations 2002', *Saskatchewan Geological Survey*, 1, pp. 143-150
- Ross, D. J. K. and Bustin, R. M. (2007) 'Shale gas potential of the Lower Jurassic Gordondale Member, northeastern British Columbia, Canada', *Bulletin of Canadian Petroleum Geology*, vol. 55, (no. 1), pp. 51-75.
- Ross, D. J. K. and Bustin, R. M. (2008) 'Characterizing the shale gas resource potential of Devonian–Mississippian strata in the Western Canada sedimentary basin: Application of an integrated formation evaluation', *American Association of Petroleum Geologist Bulletin*, 92, (), pp. 87-125.
- Rushing, J. A. and Blasingame, T. A. (2008) 'Rock typing - Keys to Understanding Productivity in Tight Gas Sands', *SPE Unconventional Reservoirs Conference* Keystone, Colorado, U.S.A., 10-12 February. pp.
- Savitzky, A. and Golay, M. J. E. (1964) 'Smoothing and Differentiation of Data by Simplified Least Squares Procedures', *Analytical Chemistry*, 36, (8), pp. 1627-1639.
- Schieber, J. and Southard, J. B. (2009) 'Bedload transport of mud by floccule ripples: direct observation of ripple migration processes and their implications', *Geology*, 37, (6), pp. 483-486.
- Schieber, J., Southard, J. B. and Schimmelmann, A. (2010) 'Lenticular shale fabrics resulting from intermittent erosion of water-rich muds – interpreting the rock record in the light of recent flume experiments', *Journal of Sedimentary Research*, 80, pp. 119-128.
- Schieber, J., Southard, J. B. and Thaisen, G. (2007) 'Accretion of mudstone beds from migrating floccule ripples', *Science*, 318, pp. 1760-1763.
- Schoell, M. (1983) 'Genetic characterization of natural gases', *American Association of Petroleum Geologists Bulletin*, 67, pp. 2225-2238.
- Schröder-Adams, C. J., Leckie, D. A., Bloch, J., Craig, J., McIntyre, D. J. and Adams, P. J. (1996) 'Palaeoenvironmental changes in the Cretaceous (Albian to Turonian) Colorado Group of western Canada: microfossil, sedimentological and geochemical evidence', *Cretaceous Research*, 17, pp. 311-365.
- Shurr, G. W. and Ridgley, J. L. (2002) 'Unconventional Shallow Biogenic Gas Systems', *AAPG Bulletin*, 86, (11), pp. 1939-1969.
- Snyder, R. W., P.C., P. and Cronauer, D. C. (1983) 'Characterisation of oil shale by FTIR spectrsocopy', *Fuel*, 62, pp. 1205-1214.
- Stott, D. F. (1993) 'Evolution of Cretaceous foredeeps: a comparative analysis along the lenght of the Canadian Rock Mountains. In: Caldwell, W.G.E. & Kauffman, E.G. (eds) Evolution of the Western Interior Basin', *Geological Association of Canada Special Paper*, 13, pp. 253-275.

- Tanaka, T., Nagao, S. and Ogawa, H. (2001) 'Attenuated Total Reflection Infrared (ATR-FTIR) Spectroscopy of Functional Groups of Humic Acid in Aqueous Solutions', *Analytical Science*, 17, pp. i1081-i1084.
- Tissot, B. P. and Welte, D. H. (1984) *Petroleum formation and occurrence*. Berlin, Federal Republic of Germany: Springer-Verlag.
- Tyson, R. V. (1995) *Sedimentary Organic Matter: Organic Facies and Palynofacies*. London: Chapman and Hall. 615p.
- Varban, B. L. and A.G. Plint. (2008) 'Palaeoenvironments, paleogeography, and physiogeography of a large, shallow muddy ramp; late Cenomanian-Turonian Kaskapau Formation, Western Canada foreland basin ', *Sedimentology*, 55, pp. 201-233.
- Walsh, W., Adams, C., Kerr, B. and Korol, J. (2006) 'Regional “shale gas” potential of the Triassic Doig and Montney formations, northeastern British Columbia; British Columbia Ministry of Energy, Mines and Petroleum Resources, Resource Development and Geoscience Branch', *Petroleum Geology Open File* 2006-0.
- Washburn, E. W. (1921) 'Note on a method of determining the distribution of pore sizes in a porous material', *Proceedings of the National Academy of Science*, 7, pp. 115-116.
- White, T. S., Witzeke, B. J., Ludvigson, G. A. and Ravn, R. (1999) 'Chemostratigraphy and sequence stratigraphy of the Albian-Turonian (Cretaceous) portions of the Kennecott Crooked River SK-16B-93-1 core, East-Central Saskatchewan ', *Summary of investigations 1999, Volume 1, Saskatchewan Geological Survey, Saskatchewan Energy and Mines Miscellaneous Report*, 99-4.1, pp. 45-51.
- Wilson, M.J. (1996) 'Clay Mineralogy: Spectroscopic and Chemical Determinative Methods', *Chapman and Hall*, London.
- Yang, Y. and Aplin, A. C. (1997) 'A method for the disaggregation of mudstones', *Sedimentology*, 44, pp. 559-562.
- Yang, Y. and Aplin, A. C. (1998a) 'Influence of lithology and compaction on the pore size distribution and modelled permeability of some mudstones from the Norwegian margin', *Marine and Petroleum Geology*, 15, pp. 163-175.
- Yang, Y. and Aplin, A. C. (1998b) 'Influence of lithology and compaction on the pore size distribution and modelled permeability of some mudstones from the Norwegian margin', *Marine and Petroleum Geology*, 15, pp. 163-175.
- Zhou, Z. J. and Law, D. H. S. (1998) 'Swelling clays in hydrocarbon reservoirs; the bad, the less bad, and the useful', *Proceedings – UNITAR International Conference on Heavy Crude and Tar Sands*, vol. 7, (1998.057).

7.4 APPENDICES

